

# Transfer of Human Motion Primitives for Digital Human Model Control in the Scope of Ergonomic Assessment

Vom Fachbereich Informatik der  
Technischen Universität Kaiserslautern  
zur Verleihung des akademischen Grades  
Doktor der Ingenieurwissenschaften (Dr.-Ing.)

genehmigte Dissertation

von

Marius Obentheuer

Datum der wissenschaftlichen Aussprache:	08. Juli 2020
Dekan:	Prof. Dr. Jens Schmitt
Berichterstatter:	Prof. Dr. rer. nat. Karsten Berns
Berichterstatter:	Prof. Dr.-Ing. habil. Sigrid Leyendecker



## Abstract

To assess ergonomic aspects of a (future) workplace already in the design phase where no physical prototypes exist, the use of digital human models (DHMs) becomes essential. Thereby, the prediction of human motions is a key aspect when simulating human work tasks. For ergonomic assessment e.g. the resulting postures, joint angles, the duration of the motion and muscle loads are important quantities. From a physical point of view, there is an infinite number of possible ways for a human to fulfill a given goal (trajectories, velocities...), which makes human motions and behavior hard to predict. A common approach used in state of the art commercial DHMs is the manual definition of joint angles by the user, which requires expert knowledge and is limited to postural assessments. Another way is to make use of pre-recorded motions from a real human that operates on a physical prototype, which limits assessments to scenarios which have been measured before. Both approaches need further post processing and inverse dynamics calculations with other software tools to get information about inner loads and muscle data, which leads to further uncertainties concerning validity of the simulated data.

In this thesis work a DHM control and validation framework is developed, which allows to investigate in how far the implemented human like actuation and control principles directly lead to human like motions and muscle actuations. From experiments performed in the motion laboratory, motion data is captured and muscle activations are measured using surface electromyography measurements (EMG). From the EMG data, *time invariant muscle synergies* are extracted by the use of a *non-negative Matrix Factorization algorithm* (NMF). Muscle synergies are one hypothesis from neuroscience to explain how the human central nervous system might reduce control complexity: instead of activating each muscle separately, muscles are grouped into functional units, whereas each muscle is present in each unit with a fixed amplitude. The measured experiment is then simulated in an optimal control framework. The used framework allows to build up DHMs as multibody system (MBS): bones are modeled as rigid bodies connected via joints, actuated by joint torques or by Hill type muscle models (1D string elements transferring fundamental characteristics of muscle force generation in humans). The OC code calculates the actuation signals for the modeled DHM in a way that a certain goal is fulfilled (e.g. reach for an object) while minimizing some *cost function* (e.g. minimizing time) and considering the side constraints that the equations of motion of the MBS are fulfilled. Therefore, three different *Actuation Modes* (AM) can be used (joint torques (AM-T), direct muscle actuation (AM-M) and muscle synergy actuation (AM-S), using the before extracted synergies as control parameters)). Simulation results are then compared with measured data, to investigate the influence of the different Actuation Modes and the solved OC cost function. The approach is applied to three different experiments, the *basic reaching test*, the *weight lift test* and a *box lifting* task, where a human arm model actuated by 29 Hill muscles is used for simulation. It is shown that, in contrast to a joint torque actuation (AM-T), using muscles as actuators (AM-M & AM-S) leads to very human like motion trajectories. Muscle synergies as control parameters, resulted in smoother velocity profiles, which were closer to those measured and appeared to be more robust, concerning the underlying muscle activation signals (compared to AM-M). In combination with a developed biomechanical cost function (a mix of different OC cost functions), the approach showed promising results, concerning the simulation of valid, human like motions, in a predictive manner.



## Danksagungen

Schnell vergisst man im Stress und bei all den Aufgaben die man im Leben bewältigt den Anteil anderer Menschen und äußerer Umstände am eigenen Erfolg. Mit etwas Abstand und einem Blick von außen zeigt sich oft, wie klein doch der eigene Anteil ist im Vergleich zu dem, wofür man eigentlich nichts kann, was man nicht in der Hand hatte, und wofür es sich lohnt dankbar zu sein. Ein wenig davon versuche ich hier zu benennen, auch wenn es bei genauerer Betrachtung wohl eine eigene Arbeit wäre.

Zuerst möchte ich meinem Doktorvater Karsten Berns danken, der mir nicht nur als fruchtbarer Diskussionspartner und Berater für allgemeine Themen was wissenschaftliches Arbeiten betrifft zur Seite stand, sondern mir auch die Freiheit ließ, mich thematisch zu entfalten und nach meinen Interessen zu forschen.

Ebenso möchte ich diesen Dank Joachim Linn aussprechen, der meine Arbeit am Fraunhofer ITWM betreute und mir stets als Gesprächspartner zur Seite stand um Problemstellungen zu konkretisieren oder aber auch weit über das eigentliche Thema hinaus zu philosophieren, manchmal bei einem Bier bis spät in die Nacht. Der menschliche verständnisvolle Umgang auch in seiner Art als Abteilungsleiter erleichterten mir den Einstieg ins Berufsleben sehr (auch wenn er immer sagte dies wäre noch weit vom „richtigen“ Berufsleben entfernt). Und auch als privater und beruflicher Stress drohten mich zu übermannen erleichterte mir diese Menschlichkeit und das Verständnis viel.

Ebenso möchte ich Klaus Dreßler danken, der mir nach einigen Vorstellungsgesprächen das Vertrauen entgegenbrachte mich einzustellen, und somit (stellvertretend für das Fraunhofer ITWM) meine Forschung finanzierte, was mir ebenfalls viel Freiheiten erlaubte.

Auch für die Kollegen am ITWM und das nette Arbeitsumfeld bin ich sehr dankbar, die Mischung aus Menschlichkeit, Gelassenheit aber auch fachlicher Kompetenz erwiesen und erweisen sich als fruchtbare Mischung. Namentlich möchte ich hier stellvertretend für viele meinen Bürokollegen Fabio Schneider nennen, der immer fair die Rittersport Tafeln mit mir teilte, oft im Handumdrehen organisatorische Dinge für mich löste (bzw. mir Lösungswege aufzeigte), für deren Erarbeitung ich sonst oft sehr viel Zeit verloren hätte, und mich oft beim lauten Denken unterstützte (manchmal auch einfach nur in dem er interessiert schaute während er weiter seine Arbeit nachging, auch das half ungemein). Außerdem Michael Roller, der mich nicht nur inhaltlich als Gesprächspartner sehr unterstützte. Ohne die Zuarbeit in Sachen Menschmodellierung und Implementierungsarbeit im Simulationscode wäre meine Arbeit so nicht möglich gewesen, vielen Dank dafür! (<= ist zwar auch kein Comic, hier mach ich aber trotzdem mal ein Ausrufezeichen).

Ebenso wichtig wie das berufliche Umfeld war auch eine harmonische und tragende Basis im Privaten, auch wenn die Übergänge hier teilweise fließend waren. Ich möchte all den lieben und tollen Menschen in meinem Freundeskreis danken, ohne eure Basis wäre ich nicht da wo ich bin, und hier spielen so viele mit hinein, daher verzeiht das ich euch nicht alle nennen kann. Nennen möchte ich aber die --BellStreetBoYz-- Thilo und Olek, ihr wart viel mehr als nur Mitbewohner – Kletterpartner, Begleiter im Abenteuer, beste Freunde, Familie eben. Dank euch habe ich nie vergessen was es noch alles andere im Leben gibt außer Arbeit und habe erfahren das gemeinsam prokrastinieren deutlich mehr Spaß macht. Unsere Zeit wird wohl für immer zu den besten meines Lebens zählen.

Auch Peli möchte ich an dieser Stelle endlich mal meinen Dank aussprechen. Ohne unsere Gespräche und dein Einwirken wäre ich wohl nie am ITWM gelandet, und auch darüber hinaus hat deine Familie sehr viel positiven Einfluss auf mich und meinen Lebensweg gehabt und war immer ein wichtiger Ankerpunkt für mich. Danke euch Toni, Max und Dorle.

Auch meinen Eltern möchte ich für ihre Geduld und die Zuversicht, aber auch für die Anerkennung danken. Und auch meinem Bruder Fabian, der mir immer wieder knallhart vor Augen führte von wie vielen Dingen (die man im Allgemeinen - als „Doktor“ aber erstrecht auf jeden Fall - wissen müsste) ich dann doch überhaupt keine Ahnung habe.

Und nicht zuletzt meinen Mädels Marta und Lulu, die viel Veränderung und Neues in mein Leben brachten. Danke Marta für deine Liebe und die Geborgenheit, und danke Lulu für die Inspirationen die Welt wieder mit Kinderaugen zu sehen und die tägliche Möglichkeit das Lernverhalten der Steuerungssysteme des menschlichen Bewegungsapparates studieren zu können.

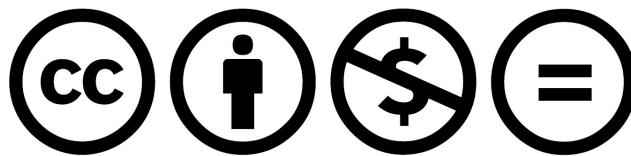
*“Nicht die Glücklichen sind dankbar. Es sind die Dankbaren, die glücklich sind”*

[Francis Bacon]

# Copyright

## Thesis

The thesis itself and all its content is licensed under the terms of the Creative Commons Attribution–NonCommercial–NoDerivatives 4.0 International (CC BY-NC-ND 4.0) license. This means that the unaltered thesis may be freely copied and redistributed except for commercial purposes. The distribution in altered forms – including shortened or annotated versions – is explicitly prohibited.



## Figures

The original figures – that do not origin from some other work – are licensed under the terms of the Creative Commons Attribution–NoDerivatives 4.0 International (CC BY-ND 4.0) license. This means that they may be used in unaltered form without restriction and without further explicit permission) as long as this thesis is properly cited.



# Contents

<b>1</b>	<b>Introduction</b>	<b>1</b>
1.1	Motivation	1
1.2	Objectives	3
1.3	Structure	4
<b>2</b>	<b>Motion generation in humans and vertebrates</b>	<b>6</b>
2.1	Anatomy	6
2.1.1	Anatomical terms of movement and body planes	6
2.1.2	Bones, joints and muscles	8
2.1.3	Voluntary motor function	13
2.2	Muscle synergies as control concept in neuroscience	17
2.2.1	Evidence for muscle synergies	17
2.2.2	Types of muscle synergies	19
<b>3</b>	<b>Control Concept for a biomechanical human model</b>	<b>22</b>
3.1	General control approaches	22
3.1.1	Muscle synergies as control concept for DHM's	27
3.2	Overall approach - overview	28
3.3	Data acquisition in the motion lab	30
3.3.1	Motion capturing	30
3.3.2	EMG Measurements	31
3.3.3	Measurement of external forces	35
3.4	Muscle synergy extraction	36
3.4.1	Non Negative Matrix Factorization for muscle synergy extraction	37
3.5	The digital human model	39
3.5.1	Implemented modelling approach	40
3.5.2	Biomechanical simulation model of the right arm	41
3.5.3	Hill muscle model	44
3.6	Optimal control framework	45
<b>4</b>	<b>The basic reaching test</b>	<b>50</b>
4.1	Motion Lab measurements	50
4.1.1	Test setup	50
4.1.2	Measured Trajectories	54
4.1.3	Measured velocity profiles	58
4.2	Measured EMG values	59
4.3	Muscle Synergy extraction	60
4.4	Simulated test	69
4.4.1	Simulation model and test setup	69
4.4.2	Simulated Trajectories	70
4.4.3	Simulated velocity profiles	73
4.4.4	Simulated EMG values	74
<b>5</b>	<b>Weight lift test</b>	<b>76</b>
5.1	Motion Lab measurements	76
5.1.1	Test setup	76
5.1.2	Measured Trajectories	78



---

5.1.3	Measured velocity profiles .....	82
5.1.4	Measured EMG values.....	83
5.2	Simulated test – Test Scenario 1 .....	86
5.2.1	Simulation model and test setup .....	86
5.2.2	Simulated Trajectories – minimal time.....	87
5.2.3	Simulated velocity profiles – minimal time .....	89
5.2.4	Simulated muscle actuations – different cost functions .....	89
5.3	Simulated test – Test Scenario 2 .....	93
5.4	Simulated test – Test Scenario 3 .....	96
<b>6</b>	<b>Industry use case – box lifting.....</b>	<b>99</b>
6.1	Motivation from industry.....	99
6.2	Motion Lab test description .....	100
6.3	Simulated Test .....	100
6.4	Results and Discussion.....	101
<b>7</b>	<b>Conclusion and Outlook .....</b>	<b>103</b>
<b>A</b>	<b>Experimental and Simulation results .....</b>	<b>107</b>
A.1	Weight lift test data.....	107
A.1.1	Weight lift test - Measured Trajectories .....	107
A.1.2	Weight lift test - Measured Velocity profiles.....	116
A.1.3	Weight lift test - Measured EMG data .....	117
A.1.4	Simulated muscle actuations TS1-f .....	136
A.2	Box lift – simulated muscle actuations .....	139
A.2.1	Direct muscle actuation.....	139
A.2.2	Synergetic muscle actuation .....	141
	<b>Bibliography .....</b>	<b>143</b>



# 1 Introduction

## 1.1 Motivation

The number of elderly work force in all branches of industry will keep on growing in the next decades due to the ongoing demographic change. Especially in branches where the amount of manual work tasks remains high, like e.g. automotive final assembly, the need for individualized, safe and ergonomic work places, processes and tools, raises continuously. The state of the art approach to assess ergonomic aspects in most of these fields is to work with human workers, which operate on physical prototypes. Such a reactive proceeding is expensive, slow, and allows only for minor modifications due to the progressed status of the product development process. Therefore, there is an increasing demand from industry for tools that allow to include models of humans in the simulation process, which enable it to predict human motions and behavior in an early stage of development, so that ergonomic evaluations can already be done when working with digital prototypes.



*Figure 1: Assembly analysis using a digital human model. Source: IPS IMMA software.*

When e.g. a construction engineer develops a new part that has to be assembled in the car body as depicted in Figure 1, many decisions have to be taken when designing the workplace layout. It has to be ensured that the worker(s) can reach the final position of the part in a way that it can be assembled. Additionally, unfavorable postures and motions (like joint angle limits) should be avoided, which means that e.g. the height, in which the chassis is positioned on the assembly line, has to be adapted or optimized. Another question would be, if the part can be lifted and mounted easily, or if some kind of support tool or a second person has to be included to reduce muscular loads of the worker. How exhausting a work task actually is, is an important information to determine cycle times and rest times in between repetitions of a task.

In classical ergonomic assessment methods, workers are simply asked after execution of a work task at a workstation, but there also exist more quantitative approaches, which measure the muscle activations with electromyography methods (EMG) during work. Anyway, it is unavoidable to somehow consider the human worker in the layout process

of workstations, to guarantee an ergonomic workplace layout and to avoid musculoskeletal disorders which result from muscle fatigue, inconvenient postures or unhealthy motions. But human beings are highly complex and eclectic creatures, regarding both, their anatomical appearance, and the cognitive capabilities and behavior. Whereas many (by no means all) of the anatomical aspects of the human body concerning motion generation are well understood, especially the control schemes of the central nervous system, which are responsible for the muscle actuation and generation of motion, still are subject of research.

Modelling an appropriate digital representation of a human worker for assembly simulation to predict human motions is a challenging task and comprises multiple topics. Although, the anatomical aspects of motion generation in humans are well understood, the transfer of their physical and biomechanical properties to a digital human model (DHM) is not trivial. When thinking about which of these anatomical properties should be transferred to a DHM, the planned control mechanism already has to be considered to some extent. For certain control concepts a pure visual representation of the human body without any physical properties can be sufficient, e.g. when mapping captured motions from real humans to an "avatar". Those approaches are widely spread in the application of computer graphics and in gaming industry, where the main focus is on a realistic visual appearance, and the calculation of physically correct data is of minor interest.

In contrast, if learning or optimization methods are used for motion generation, the DHM needs at least some physical properties to simulate for example walking (and falling), and to have control parameters that can be adapted by the learning or optimization algorithm. If these approaches are inspired by nature, there might even be the need for a more realistic modelling approach to be able to optimize or learn on the same parameters as the central nervous system (CNS) does (for example muscle loads). But which level of detail is necessary for that end? There is a wide range of scientific approaches for digital human modelling considering physical quantities, leading from very simplified stick-figure like pure kinematical representations (e.g. Calspan3D CVS [Mühlstedt 12] over more detailed biomechanical multibody system approaches with simplified muscles [Damsgaard 06] to very complex nonlinear finite element models considering viscoelastic effects of human tissue coupled with chemo-electrical co simulations [Röhrle 16, Heidlauf 14]. At this point, computation times already have to be considered to some extent, to ensure that the DHM will suit the intended purpose in the end. For ergonomic assessments, the overall posture or motions of a human respectively DHM for predictions is of high relevance, but also the loads on the manikin (external) and the resulting inner strains on joints (torques) or muscles.

Beside the demanding question of modelling the anatomical and biomechanical aspects of the human body, finding an appropriate control approach, might even be the more challenging task. The complexity of the human body, regarding both, the anatomical appearance and the characteristics of the CNS, result from a million of years of evolution. It allows human beings to easily adapt to new situations, change the motion strategy in case of injuries or with an altering surrounding and to quickly react on disturbances. One important base for this property is the principle of redundancy, which can be found everywhere and on every level of detail in the human body. So, e.g. the control system, that keeps our body in balance is a combination of our visual system (eyes), vestibular system (inner ear) and skeletal system, whereas the information are processed by the brain

and combined with already learned knowledge and information (e.g. position in the room and proprioception).

In the sense of selection advantage and survivability this seems to be a very efficient and convenient concept, that allows for a high flexibility. But exactly this flexibility makes it very difficult to predict human motions and behavior due to the numerous possible solutions for one and the same problem. Even a simple “reach and grasp” task can be fulfilled by a multitude of possible solutions. Which trajectory does a human choose, which velocity, which acceleration? On which factors does this decision depend on? Which muscles will be activated? And how and why does the CNS decide to exactly take this solution out of so many possible ones? How does it find this often (near) optimal solution so quickly, even in new and unknown situations?

These are long standing questions in medicine, neuroscience and biology, and also in related fields like robotics, where scientist try to transfer control approaches inspired by nature to robots or technical systems. When thinking of a controller for a humanoid robot and the “reach and grasp” example, the main focus is on finding a robust control policy that somehow fulfils the task, while keeping the robot in balance and avoid collisions. For the simulation of a human worker with a DHM, the “robustness” of the controller is much easier to ensure due to the pure virtual representation, but therefore some more aspects are important for the generated motions. To get significance for ergonomic evaluations, the simulated motion has to be human like. This means that the controller should find a solution to fulfill the task similar to the one a real human would choose (trajectories, velocities, accelerations...). Or, thinking of reachability and mountability analyses, a real human should at least be able to perform the predicted motions.

When the DHM is modelled as more detailed biomechanical system with muscles as actuators, the problem of anatomical redundancy comes up additionally. Due to the fact that humans have much more muscles than kinematical degrees of freedom (DOF), even one and the same kinematical motion can be performed by a multitude of muscle actuations. Here, it would also be favorable if the controller would not just be able to handle the anatomical redundancy, but to solve it in a human like way. This would deliver important values for an ergonomic workplace layout and help to predict muscular overload and fatigue. One hypothesis in neuroscience to explain how the (anatomical) redundancy is solved or reduced in vertebrates is that the CNS makes use of pre-defined groupings of muscles, so called muscle synergies, instead of actuating every single muscle in particular. It is assumed that this reduces the number of possible solutions to fulfill a certain task and by that simplifies motion control. Transferring the principle of muscle synergy actuation from neuroscience to a control algorithm for a biomechanical DHM could help to solve the muscle redundancy problem, lead to human like motions and reduce the dimensionality of the control problem.

## 1.2 Objectives

The main objective of this work is to develop and investigate a DHM control framework, which allows to use **muscle synergies as control parameters** for a biomechanical DHM and to investigate the influence of such a control concept. This comprises multiple sub problems which have to be solved. For one, muscle synergies cannot be estimated or measured in a direct way. This means that they have to be extracted implicitly. Therefore, different algorithms are used in neuroscience, which allow to extract muscle synergies

from measured EMG data. Many of these experiments are done with animals and invasive procedures which are not suitable for experiments with humans. So, one objective will be to **design an appropriate experimental setup**, which allows to **extract muscle synergies from human EMG data**. This includes the choice of (measureable) muscles and expedient motions, EMG marker placement, EMG data post processing and filtering, muscle synergy extraction and validation and many more subtasks. As there exist several different mathematical representations of muscle synergies in literature, a suitable representation has to be chosen and transferred into a control concept.

Muscle synergies themselves can be seen as control parameters, which e.g. group several actuators (muscles) into functional units. To generate motions with a DHM, there still is a need for some kind of control policy, which calculates activation signals for these functional units. Such activation signals can be computed by means of an optimal control framework, whereas optimal control models of biological movement have explained behavioral observations on multiple levels of analysis and have arguably been more successful than any other class of models [Todorov 04]. In this thesis, an already **existing prototypical optimal control (OC) framework is used** [Leyendecker 10, Maas 13, Roller 17]. This framework allows to build up arbitrary multibody system (MBS) models, which can be actuated by joint torques, or by using simplified muscles as force elements. The OC code then calculates the actuation signals in a way, that a certain goal is fulfilled (e.g. reach for an object) while minimizing some cost function (e.g. minimizing time) and considering the side constraints that the equations of motion of the MBS are fulfilled. The developed muscle synergy representation should be applicable to these existing muscle models to be able to make use of the (enhanced) OC framework for motion generation (and control simulation models built up in this framework).

Another objective of this work will be to investigate the influence of the derived muscle synergy actuation. In consideration of the optimal control framework as control policy for motion generation, this involves several subtasks which have to be examined. As the OC framework allows the actuation of an arbitrary MBS with joint torques as well as alternatively single muscles, these **Actuation Modes (AM) should be investigated** as well and **compared with a muscle synergy actuation**. The advantages and disadvantages of each Actuation Mode (beside others regarding calculation times, kinematical solutions, convergences) should be examined. To be able to validate how "human like" the resulting motions or actuation signals are, and to be able to assess the influence of the different action modes, the simulated solutions should be **validated against measured motion lab data**. To get significance for a comparison of measured and simulated motion data, many influencing factors have to be considered. Therefore, a suitable concept has to be worked out. One factor here is e.g. that the anthropometry of the built up DHM simulation models fits to the anthropometry of the subject(s) performing the experiments in the motion lab.

### 1.3 Structure

This thesis is structured as follows: In Chapter 2, the basics for motion generation in humans and vertebrates are introduced. The anatomical basis like bones and muscles are explained, directly with regard to the challenges for DHM modelling and motion validation (simulated vs. measured). The underlying control structures for voluntary motor functions are explained including force generation and activation mechanisms of muscles, and the muscle synergy hypothesis is introduced. Experiments from neuroscience which give

evidence for the existence of muscle synergies as control concept of the CNS are summarized and the different mathematical representations of muscle synergies are explained.

The DHM control concept developed in this work is introduced in Chapter 3. After a short overview of alternative control approaches and the state of the art commercial DHMs for ergonomic assessment, the developed overall approach and the outputs from each sub step and their interaction are outlined. Afterwards each step is elucidated in more detail. The background and technical setting for data acquisition in the motion lab concerning EMG data and motion capturing methods are expounded, as well as the used algorithms for muscle synergy extraction and the methods for validation of the calculated muscle synergies. Further on, the construction of the DHM used for simulation in this thesis work with the implemented muscles and their biomechanical functionality is described, followed by an outline of the used optimal control framework for motion generation.

In the following two chapters, the developed DHM control approach is applied to some concrete use cases. In the *basic reaching test*, which is described in Chapter 4, test persons are standing in front of a plane and are told to reach several target points on the plane as fast as possible, whereas the target points and the distances to the plane are adapted to the test person's anthropometry. The chosen trajectories, velocity profiles and EMG signals are analyzed and muscle synergies are extracted from EMG data. The reaching tasks are then simulated under similar specifications as performed in the motion lab with a human arm model, the motion data are analyzed and compared to the measured data, and the influence of the different Actuation Modes AM (joint torques, single muscles and muscle synergies) is investigated with the main focus on trajectories and velocity profiles.

The weight lift test (Chapter 5) is then performed to investigate the muscle activation patterns with special focus on the muscle redundancy problem. In this scenario, test persons lift a dumbbell with different weights by flexing their elbow (single biceps curl). Due to the restricted motion only one rotational DOF is set free in the elbow joint. Besides motion data was captured and compared, the main focus is on the EMG data and simulated muscle activation patterns at this test, simulated again with the same arm model as used in chapter 4. Again the influence of the different Actuation Modes AM is investigated now with the focus on the resulting muscle activation signals. Additionally, the influence of the solve OC cost function is examined.

In Chapter 6, the parameters for control derived in the previous chapters are applied to a simple, yet industry relevant use case. A box lifting scenario, which is also performed in the motion lab before, is simulated with a full body model with both arms actuated by Hill type muscles [Hill 38]. Simulated and observed motion data are compared (on a less detailed level than in the previous chapters), and capabilities and limitations of the developed approach for DHM simulation in the scope of ergonomic assessment are discussed. In Chapter 7, the thesis results are concluded and potentials for future work are discussed.

## 2 Motion generation in humans and vertebrates

From an evolutionary point of view, motion generation in vertebrates is an essential behavior, allowing such fundamental things like foraging or escaping from predators. Also we fulfill many daily tasks with naturalness, the human locomotor system turns out to be a highly sophisticated system when having a closer look, allowing e.g. well trained sports climbers to do pull ups on only one finger, and on the other hand watchmakers or musicians fulfill very fine tuned precision tasks using the same “tools” (hands / fingers). The adaptability and capability to learn is a crucial skill for survival, but it also allows e.g. workers in our today’s life to adapt on (repetitive) tasks quickly, which can then be performed with a fractional amount of energy after some training. This can be very well observed e.g. on new workers on an assembly line, which in the beginning need support by a stand-by person to not exceed cycle times and after some training period fulfill the same task with ease. In humans and vertebrates, motions are generated by the musculoskeletal system. The bones of the skeleton are connected via joints (connective tissue like tendons, cartilage, ligaments), and *antagonist muscles* create pulling forces at the bones they are connected to which result in a joint torque. The activation of the muscles is controlled by the central nervous system (CNS).

As the scope of this work is to simulate human motions in a predictive manner using a biomechanical human model, a rough overview of the anatomical basis of the relevant parts of the body as well as terms of movements and underlying control structures is given in this Chapter. Thereby the focus is on pointing out the challenges of transferring the anatomical and biomechanical properties of human joints, muscles or muscle control to a musculoskeletal DHM using classical multibody system formulations for modelling and optimal control for motion generation. This is important in order to understand and interpret simulation results, especially when they are compared with measured motions and muscle actuations for validation as done in the Chapters 4, 5 and 6. To get a deeper insight into human anatomy, [Schünke 18] and [Vaupel 15] can be highly recommended as well as [Kapandji 16] for the properties of human biomechanics. Also a good overview from a more engineering point of view, especially interesting for DHM creation and understanding is given in [Herman 16] and [Hamill 14].

### 2.1 Anatomy

#### 2.1.1 Anatomical terms of movement and body planes

In the following, a short overview of anatomical terminology used to clearly describe positions, orientations and motions is given. Many redundant terms are used in literature, which can be confusing when reading publications of different authors, especially for readers from non-medical disciplines. Further on, motions can be defined by a DOF of a joint, or by the way a limb moves relative to a body plane or axis. So, e.g. the *flexion* of the shoulder joint can also be described as *anteversion* of the upper arm (moving towards the sternum (*Ventral*)). In Figure 2, the human body planes are depicted and a good overview of directional terms with the existing terminologies is given.

The *Frontal Plane* is a vertical plane running from side to side that divides the body into *anterior* (front) and *posterior* (back) portions. The *Sagittal Plane* is a vertical plane running from front to back dividing the body into right (*Dextral*) and left (*Sinistral*), and the *Transversal Plane* is a horizontal plane dividing the body into upper and lower parts.



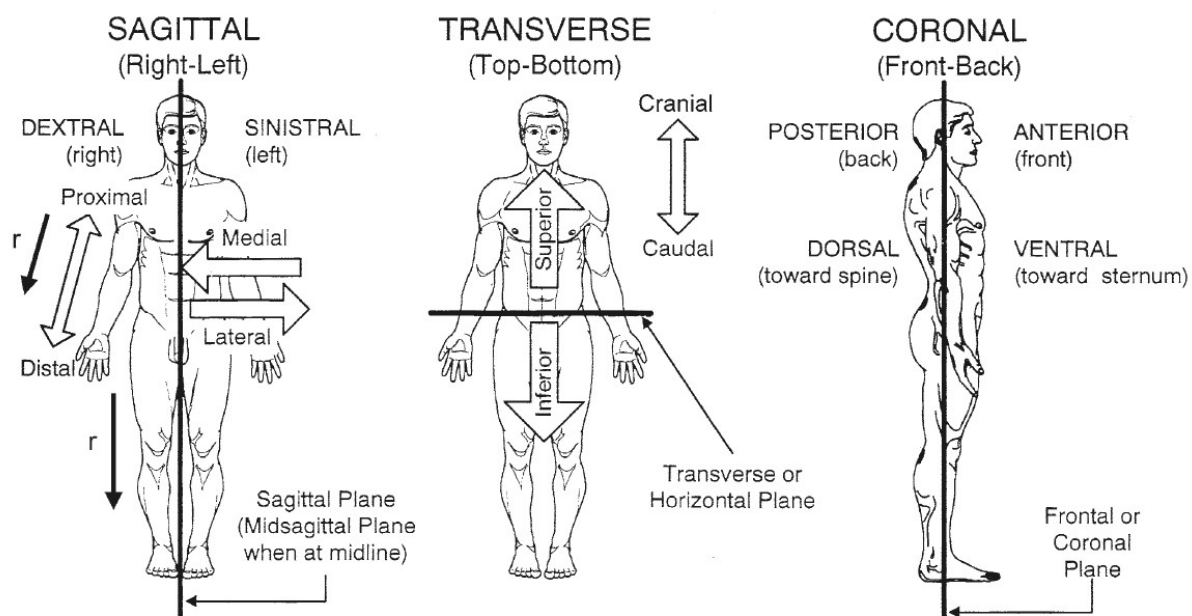


Figure 2: Human body planes and directions. From [Herman 16].

Additional to these terms of directions, several terms of motions are defined for distinct parts of the human body. Those relevant in this work concern the extremities and are as follows:

- **Flexion – extension:** Bending / straightening a joint, especially a joint between the bones of a limb so that the angle between them is decreased / increased.
- **Anteversion – retroversion:** Moving a limb towards *Ventral* (sternum) / *Dorsal* (spine).
- **Abduction – adduction:** Move a limb away / towards the vertical *Middle Axis* of the body / the extremities.
- **Internal - external rotation:** Inwards / outwards rotation of shoulder or hip joint.
- **Pronation – supination:** Inwards / outwards rotation at forearm or foot.
- **Radial abduction – ulnar abduction:** Moving the hand towards *Ulnar* / *Radius*.

Note that the degrees of freedom of the *shoulder girdle* are not listed here. The shoulder joint is a quite complex joint and actually consists of a group of four joints (see Chapter 2.1.2). As the shoulder joint used in the simulation model in this work is simplified as ball and socket joint, only the degrees of freedom possible with this joint are considered here (and also in the motion lab test setups later on). As the main focus in the simulated and measured tests in this work focus on arm motions, the used terms for the possible degrees of freedom for the shoulder, elbow and wrist are defined in detail in the following.

Moving the arm away from the *Midsagittal Plane* is called shoulder *abduction*, moving it towards the *Midsagittal Plane* is called shoulder *adduction* (see Figure 3 left). When moving the arm parallel to the *Sagittal Plane* to the front (towards *Ventral*), a shoulder *flexion* is performed, an in opposite direction a shoulder *extension* (see Figure 3 middle). Moving the flexed arm in parallel to the *Horizontal Plane* to the left is called *horizontal*

*adduction*, and in opposite direction *horizontal abduction* (see Figure 3 right top). Rotating the arm in the shoulder joint outwards is called *external rotation*, rotating it inwards is called *internal rotation* (see Figure 3 right bottom).

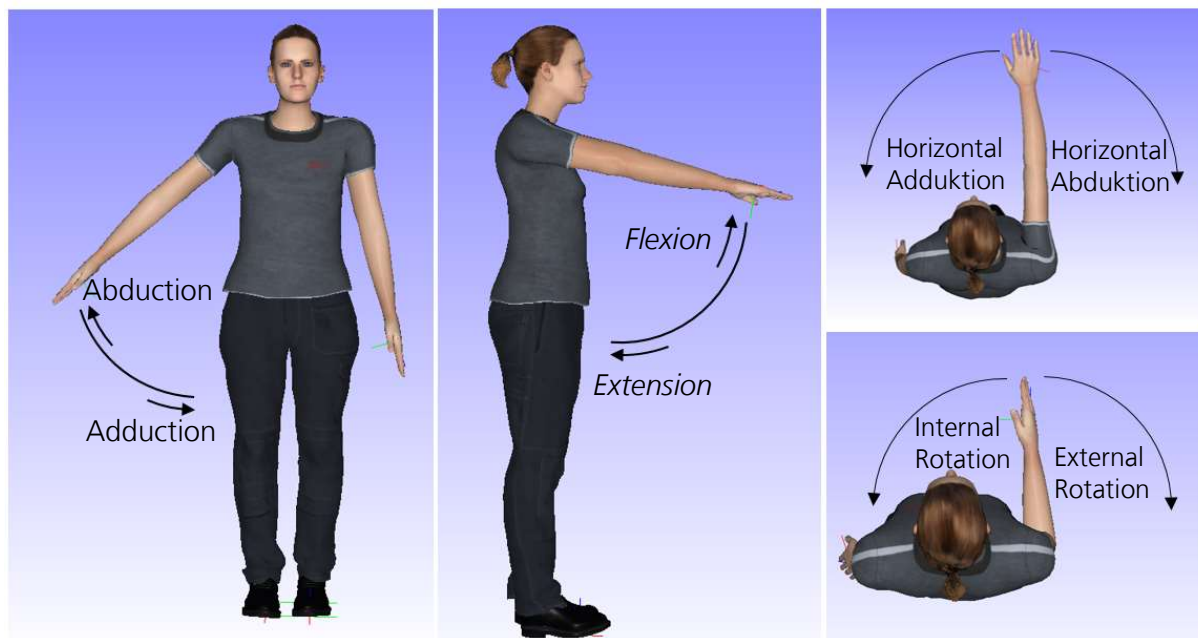


Figure 3: Anatomical terms of motion for the shoulder joint used in this work.

A *flexion* and *extension* of the wrist is performed as depicted in Figure 4 left. An outwards rotation of the forearm (rotated in the elbow joint) is called *supination*, and an inwards rotation is called *pronation*. Bending the wrist towards the *Radius* is called a *radial deviation*, and in the direction of the *Ulnar* an *ulnar deviation* (Figure 4 middle).

Bending the elbow joint so that the angle between forearm and upper arm decreases is called an *Elbow flexion*, straightening this joint is called an *Elbow extension* (Figure 4 right).

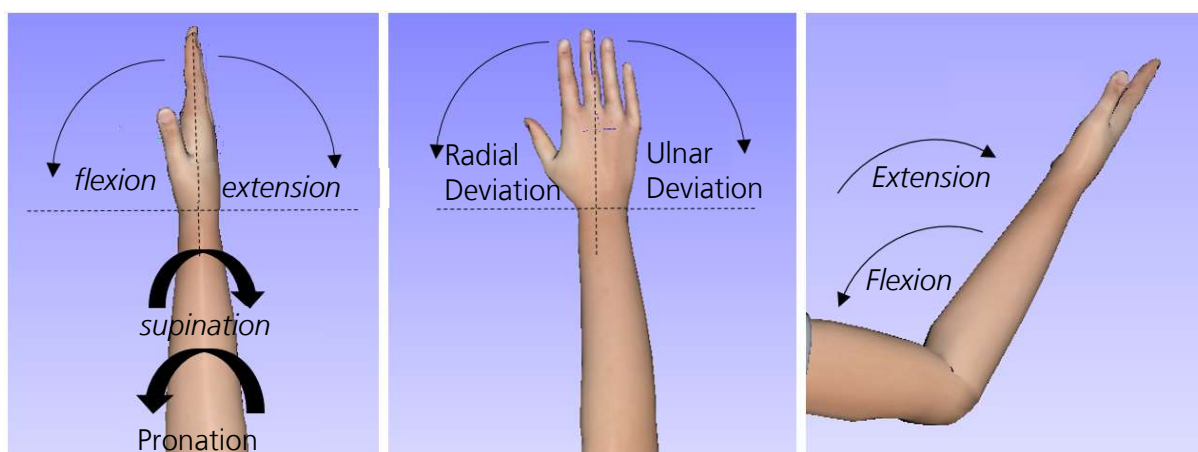


Figure 4: Anatomical terms of motion for the wrist and elbow joint used in this work

### 2.1.2 Bones, joints and muscles

The human skeleton is the internal framework of the human body which consist of about 206 **bones** [Marshall 10]. Bones exist in a variety of shapes and sizes, have complex

internal and external structures and are very lightweight while being strong and hard. Beside other functions they fulfill the task of supporting and maintain the body shape and movement. Motions are allowed by the joints between the bones and powered by muscles attached to the bones. In Figure 5, the bones of the human arm and the joints they are connected by are depicted, which will be described in more detail in the following.

The **joint** of the shoulder and shoulder girdle (*Clavicle* and *Scapula*) is one of the most complex human joints and has the greatest range of motion in the human body. It actually consists of four distinct joints working together. The *Glenohumeral joint* is formed between the ball of the *Humerus* and a shallow socket of the *Scapula*. The *Acromioclavicular joint* is formed between *Clavicular* and the *Acromia*, a process of *Scapula*. The *Sternoclavicular joint* is formed between the *Clavicular* and the main skeleton at front of the chest. The fourth joint is the *Scapulothoracic joint*, which is formed of shoulder blade (*Scapula*) which glides along the rib cage.

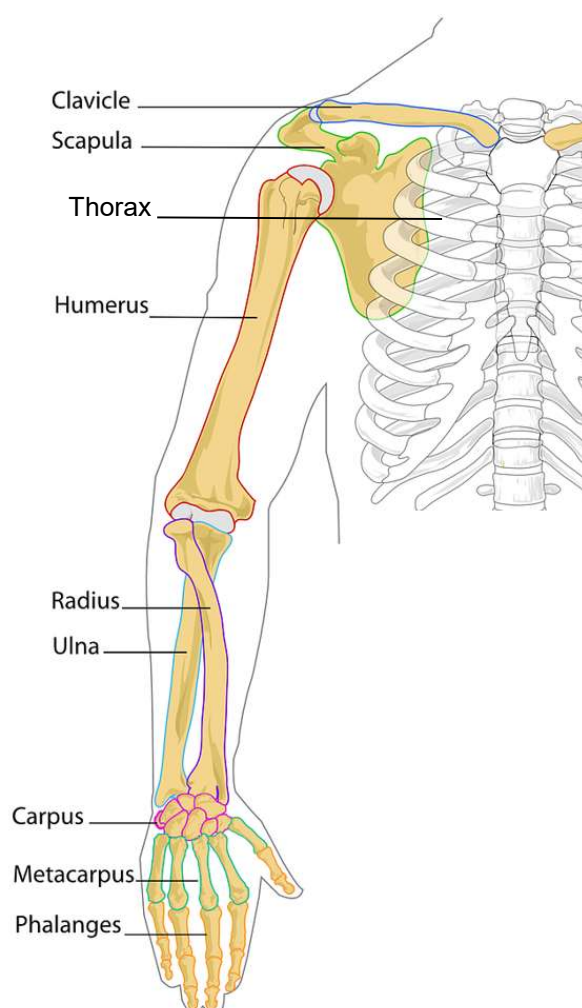


**Figure 5: Bones of the human arm.**

The *Glenohumeral joint* is denoted as the actual shoulder joint and is formed as a ball-and-socket joint. The joints of the shoulder girdle (*Clavicle* and *Scapula*) mainly have the function of lifting / lowering (*elevation / depression*), moving forward / backward (*protraction / retraction*) and rotating the shoulder girdle to extend the range of motion.

In the simulation model used in this work, only the *Glenohumeral joint* is modelled (as ball-and-socket joint) to represent the shoulder joint. This simplification can be regarded as “correct”, as long as simulated motions do not exceed the range of motion of the human *Glenohumeral joint*. This is regarded in the simulated and measured tests (motion lab), so e.g. the center of the shoulder is always kept in position and the arm is not abducted above shoulder height.

The elbow joint is a *Synovial Hinge joint* between upper arm and forearm. As the forearm consists of two bones, the *Radius* and the *Ulnar*, the elbow joint is a complex compound joint as well (formed by several “sub joints”). The *Humeroradial joint* is formed between *Humerus* and *Radius*, the *Humeroulnar joint* between *Humerus* and *Ulnar*, and a third joint (or articulation) is formed between the contact areas of the head of the *Radius* and *Ulnar*. Simplified the *Humeroulnar joint* can be regarded as the hinge joint allowing the *flexion / extension* of the elbow. Further on, the *Radius* can rotate around the *Ulnar* (which keeps in position), which causes a *pronation / supination*. In a *supinated* orientation, *Radius* and *Ulnar* are parallel. When the forearm is *pronated*, the *Radius* rotates around its longitudinal axis, and the motion is limited by the contact of *Radius* and *Ulnar* as depicted in Figure 5. This means that every muscle being attached to the *Radius* has the potential to perform beside an elbow *flexion* also a *supination / pronation* of the forearm, whereas muscles attached to the *Ulnar* only contribute to a pure *elbow flexion*. This has to be carefully considered when building up a musculoskeletal digital human model. The wrist joint is a *Radiocarpal Synovial joint*. It involves the three *proximal* carpal bones of the *Carpus* and the distal end of the *Radius*, whereas the *Ulna* is “covered” by an articular disc. It allows for the in Figure 4 depicted degrees of freedom, whereas the shape of the bones limits the range of motion (e.g. the *Styloid process* of the *Radius* extends further than the *Ulnar Styloid*, which means that an abduction is more limited than an *adduction*), which has to be considered when modelling this joint as well.

**Muscles** exert forces on the bones they are connected to via tendons and thus are the major contributors to human movement. In most cases, one attachment point of a muscle is fixed in position (muscle *origin*), while the other attachment point moves during contraction (muscle *insertion*). The *insertion* is usually *distal* (further away) while the origin is *proximal* (closer to the body, relative to the insertion) [Kapandji 16]. When a muscle is activated by the nerve system (see Chapter 2.1.3), it contracts, which means that the muscle generates tension (and shortens). This means that muscles can only create pulling forces, and motions are created due to the fact that the muscle crosses a joint [Hamill 14]. Concerning motions, muscles have three major functions. First of course to create movement, which means that the pulling forces created by muscles acting on a bone lead to a motion. The second function is to maintain postures and positions, which is mostly performed by muscle activations of a lesser magnitude and continuous muscle activation. The third important function is to stabilize joints. The muscle tensions applied across the joint via tendons provide stability. Indeed, the muscles spanning the joints are among the primary stabilizers in many joints as e.g. the shoulder joint [Hamill 14].

When simulating motions with a biomechanical musculoskeletal DHM, this is a challenging issue, as a joint formulated in a classical multibody system model can “absorb” forces in all directions it has no defined DOF’s. This means that, using e.g. optimization methods to simulate a motion and fulfill a given task that involves flexing

the elbow joint, from an optimal point of view it does not make any sense to activate also muscles which pull in other directions at the elbow joint.

Another phenomenon which implicates similar challenges concerning DHM control is the muscle *co-contraction* (or *co-activation*). As muscles can only create pulling forces, at each joint the *antagonistic* principle can be found. When doing a biceps curl (weight lift, *flexing* the elbow joint), the elbow flexor muscles are seen as the *agonists* muscles, as they cause a movement to occur through their own activation [Willert 01]. This is not only the case in the lifting phase, but also when the weight is lowered slowly (the *agonist* muscles lengthen while resisting gravity). The *antagonist* muscles are simply the muscles that produce an opposing joint torque to the *agonist* muscles, which would in this case e.g. be the triceps muscle. Which muscle(s) is called *agonist* and which plays the role of the antagonist depends on the performed movement, so when doing "push ups", the role of the elbow muscles would change so that the triceps would now be seen as *agonist* and the elbow flexors as *antagonist* muscles.

*Synergist* muscles are muscles which produce a similar joint torque as the *agonists*, so they support the *agonist* muscles. They are named as "*synergists*" as they have similar functions, and especially in the scope of this work not to be confused with *synergetic* muscles which are activated in a fixed balance (independent of their function) as they are grouped in one muscle synergy as introduced in Chapter 2.2. Still *agonist* and *antagonist* muscles produce opposite joint torques, the CNS often co-activates both at the same time, which is still a not well understood phenomenon. For the muscles of the leg it has already been observed at the beginning of the last century and is well known as the *Lombard's paradox* [Lombard 07], and has later on been explained as an efficient strategy of movement, especially during gait [Andrews 87]. Further explanations for muscle co-contraction are that the resulting joint stiffness allows for a better stability and control when the joint has to react on unexpected loads [Le 17, Riemann 02]. Other investigations show that muscle co-contraction is necessary for learning a fine motor skill [Lundy-Ekman 13] and that it accelerates the rate of dynamic motor learning in reaching tasks [Heald 18]. In [Heald 18] it is also shown, that a muscle co-contraction decreases as an accurate internal model develops after a learning phase. Besides controlling the muscle activation of a musculoskeletal DHM, an appropriate modelling or representation of the anatomical human muscles with all their biomechanical properties is already a quite complex and challenging tasks.

The human body has over 600 muscles [Herman 16], with over 20 muscles responsible to control movements of the arm. The challenges of modelling human muscles in a DHM will be explained at the example of the delta muscle and the biceps muscle: The delta muscle is a large triangular-shaped muscle that spans around the shoulder (named by the greek letter  $\Delta$ ). It has several origins (*proximal attachment* points) at the *Clavicle* and the *Scapula* and its *insertion* (*distal attachments*) is at the *Humerus*. The delta muscle is classically divided into three parts, based on the findings that the insertion of the intramuscular tendons of the deltoid muscle form three discrete sets of muscle fibers (often referred as "heads") [Schünke 18]. The *anterior* part (or *clavicular* part/ front delt) have their origin at the *anterior* border and upper surface of the lateral third of the *Clavicle* (see Figure 6 red). The *lateral* part (or *acromial* part / middle delt) has its origin at the superior surface of the *acromion process* of the *Scapula* (see Figure 6 green). The *posterior* part (or *spinal* / rear delt) has its origin at the *posterior* border of the spine at the *Scapula*

(see Figure 6 *blue*) [Schünke 18]. Due to their distinct muscle paths and attachment points, each part of the delta muscle creates a different torque in the shoulder when being activated.

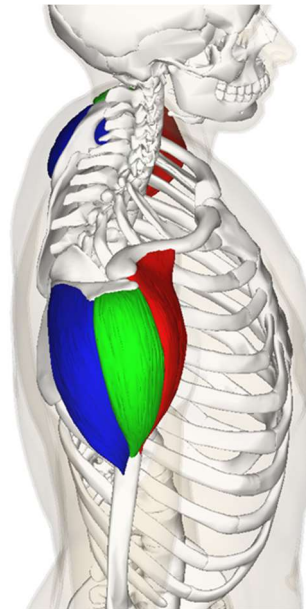


**Figure 6:** *The three parts of the delta muscle: Clavicular part (red), acromial part (green) and spinal part (blue). Source: Bodyparts3D, Japan (CC BY-SA 2.1jp).*

To model such a broad muscle as e.g. the delta muscle in a musculoskeletal DHM using simplified Hill muscle models [Hill 38] as done in this work, some challenges have to be focused. Hill muscle models are simplified 1D string muscles, which capture the basic characteristics of muscles as force-length and force-velocity dependency (see Chapter 3.5.3). As they do not have any 3D- volume, the challenge is now to find an appropriate number of Hill muscles which represent the function of the delta muscle and further on to define proper origins and insertion points as well as eventually via points to define the muscle path (as Hill muscles are 1D elements they always form a straight line between their attachments and can be led over via points to reproduce human muscle paths). From a biomechanical point of view, at least each head of the delta muscle should be modelled as distinct Hill muscle, to be able to create a similar range of joint torques. However, latest research results have shown that the CNS can not only coordinate the three heads of the delta muscle independently, but seven parts of the delta muscle [Brown 07]. The used modelling approach has to be carefully considered when interpreting or comparing simulated and measured muscle activation signals.

For the controller of the musculoskeletal DHM, each Hill muscle used to model a distinct muscle head is an independent actuator of the MBS. In the case of the delta muscle it was shown that this is also the case at human motion generation [Brown 07], but at other muscles this is still not clear in how far the CNS can activate distinct muscle heads independently. The biceps muscle e.g. is one of the dominant elbow flexors and has two distinct muscle heads, the long and the short head, which have their origins at distinct points at the *Scapula* and then join to form a single muscle belly, whereas several anatomic studies have demonstrated that the muscle bellies remain distinct structures without confluent fibers [Eames 07, Platzer 14]. The insertion point is at the *Radius* and the

antebrachial fascia (a dense, membranous investment, which forms a general sheath for the muscles at the forearm) as depicted in Figure 7. So, the biceps is a *biarticular* muscle that spans of the shoulder joint and the elbow joint. The different attachment points of each head influence the resulting joint torque when the muscle (head) is activated. Also it was shown that the distinct heads can be activated by the CNS in different ratio [Pérot 96], it is not clear if they can be activated completely independent. This means, when the heads of the biceps muscles are modelled as distinct Hill muscles in the musculoskeletal DHM model, the question of how they should be controlled has to be answered as well. A defined co-activation of each head could e.g. be achieved by using the in this work derived approach of *synergetic* muscle activation.

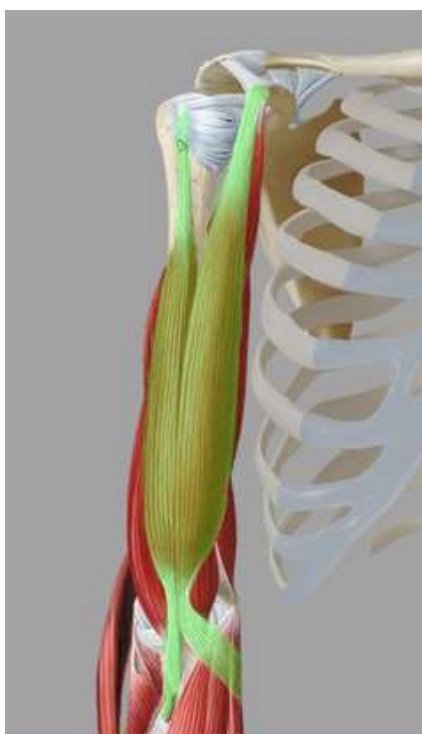


*Figure 7: Muscle path of the biceps muscle – short and long head. Source: University of Zurich, Institute of Anatomy.*

So, beside the challenging task of finding an appropriate modelling approach which reflects the biomechanical properties of human muscular force generation by the use of Hill muscle models in an adequate manner, the question of finding a “human like” controller is at least equally challenging. The neuronal control structures of the CNS concerning human muscle activation are treated in the following.

### **2.1.3 Voluntary motor function**

The human movement is controlled by our nervous system, which can be divided in the central nerve system (CNS) and the peripheral nerve system. The CNS consists of the brain and the spinal cord and can be regarded as the part being responsible to initiate and control movement. The peripheral nerve system consists of all other nerves outside the spinal cord, whereas for muscle activations the spinal nerves are of importance. They can be grouped into the sensory neurons, which enter the spinal cord and transmit information into the system (from the muscles), and the *lower moto neurons*, which exit the spinal cord and carry impulses away from the system to the muscles [Hamill 14]. The

motor cortex which is located in the frontal lobe of the brain is responsible for our voluntary motor functions. These nerve cells (also referred as upper motor neurons), then activate the *lower motor neurons* over long pathways through the medulla of the spinal cord. The *lower motor neurons* then activate the muscles they have connections to. An important fact of this control structure is that there are no direct connections from the brain to the muscle. All information are transmitted over the *lower motor neurons* in the spinal cord as depicted in Figure 8. This allows for some hypothesis concerning the control mechanisms as e.g. the muscle synergy hypothesis as we will see in the next Chapter.

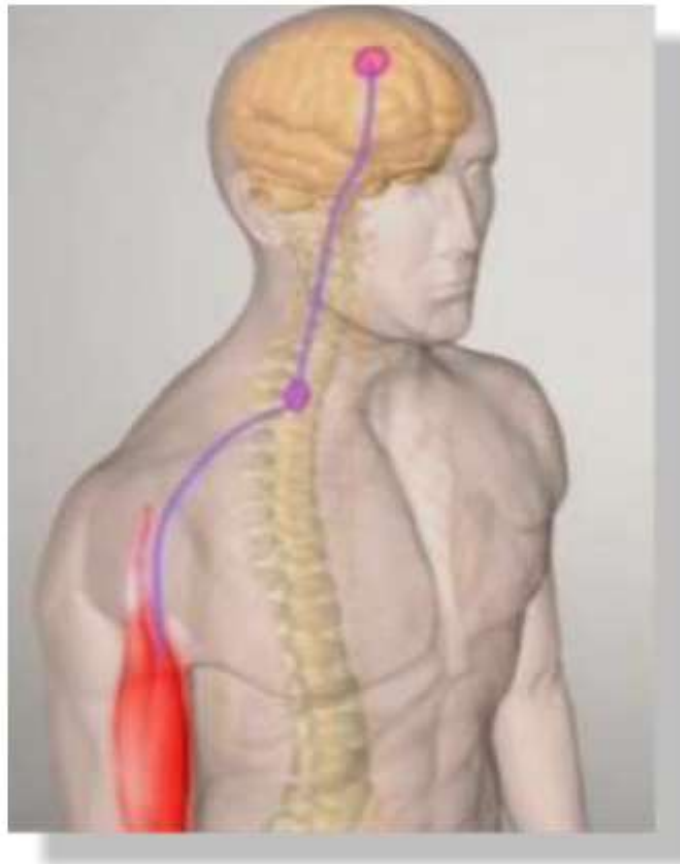


**Figure 8: Control architecture for voluntary motor function. Nerve signals from the motor cortex of the brain are transmitted to the lower motor neurons in the spinal cord which then activate the muscles. Source: Unteregger, Swiss.**

A *lower motor neuron* has connections (axons) to several muscle fibers, which are individual contractile units within a muscle as depicted in Figure 9. The smallest functional unit for neuronal muscle control is a so called *motor unit* (MU). A *motor unit* is defined as a *lower motor neuron* with its axon and all muscle fibers it has connections to [Enoka 89]. *Motor units* can consist of only a few muscle fibers, e.g. at the very precise optical muscle of the eyes, or may have up to 2000 muscle fibers, e.g. at a calf muscle [Hamill 14].

If a *motor unit* is firing, it sends an electrical pulse, a so called *action potential*. This *motor unit action potential* (MUAP) is forwarded along the nerve pathway of the MU to all muscle fibers it has connections to. Thereby, the MUAP spreads over the axons to branches at the muscle fibers, the *motor endplates*, which are located near the center of each muscle fiber. The area of these *motor endplates* is called neuromuscular junction. The *motor neuron* does not have direct contact to the muscle fibers here. Instead, there



is a small gap in between, the synaptic gap (or synapse), so that the electrical signals are chemically transmitted over the gap to reach the muscle fibers.

Skeletal muscle tissue is one of the most sensitive and responsive tissues in the body, meaning that it is highly excitable and can react very quickly on the chemical neurotransmitter released at the synaptic gap, which allows for significant control of muscle fiber recruitment for movement.

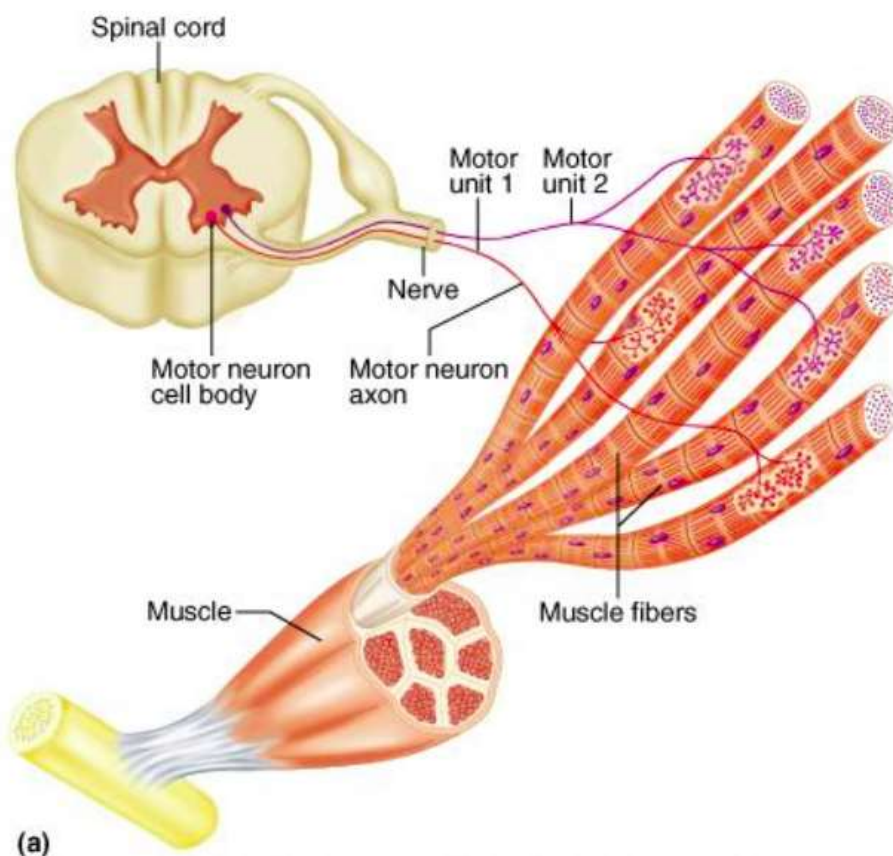


**Figure 9: Illustration of a motor unit, the smallest functional unit to control muscle contraction, consisting of a lower motor neuron, its axon and all muscle fibers it innervates. Source: Addison Wesley Longman Inc., Cummings 2001.**

The irritability of the muscle cells can be explained by the model of the semi-permeable membrane of the muscle fiber membrane. An ion imbalance inside and outside the muscle cell forms a resting potential on the muscle fiber membrane (about  $-80\text{mV}$  to  $-90\text{mV}$  in non-contracted muscle), which leads to a negative charge inside the cell.

When an *MUAP* reaches the neuromuscular junction, acetylcholine is released which causes an increase in permeability of the muscle membrane. This leads sodium ions to stream inside the cell, which leads to a depolarization of the muscle fiber membrane. If a certain threshold is reached, this depolarization leads to an action potential from about  $-70\text{mV}$  to about  $+40\text{mV}$ . This depolarization is directly followed by a repolarization as depicted in Figure 10. Starting at the motor endplates, this action potential spreads bidirectionally along the muscle fibers and leads to a release of calcium ions which promote cross-bridge formation, which results in an interaction between the *actin* and

*myosin* filaments. So, the calcium ions link *action potentials* in a muscle fiber to contraction by binding to the filaments and turning on the interaction of the *actin* and *myosin* to start contraction of the *sarcomere* [Hamill 14].

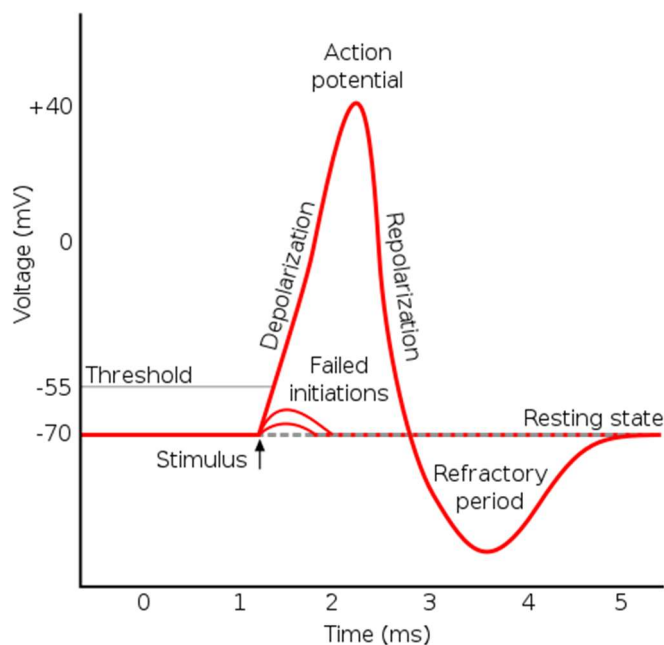


**Figure 10: Action potential of a muscle cell.** Source: Creative Commons by Chris 73 (CC BY-SA 3.0).

Muscle fibers contain numerous *myofibrils*, which are composed of repeating sections of *sarcomeres*, the basic units of (striated) muscle tissue. They are composed of long, fibrous proteins as filaments that slide past each other when a muscle contracts (or relaxes). The two most important filament proteins are *actin* and *myosin*. *Myosin* forms the thick filament and *actin* the thin filament as schematically depicted in Figure 11.

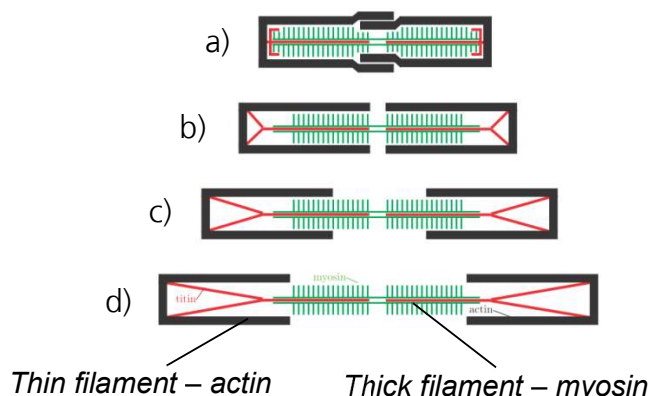


**Figure 11: Schematic depiction of the muscle filament proteins leading to a force-length dependency.** From [Maas 14].

By the formed cross bridges, the *actin* filaments glide along the *myosin* filaments. This happens at many thousands *sarcomeres* in series, which leads the muscle to contract and

results in a muscle force. The amount of force a muscle can create is directly proportional to the number of cross bridges that can be built. If a muscle is continuously lengthened, the possible cross bridges become less (Figure 11-c) until it reaches a point where no cross bridges can be built up any more as there is no more overlap between actin and myosin filaments (Figure 11-d). If a muscle is continuously shortened, at some point the actin filaments start to slide past each other (actin double overlap), which also prevents cross bridges to be built up and possible muscle force decreases (Figure 11-a). If the muscle has its "optimum" length, the overlap of myosin and actin filaments is at its maximum and the muscle can produce its maximum force (Figure 11-b).

## 2.2 Muscle synergies as control concept in neuroscience

As described above, the human body has over 600 muscles, each with a multitude of muscle fibers and innervated by numerous motor units. This means that even for a simple reaching tasks the CNS has to activate many thousands of motor units in numerous muscles [Bizzi 08], with a high redundancy on several layers of control. This complexity was already described by the neurophysiologist Nicolas Bernstein in the late sixties, who formulated the DOF Problem [Bernstein 67].

- **Kinematical:** We can perform each motor task by a multitude of different trajectories, velocities and accelerations. So for e.g. grabbing an object, we have to decide between a multitude of possible trajectories in the room as well as where and how we grab the object.
- **Anatomical:** Even a well-defined kinematical solution (e.g. a 1 DOF elbow *flexion*) can be performed by a multitude of different muscle actuations, as the human body consists of much more actuators (muscles) than kinematical DOF's (joints).
- **Neurophysiological:** Even when it is clear which muscle will be activated, the CNS has to choose between a multitudes of motor units which innervate this muscle.

Which strategies the CNS might follow to reduce this complexity is a long standing question in neuroscience and also other fields. One hypothesis is, that the CNS makes use of predefined groupings of muscles, which can be activated as functional units, so called *muscle synergies* [Bizzi 08], with each muscle being present in such a synergy with a fixed amplitude that does not change over time. This pre-grouping of muscles could facilitate motor complexity as it reduces the number of control parameters to be defined.

Some investigations which give evidence for the existence of muscle synergies as underlying control architecture in vertebrates are shortly introduced in the following.

### 2.2.1 Evidence for muscle synergies

To investigate the underlying strategies of the CNS to produce a specific motor output or reduce complexity of motor control, several approaches have been followed in the past until today. One of the earliest approaches which initiated the idea of a modular control architecture of the spinal cord were the stimulation approaches. In these approaches, different regions of the spinal cord of vertebrates were excited electrically (microstimulation) or chemically (NMDA iontophoresis) and the resulting motor outputs were investigated.

In tests with spinalized frogs for example [Bizzi 91], the hind limb was fixed in different positions of the legs workspace (Figure 12-a), and the resulting force output at the ankle was measured when stimulating a specific area of the spinal cord. For each position of the ankle, a specific force was measured, leading to a force field for this area of the spinal cord. This was performed for several areas of the spinal cord.

The majority of the resulting force fields converged to an equilibrium point where no force was created (Figure 12-b) and could further on be grouped into a few classes [Bizzi 08]. Several control experiments indicated that distinct interneuronal networks of the spinal cord must be the source of specific types of convergent force fields (CFF), and that the resulting CFF when different sites are stimulated simultaneously follow the law of vector summation [Bizzi 91, Mussa-Ivaldi 94, Lemay 01]. This indicates that the complex nonlinearities among neurons and between neurons and muscles are eliminated in some way and led to the hypothesis of movement creation based on combination of a few modules [Bizzi 08], which was later on verified to be suitable to create a wide repertoire of movements [Mussa-Ivaldi 92, Mussa-Ivaldi 97].

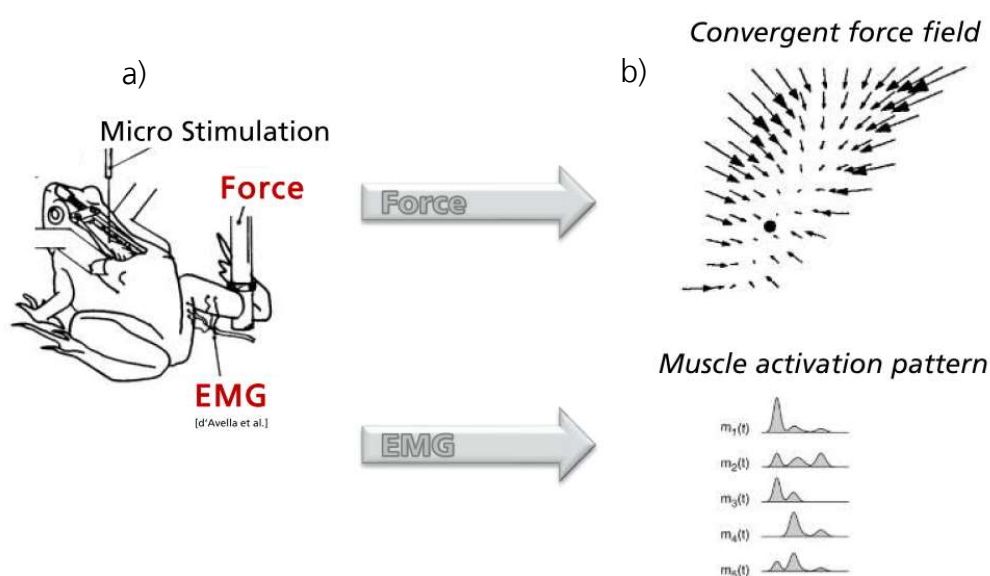


**Figure 12: Microstimulation of spinalized frogs leading to convergent force fields. Modified from [Giszter 93].**

Further investigations using stimulation methods with rats [Tresch 99, Haiss 05], cats [Krouchev 06, Haiss 05, Ting 05, Lemay 04], prosimians [Stepniewska 05] and macaques [Overduin 08 Overduin 14] generated corroborative evidence and supported the hypothesis of a modular organization of movement.

Other approaches are based on behavioral studies of intact or deafferented animals (elimination of afferent nerve impulses) or of humans. In these approaches, the muscle activations are measured via electromyography (EMG) while a natural or specific task is performed. From the measured EMG data, muscle synergies are extracted using computational methods. The measured EMG signals should then be reproducible by linear combinations of the extracted synergies. In studies with cats it was shown, that 95% of the measured hind limb muscle activations could be reproduced by the use of four muscle

synergies [Ting 05]. In similar investigations it could later on be shown that five synergies account for 80% of the total variability in the data [Torres-Oviedo 06]. Measured EMG data of monkeys while performing grasping tasks could be reproduced with only three muscle synergies accounting for 80% of variability.

Also in tests with humans four synergies were able to reproduce measured data with a *variance account for* (VAF) of over 90% [Israely 18], and also other studies on humans showed that a few synergies were able to reproduce measured data of different reaching motions [Obentheuer 17, d'Avella 06] or natural behavior [Cheung 05, Weiss 04] with a high accuracy.

## 2.2.2 Types of muscle synergies

There exist two major representations of muscle synergies, *time variant* and *time invariant* muscle synergies (although d'Avella et al. introduced with *time varying synergies* more complex descriptions of muscle synergies [d'Avella 06]). Time variant muscle synergies describe a neuronal muscle activation waveform which is shared across muscles. These temporal components capture temporal regularities in the motor output (therefore a.k.a. *temporal components*) and are commonly used for approaches where rhythmic motions are investigated like e.g. human gait or locomotion of vertebrates. Time invariant muscle synergies are patterns of co-activations of muscles recruited by a single neuronal activation signal. This pattern of muscle activation does not change over time (therefore "time invariant synergies"). By that, time invariant muscle synergies capture spatial regularities in the motor output. The latter are investigated in this work, as they seem convenient to handle e.g. the problem of muscle redundancy and muscle co-contraction and the focus in this work is on arbitrary (arm) motions at which are not rhythmic.

For a better understanding, a mathematical representation of time invariant muscle synergies is schematically depicted in Figure 13. On the left side (A), three muscle synergies are depicted (columns), colored in red, green and blue. In each synergy, each muscle ( $m_1$  -  $m_5$ , rows) is present with a certain amplitude. This amplitude is fix and does not change over time. Muscles can now be controlled by activating one or several of the time invariant synergies with a certain level and sum up the outputs for each muscle from each synergy. In this representation this is done by multiplying each synergy  $w$  with a certain weight  $c$  so that  $m = \sum_{i=1}^N c_i w_i$  ( $N$  equals the number of synergies).

Having a look on Figure 13 – B, in the first column we have only synergy  $w_1$  active as there is only the weight  $c_1$  greater than zero (red – bottom). The resulting output of muscle activations (row 1-5, 1<sup>st</sup> column) is by that a scaling of the first synergy. The same case we have in column two and three, now with a higher weight  $c_1$  and by that higher outputs for muscle activities, but still a scaling of the amplitude pattern of synergy  $w_1$ .

In column four we now have synergy  $w_1$  and  $w_2$  active (red and green weight  $c_1$  and  $c_2$ ), so that the resulting output for each muscle is the summed up output from these two synergies. Same is shown in column five for synergies  $w_1$  and  $w_3$ , and in the last case (column 6) all three synergies are active.

The basic idea is now that the CNS only has to control three muscle synergies instead of five distinct muscles, which reduces complexity and could simplify motor control. When thinking of controlling a musculoskeletal biomechanical DHM, this control strategy appears to be quite attractive for several reasons.

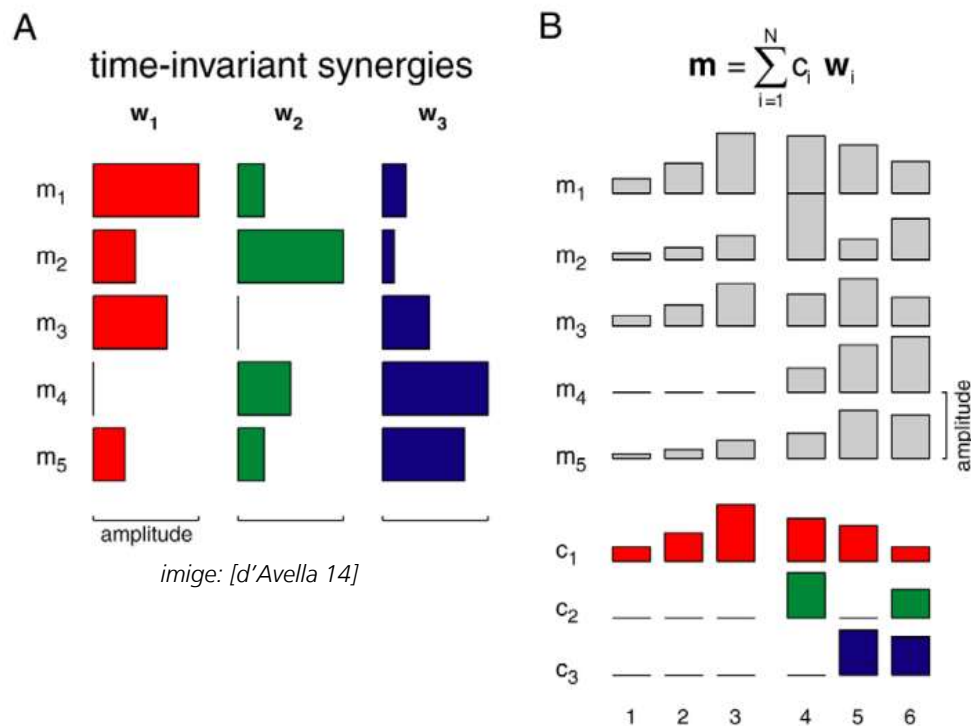


**Figure 13: Mathematical representation of time invariant muscle synergies. Modified from [d'Avella 14].**

One point of course is, that, if a synergetic muscle control is an underlying control strategy of the CNS in humans, a control approach being close to nature is quite promising if the aim is to find the same solutions with a DHM for a given tasks as humans do (trajectories and muscle actuations). But even if muscle synergies are not a "hard coded" control architecture of the CNS, they could be very useful for DHM control. As shown in the example above, the complexity is reduced by reducing the number of control parameters. In musculoskeletal DHMs, the number of actuators increased dramatically (compared to a joint torque actuation), especially when every human muscle head is modelled as distinct Hill muscle (see Chapter 2.1.2 and 3.5.3). At this point, muscle synergies could be very helpful to reduce the number of control parameters, and also to e.g. map the activation correlations of distinct muscle heads. Further on, a synergetic actuation could help to solve the muscle redundancy problem. As described above, joint stiffness in humans as well as joint stability is achieved and regulated by muscle co-contraction and muscle co-activation. Beside other functions a certain joint stiffness can help to better react on unexpected external loads or disturbances. This is a circumstance which does not occur in open loop optimal control systems, as here the whole "scenario" from the given start configuration to the desired end configuration is well known. This is one reason why optimal control strategies lack to predict a muscle co-contraction [Cholewicki 95].

A joint stability in a biomechanical DHM using MBS approach to model the human skeleton and joints is given by the definition of the MBS joint description. So, there is also no need for a controller to generate an according muscle actuation as done in humans.

In both cases, for muscle co-contraction and muscle co-activation patterns, muscle synergies could be a useful approach to generate an human like muscle activation,

especially if these muscle synergies are captured from humans as in the above described behavioral approaches used by neuroscientists. When muscle synergies are extracted from measured EMG signals of humans, they in some way capture the activation patterns generated by the human CNS. From this point of view, they might also be an advantageous control strategy for a DHM, even if they do not exist as hard wired building blocks in the human body (and instead result e.g. from an optimization strategy of the CNS [de Ruyg 13, Steele 13]).

So, muscle synergies could be a promising approach to solve or reduce the muscle redundancy problem and generate human like muscle actuations (and by that motions).

## 3 Control Concept for a biomechanical human model

### 3.1 General control approaches

There exist several fields of applications where motions for digital human models or virtual avatars have to be generated. Further on, there are also fields like robotics, where motions for a physical agent or humanoid robot have to be controlled, which poses similar challenges similar problems.

The generation of motions of a physical robot comprises many challenging tasks like finding an appropriate controller which guarantees for stability (including fast reactions on disturbances) appropriate motion planning based on sensor information and sensor information processing in general (including handling of sensor noise, variation of internal and external state of the robot and many more). All these problems do not occur when controlling an avatar in a pure virtual and well known environment. Still, the kinematical redundancy problem has to be solved somehow, preferably in a human like manner to obtain acceptance of humans working or interacting with a humanoid robot. Wide spread approaches here are the use of motion capture data of e.g. reaching motions or biped walking. Therefore, humans perform a desired task and the captured trajectories are then used as guideline for the robot which tries to mimic them by the use of learning algorithms (e.g. reinforcement learning) or optimization methods [e.g. Pollard 02]. Instead of using motion capture data, some approaches simply guide an end-effector of a robot to the desired goal (external teach in) [e.g. Ott 13]. Other approaches make use of optimization methods to generate a desired trajectory as guideline for the controller (*open loop optimal control*) [e.g. Mostafa 10] or even involve sensor information to adapt optimization on the actual state of the robot (*closed loop optimal control*) [e.g. Seekircher 17]. In both cases, these optimization approaches need a more detailed virtual model of the physical agent and solve a desired task (e.g. walking or reaching for an object) by minimizing an *OC cost function* (aka. *objective function*), e.g. *time*, *energy consumption* or *smoothness*. *Open Loop OC* is also used in this thesis to generate motions and further described in Chapter 3.6. Further on, to find a desired trajectory for robot arm movement or effective reflexes on disturbances while walking, some biologically inspired approaches try to transfer human control concepts not only on a kinematical level and instead investigate the underlying muscle actuations generated by the CNS. Therefore, some approaches use as a "high level controller" a musculoskeletal model to transfer measured human muscle activations (EMG) into the resulting joint torques, which can then be applied to the robots actuator. As the number of actuators highly increases in musculoskeletal models, some approaches use muscle synergies to reduce complexity and reduce computational times [e.g. Cimolato 16].

Meanwhile one of the biggest sectors dealing with motion generation of virtual avatars is the film, television and gaming industry. In these branches, it is necessary to generate very natural and realistic looking motions, as humans are quite acute at recognizing implausible motions. In these fields, the physics behind the motions (e.g. internal or external forces, inertia effects) is unimportant. The most common approach in these fields is to capture motion data from a real human which is transferred to a virtual avatar. To create motions in animation films, they are quite often captured and transferred one to one from a real human to the avatar, so that all scenes have to be captured from and actor performing them.



In gaming industry there are some approaches which capture e.g. a multitude of different martial art kicks to different targets (height, distances), and then extract a set of kinematical motion primitives, which then can be combined to generate realistic looking kicks to new targets. These approaches are well suited to “simulate” small deviations of an already captured task, but lack the ability to predict motions of a completely new scenario. Further on, as they only focus on a visual representation, they do not involve any physics and do not allow a direct statements about inner or external forces and strains.

In the last decades, a multitude of digital human models for the use in the fields of ergonomics, human engineering and work science have been developed (around 100 listed e.g. in [Mühlstedt 12]). Commonly used state of the art commercial digital human models are e.g. JACK [Badler 97 Blanchonette 09], CATIA-Human, RAMSIS [Van der Meulen 07], SAMMIE [Porter 90], SANTOS [Abdel-Malek 07] and Pro/ENGINEER Manikin. All these tools have their historical origin in a specific field of application. RAMSIS e.g. was developed as a co-operative arrangement between German automotive manufactures and still is widely used for the design of vehicle interiors (specialized for sitting postures). Similar SAMMIE is used in areas such as tram driver workstation and aircraft cockpit design and Jack was developed to support the design and development of workspaces, with the emphasis on optimizing the human machine interface [Blanchonette 09]. These software packages involve a wide range of analyzing tools to assess e.g. reachability or visibility and involve databases to simulate different anthropometries.

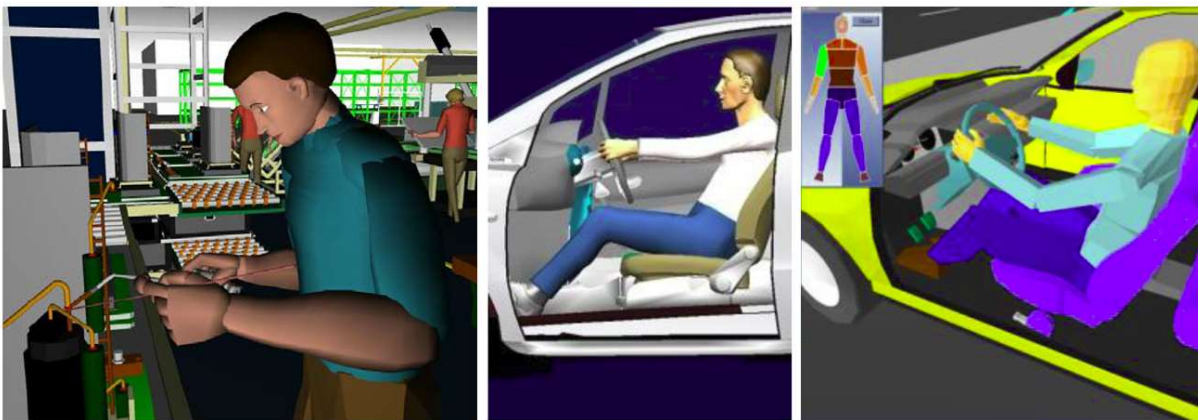


**Figure 14:** The commercial digital human models JACK (left), RAMSIS (middle) and SAMMIE (right). From [Zhang 19, Mühlstedt 12].

When it comes to motions, two major approaches are used in these tools. The user can simply position the manikin by hand (mouse and keyboard), whereas positions of linked body segments (connected via joints) are determined by inverse kinematics when moving a certain segment. To simplify this control strategy, some tools have predefined postures which can be selected and then refined. Still, this procedure is very time consuming especially when whole motion sequences should be created, meaning that for each time frame manikins have to be positioned by hand analyses can become very time-devouring [De Magistris 13]. Further on, to estimate realistic postures for a given tasks, specialist knowledge of ergonomists is necessary. Still, these strategies inherit the danger of delivering user dependent results, as each user defines the resulting postures or motions himself.

Another approach for motion generation used in these tools is, similar as described above, the use of motion capture data [De Magistris 13]. In these cases, the motions look realistic, and can be used for a post processing and ergonomic evaluation of a captured task performed with a real human on a physical prototype or existing workplace. But validity of the motions is restricted to the cases (loads, geometry, worker) they have been captured at. This inherits the risk of producing good looking motions in a simulation for a new task which might be wrong, e.g. in cases where the loads to be handled changed, which means that the real human would now behave different with the new load, which is not the case in the simulation. Further on, the captured motions are in principle only valid for the persons they have been measured with, and cannot simply be transferred to new workers with different strength or anthropometry.

To get information about inner loads, motion capture data can be post processed and joint torques used to create this motion be calculated by inverse dynamics methods (e.g. classical iterative Newton-Euler methods [Winter 09, Tsai 13]). This comprises the need of having a good model of the measured test person including several uncertainties as e.g. determination of body segment parameters [Drillis 64]. Therefore, also special tools exist which allow further on guessing muscle loads needed to produce the calculated *joint torque time series*. The *AnyBody Modeling System* is one of the most advanced musculoskeletal modeling systems for this case [Damsgaard 06]. For the involved *GaitLowerExtremity* model it has been shown that predicted muscle actuation showed a good agreement to measured EMG values in human gait [Wibawa 13]. For more complex motions as assembly tasks no direct validation studies are available.

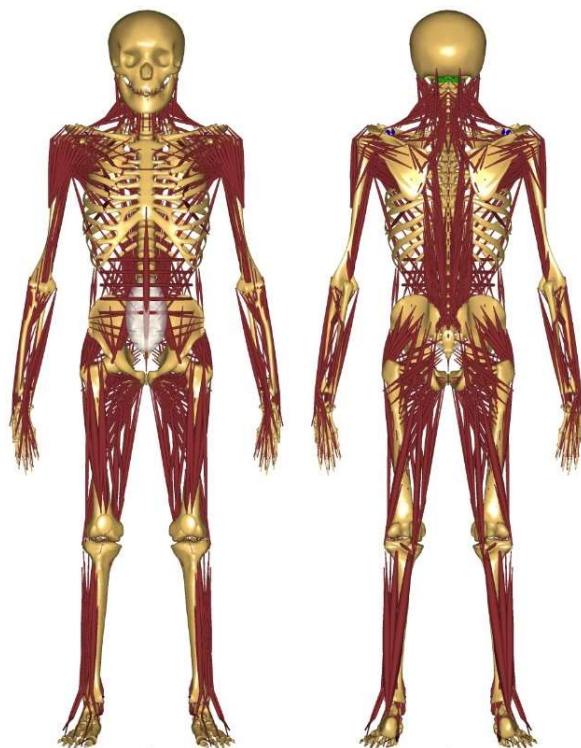


Figure 15: The ANYBODY model. From [Bio 14].

Also it is a quite complex and very time consuming process of inverse dynamics calculations to get from motion capture data over joint torques to muscle activations, it

can be useful to get information about inner loads for use cases where valid motion capture data exists. Still, these approaches are limited to scenarios which have been measured before (so that physical prototypes have to exist) or small deviations of these scenarios [De Magistris 13] and inherit several uncertainties due to their inverse nature. To avoid the need of motion capture data, there are also approaches existing which link simulated motions of a DHM as e.g. the EMA model (see below) to the AnyBody model [Peters 18]. In these approaches, the validity of the generated motion is an additional uncertainty, as torques and muscle forces are not directly taken into account for motion generation (as done in humans when creating MoCap data), so that the behavior of the DHM cannot adapt or optimize on these parameters.

The difficulty of motion generation in unknown scenarios and environments has pushed the development of new digital human models, also driven by the demand from industry which became aware of the potentials of DHMs. Two examples here are the commercial software packages EMA & IMMA, which follow (besides having the classical analyzing tools) new approaches for motion generation. EMA [Leidholdt 16] makes use of a sequence of building blocks (activities / daily tasks in industrial application) which are defined by the user and then are translated into motions [Mühlsted 12]. Therefore, a catalog of pre-recorded/defined fundamental motions is used (including e.g. the use of tools), which are assigned to a corresponding building block. This allows to setup scenarios with good looking macroscopic motion sequences, to estimate e.g. cycle times of a work station. When it comes to detailed simulations, this approach is also limited to what has been measured before (catalog of building blocks). And as it is based on pre captured kinematical motions, it does not allow to optimize on e.g. loads acting on the manikin or other biomechanical properties, which would change the behavior. The IMMA manikin [Hanson 19, Högberg 16] uses an optimization approach to estimate a posture, directly adapted to the given task. Therefore, the user defines certain constraints (e.g. grasp an object, look at an object), and a mix of mathematical functions is minimized, so that the manikin chooses the most comfortable posture which fulfills the defined constraints. This comprises minimizing joint torques, avoiding undesirable joint angles, automated force distribution (feet and support points at the hands) and many more.



Figure 16: The digital human model EMA (from [imk 19]) and IMMA (right).

Motions are then generated as a sequence of optimized postures, e.g. by following an object which is assembled. Combined with a very powerful path planner for collision avoidance, the IMMA software allows to simulate very detailed tasks, e.g. assembly of parts in narrow spaces without the use of any prerecorded motions. In cases where motions also in a real environment are performed very precise (slow / quasi static), the software delivers very realistic and human like behavior. But it finds its limitations in use cases, where humans move faster (dynamic) so that inertia effect play a role or where the human even makes deliberately use of inertia effects e.g. when using a hammer.

Summing up, the crux of DHM control in the scope of ergonomic assessment, human engineering and work science remains the generation of human like motions. For a given workplace (or physical prototype), this can be very well done by the use of motion capture data, which, transferred to the manikins of a software tool allows to use the analyzing tools of this software package. But validity of these motions is limited to the scenario they were captured and the worker performing the tasks. The EMA software extends the generality of this approach by dividing captured motions into fundamental sub-motions which can be rearranged into new tasks. But this approach based on kinematical sub motions does not allow for an optimization on biomechanical properties (e.g. muscle loads) and is only suitable for simulation of macroscopic motions (walking in open room, rough simulation assembly task). The only commercial DHM software creating motions without any captured motions and directly optimizing on the given task and biomechanical loads is IMMA. But also here, only postures are optimized, so that validity is restricted to quasi static motions. In cases where a human "optimizes" over a longer time window or makes use of inertia effects, the resulting motions might differ. To get any information about muscle forces, the software AnyBody is available, which needs motion data as input resulting from e.g. motion capture or DHM simulations. It is a very time consuming process and involves several uncertainties due to the inverse calculations.

So, a DHM control approach which allows to automatically create motions for a given start and end configuration, directly including dynamics (inertia effects), stability criterions and optimizes over a longer time window could be a big improvement. Optimization methods used to find the best solution for a completely new task with respect to e.g. anthropometry and strength of the model, allowing the usage of the approach with a high generality. Thereby, the main scope to guarantee validity of simulation results has to be to generate human like motions.

In this work it is assumed that this can be achieved by the use of human like actuation and control principles. As humans use muscles as actuators with their specific properties (e.g. create only pulling forces, force length- and force velocity- dependency), this is an important feature of the human locomotor system and influences the resulting "optimal" motion for a given goal. So, one assumption is, that using (simplified) muscles as actuators instead of e.g. joint torques, an optimal control approach might converge to a similar solution as the one the human CNS chooses or converges to after a learning period. As described above, the muscular actuation system in humans is highly redundant [Bernstein 67], which raises complexity of control. One approach to reduce this complexity could be the use of pre-defined groupings of muscles, as introduced above as muscle synergies. As this is hypothesized as a control mechanism of the CNS, this is an approach it is worth to follow, as a human like control strategy might lead to human like motions and also muscle actuations, which is an important topic concerning ergonomics. But even

if muscle synergies do not exist as hard wired building blocks in the human body (and instead result e.g. from an optimization strategy of the CNS [de Rugy 13, Steele 13]), it can be a very expedient approach as they capture human like muscle activations. The human muscle activation patterns might also (partly) result from optimization objectives of the CNS which are not present in a simplified human model (e.g. joint stability generated by muscle activations– see Chapter 2). This means that optimization methods would lack to predict these activation patterns in a DHM, simply due to the fact that there is e.g. no need to “stabilize” a ball and socket joint defined in a multibody system. Muscle synergies captured from humans and used as control concept might be a way to transfer the human muscle activation characteristics to a musculoskeletal DHM and further on lead to human like motions.

The in this work proposed and developed control approach uses optimal control for motion generation of a biomechanical digital human model (see Chapter 3.6 ). The optimal control framework was preexisting [Leyendecker 10, Roller 17, Björkenstam 18] and is used as a “black box” in this approach, whereas its properties (e.g. resulting motions) are investigated. The focus thereby is on the comparison of different Actuation Modes (joint torque actuation, single muscle actuation and synergetic muscle actuation) and the influence of the solved OC objective function. The resulting motions for the different control parameters are validated against measured human motions. To extract a set of muscle synergies from measurements at humans that can then be used as control parameters, a variety of steps has to be performed as described in the following Chapters. Muscle synergies have in other approaches already been shown to be suitable as control parameters.

### 3.1.1 Muscle synergies as control concept for DHM's

In several review studies, it has been examined and approved that the muscle synergy hypothesis can be an efficient method for motor control [Singh 18, Taborri 18, Ting 08, Tresch 09]. Still, few works are published which actually use muscle synergies as control strategy for motor control. And although these approaches commonly use “muscle synergies” in some way for motion control, the ways of implementation or the way the properties of muscles synergies are exploited for control are of different nature.

Several studies like Neptun et al, Allen et al. or Sartori et al. extracted muscle synergies from humans while walking, and showed that these synergies allowed for effective gait control of a musculoskeletal model [Neptune 09, Allen 12, Sartori 13]. These types of studies use *time variant muscle synergies* to capture the temporal regularities of human motion control to simulate a rhythmic motion task. Berniker et al. showed that muscle synergies extracted from frogs could efficiently control a 17-dimensional nonlinear dynamical system (masses and inertia of the hind limb skeleton and 13 muscles) of the frog's hind limb, and delivered very similar results to a full dimensional controller (individual muscle control) [Berniker 09]. In this case, *time invariant muscle synergies* extracted from EMG measurements were used as parameters for a controller of a dynamic system. Similar McKay et al. showed that five muscle synergies were capable to control a cats hind limb muscle activity in different postures with the same efficiency as controlling the 31 muscles individually, using a detailed 3D static model of the hind limb for validation [McKay 08].

Rasool et al. used muscle synergies extracted from EMG as “look up table” to discriminate between several tasks, which is performed in real time (from EMG measurements) and used to control lower arm prosthesis [Rasool 16]. A similar approach was used by [Afzal 17] with EMG signals of the human leg for classification of different locomotion modes (walking, stair ascent, ramp ascent).

Razavian et al. have shown that muscle synergies can control a musculoskeletal arm model in real time. A higher level controller is used to map a reference trajectories to muscle activations on a lower level by the use of muscle synergies [Razavian 16]. The dimensionality reduction results in 20 times faster calculation times while producing close to optimal muscle activations [Razavian 15]. Also Cimoloto et al. used muscle synergies for an EMG-driven Human-Machine interface to control the arm of a humanoid robot in real-time [Cimoloto 16]. In these cases, *time invariant muscle synergies* are used to reduce dimensionality of control to speed up computational times to map a by a controller calculated force to a certain muscle actuation (to get information about muscle loads or actuate a musculoskeletal system) or, in the other direction, map measured muscle activations to a desired controller task (force or motor command for prosthesis / robot control). Although these approaches have shown that muscle synergies can be useful as controllers, there are still many uncertainties about muscle synergies which makes approaches hard to compare and the integration of muscle synergies in a control strategy remains a complex task. In all of the above mentioned approaches, some kind of adaptations were necessary, if by hand (manually parameter fitting) or by the use of some kind of optimization method. Further on, the way of how to extract muscle synergies (e.g. test setup, EMG sensor placement, extraction algorithm) and an appropriate number of synergies for control itself remain an open questions which depend on the control approach, simulation tasks and many more things. How these problems are handled in this thesis will be described in the remaining subsections of this Chapter.

### **3.2 Overall approach - overview**

The control approach developed in this work allows to identify modelling parameters of the DHM used for simulation, extract muscle synergies from measurements which can then be used for actuation and can be compared with a direct muscle actuation and joint torque driven actuation. Additionally, the resulting motions can be validated against measured motions and the influence of the optimal control objective function can be investigated.

As described in 2.2, muscle synergies are one hypothesis from neuroscience to explain, how the CNS might reduce complexity of motor control in vertebrates. Using solutions inspired by nature is a wide spread practice in robotics, engineering and other applied fields, simply due to the fact that these solutions result from a long period of evolution and have proven their functionality over time. Beside this, as the control approach aims to produce human like motions of a DHM, it is additionally somehow obvious to also use or search for a “human like” control approach. But even if muscle synergies do not exist as hard coded underlying building blocks in vertebrates, they might be a useful approach to control a DHM, as they are copied from nature and might capture human like or natural activation characteristics. Motions in this approach are planned by the use of optimal control, whereas the DHM is represented as multibody system that can be actuated via joint torques or by simplified muscles. In Figure 17, an overview of the workflow of the developed control approach with the main steps for parameter identification and

validation is depicted. First, measurements of certain tasks in the motion lab are performed, from which EMG data of the involved muscles and trajectories are measured. The choice of motions and muscles to be measured depends on the parameters that should be identified or validated (muscle synergies, objective functions) and will be further described in the Chapters 4 and 5. From the measured EMG data, muscle synergies can be extracted after data processing and filtering by using a *non-negative matrix factorization* (NMF) algorithm [Dhilon 05]. A procedure developed within this thesis work allows to validate the extracted muscle synergies and to determine a useful number of synergies, which is a free parameter of the NMF algorithm. The extracted muscles synergies can then be implemented in the OC framework to be used as control parameters for the DHM.

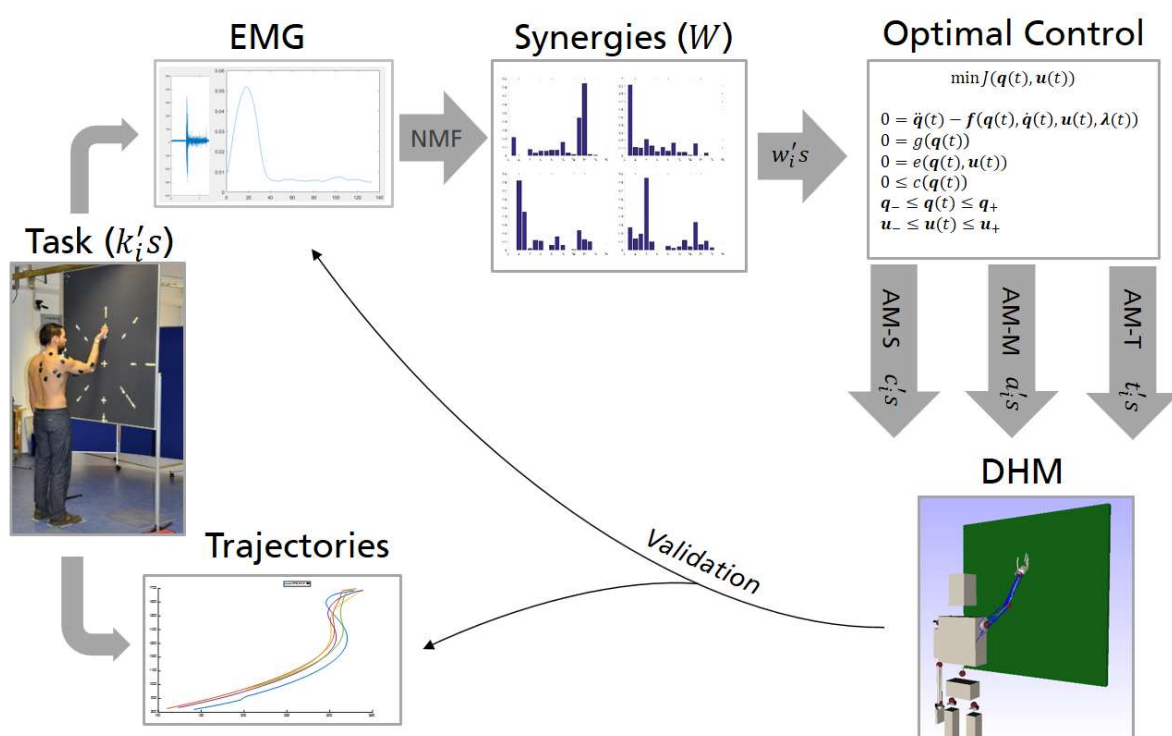


Figure 17: Workflow of the overall control approach developed in this thesis [Obentheuer 17, Obentheuer 18, Obentheuer 19].

In the next step, simulations are performed in the OC framework under similar specifications as the measurements were done in the motion lab, e.g. reaching a point as fast as possible or lifting a weight. Therefore, a specific DHM model can be build up with the focus on the needs for the actual test. If a whole body motion is investigated, a full body model can be used. Or, if the focus is e.g. on only one arm, e.g. in tests where the shoulder is kept in position while moving, a reduced model with only the relevant parts of shoulder and arm can be build up. The dimensions of the model, like length of the limbs, can be adapted to the anthropometry of the test persons, so that the motion data gets comparable more quantitative. Additionally it can be defined for each joint, how it will be actuated. Therefore, three different **Actuation Modes (AM)** are available:

In the model setup denoted as **AM-T (Actuation Mode – Torques)** joint torques are used as actuators, so the OC code calculates a time series of joint torques actuation

signals ( $t_i$ 's). These actuation signals move the DHM in a way, that the task to be simulated is fulfilled, while a defined objective function is minimized and the side constraints that the equations of motion of the MBS are fulfilled. In the **AM-M** approach (**A**ctuation **M**ode – **M**uscles) the model is actuated by muscles, whereas each muscle is activated separately, so that the OC calculates a times series of muscle actuation signals ( $a_i$ 's) which fulfill the given tasks. In the **AM-S** approach (**A**ctuation **M**ode –**S**ynergies), the muscles are grouped to muscles synergies which act as control parameters. Here, the OC code calculates a time series of corresponding weights ( $c_i$ 's). These weights define how active each synergy is, and by multiplying them with the muscle synergy matrices, the activation level for each single muscle results. The different Actuation Modes can be combined in one model, so that e.g. the arm can be controlled by muscles, whereas the rest of the DHM is actuated by joint torques. The resulting simulated trajectories and actuation signals can then be compared with those measured in the motion lab. By that, the influence of the different Actuation Modes AM and the distinct OC objective functions to the resulting motions and actuation signals can be compared and validated against measured motion data. Additionally, this procedure allows to identify modelling parameters like e.g. the number of muscle synergies, maximum muscle forces or muscle insertion points.

### 3.3 Data acquisition in the motion lab

As described above, motion capturing in this control approach is only done to validate the simulation results and to identify parameters of the DHM respectively the OC framework. In general, it is not necessary as input for the OC framework to set up a simulation and generate motions for a new task. Same holds true for the measured EMG data and the control parameters derived from EMG measurements. Once, muscle synergies are extracted from measured EMG data, they can be used to simulate arbitrary new tasks. How generic muscle synergies extracted from a certain task actually are has to be investigated. All kind of data that was acquired (optical tracking, EMG, external force sensors) was synchronized by the used measuring system, which allows to identify e.g. the start of a certain motion by the captured visual motion data and investigate the related EMG data.

#### 3.3.1 Motion capturing

The term “Motion Capturing” stands for the process of recording movements of persons or objects. The performed motions are sampled with a certain framerate (many times per second). The main purpose in this DHM control approach is to track motions performed in distinct tests, to be able to compare measured trajectories, velocities and accelerations of human limbs or involved objects with simulated motion data. For motion capturing different techniques exist. In the tests described in this work, optical systems with passive markers are used. In these systems, several cameras track the positions of reflective markers that are placed on the human body or on objects, as depicted in Figure 18. By triangulation, the 3D position of each marker can be calculated, and with the knowledge of where the markers are placed on the human body or an object, the performed motions can be reproduced.

In principle, markers can be placed on arbitrary positions on the human body, but there are positions which are more favorable, e.g. those where the skin does not move while performing a motion, so that markers keep their relative positions to the limb. Guidelines



and landmarks for marker placement are e.g. given in [Van Sint Jan 07]. Additionally, the optimal number and positioning of markers depends on the test setup and the needed level of detail of motion resolution. The details of marker placement, tracking systems and data acquisition are described in each test in detail (see Chapter 4 and 5).

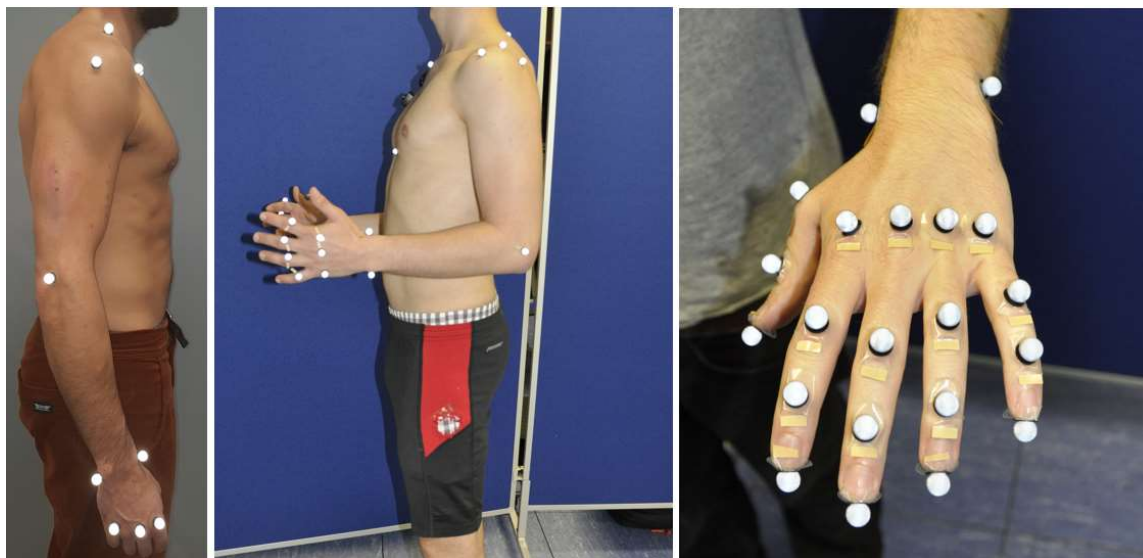


*Figure 18: Placement of optical reflecting markers for motion capturing.*

### 3.3.2 EMG Measurements

Electromyography (EMG) is a method used in several fields of application like medicine, ergonomics, sport science or biomechanics that allows to determine and record the neuronal activity of a skeletal muscle. In the control approach developed within this thesis, EMG measurements are performed for two reasons: For one, from the measured muscle activation signals muscle synergies are extracted which are then used as control parameters. Further on, the measured EMG values can be used to validate simulated muscle activations and, similar as done with trajectories, can help to adapt modelling parameters.



*Figure 19: Placement of several wireless bipolar surface EMG electrodes on upper arm and forearm.*

To measure EMG data, a sensor is placed on the skin over the relevant muscle (surface EMG) or into the muscle (intramuscular EMG). Intramuscular EMG measurements are categorized as invasive procedures fraught with risk to health that have to be approved by a medical ethic commission (Germany). Due to that, measurements in this work are done with surface EMG only (in literature sometimes abbreviated as sEMG, in the following simply as EMG). In Figure 19, the placement of several wireless EMG electrodes placed over muscles on the upper arm and forearm are depicted.

As described in Chapter 2.1, the “firing” of a motor unit leads to a depolarization of the innervated muscle cells from  $-80mV$  to  $+30mV$ , which is directly followed by a repolarization with the same magnitude (symmetric signal). Starting from the motor end plate, this action potential spreads bidirectional along the muscle fiber. This electrical excitation leads to a release of calcium ions, which causes, due to an electro mechanical coupling, the contraction of the muscle cells. This model describes a highly correlated relationship between electrical excitation and mechanical contraction [Konrad 11]. This depolarization-repolarization cycle leads to a depolarization wave (electrical dipole) along the muscle fiber which can be measured on the surface (skin). The action potentials of all muscle fibers belonging to one motor unit sum up to a motor unit action potential (MUAP). The (raw) EMG signal that can actually be measured on the surface (skin), the so called interference signal, is the summed up signal of all MUAP's of one muscle, a bipolar signal with a symmetrical distribution of positive and negative amplitudes.

Depending on the distance of the active muscle fiber to the EMG sensor, signals will be acquired with different amplitudes. Muscle fibers which are closer to the surface and by that to the electrode produce higher values than those located deeper inside the muscle. For measuring the neuronal activity of a muscle with EMG, bipolar electrodes with a differential amplifier are placed in longitudinal direction of the muscle on the skin. As these electrodes capture the differences of the two measurement points (poles) which reaches the highest values if aligned longitudinal to the muscle fiber (in direction of the depolarization wave), the orientation of the muscle fiber to the electrode also influences the magnitude of the captured signal.

The CNS has two major mechanisms to control the contraction process and by that the generated force output, the recruitment and the firing rate of motor units. Both mechanisms are reflected directly in the measured EMG signal: if the number of recruited MUs or the firing rate increases, the summarily signal amplitude rises as well. In Figure 20, the EMG raw signal of three isometric biceps brachii contractions is depicted. The relaxed muscle produces a more or less flat zero signal, whereas the measured baseline noise is an important factor to check the signal quality and marker placement. The measured signals of a muscle contraction have a stochastic character, meaning that no measured EMG signal can be reproduced in exactly the same appearance.

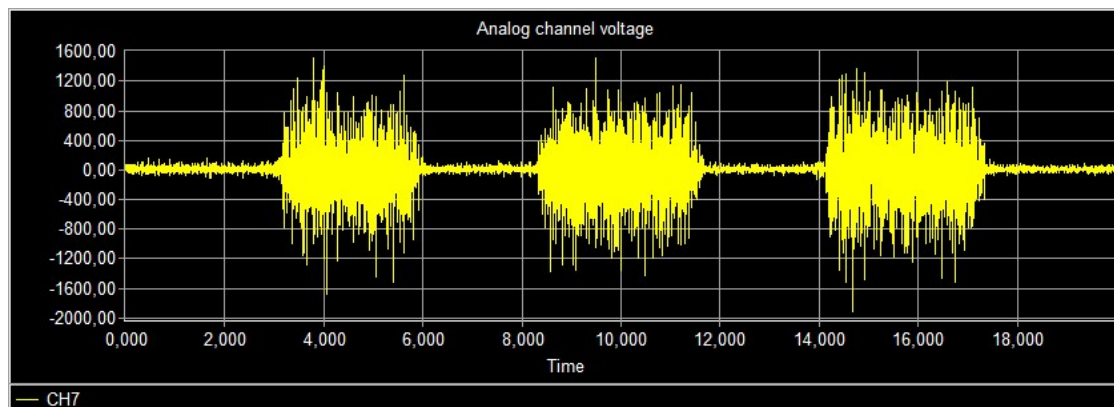


*Figure 20: EMG raw signal of three isometric biceps brachii contractions.*

Beside noise and other artefacts this is mainly due to the fact that the compilation of recruited MUs changes within each voluntary contraction, so that their physical configuration in the muscle changes continuously. As muscle fibers closer to the EMG electrode produce higher signal outputs than those located deeper inside the muscle, the resulting summarily amplitude changes each time. This mainly shows up in configurations with many muscle fibers close to the surface, which then produce very high spikes for a short time. The non-reproducible part of the EMG signal can be eliminated (or at least reduced) by using appropriate smoothing algorithms. EMG Measurements can deliver important information about neuronal activities and muscle recruitment strategies of the CNS, but there are some limitations of the method and influencing factors which have to be carefully considered before planning a test setup and when assessing or interpreting measured EMG signals:

- **Properties of human tissue:** The electric conductivity of human tissue varies between subjects, but also within measuring points of one and the same subject. Additionally the temperature or daily changing properties like e.g. thickness or amount of water in the subcutaneous fat have a big influence on the measured signal. Due to that, EMG signals of different persons, measuring points or tests cannot be compared quantitatively (without filtering / normalization).
- **Physiological crosstalk:** EMG sensors can capture activity signals from neighbored muscles (typically the amount does not exceed 10-15% [Konrad 11]). This has to be considered especially where muscles are located very close to another, like e.g. in the forearm, and in test setups with dynamic motions (see next point).
- **Changing distances or orientation between muscles and electrodes:** A changing distance or orientation between muscle and electrode leads to changes of the signal amplitude. This causes problems especially when measuring dynamic motions, where the muscle moves and changes its position or orientation under the electrode. Larger displacement also influence the amount of measured crosstalk, especially where muscles are located very close to another.
- **External interfering voltage and materials:** There are many factors that have to be considered e.g. when choosing the used electrodes and differential amplifiers. Additionally, surrounding electrical equipment can produce noise or artefacts while measuring. By using modern equipment, skilled personnel and a

proper calibration before measuring (e.g. check baseline noise), their influence should be negligible.

- **No deep layer muscles measurable:** With surface EMG, only muscles located directly under the skin are measurable. This means that muscle data of deep layer muscles cannot be acquired, and due to that are not considered in this approach. Neither for validation, nor for the use as control parameters in the muscle synergies. (This could be resolved by using fine wire EMG, or by newer approaches [Koshio 2012] which assume to be able to measure deep layer muscles with surface EMG)
- **Number of available EMG channels:** Although the number of EMG measuring channels are not directly limited from a technical point of view (depending on the used system), most motion laboratories have a fixed number of channels available (commonly between 8-16 Channels). For muscle synergy extraction, this can become a problem, as all involved (measurable) muscles have to be measured in parallel.

As described above, the EMG raw signal has to be filtered to eliminate e.g. spikes and other non-reproducible parts. Beside this, a certain post processing has to be done before extracting muscle synergies and to be able to compare the measured EMG signals with the activation signals of the used muscle models in the simulation model (see Chapter 3.5). The main steps of data editing for the EMG raw signal performed in this approach are as follows:

- **Zero calibration:** Due to the nature of the EMG signal (symmetry), the mean value should be zero. This is also a checkpoint for calibration before measuring (baseline noise and mean value). For some reasons the mean value can shift or drift while measuring. This effect can be re-calibrated by subtracting out the mean value of the measured raw signal.
- **Full wave rectification:** This is an essential step in the post processing and simply means taking the absolute values of the signal, so the negative swings turn into positives. This is important for two reasons. For one, to study the characteristic of the measured EMG signal, it is beneficial to "extract" its shape or envelope using an appropriate filter. But, due to the zero mean nature of EMG signals, a low pass filtering of an unrectified signal would just deliver zero. Further on, the used hill muscles in the DHM simulation model are activated with positive activation signals. So, to enable a comparison of those two signals, and to use muscle synergies as control parameters, the measured EMG has to be rectified (and normalized, see below).
- **Low pass filter:** This is the actual step to extract the characteristic envelope of the measured EMG signal. Usually, cut off frequencies between 5-100Hz are used. Typically used filtering methods are sliding average window (finite Impulse response filter), sliding root mean square (RMS) window or discrete versions of classical low pass filters like Butterworth or Chebyshev (infinite impulse response filter, IIR). In this approach, a Butterworth low pass is used, which is applied in forward and backward direction, which guarantees a zero phase shift (the phase or timing of the original signal is not altered). For details and used cut off frequencies see test descriptions (Chapters 4 and 5).

- **Down sampling:** To reduce data points and speed up calculation times, and as simulations are performed with a framerate of about 100Hz maximum, the filtered EMG data is down sampled to 100Hz as well after filtering.
- **Normalization:** As described above, EMG signals of different persons, measuring points or tests cannot be compared quantitatively in a direct way. Therefore, measured and filtered EMG data is normalized to the highest values measured at a maximum voluntary contraction (MVC). To determine MVC values, certain tests according to [Freriks 99] are performed at each lab test (for details see test descriptions, Chapters 4 and 5). In these tests, the measured muscle is contracted as high as possible (by lifting a weight or pulling/pushing isometric against a resistance with maximum power). The MVC values can be interpreted as “100% muscle activation” and correspond to a fully activated Hill muscle for comparison and validation.

In Figure 21, the EMG values of the musculus biceps brachii of three repetitions of a dynamic arm motion are depicted. The left side shows the unfiltered raw signal. On the right side, the EMG signals are filtered with the above described procedure, normalized to the MVC values, and overlaid. After this process, the plots become much more expressive. It can e.g. be directly seen, that timings and characteristics of the EMG signals are very well comparable (start- and end frames were visually identified on the corresponding motion capture data). This shows that the measured EMG values are not just some kind of artefact or of a pure stochastic nature, they are instead very well reproducible within repetitions.

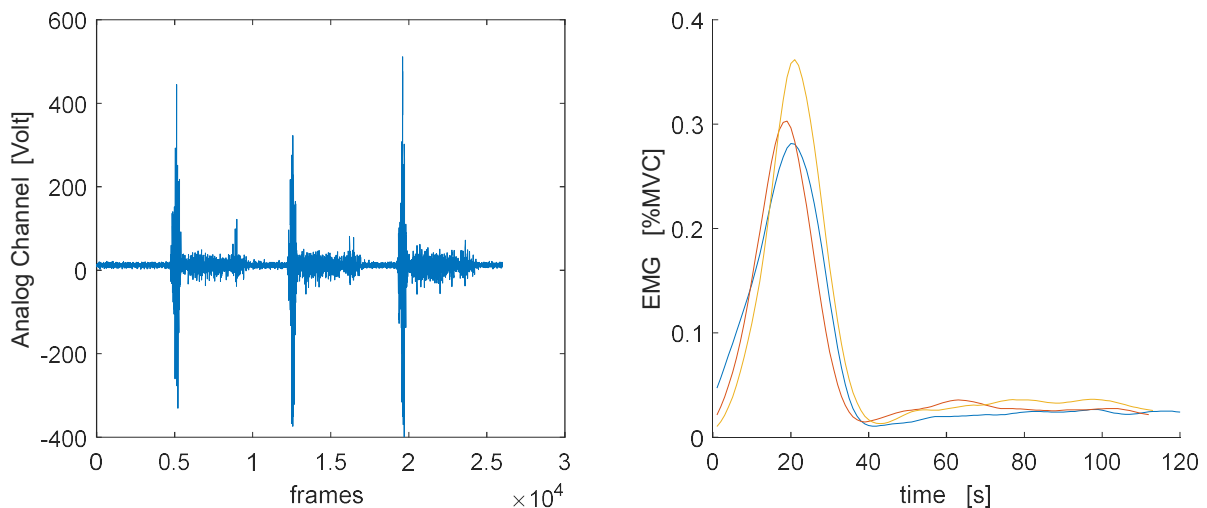


*Figure 21: EMG values of the biceps brachii of three repetitions of the same motion. Raw signal (left) and filtered and normalized signal of one repetition (right).*

### 3.3.3 Measurement of external forces

It can be helpful to measure external forces like reaction forces (foot ground reaction forces, grasping forces, loads on objects to be manipulated etc.) for validation purposes or as side constraints for the simulation setup.

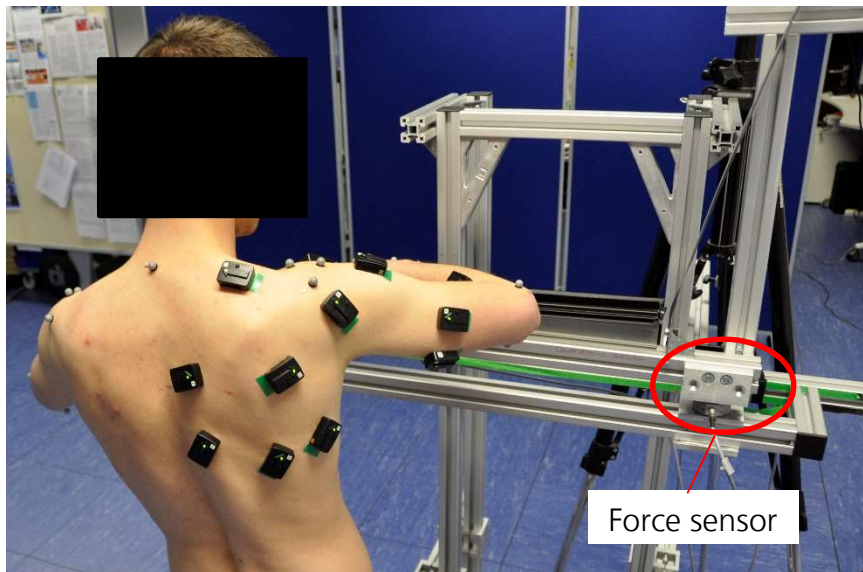


*Figure 22: Assembling of a car door sealing on a test bench with force sensors to measure the axial installation forces.*

In Figure 22 for example, the axial installation forces while assembling a car door sealing are estimated as well as motion data and EMG values of involved arm and shoulder muscles. Tasks where flexible parts are assembled in industry like e.g. a sealing are of high interest for ergonomists. Those parts often get jammed while mounting, which makes high hand forces necessary for installation. Jamming and easy gliding of a sealing often alternate while mounting, and this behavior is hard to simulate (even with complex material models), which makes the needed forces almost unpredictable with simulation models. When simulating this test, one workaround could be to set the measured forces as side constraint in the simulation scenario, and use the measured motion data for validation.

### 3.4 Muscle synergy extraction

As described in chapter 2.2, the muscle synergy hypothesis from neuroscience describes a strategy which the CNS might use to reduce the complexity of motor control. Instead of actuating each muscle directly, it assumes a modular architecture of the underlying motor circuits, meaning that muscles are grouped to functional units (muscle synergies). To investigate muscle synergies or use them as control concept, one has to focus the problem that it still remains a hypothesis which is not proven and muscle synergies cannot be estimated or measured in a direct way.

Commonly, muscle synergies are extracted from measured EMG data from experiments which are arranged in a matrix. Finding a set of source signals from a given set of mixed signals (without any or with minor knowledge about the source signal) is a well-known problem in different fields of application, and there exist several algorithms for so called blind signal separation (BSS) [Cardoso 98]. The BSS algorithms which are qualified to be used to extract muscle synergies from a Matrix containing measured EMG data are reduced by two facts. First, if muscle synergies should reduce complexity of motor control, the number of synergies ( $n_w$ ) should be smaller than the number of muscles ( $n_m$ ). This allows the usage of conventional linear methods. Second, the activation signals of the CNS are always positives. Due to that, algorithms using non negative factors are ineligible.

Commonly used algorithms for muscle synergy extraction are Principal component analysis (PCA), Independent component analysis (ICA), Factor analysis (FA), Non-negative matrix factorization (NMF) and second-order blind identification (SOBI). Several studies have investigated and compared the performance of these algorithms for muscle synergy extraction. Therefore, the algorithms were applied to real EMG data as well as to artificial EMG signals produced by artificial muscle synergies (to allow a direct validation of the extracted Synergies) and superimposed by noise. [Ebied 18] recommend the use of NMF and identified it as the best working algorithm, especially when the number of (EMG) channels is higher than the number of synergies. [Tresch 06] showed that NMF was very robust to noise and grouped it to the best performing algorithms as well, which all identified synergies very similar to another. Due to the findings and recommendations in these studies, a NMF algorithm for muscle synergy extraction is used in this approach as well.

### 3.4.1 Non Negative Matrix Factorization for muscle synergy extraction

To extract muscle synergies, a NMF algorithm in a customized software written in Matlab is used in this approach, as schematically depicted in Figure 23. Therefore, the NMF algorithm is applied to the muscle synergy extraction Matrix  $M_e$  which contains the filtered EMG data of all measured muscles of one Test Scenario (size  $n_t$  by  $n_m$ , where  $n_t$  is the number of time samples of all included trials, and  $n_m$  is the number of measured muscles). Input data of several trials is concatenated vertically. A "trial" is e.g. one single reaching motion from the defined start to the desired end position. Start and end frame of each trial are identified visually by investigating the captured motion data.

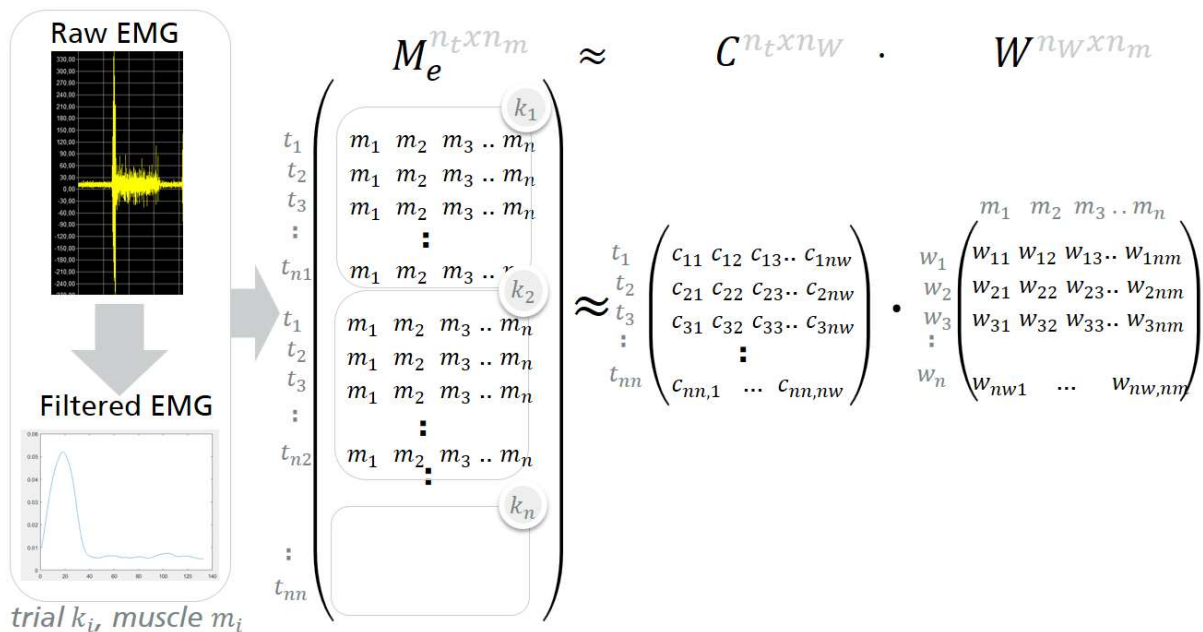


**Figure 23: Muscle synergy extraction: Filtered EMG signals of all trials (e.g. single reaching motions) are concatenated vertically in the Matrix  $M_e$ . Applying the NMF algorithm to  $M_e$  delivers the weight Matrix  $C$  and the synergy Matrix  $W$ . The number of synergies  $n_w$  is not an output of the NMF algorithm and is determined in a separated procedure.**

The NMF algorithm provides two Matrices  $C$  and  $W$  (of dimension respectively  $n_t$  by  $n_w$  and  $n_w$  by  $n_m$ , where  $n_w$  is the number of muscle synergies) such that

$$M_e = C \cdot W + \text{residuals} \quad (1)$$

where the number of muscle synergies  $n_w$  is a free parameter of the NMF algorithm, and has to be set by the user. For each value of  $n_w$  we ran the NMF algorithm 25 times to reduce the probability that it converges to a local minimum.

As described above, the factorization of  $M_e$  is a lower rank approximation, where the factors  $C$  and  $W$  are chosen to minimize the root-mean-squared residual between  $M_e$  and  $C \cdot W$ . The Matrix  $W$  is interpreted as the muscle synergy matrix, where each row vector  $\bar{w}$  stands for one time invariant muscle synergy and each entry  $\bar{w}_j$  of  $\bar{w}$  defines, with which magnitude each muscle is present in this synergy. This balance does not change over time, and the Matrix  $W$  is used as control policy in the OC framework when performing simulations in AM-S. The Matrix  $C$  represents the according weights, which (multiplied with  $W$ ) reproduce the measured muscle actuations ( $M_e$ ) best. So, each entry  $\bar{c}_i$  of the row vectors  $\bar{c}$  of the Matrix  $C$  defines, how active each synergy is at one discrete time step. Following the law of matrix multiplication, this means that the activation level for a muscle  $m_j$  at a certain time step results by summing up the scaled outputs of each synergy for this muscle so that

$$m_j(t) = \sum_{i=1}^{n_w} c_i(t) \cdot w_{ij}. \quad (2)$$

For the given input set of muscle activations ( $M_e$ ) these weights  $c_i$  are an output of the NMF algorithm. In the simulations in AM-S, they are calculated by the OC framework (respectively the according activations  $a_j$  of the artificial Hill muscles in the simulation model). To determine the number of muscle synergies  $n_w$ , in a first step a criterion based on the variance account for VAF defined as follows [Chiovetto 13]

$$VAF(n_w) = 100 \cdot \left(1 - \left(\frac{\|M_e - D\|^2}{\|M_e - \text{mean}(M_e)\|^2}\right)\right) \quad (3)$$

was used, where  $D$  is the approximation of  $M_e$  obtained by multiplying  $C \cdot W$ , and  $\text{mean}$  is an operator that computes a matrix of the same dimension as the matrix  $M_e$  and whose rows are equal point by point to the mean values of the corresponding rows of  $M_e$  [Chiovetto 13].

There exist distinct procedures in literature to determine the right number of muscle synergies based on the VAF criterion. A well spread option is to define a number of muscle synergies which reproduces a certain percentage of the VAF (commonly between 85-95%) as threshold, assuming that the measured EMG values to be reproduced include noise and uncertainties, so that it is not convenient to go above this threshold.



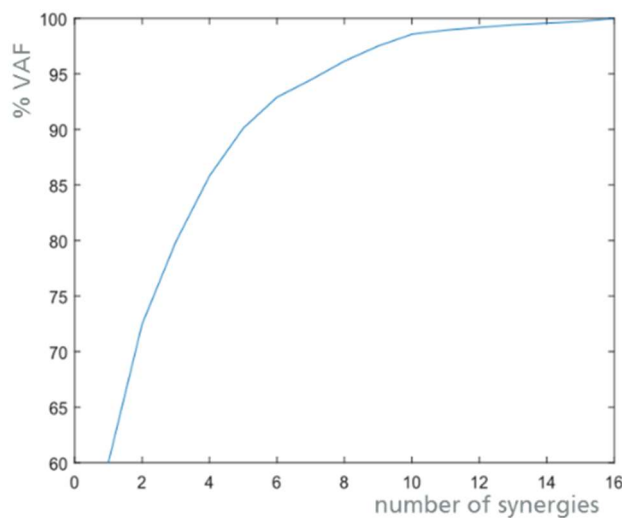


**Figure 24:** Plot of the Variance Account For (3) depending on the used number of muscle synergies.

Another practice is to plot the VAF versus the used number of muscle synergies (typically from 1 to  $n_m$ ) as depicted in Figure 24, and identify the number of muscle synergies where the graph shows a significant change of slope, after which the slope becomes constant [Ferré 95]. This can be done automatized e.g. with a linear regression procedure [Cheung 05, d'Avella 06], or simply by identifying this point visually as done in this approach.

Up to this point, it is only checked if the muscle synergies are capable of reproducing measured EMG signals, which were used as input values for the NMF algorithm (respectively how many synergies are necessary to reach a certain reproduction quality for these signals based on the VAF criterion). As it is planned to use the muscle synergies as control parameters not only for scenarios they were extracted from, their generality is estimated in a further step. Therefore it is checked if measured muscle activation signals that were not included in the matrix  $M_e$  used for synergy extraction can also be reproduced with the extracted synergies. To approximate a new set of measured muscle activations, the measured EMG signals, are arranged in the validation matrix  $M_v$  (with number of columns equal to  $M_e$ ). Then, a customized software written in Matlab and developed within this thesis is used, which similar as in (1) minimizes the root-mean-squared residual between  $M_v$  and  $C \cdot W$ , now with  $M_v$  and  $W$  given. Further on, the quality of the used (number of) muscle synergies was investigated by a visual comparison of the plots of the original filtered EMG signal and the signals being reproduced with the use of muscle synergies. This was done for reproduced signals that were used as inputs for the NMF algorithm ( $M_e$ ) as well as for measured EMG signals that were not included in the NMF algorithm.

### 3.5 The digital human model

As described above, in this thesis it is hypothesized that a modelling and control approach inspired by nature leads to “human like” motions. This means that a biomechanical simulation model has to be used so that properties of the human locomotor system are somehow transferred to the DHM, which allows the optimal control framework to directly optimize on similar objectives as the central nervous system might do (e.g. muscle loads). But also in the field of biomechanics, there is a wide range of different modelling

approaches and levels of detail. Many of these approaches have their focus on special parts of the body (e.g. a distinct joint), special load cases or motions (sport science) or detailed properties of human tissue. In [Röhrle 16] e.g. a model of the arm is simulated, where all components are represented as continuous, three-dimensional, volumetric objects (nonlinear hyperelastic materials). This approach allows predicting realistic moment arms and muscle forces while giving insights into existing contact forces and their influence on the muscle fibre stretch. Other approaches (e.g. [Heidlauf 14]) simulate muscle activations on the microscopic sarcomere level delivering key characteristics of skeletal muscles. Those detailed approaches are computationally highly intensive and not suitable to simulate a full body model or a large range of motions. To speed up computational times but still being accurate in the parts of interest, many hybrid approaches are used. In [Anderson 17], a biomechanical model of the human head and neck consists of a combination of finite element models (FEM), rigid body, and spring-like components. It is controlled by muscles which can be activated to mimic complex actions such as swallowing, chewing, and speech. There exist many other approaches driven by medicine to support diagnostics but also motivated by sport science to support specific training or rehabilitation of athletes. Mostly they focus on e.g. a distinct joint, using very detailed models of the respective part of the body. In [Herrmann 19], a detailed musculoskeletal kinematic multibody model of the shoulder is used to analyze shoulder dynamics after total replacement. In [Westover 16], a model of the knee allows quantifying the laxity in the anterior cruciate ligament and individual knee joint structures. In all of these approaches, the high level of detail leads to a huge number of parameters which have to be defined (respectively fitted). In most cases some image based motion data is used, often combined with special load cases, where e.g. external forces are measure. In [Westover 16] e.g. a custom knee loading apparatus in conjunction with magnetic resonance imaging is used to feed the model. These approaches can deliver important insights on e.g. the role of tendons and ligaments for joint stability, the pressure distribution in cartilage during a specific sport task and many more, but they are by that restricted to these specific application and too complex to build (and control) a human full body model. In this thesis, the biomechanical multibody system model approach is simplified to a level that the basic dynamical properties of the human locomotor system like (center of) masses of the body and limbs, joint range of motion and actuation principle by muscles are transferred, but computational times are still fast. It will be investigated how far this simplification is sufficient to predict human motions.

### **3.5.1 Implemented modelling approach**

To build up a digital human model, a dynamic MBS code based on [Featherstone 14] is utilized that uses minimal coordinates and facilitates fast computational algorithms to determine forces and velocities [Björkenstam 16, Björkenstam 18]. It allows to define rigid bodies (bones), joints and actuators freely in arbitrary configurations, so that models can be built up adapted to what should be investigated. As joints, spherical joints and revolute joints are available, which can be limited to simulate the human range of motion. As rigid bodies, cones and cylinders can be defined, with mass, length and diameter as modelling parameters.

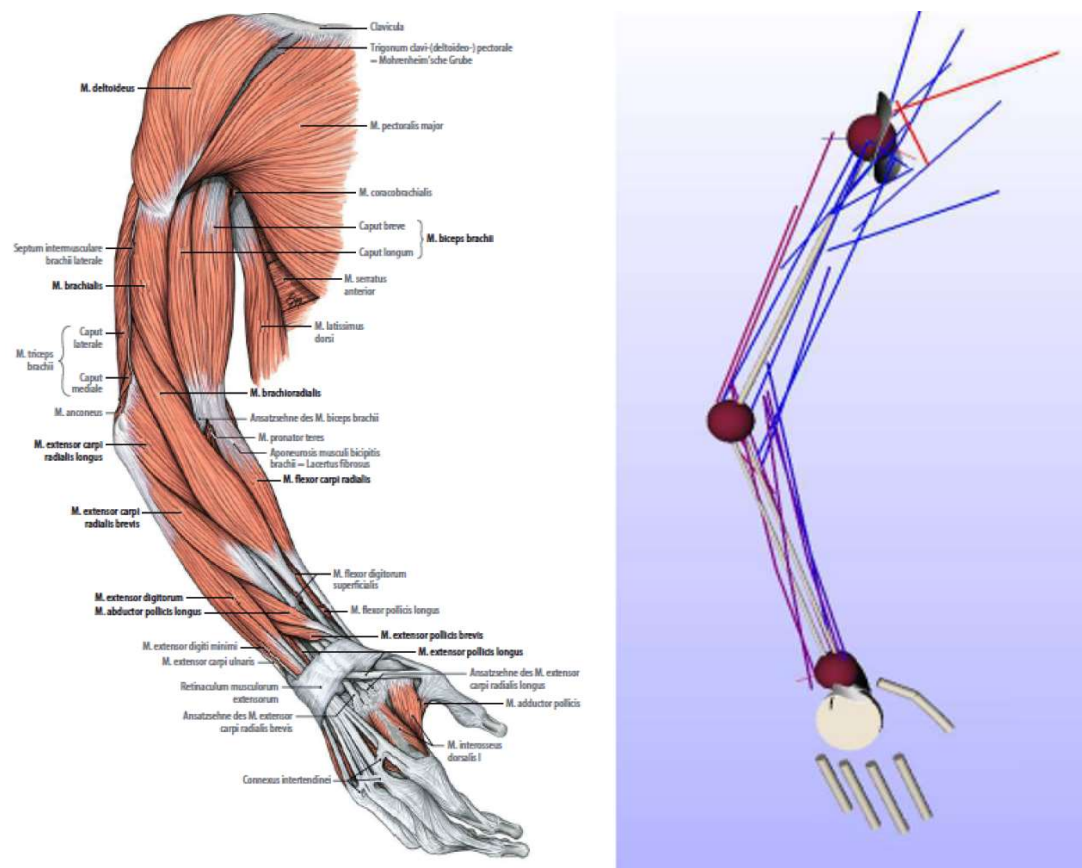


Figure 25: human arm model: anatomical representation (left, from [Tillmann 05]) and simulation model (right).

As actuators, motors (torques between rigid bodies) and Hill-type muscles (force elements between rigid bodies) can be specified. The tests that were measured in the motion lab and simulated in the OC framework presented in this work focus on human arm motion. For these tests, a model of the human arm including 29 Hill muscles was used for simulation, which is depicted in Figure 25 (right) and described in more detail in the following. To get measured motion data comparable with simulated results, dimensions of the simulation model were adapted to the anthropometry of the subjects that performed the test. Therefore, a program was developed, which automatically adapts muscle parameters (origin, via- and insertion points, see below) to a given set of measurable input data like length of forearm, upper arm and hand.

### 3.5.2 Biomechanical simulation model of the right arm

As described in chapter 2.1, skeleton muscles in humans are attached to bones at their ends by tendons, and by contraction they exert force on the bones. One end of the muscles, the so called origin, is closer to the body (proximal) and does not move during contracting. The other end, the insertion, is further away (distal) and does move when the muscle contracts. Origin and insertion points are important parameters for biomechanical modelling as they influence the resulting motion respectively ratio of the resulting joint torque when the muscle contracts. Another important parameter is the muscle path. In humans, muscles wrap around bones or other muscles and get thrust aside when other muscles contract and by that get thicker. The Hill muscles used in this approach (see chapter 3.5.3) always form a straight line between their attachment points and do not

consider contact to geometries of the MBS (bones). To simulate a more realistic muscle path, they can be led over via points. Muscle origin, insertion- and via points used in this model were identified by studying the human anatomy. Additionally, it was checked if the resulting motion when contracting the muscle in a forward simulation were in conformity with muscle actions in humans.

Especially bigger muscles often have several distinct insertion points (muscle heads). Those different parts of a muscle were modelled as distinct Hill muscles in the simulation model. This modelling approach is not only derived and useful from the (bio) mechanical point of view. The delta muscle for example is divided in three different parts with distinct insertion point (anterior, medial and posterior). It was shown that these parts can even be subdivided into at least seven functional units, which can be activated by the CNS individually [Brown 07]. This supports the above described modelling approach as these findings lead to the assumption that the CNS as well can exploit the mechanical properties of each single muscle head in particular as it were activating a single muscles. Overall, 29 Hill muscles were implemented in the simulation model of the human arm. The name of the Hill muscles (which refer to real human anatomical muscles or muscle parts), their origin and insertion, as well as the action of the muscle (part) are listed in Table 1.

Note that origins of the Hill muscles of the shoulder (referring to *Scapula / Clavicle* ) are chosen at the coordinates of human origins at those bones (in a neutral shoulder position), but as *Clavicle* and *Scapula* are not modeled, they are all connected to one and the same rigid body ("root"). Same holds true for the distinct metacarpal bones of the hand, which are modeled as one rigid body "palm".

**Table 1: Implemented Hill muscles**

<b>Name</b>	<b>Origin</b>	<b>Insertion</b>	<b>action</b>
Infraspinatus	<i>Scapula</i>	<i>Humerus</i>	external rotation <i>Humerus</i>
Coracobrachialis	<i>Scapula</i>	<i>Humerus</i>	Internal rotation, <i>adduction</i> , anteversion <i>Humerus</i>
Deltoid Posterior	<i>Scapula</i>	<i>Humerus</i>	<i>abduction Humerus</i> (along frontal plane). Shoulder <i>extension</i> , lateral rotation
Deltoid Middle (lateral)	<i>Scapula</i>	<i>Humerus</i>	<i>abduction Humerus</i> (along frontal plane), transverse abduction
Deltoid Anterior	<i>Clavicle</i>	<i>Humerus</i>	<i>abduction Humerus</i> (along frontal plane), shoulder <i>flexion</i> ,medially rotation <i>Humerus</i>
LatissimusDorsi	multiple	<i>Humerus</i>	Internal rotation, <i>adduction</i> , retroversion <i>Humerus</i>
PectoralisMajorClavicular	<i>Clavicle</i>	<i>Humerus</i>	<i>anteversion</i> , <i>adduction</i> , internal rotation

PectoralisMajorSternal	Sternum / ribs	<i>Humerus</i>	<i>anteversion, adduction, internal rotation</i>
SubScapularis	<i>Scapula</i>	<i>Humerus</i>	<i>internal rotation, adduction</i>
Supraspinatus	<i>Scapula</i>	<i>Humerus</i>	<i>abduction, external rotation</i>
TeresMajor	<i>Scapula</i>	<i>Humerus</i>	<i>internal rotation, adduction, retroversion</i>
TeresMinor	<i>Scapula</i>	<i>Humerus</i>	<i>external rotation, adduction, retroversion</i>
Biceps brachii short head	<i>Scapula</i>	<i>Radius</i>	<i>supination forearm, flexion ellbow</i>
Biceps brachii long head	<i>Scapula</i>	<i>Radius</i>	<i>supination forearm, flexion ellbow</i>
Brachialis	<i>Humerus</i>	<i>Ulnar</i>	<i>flexion ellbow</i>
Brachioradialis	<i>Humerus</i>	<i>Radius</i>	<i>flexion ellbow, pronation / supination</i>
PronatorTeresHumoral	<i>Humerus</i>	<i>Radius</i>	<i>pronation</i>
PronatorTeresUlnar	<i>Ulnar</i>	<i>Radius</i>	<i>pronation</i>
SupinatorHumoral	<i>Humerus</i>	<i>Radius</i>	<i>supination</i>
SupinatorUlnar	<i>Ulnar</i>	<i>Radius</i>	<i>supination</i>
TricepsBrachiiLateral	<i>Humerus</i>	<i>Ulnar</i>	<i>extension ellbow</i>
TricepsBrachiiLong	<i>Scapula</i>	<i>Ulnar</i>	<i>extension ellbow</i>
TricepsBrachiiMedial	<i>Humerus</i>	<i>Ulnar</i>	<i>extension ellbow</i>
ExtensorCarpiRadialisBreve	<i>Humerus</i>	Meta-carpus	<i>Elbow extension, dorsal flexion wrist, abduction hand</i>
ExtensorCarpiRadialisLongus	<i>Humerus</i>	Meta-carpus	<i>Elbow flexion, dorsal flexion, radial abduction</i>
ExtensorCarpiUlnaris	<i>Humerus</i>	Meta-carpus	<i>Ulnar abduction</i>
FlexorCarpiRadialis	<i>Humerus</i>	Meta-carpus	<i>Palmar flexion, radial abduktion, (pronation)</i>
FlexorCarpiUlnaris	<i>Humerus</i>	Meta-carpus	<i>Palmar flexion, Ulnar abduction</i>
PalmarisLongus	<i>Humerus</i>	Meta-carpus	<i>palmar flexion</i>

As described in chapter 2.1, the human shoulder joint is quite complex and actually consists of four individual joints between *Humerus*, *Scapula* and *Clavicle*. In the simulation

model, the shoulder joint is simplified by a spherical joint (between *Humerus* and root). The test setups in the motion lab described in this work were designed in a way that the shoulder itself was kept in position and the range of motion that was utilized did not exceed the limits of the *Glenohumeral* joint (shoulder *flexion / extension*, *adduction* and *abduction*). The human *Glenohumeral* joint is formed between the ball of the *Humerus* which moves in a socket of the *Scapula*, and can by that be approximated by a ball and socket joint.

The Elbow joint is modelled as two successive revolute joints between forearm and *Humerus*, which allow an elbow *flexion / extension* and a *pronation / supination* of the forearm. The forearm itself is modelled by two rigid bodies (*Ulnar* and *Radius*), which cannot move relative to each other. The palm of the hand is model by one rigid body which is connected to the forearm by two successive revolute joints again, allowing a *radial / ulnar* deviation as well as a *flexion / extension* of the hand. Each finger is modelled as three rigid bodies, connected to each other respectively the palm by one revolute joint. Fingers in humans are controlled by the muscles of the forearm, which are connected to the fingers by long flexor tendons. This is not implemented in this arm model, so that the fingers can only be actuated by joint torques. The seven DOF of the shoulder, elbow and wrist can be controlled by the included muscles.

### 3.5.3 Hill muscle model

As muscle model, a string type Hill model [Hill 38] variant as suggested by [Maas 13] is used that consists of a contractile component (CC) and a parallel elastic component (PEC) (see Figure 26).

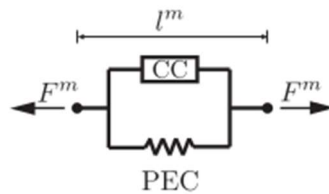


Figure 26: Hill muscle model. From [Roller 17].

To simulate the natural characteristic of muscular force generation (see Chapter 2.1), the pulling force  $F^{CC}$  created by the CC depends on the actuation level  $a \in [0,1]$ , the length of the muscle ( $l^m$ ), the contraction velocity ( $\dot{l}^m$ ) and the maximum isometric force and is given by  $F^{CC} = f_l(l^m)f_v(\dot{l}^m)aF_{max}$ . The length and the velocity dependency are approximated by

$$f_l(l^m) = 1 - \frac{(l - l_{opt})^2}{(l_{opt} - l_0)^2} \quad f_v(\dot{l}^m) = \begin{cases} \frac{v_{max} - v}{v} & v \geq 0 \\ v_{max} + \frac{v}{\gamma} & v < 0 \end{cases} \quad (4)$$

and depicted in Figure 27. Here  $l_0$  represents the minimal and  $l_{opt}$  the optimal muscle length. The negative scalar  $v_{max} < 0$  is the maximal contractive velocity of the muscle, and  $\gamma$  is a shape factor, while  $A, B, C \in \mathbb{R}$  are chosen such that the function is differentiable in  $0$  [Roller 17].

The PEC, a linear elastic spring which is connected in parallel to the CC, represents the passive stiffness of the tissue and is given by  $F^{PEC} = k(l - l_0)$  with stiffness  $k \in \mathbb{R}_+$ . The muscle force  $F_m$  is achieved by linear superposition of  $F^{PEC}$  and  $F^{CC}$  so that

$$F_m = F^{PEC} + F^{CC} = k(l - l_0) + f_l(l^m)f_v(l^m)aF_{max} \quad (5)$$

The muscles are connected to the MBS through at least two body points (between which they build a straight line) and can be led over via points to adjust the muscle paths.

The muscles are directly included in the simulation scenario (in contrast to approaches where motions e.g. are generated by using joint torques and the muscle loads needed to generate these torques are calculated in a post processing step). This allows the optimization to directly optimize on the biomechanical muscle parameters and consider dynamic quantities like e.g. the force velocity dependency.

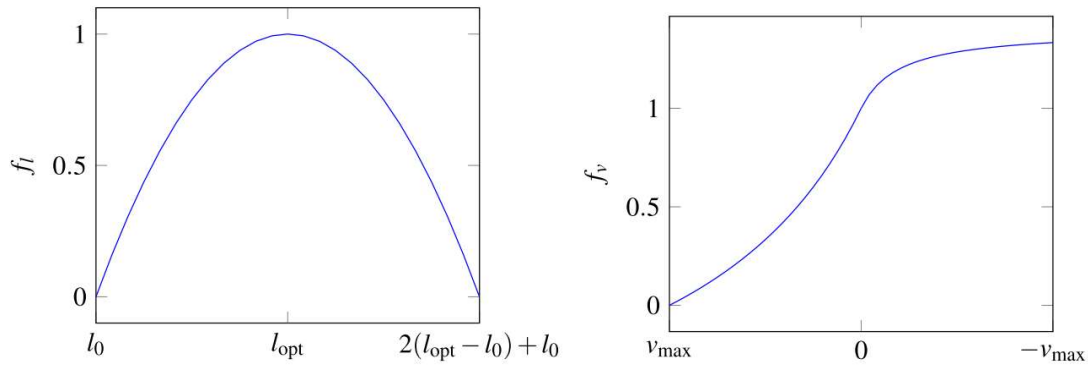


Figure 27: Force length and force velocity dependency of the implemented Hill muscle model.

### 3.6 Optimal control framework

The optimal control theory is a special class of infinite optimization problems on function spaces [Gerdt 11] and is a control strategy that is quite attractive in the application of DHM actuation. It deals with finding a control law for the described biomechanical multibody system such that a certain optimality criterion is fulfilled. The optimality criterion is brought into the system by an *objective function* (a.k.a. *cost function*) that is minimized. Emanuel Todorov explains in a review article that “optimal control models of biological movement have explained behavioral observations on multiple levels of analysis (limb trajectories, joint torques, interaction forces, muscle activations or EMGs) and have arguably been more successful than any other class of models” [Todorov 04.]. The OC framework used for motion generation in this thesis was preexisting [Leyendecker 10, Roller 17, Björkenstam 18], so it’s (mathematical) functionalities are only shortly summarized in the following.

The OC framework calculates the actuation or control signals (joint torques  $t_i$ , muscle actuations  $a_i$  or synergy weights  $c_i$  – see chapter 3.2) in a way, that a certain goal is fulfilled while minimizing the defined objective function and considering the side conditions that the constrained equations of motion of the MBS are fulfilled. For the MBS

used to model biomechanical DHMs in this work, the set of governing equations can be stated as follows:

$$\text{Minimize } J = \int_{t_0}^{t_F} \phi(q, \dot{q}, u) dt + \chi(q|_{t_0}, q|_{t_F}, t_0, t_F), \quad (6)$$

$$\frac{\partial L}{\partial q}(q, \dot{q}) - \frac{\partial}{\partial t} \frac{\partial L}{\partial \dot{q}}(q, \dot{q}) + F(q, \dot{q}, u) + G^T(q)\lambda = 0, \quad (7)$$

$$g(q) = 0, \quad (8)$$

$$c^- \leq c(q, u, \lambda) \leq c^+. \quad (9)$$

The main goal, minimizing the objective function  $J$ , is introduced in (6). The function  $J$  is split in the function  $\phi$ , which is a measure of the state of the system in the interval  $I = [t_0, t_F]$ , and  $\chi$  is only rating the bounds of  $I$ . The vector  $q$  collects the configuration variables of the multibody DHM as a function of time, such that  $q(t)$  represents the trajectory of DHM configurations in its configuration space. The function  $u$  represents an external actuation ( $t_i$ 's or  $a_i$ 's)

The Lagrangian  $L$  of the system is given by  $L = T - V$ , where  $T$  is the kinetic energy and  $V$  the potential energy. As side condition, the constrained equations of motion (7) and (8) have to be fulfilled by the mappings of  $q(t), u(t)$  and  $(t)\lambda$ , whereas  $\lambda$  are the Lagrangian multipliers associated to the constraints  $g(q) = 0$  (8).  $F$  represents non-conservative external forces acting on the system and  $G$  is the constraint Jacobian  $G = \partial g / \partial q$ , whereas  $g$  are additional holonomic constraints which have to be fulfilled when a closed loop occurs in the MBS (e.g. at the box lift, see chapter 6). By (9), additional equality and inequality constraints are included into the optimal control problem, whereas  $c^-$  is the lower and  $c^+$  the upper bound of the constrained function  $c$ . This is a generic description for many different constraints as e.g. box constraints on the controls or path constraints. Further on, the time interval for the motion can be defined, or  $t_0$  and  $t_F$  can be set as unknown variables (constrained to limits, for more details see [Roller 17]).

In contrast to most other control strategies, the goal can be described in a quite generic manner and no further control signals have to be defined. It is sufficient to describe the start and the end configuration of the multibody system, and all further control signals are an output of the OC framework. This is e.g. done for the arm model in the *basic reaching test* (see chapter 4), where the start and end posture of the arm model are defined (at zero velocity), and by setting "*minimal time*" as *cost function*, the OC framework calculates the according actuation signals to move the MBS from the start to the end configuration as fast as possible. In this simulation environment, the time continuous OC problem is discretized by the DMOCC approach [Leyendecker 10] where a variational integrator is used to solve the equations of motion. The resulting finite dimensional optimization problem is solved with the interior point method implemented in the solver IPOPT [Wächter 06].

The pre-existing OC framework has been developed on the basis of previous works [Leyendecker 10, Roller 17, Björkenstam 18], so its development is not part of this work.



Instead, in this thesis it is regarded as “black box” used for motion generation, and part of this thesis is to investigate the properties of the framework. Depending on the defined inputs (e.g. cost function, Actuation Modes), the resulting outputs (motions) are compared or validated against measured motions from humans. The defined input values and investigated outputs of the OC framework are depicted in Figure 28. In detail, these are the following:

### Inputs

- **Cost Function:** As cost function, or objective function, four different functions which are minimized as described in (6) can be defined. These cost functions can be linearly combined to create a mixed cost function. This allows to utilize them in a “controller like manner” and exploit the influence of each objective function to the resulting outputs. The implemented cost functions that can be minimized are:
  - Time:  $J^t = t^f - t^0$   
The optimizer tries to fulfill the defined goal as fast as possible.
  - Kinetic energy:  $J^T = \int_{t^0}^{t^f} T dt$   
The optimizers minimizes kinetic energy.
  - Control:  $J^u = \int_{t^0}^{t^f} u \cdot u dt$   
The signals used to actuate the simulated model are minimized. Depending on the used Actuation Mode, this are the joint torques ( $t_i$ 's) or the muscle activations ( $a_i$ 's). (When the model is actuated via muscle synergies (AM-S), the optimizers tries to find a set of weights ( $c_i$ 's) which as well minimize the resulting muscle activations ( $a_i$ 's)).
  - Control change:  $J^{\dot{u}} = \int_{t^0}^{t^f} \dot{u} \cdot \dot{u} dt$   
The optimizer minimizes the time derivatives of the used controls (see previous point)
  - Mixed:  $J^{mix} = c^t J^t + c^T J^T + c^u J^u + c^{\dot{u}} J^{\dot{u}}$   
The optimizer minimizes a linear combination of the above described cost functions.
- **MBS Model:** The description of the simulated model. This comprises the defined rigid bodies (including geometries, length, diameter, masses, orientations), the defined joints (including joint type and limits of the defined range of motion). Additionally the used actuators as joint torques (rotation axis, min and max torque) or muscles (origin, via points, attachments and all muscle parameters as described in 3.5.3).
- **Actuation Mode:** The defined model can be actuated by three different Actuation Modes.
  - AM-T: The model is actuated via joint torques.
  - AM-M: The model is actuated via the implemented Hill muscles. In AM-M, each distinct Hill muscle can be controlled independently.
  - AM-S: The model is actuated via the implemented Hill muscles. In AM-S, some muscles are grouped to muscle synergies, so they cannot be activated

independently. Those muscles not included in the defined synergies are treated as in AM-M.

- **Bounds:** The boundary conditions define the start configuration and the goal of the simulated task as well as restrictions for the motion. So, *left bounds* define the start configuration of the simulation model, e.g. angles of joints or orientations of the rigid bodies. *Right bounds* define the desired goal, e.g. by setting the complete configuration of the model (angles, orientations), or just by defining a certain point on a rigid body to match a point in the room or reach over a certain height (z-value) in the global coordinate system. Further on, boundary conditions active during the whole simulation can be defined, e.g. for a joint angle to not exceed a *min* and *max* value. All tests performed in this thesis start at zero velocity and end at zero velocity. All the defined boundary conditions used for simulation are described in the according tests
- **Time Steps:** This defines the number of steps for the discretization of the OC problem. Most simulations performed in this thesis are performed with between 20 and 50 steps, which resulted in smooth looking motions when assessing video data. At all performed Test Scenarios, several simulations were performed with up to 250 steps, to ensure that the OC solver does not converge to a different solutions.
- **Time Interval:** The minimum values  $t_F^{min}$  and maximum values  $t_F^{max}$  for the simulation time (interval  $[t_0, t_F]$ ) can be defined. In all simulations performed in this thesis the start time and values for the minimum time are set to zero ( $t_F^{min} = t_0 = 0$ ). The maximum values  $t_F^{max}$  are in most simulations not reached, so they result as output ( $t_F$ ). If the limit ( $t_F^{max}$ ) is reached, this is always mentioned when discussing results.

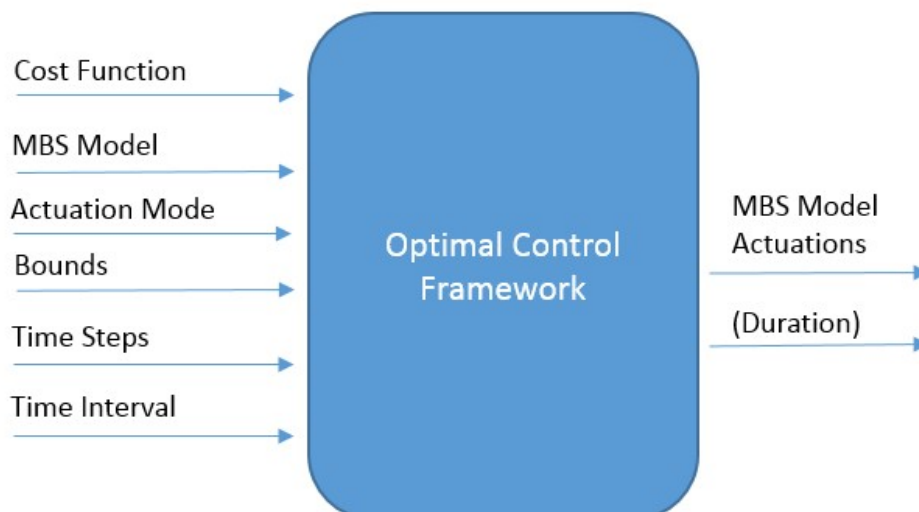


Figure 28: Black Box view of the optimal control framework used for motion generation.

## Outputs

- **MBS Model Actuations:** The OC framework calculates a series of actuation signals, which move the simulation model in a way, that the defined boundary conditions and the constrained equations of motion are fulfilled, while minimizing the given cost function. The number of actuation signals equals the number of discretization steps. In AM-T, a series of joint torque actuation signals ( $t_i$ 's) is calculated and in AM-M a series of Hill muscle actuations ( $a_i$ 's). In AM-S the output is a series of weights ( $c_i$ 's), which multiplied with the synergy matrices result in the Hill muscle actuations which finally actuate the model.
- **Duration:** The value for the total duration ( $t_F$ ) for a performed simulation result from the OC solver. As described above, minimum values  $t_F^{min}$  and maximum values  $t_F^{max}$  can be defined as inputs. So, in cases where duration equals the defined maximum values ( $t_F = t_F^{max}$ ), the duration is not a "real" result of the simulation. If this is the case, it is mentioned when discussing results.

In the following chapters, the derived control and validation approach is applied to several use cases. At the *basic reaching test* (chapter 4), minimal time is used as cost function in all tests for simulation, as test persons in the motion lab are advised to move as fast as possible. At the *weight lift test* (chapter 5), the influence of the distinct cost functions is investigated in more detail and a mixed cost function derived. With the *box lift test*, a use case from industry is simulated in the end, to check if the derived control parameters and the entire control approach can be applied to more complex use cases.

## 4 The basic reaching test

The first practical experiment that is realized is the *basic reaching test*. In this test, a multitude of different reaching motions is performed in the motion lab and the EMG values of the involved arm and shoulder muscles as well as the used trajectories are captured. The test setup is chosen in a way which is expedient to investigate distinct aspects.

To examine if EMG values of one and the same task are reproducible, each distinct reaching motion is performed five times. This allows to investigate if characteristics of muscle activations remain similar within repetitions, respectively if a consistent characteristic can be measured with EMG. This obviously is a basic requirement if control parameters should be derived from measured signals. Further on, if a basic characteristic remains recognizable within repetitions, this allows to identify appropriate parameters for EMG post processing like e.g. adequate cut off frequencies of the used low pass filter, which eliminate spikes but keep the basic nature of the signal. The multitude of different reaching motions allows to extract muscle synergies from different subsets of motions (Matrix  $M_e$ , see chapter 3.4.1), and check if measured EMG signals of reaching motions that were not included in the Matrix  $M_e$  can also be reproduced with these synergies. This is done to validate if the extracted synergies have a certain generality. Comparing the "goodness" of the muscle synergies extracted from distinct subsets of reaching motions, can also help to identify an adequate or minimum number of motions which is necessary to extract meaningful muscle synergies. This can help to plan test setups for future experiments.

Another important aspect is to validate simulated reaching trajectories and velocity profiles against those that are measured, and to investigate the influence of the used Actuation Mode in the simulation model. Therefore, additional optical markers are placed at the hand, to get detailed information of the chosen trajectories of the hand. The target points for the reaching motions are adapted to the anthropometry of the test persons (see test setup below). The idea behind this is to get motion data of different test persons comparable. By that it can e.g. be checked if different test persons use similar trajectories to reach a point, that is located in the sagittal plane in the height of the shoulder with a distance of 90% of the reaching range. In contrast, if test persons with different anthropometries (e.g. body height and arm length, leading to strongly deviating reaching ranges when keeping the shoulder in position) would reach for one and the same point with an absolute distance similar in all test, the reaching motion and final joint orientations would obviously strongly differ.

### 4.1 Motion Lab measurements

#### 4.1.1 Test setup

The Experimental design is defined as follows. The test person stands in front of a plane with 17 marked target points on it (Figure 29 *left*). The arrangement of these points is adjusted to the test persons anthropometry as depicted in Figure 29 *middle left*. The inner *Radius* ( $R_i$ ) corresponds to the upper arm length, the outer *Radius* ( $R_a$ ) equals 90% of the maximal reachability ( $R_{\max\_reac}$ ) of the test person. The maximal reachability is estimated, in frontal position and in distance  $d_1$  (see below) to the test plane, as follows:

The subject is instructed to move the tip of the middle finger to the highest reachable point on the plane while keeping his trunk and the center of the shoulder joint in position. This is repeated for the lowest reachable point as well as those being most far to the right and the left on the horizontal line in the height of the shoulder. From the four resulting distances the smallest one is defined as  $R_{\max\_reach}$  (whereas all of them are in the same range).

The target points are placed on the intersections of  $R_i$  and  $R_a$  with the horizontal and the vertical lines and their bisectrices. The center of  $R_i$  and  $R_a$  is positioned concentric with the center of the shoulder joint (projected to the plane) in a relaxed and upright standing position. Two distances are specified between the plane and the test person ( $d_1$  and  $d_2$ ) which are also determined based on the test persons anthropometry as shown in Figure 29 *middle right*. Distance  $d_1$  corresponds to the length of the forearm whereas  $d_2$  is defined as the distance between the subject and the plane when standing in a frontal position to the plane with the forearm parallel to the ground and the angle  $\alpha = 45^\circ$  between the upper arm and the subjects coronal plane.

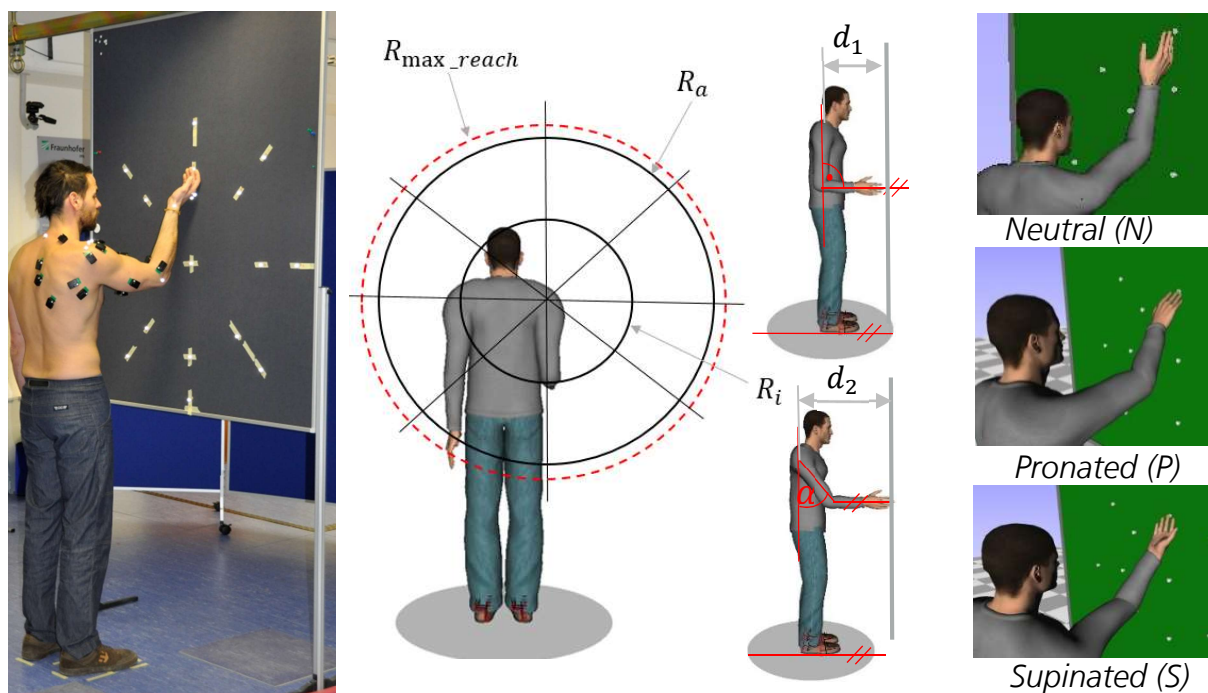


**Figure 29:** The basic reaching test: (left) Test execution in the motion lab; (middle left) the three final hand orientations; (middle right) adaption of the target point placement to the test persons anthropometry; (right) distances  $d_1$  and  $d_2$  to the measuring plane, adapted to the test persons anthropometry.

The test is executed as follows. Twelve different **Test Scenarios** (TS1 - TS12) are performed, which are shown in Table 2. In all scenarios the test persons are instructed to stand in a straight and upright posture at the marked positions on the ground with the arms hanging relaxed in a natural position. Tests are performed from two distances ( $d_1$  and  $d_2$ ) and two distinct orientations to the test plane (frontal and lateral). In the frontal positions the subjects coronal plane is parallel to the test plane, in lateral positions the subjects sagittal plane is parallel to the test plane (right arm oriented towards the test

plane). The test persons are instructed to move the tip of the middle finger (after the start signal) quickly to the target point on the plane and keep it in the final position for about one second. We define three final hand orientations: Neutral (N), pronated (P) and supinated (S) as seen in Figure 29. Additionally we make measurements with a weight cuff adjusted to the test person's wrist (1kg). Each task is repeated five times. The start signal just indicates that data recording started, the timing (start, end, holding time) for each repetition is not restricted by signals and freely chosen by the test persons. The subjects are advised to keep shoulder and trunk in position while moving the arm. A palmar *flexion* and a dorsal *extension* of hand and fingers as well as an *Ulnar* abduction and a radial abduction should be avoided (which means that the forearm, hand and fingers should be kept stiff as one rigid body). The motions are not restricted by any kind of apparatus to keep them natural.

**Table 2: The different scenarios of the basic reaching test**

	<i>Distance</i>	<i>Weight</i>	<i>Orientation</i>	<i>Number Target Points</i>	<i>Hand pos.</i>
<i>Test scenario 1</i>	$d_1$	No	Frontal	17 (P1-P17)	N
<i>Test scenario 2</i>	$d_1$	No	Frontal	17 (P1-P17)	P
<i>Test scenario 3</i>	$d_1$	No	Frontal	17 (P1-P17)	S
<i>Test scenario 4</i>	$d_2$	No	Frontal	9 (P9-P17)	N
<i>Test scenario 5</i>	$d_2$	No	Frontal	9 (P9-P17)	P
<i>Test scenario 6</i>	$d_2$	No	Frontal	9 (P9-P17)	S
<i>Test scenario 7</i>	$d_2$	No	Lateral	5 (P1,P5,P9,P13,P17)	N
<i>Test scenario 8</i>	$d_2$	No	Lateral	5 (P1,P5,P9,P13,P17)	P
<i>Test scenario 9</i>	$d_2$	No	Lateral	5 (P1,P5,P9,P13,P17)	S
<i>Test scenario 10</i>	$d_1$	Yes (1kg)	Frontal	17 (P1-P17)	N
<i>Test scenario 11</i>	$d_2$	Yes (1kg)	Frontal	9 (P9-P17)	N
<i>Test scenario 12</i>	$d_2$	Yes (1kg)	Lateral	5 (P1,P5,P9,P13,P17)	N

In the Test Scenarios 1 to 3 the subjects are standing in frontal position to the test plane in distance  $d_1$ . Reaching motions to all 17 target points are measured, each point with the three final hand orientations and without weight. The labeling of the target points is depicted in Figure 30. In the scenarios 4 to 6 the subjects are standing in frontal position to the test plane in distance  $d_2$ . As the maximal reachability is determined in distance  $d_1$ , only the target points on the inner circle (P9-P17) are measured. Again each point with the three above described different final hand orientations and without extra weight. In scenario 7 to 9 the subjects are standing in lateral position to the test plane in distance  $d_2$ . Target motions to the target points on the vertical line are measured (P1, P5, P9, P13, P17), each point with the three different final hand positions and without weight. In scenarios 10 -12 we made measurements with the weight cuff adjusted to the subjects hands. In scenario 10 the subjects are standing in frontal position to the test plane in distance  $d_1$  and target motions to all 17 target points are measured with a neutral final hand position. In Test Scenario 11 the subjects were standing in frontal position to the test plane in distance  $d_2$  and target points on the inner circle (P9-P17) are measured with a neutral final hand position. In the last scenario the subjects are standing in lateral position to the test plane in distance  $d_2$  and target motions to the points on the vertical line are measured (P1, P5, P9, P13, P17) with a neutral final hand position. In sum, 124

*distinct motions* (tasks) are measured whereas every motion is repeated and recorded five times (repetitions).

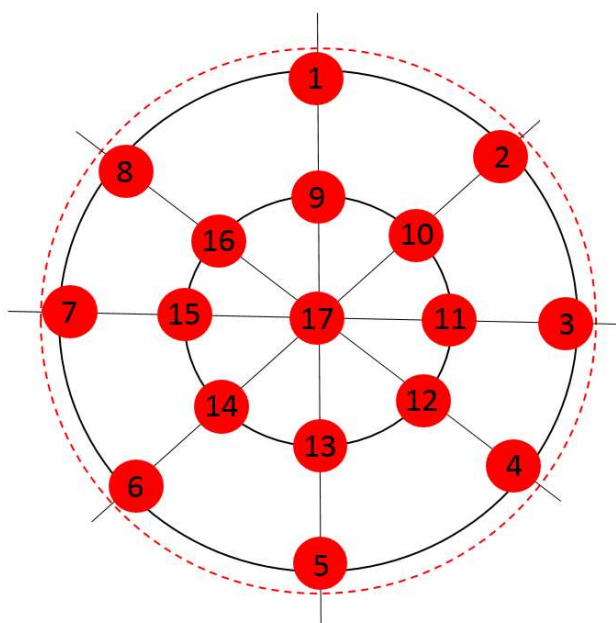


**Figure 30: Labeling of the target points P1-P17.**

To have values for normalization of the measured EMG signals, the *maximal voluntary contraction (MVC)* of the measured muscles are estimated as well. Therefore the EMG values are measured when performing the MVC tests as described in [Konrad 11]. The MVC test were performed directly after test execution of the basic reaching test.

During test execution, the following data is acquired. In all Test Scenarios the position of the right hand, forearm, upper arm, shoulder and the thorax as well as the placement of the target points and the activity of 16 involved arm and shoulder muscles are recorded. The positions are tracked with an optical motion capture system (Qualisys, 9 cameras, Oqus 400 and Oqus 310+) with an accuracy of < 1mm and a sample frequency of 240Hz. The Markers on the test persons are placed according to the recommendations of the international society of Biomechanics (ISB) as described in [Wu 05]. Additional markers are placed on the hand, to get a higher resolution of hand motions. Palpation of anatomical landmarks is accomplished manually, following the guidelines of [Van Sint Jan 07]. Additionally, marker are placed on each of the 17 target points on the test plane to be able to assess the characteristics of close-to-goal velocities / trajectories and the influence of motion precision. The surface EMG signals are acquired with a wireless 16-channel Delsys system with a sample frequency of 2000Hz. The measured muscles are listed in Table 3. The EMG sensor locations were chosen following the recommendations of SENIAM and Konrad [Freriks 99, Konrad 11, SENIAM]. Before applying the sensors, the skin is shaved, cleaned with alcohol and rubbed with abrasive gel as recommended in [Freriks 99]. Data recording (motion data as well as EMG signals) for each task started with a signal about one second before the first motion and was recorded continuously during all repetitions of each task.

The trapezius muscle (Channels 1-3) is also involved in the measured muscles, also this muscle does not count as arm or shoulder muscle (it is part of the shoulder girdle). It is a large paired surface muscle that extends laterally to the spine of the *Scapula* and

longitudinally from the occipital bone to the lower thoracic vertebrae of the spine. Its main function is to stabilize and move the *Scapula*, and by that support the arm and shoulder muscles. By moving the *Scapula* upwards to the side, the arm can e.g. be moved over the horizontal. As the *Scapula* is not modelled in the simulation model, the *Trapezius* muscle is not included in the simulation model neither (as it has insertion points on the *Scapula*). The main function of the *Trapezius* muscle is to stabilize and move the *Scapula*. It was still decided to measure the EMG signals of this muscle and include the signals for muscle synergy extraction, as this muscle is always involved in shoulder or arm motions, and by that could be involved in corresponding muscle synergies.

**Table 3: List of measured muscled**

EMG Sensor	Muscle	Short name
01	M. trapezius desc.	TraDesc
02	M. trapezius transv.	TraTrans
03	M. trapezius ascend.	TraAsc
04	M. deltoideus clavicularis (ant.)	DeltAnt
05	M. deltoideus acromialis (med.)	DeltMed
06	M. deltoideus spinalis (post.)	DeltPost
07	M. biceps brachii	Bic
08	M. triceps brachii longus	TriLong
09	M. triceps brachii lateralis	TriLat
10	M. brachioradialis	BrRad
11	M. pectorialis major clavic.	PectClav
12	M. pectorialis major sternal	PectSter
13	M. infraspinatus	InfraSp
14	M. teres major	TeresM
15	M. latissimus dorsi	LatDors
16	M. pronator teres	PronTer

The basic reaching test is executed with two right handed males in the age of 25 and 35 after giving their informed consent. No (pre-existing) injuries or impairments of the skeletal and locomotor system of the arm and upper body were known at the time of test execution.

#### 4.1.2 Measured Trajectories

In the following plots, the trajectories and velocity profiles of the marker HL3R of one test person are shown. The marker is placed at the metacarpophalangeal joint of the middle finger as depicted in Figure 31 (*left*). The z-direction of the coordinate system for the plots points upwards, x-direction points into the viewing direction of the test person, and y-directions points to its left (Figure 31 *right*).

From distance  $d_1$  in frontal orientation, reaching motions to all 17 target points (TP) are measured. In Figure 32 the trajectories for Test Scenario (TS) TS1 (supinated final hand orientation (S)), TS2 (pronated final hand orientation (P)), TS3 (neutral final hand orientation (N)) and TS10 (weight cuff attached (W)) are plotted. For each point, one (arbitrary) repetition is depicted.



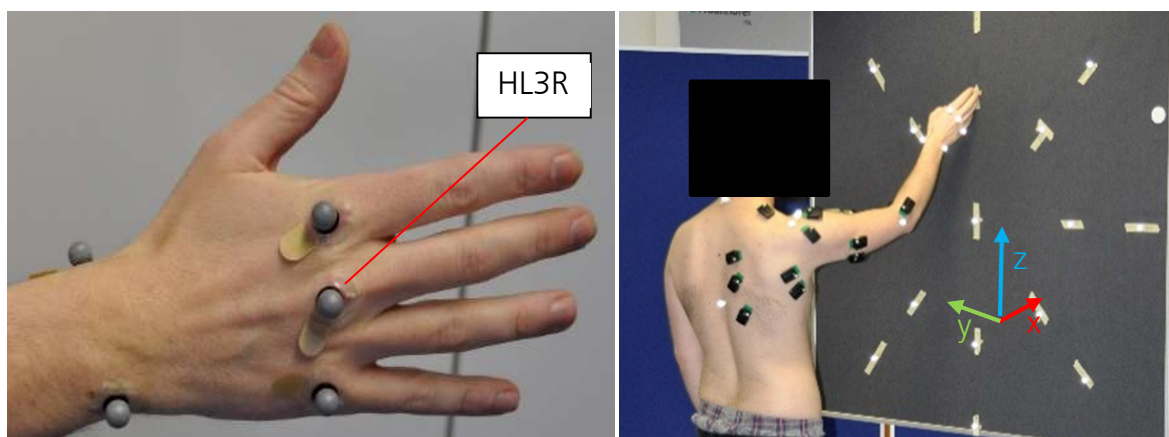


**Figure 31:** Position of optical marker HL3R (left) and coordinate system orientation (right) used for the plots of the measured trajectories.

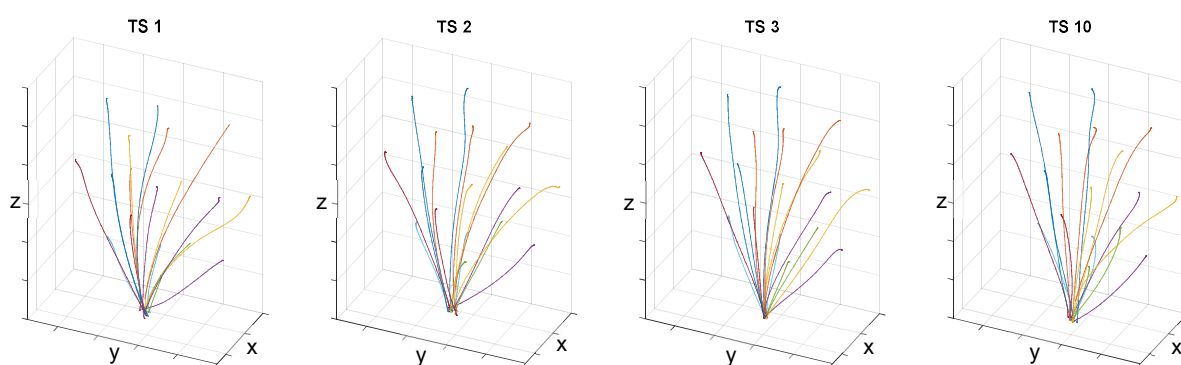


**Figure 32:** Measured reaching trajectories to all points from distance  $d_1$  and performed in a frontal orientation. Test Scenario TS1-3 (neutral, supinated and pronated final hand orientation) and TS10 (neutral final hand orientation, weight cuff attached to the wrist).

In Figure 33, the reaching motions from TS1 (S - blue line), TS2 (P - red line) TS3 (N - yellow line) and TS10 (W - purple line) to a single target point are compared (1<sup>st</sup> row TP1, 2<sup>nd</sup> row TP3 and 3<sup>rd</sup> row TP7). In the first column the 3D plots are depicted, in the second column the projection to the x-z plane (sideview from the right), in the third column the projection to the y-z plane (viewing direction of the test person) and in the fourth column the projection to the y-x plane is plotted (top view). The chosen trajectories do not differ a lot for the different Test Scenarios and lie in the range of variation that was measured in between single repetitions for one specific task. Hence, the final hand orientation as well as the weight cuff do not seem to influence the characteristics of the global trajectory. In all 2D projections, a more or less pronounced bow- to s-shape like characteristic of the measured trajectories can be observed. All Trajectories have a smooth appearance, without any sharp edges or sudden changes in direction.

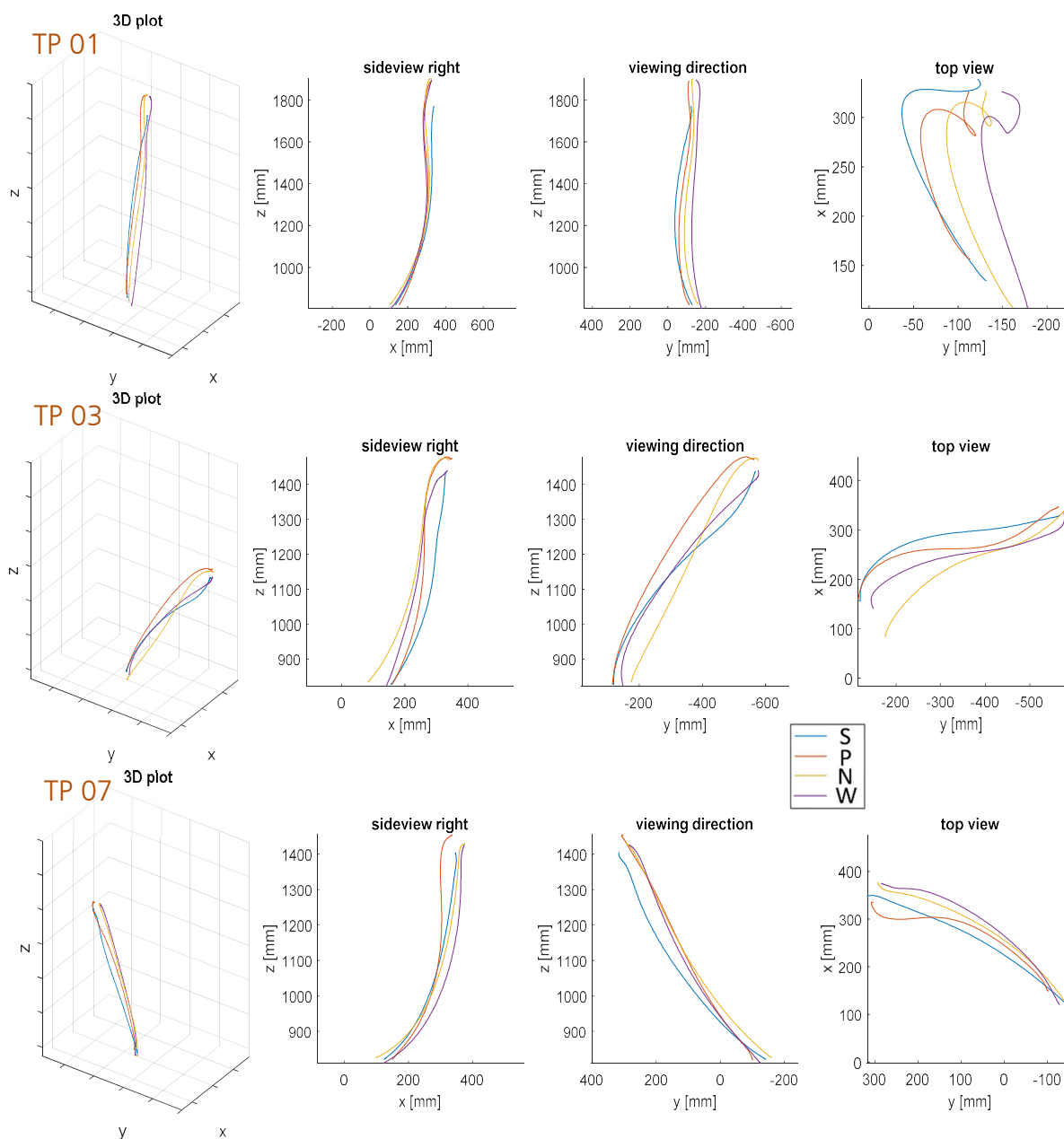


**Figure 33:** Measured reaching trajectories to target point TP1 (1<sup>st</sup> row), TP3 (2<sup>nd</sup> row) and TP7 (3<sup>rd</sup> row), for the different Test Scenarios. TS1 (neutral final hand orientation – yellow line), TS2 (pronated – red), TS3 (supinated – blue) and TS10 (neutral with weight cuff – purple).

From distance  $d_2$  in frontal orientation, only reaching motions to target points 09-17 are measured (as target points on the outer circle are out of reach when keeping the shoulder in position). In Figure 34, the trajectories for Test Scenario (TS) TS4 (supinated final hand orientation), TS5 (pronated final hand orientation), TS6 (neutral final hand orientation) and TS11 (weight cuff attached) are plotted. For each point, one (arbitrary) repetition is plotted.

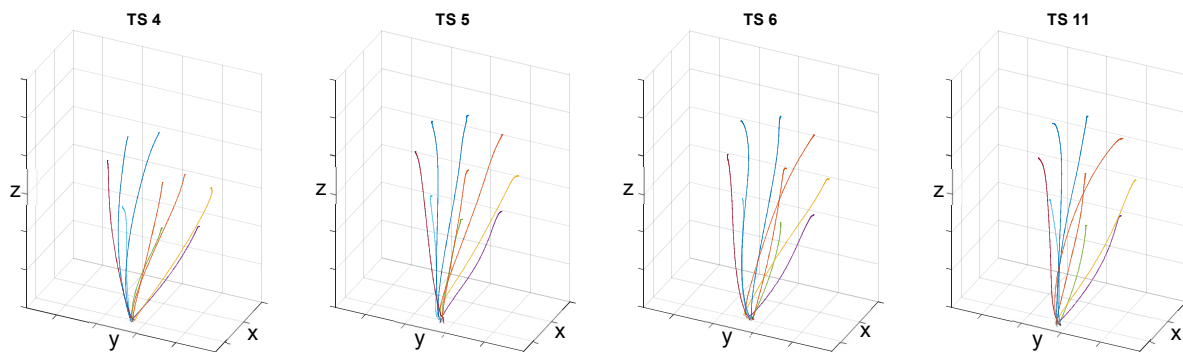


**Figure 34:** Measured reaching trajectories to all points from distance  $d_2$  and performed in a frontal orientation. Test Scenario TS4-6 (neutral, supinated and pronated final hand orientation) and TS11 (neutral final hand orientation, weight cuff attached to the wrist).

In Figure 36 and Figure 36, the reaching motions from TS4 (S - blue line), TS5 (P - red line), TS6 (N - yellow line) and TS11 (W - purple line) to a single target point are plotted (Figure 36 1<sup>st</sup> row TP9 2<sup>nd</sup> row TP11 and Figure 36 1<sup>st</sup> row TP13 and 2<sup>nd</sup> row TP15). In the first column the 3D plots are depicted, in the second column the projection to the x-z plane (sideview from the right), in the third column the projection to the y-z plane (viewing direction of the test person) and in the fourth column the projection to the y-x plane is plotted (top view).

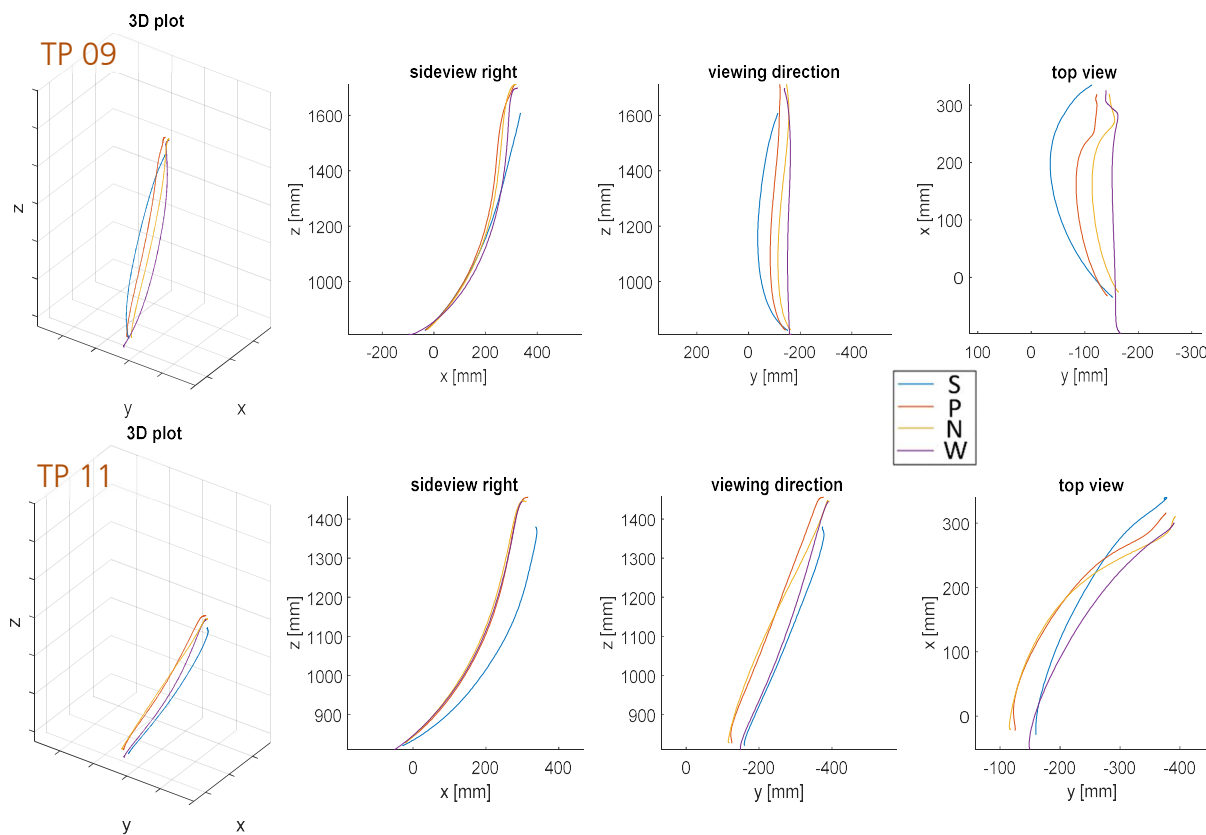


**Figure 35:** Measured reaching trajectories from Test scenario TS 4-6 and 11 to target point TP9 (1<sup>st</sup> row) and TP11 (2<sup>nd</sup> row).

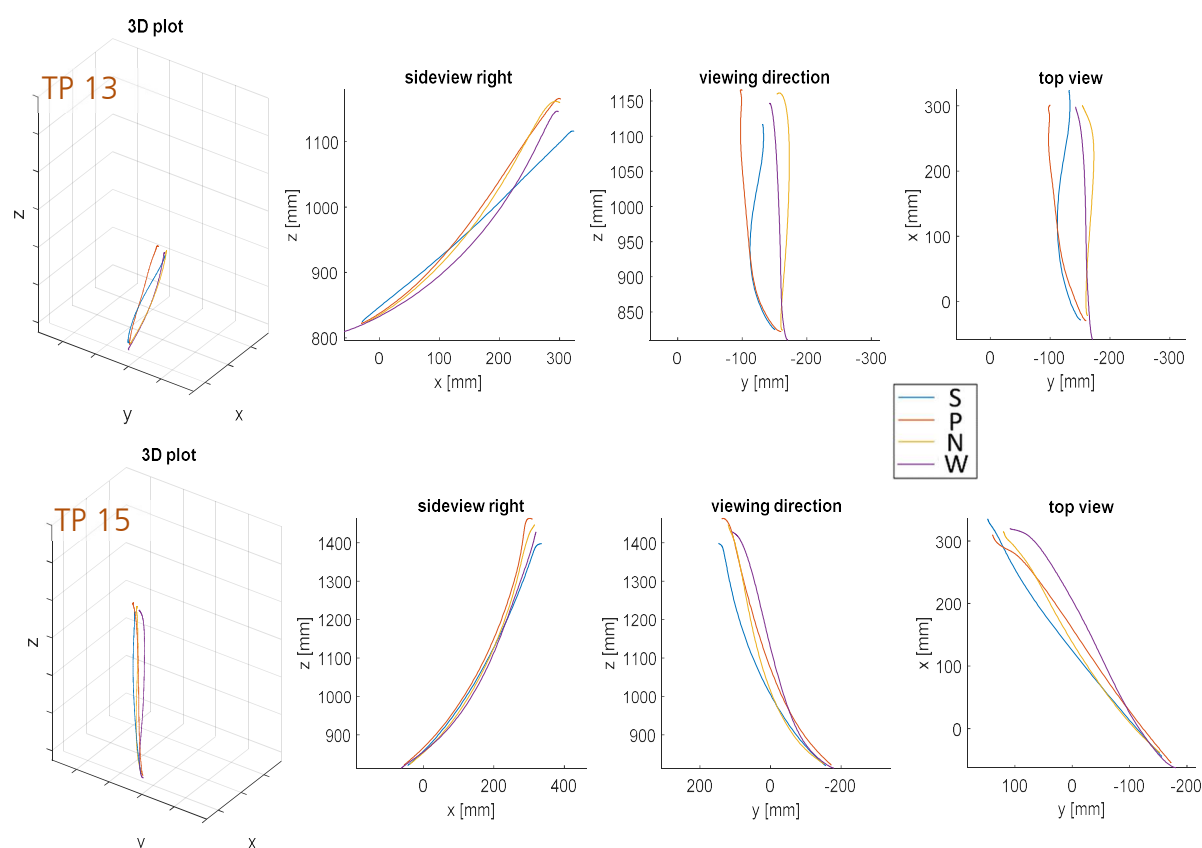


**Figure 36:** Measured reaching trajectories from Test scenario TS 4-6 and 11 to point 13 (1<sup>st</sup> row) and point 15 (2<sup>nd</sup> row). TS4 (neutral final hand orientation – yellow line), TS5 (pronated – red), TS6 (supinated – blue) and TS11 (neutral with weight cuff – purple).

The observed characteristics of the measured trajectories remain consistent for reaching motions from distance  $d_2$ . It can be said that reaching motions with a supinated final hand orientation have a slightly more distinct bow shape, especially for target points on the vertical line (see Figure 32 *left* (TS1), Figure 34 *left* (TS4) and top views TP 01, TP 09, TP 13 Figure 33 and Figure 36).

### 4.1.3 Measured velocity profiles

In Figure 37, the velocity profiles (absolute velocities) of reaching motions from distance  $d_1$  to TP 1-17 (*left*) and distance  $d_2$  to TP 9-17 (*right*) with a neutral final hand orientation are depicted. The velocity profiles have a bell shaped characteristic, whereas the peak velocity is reached at about one third of the duration. The maximum velocity increases with the distance between start- and end position of the hand, the maximum speed is reached at TP1 from distance  $d_1$ , and is about 3 m/s, i.e. about four times higher than the minimum velocity peak (0.7 m/s at TP 5). On the other hand, the duration of the motion for the shortest distance ( $d_1$ , TP 5, distance 25 cm, duration 0.8s) and the longest distance ( $d_1$ , TP 1, distance 109 cm, duration 1.1s) only varies by a factor of 1.38.

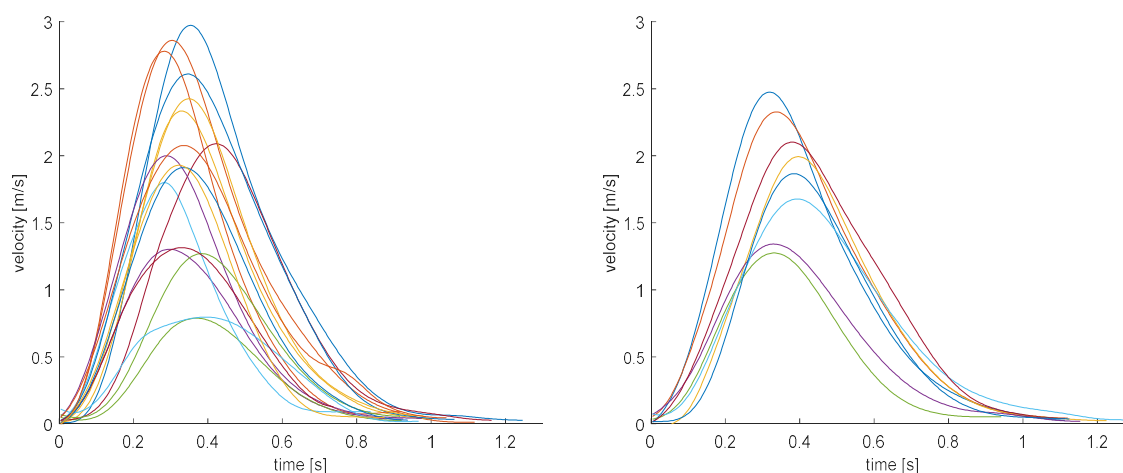


*Figure 37: Velocity profiles of measured reaching motions from distance  $d_1$  (left) and distance  $d_2$  (right).*

## 4.2 Measured EMG values

In Figure 38, the EMG values of all 16 measured muscles for five repetitions of one reaching task are plotted (Test scenario TS1 – target point TP 09). The EMG signals are normalized to the measured MVC values.

It is conspicuous that the signals of some muscles / repetitions do not start from zero. This can be explained by the fact that start- and end frames are chosen by visually identifying the beginning and end of the visible motion. The delay between activation of a muscle (measurable with EMG) and the force exerted on the bone (leading to a visible motion) is known as electromechanical delay (EMD). One explanation for the EMD is that the muscle has to take up the slack between all the connected tissues in the muscle and the tendons. There are several potential sources that might have an influence to the EMD values, like contraction speed and direction (eccentric / concentric), initial muscle length and (passive) tension, muscle fiber types (slow- and fast twitch fibers) and others. Published values for EMD in literature differ, e.g. for the knee extensor muscle between 18ms [Jöllenebeck 99] and 118ms [Horita 87]. Due to those uncertainties, it is hard to predict EMD values or use heuristic models for simulation of EMD values. There exist approaches with more complex Hill type muscle models which investigated to which extend these models can explain the electro-mechanical delay [Mörle 12]. In the Hill type muscle model used in this approach, EMD effect are not considered, meaning that an activation of the muscle directly leads to a force reacting on the rigid body it is connected to.

The measured EMG values show a high conformity in between the trials of the same task. This holds true for the height of the signal as well as the characteristic of the actuation signal in almost all measured muscles. This indicates that the measured actuation signals reflect the motor signals generated by the CNS, and that artefacts and other non-reproducible parts of the EMG signal are eliminated to the greatest extent by the applied filtering methods ( see chapter 3.3.2).

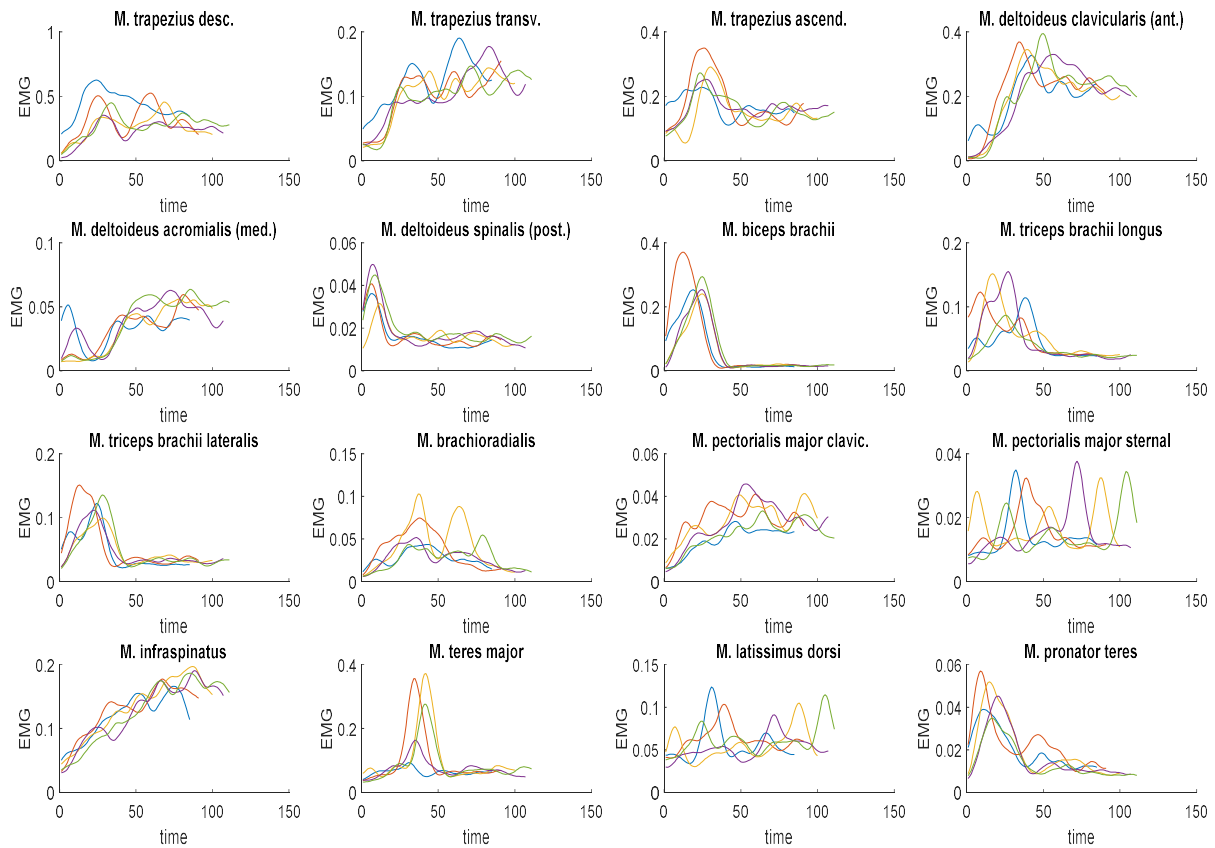


**Figure 38:** Measured EMG signals (normalized to MVC values) of Test Scenario TS1. Plotted are all five repetition of reaching motions to target point 09.

### 4.3 Muscle Synergy extraction

The raw EMG signals are processed in a customized software written in *Matlab* (Mathworks). As described above, the EMG data is acquired continuously during execution of all five repetitions of each tasks. The signals are then separated repetition-wise into single sequences by visually identifying the start and the end of each motion. As start, we define the first visible movement of the arm / shoulder from the hanging rest position, and the end of the motion is defined as the moment when the tip of the middle finger reaches the target point and movement comes to rest. In order to capture all EMG signals potentially involved in the motion generation process, 300 frames ( $\pm 0,15s$ ) before the first visible movement and after reaching the final hand position are included in each sequence. The EMG signals of each sequence are zero calibrated (by subtracting out the mean values), full wave rectified and low pass filtered (butterworth filter, cut off frequency 5 Hz, filter order 2) as described in chapter 3.3.2.

The EMG signals of each repetition are then arranged in the Matrix  $R_i$  (size  $n_t$  by  $n_m$ , where  $n_m$  is the number of measured muscles and  $n_t$  is the number of time samples of this repetition), that are concatenated vertically for muscle synergy extraction. In a first step, the NMF algorithm is applied to the Matrix  $M_{e.all}$ , which contains all measured tasks (and repetitions), providing two matrices  $C_{all}$  and  $W_{all}$  such that

$$M_{e\_all} := \begin{bmatrix} R_1 \\ \vdots \\ R_n \end{bmatrix}; M_{e\_all} = C_{all} \cdot W_{all} + residuals \quad (10)$$

As described in chapter 3.4.1, the number of muscle synergies ( $n_w$ ) is a free parameter of the NMF algorithm and has to be defined manually. To identify an appropriate number of synergies, the criterion based on the variance account for (VAF) is used in a first step. We calculate the VAF (see Figure 39) as described in (3) based on [Chiovetto 13] for values of  $n_w$  between one and sixteen (which equals the number of measured muscles  $n_m$ ), each by running the NMF algorithm 25 times to prevent it to converge to a local minima.

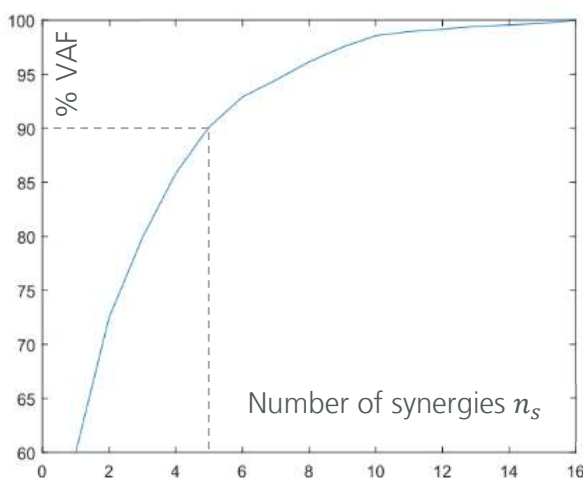


**Figure 39: Variance Account For (VAF) for a different number of muscle synergies.**

Commonly, the value for  $n_w$  is chosen where a certain threshold is reached (usually 90% VAF) or the graph of the cumulative VAF presents a significant change of slope. In our case, the 90% VAF threshold is reached with 5 synergies, which would reduce the number of actuators by two thirds. In Figure 40, the 5 synergies are depicted as bar plots, showing with which amplitude each muscle is involved in each synergy.

The muscle synergy hypothesis originates from neuroscience, and most approaches working with it aim on proving a control scheme of the CNS. Due to that, many of them only investigate the input-space side (measured EMG signals of natural or stimulated motions- see chapter 2.2). Only few studies focus on which impact e.g. a certain percentage VAF that cannot be reproduced has on the output-space side (actuation side, resulting motions) [Alessandro 13]. This becomes obvious, when thinking about that one synergy is already capable of reaching 60% VAF (Figure 39). On the output-space side, with only one synergy, the producible range of motion would be very poor and the number of reachable points in this test would probably far below 60%. The 90% VAF criterion is often substantiated by the statement that EMG measurements involve noise and artefacts, and due to that it would not be reasonable to aim on reproducing the measured signals with a higher accuracy.

Another property of an assessment criterion based on variance as in (3) as well as the NMF algorithm itself, is, that smaller values carry less weight (both based on mean square errors). This means that the NMF algorithm as well as the VAF criterion might “accept”

deviations between measured and reproduced EMG signals in cases (muscles), where the (normalized) magnitude of the measured signal is low (compared to other muscles).

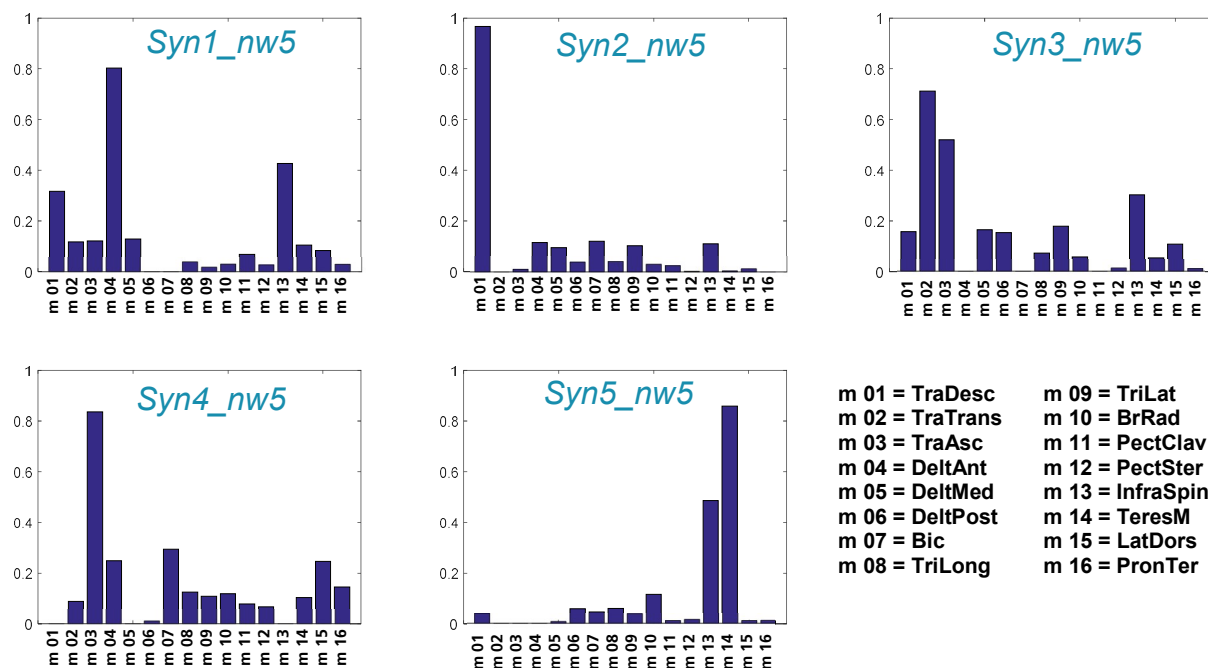


**Figure 40:** The five extracted muscle synergies that reproduce 90% VAF - all measured tasks used as input for the NMF algorithm (matrix  $M_{e\_all}$ ).

For the extracted synergies, this means that muscles that are present with high magnitudes in the extraction Matrix, will “try to” dominate a certain synergy (as it is important to reproduce the measured values of these muscles with a high accuracy as deviations here carry more weight). As soon as the number of synergies equals the number of dominant muscles, the VAF value will become high and the plot will show a significant change of slope. This is not necessarily wrong or undertheorized to reflect an underlying control principle of the CNS, but in our opinion it should be handled with care when assessing the “goodness” of the extracted synergies. In our estimation, EMG signals that have a clear and consistent characteristic within repetitions, should be well reproducible with the extracted muscle synergies, although they are present only with small magnitudes.

Therefore, the quality of the extracted synergies was additionally assessed by visually studying the measured and reproduced EMG signals. Therefore, the measured (and filtered) EMG signals are plotted for one task within all repetitions and compared with the signals created by the extracted muscle synergies. In our first case, where all tasks are included in the extraction Matrix  $M_{e\_all}$ , the NMF algorithm provides beside the synergy Matrix  $W_{all}$  additionally the weight matrix  $C_{all}$ , which approximates the measured EMG signals ( $M_{e\_all}$ ) best. This means we get the approximation matrix by multiplication of weight and synergy matrix so that  $D_{e\_all} = C_{all} \cdot W_{all}$ .

In Figure 41, this procedure is shown exemplarily for three muscles, the anterior part of the delta muscle (*left*, high magnitude), the biceps muscle (*middle*, medium magnitude) and the lateral part of the triceps muscle (*right*, low magnitude). The first repetition of the



original signal ( $M_{e\_all}$ ) is plotted with green squares, the repetitions 2-5 are plotted with purple, blue, yellow and red lines. The reproduction of the first repetition of the original signal by using muscle synergies ( $D_{e\_all}$ ) is plotted in blue stars.

Used are the five muscle synergies as depicted in Figure 40. As expected, the EMG signals of the anterior part of the delta muscle can be very well reproduced, as this muscle is dominant in the first synergy  $Syn1\_nw5$  as it shows high magnitudes in most of the measurements.

In contrast the reproduced EMG signals of the biceps (Figure 41 *middle* – blue stars) are less satisfying, even so this muscle is present with medium activity levels. All five repetitions of the original signal (green squares and colored lines) show a very clear characteristic with a high bell-shaped peak in the beginning followed by a flat signal close to zero. This characteristic is only slightly hinted by the reproduced signals (blue stars).

The original signal and the reproduction of this signal of the lateral part of the triceps do not match one to one, but the deviation lies in the range of variation in between trials and the reproduced signal reflects the characteristic of the measured signals.

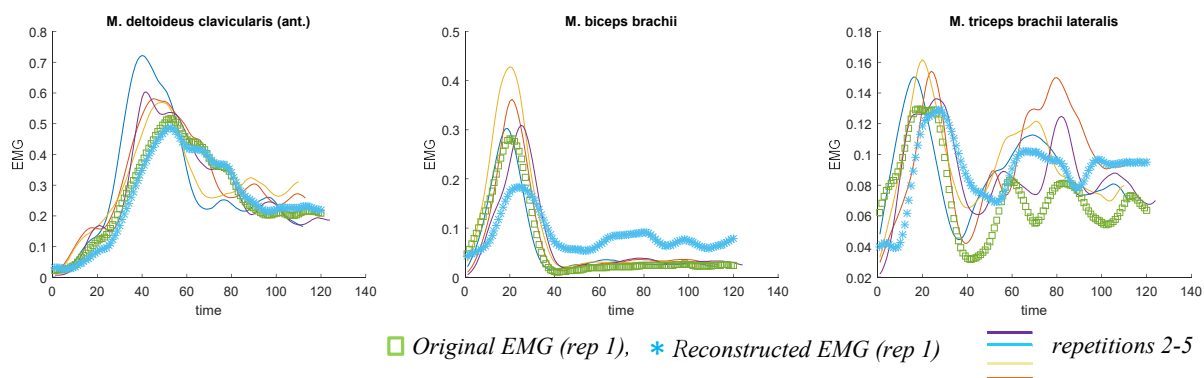


**Figure 41:** The reconstruction of measured EMG signals of one reaching tasks for three involved muscles using five muscle synergies. The original signal of the first repetition (green squares) is reproduced (blue stars) by the use of the five muscle synergies and corresponding weights resulting from the NMF algorithm. Repetitions 2-5 show a clear, consistent characteristic of the measured EMG signals resulting from this motor task.

In a next step, the number of synergies  $n_w$  is continuously raised (still by using the extraction matrix  $M_{e\_all}$ ) and the quality of the reproduced signals checked visually in the above described way. In Figure 42, the resulting muscle synergies for  $n_w = 7$  are plotted. The variance account for (VAF) for an number of muscle synergies of  $n_w = 7$  reaches 94,5%.

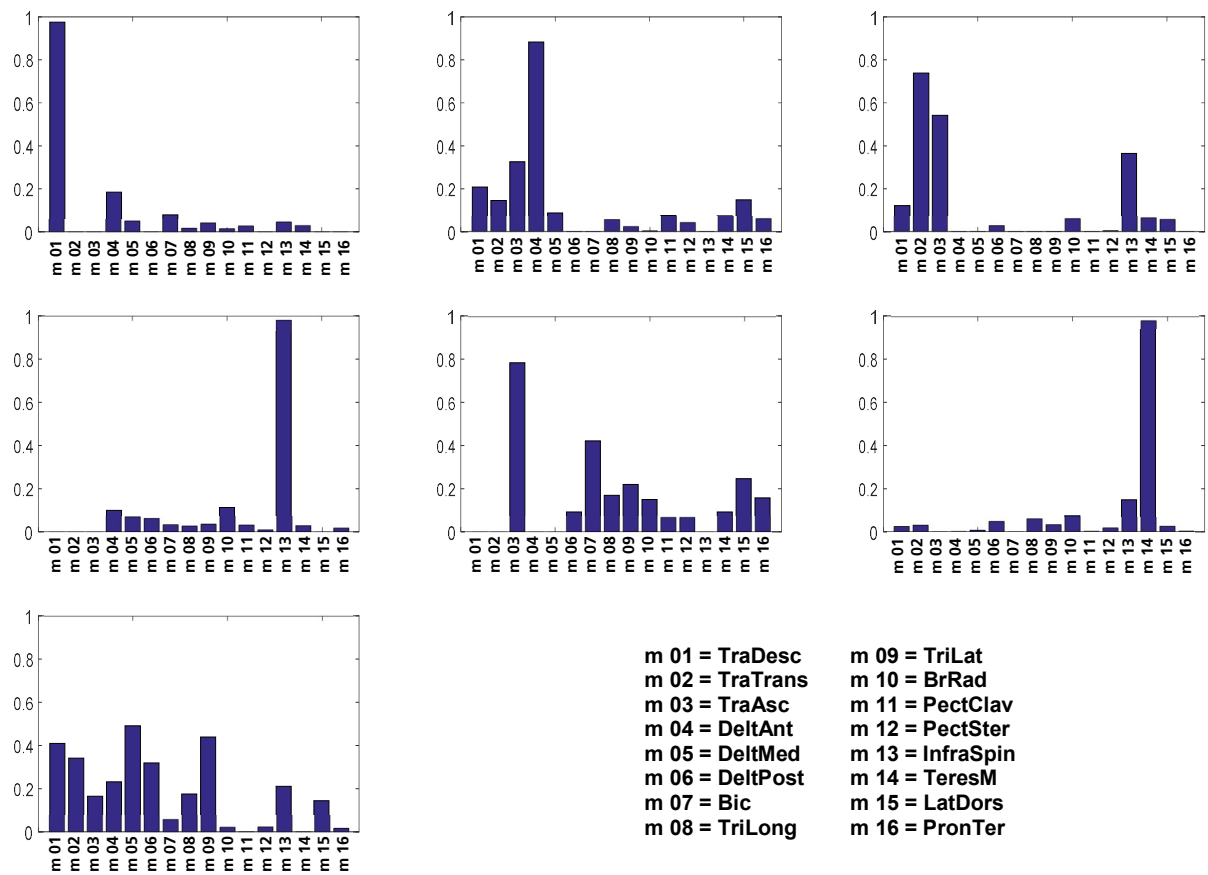


Figure 42: The resulting synergies when the number of synergies is raised to  $n_w = 7$  - all measured tasks used as input for the NMF algorithm (matrix  $M_{e\_all}$ ).

Figure 43, it can be seen that the properties of the reproduced EMG signals using seven muscle synergies remain similar for the regarded task and repetition. The reproduced signals (blue stars) of the delta muscle (*left*) and the biceps (*middle*) remain similar compared with the signals resulting from five synergies. The reproduced signals of the lateral part of the triceps (*right*) are even worse with seven synergies as the significant peak in the beginning is not well reproduced (but would still be acceptable).

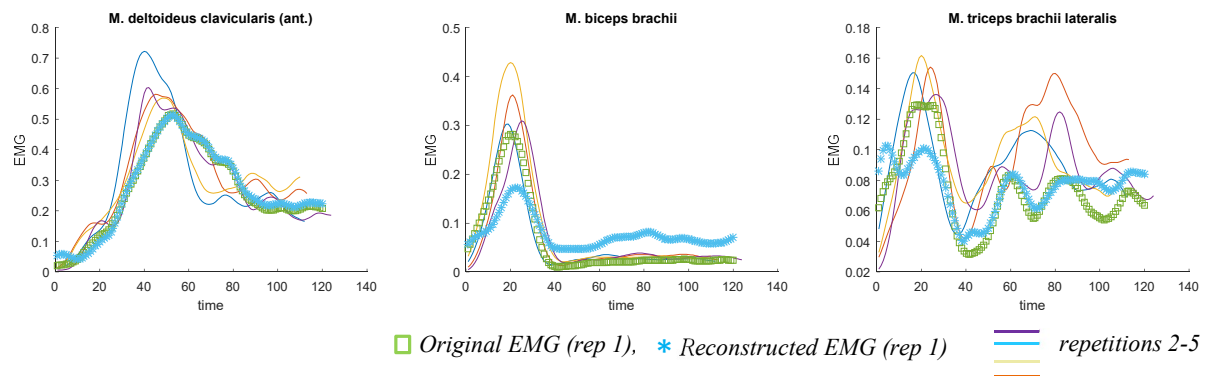


Figure 43: The reconstruction of the measured EMG signals of the same reaching task and involved muscles, now using seven muscle synergies.

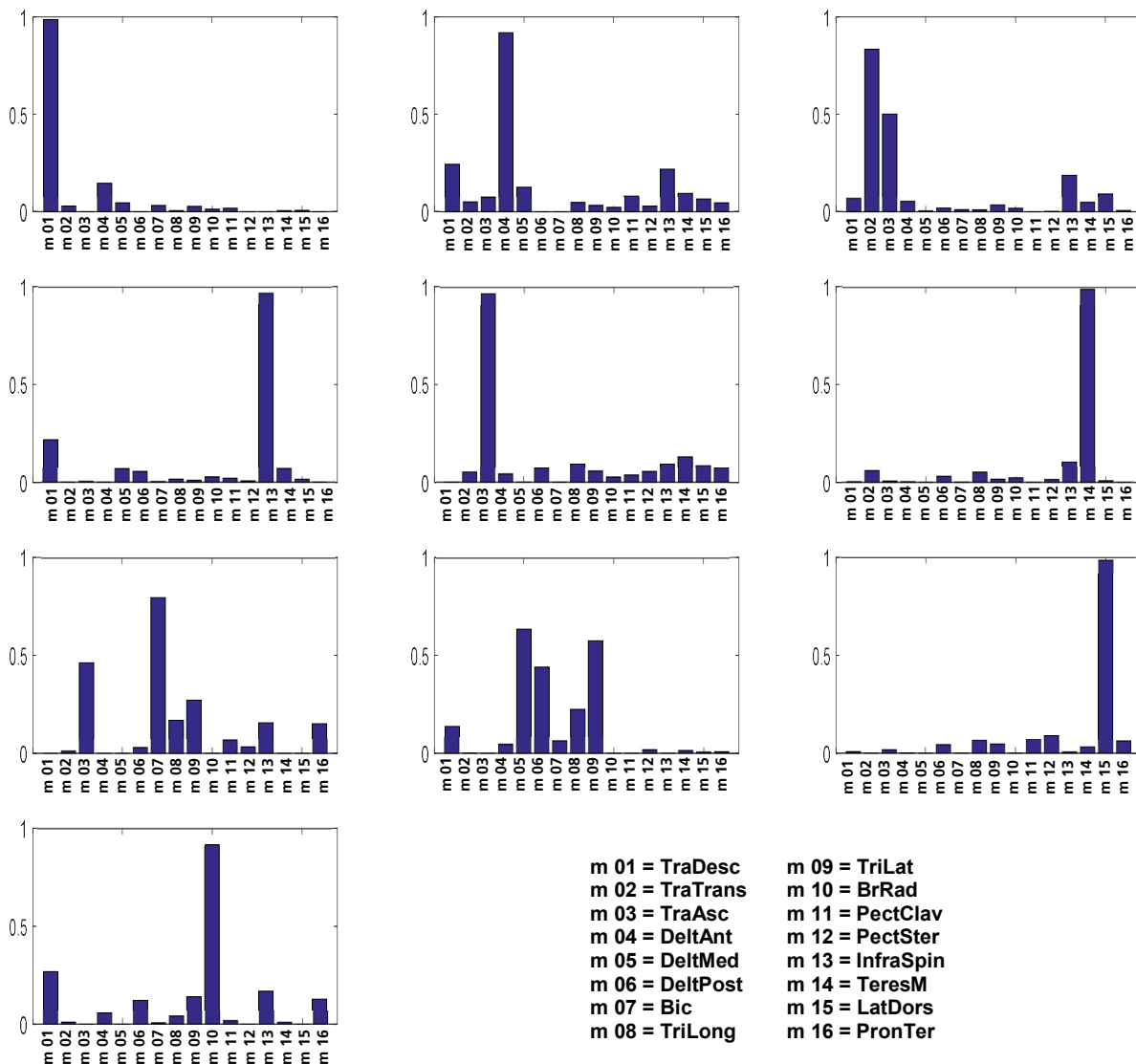
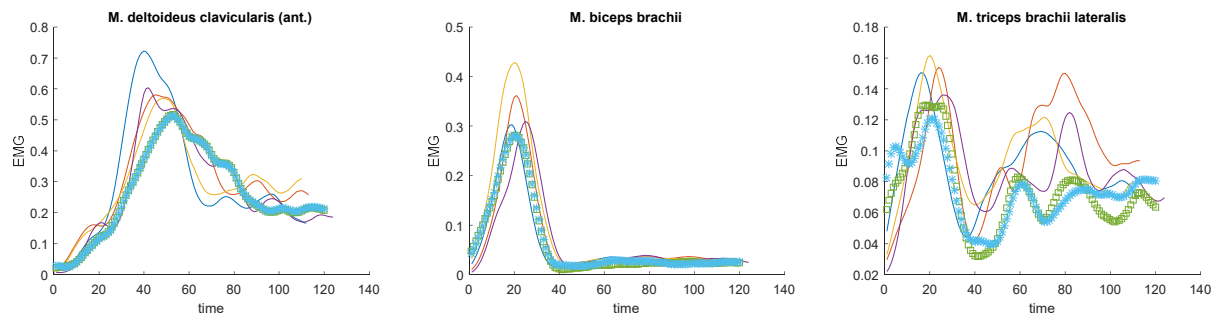


Figure 44: The resulting synergies when the number of synergies is raised to  $n_w = 10$  - all measured tasks used as input for the NMF algorithm (matrix  $M_{e\_all}$ ).

In Figure 44, the resulting synergies for  $n_w = 10$  are plotted (extraction matrix  $M_{e\_all}$ ). The VAF reaches 98.6%, and additionally the VAF plot (Figure 39) shows a change of slope at  $n_w = 10$ .

In the plots of the measured ( $M_{e\_all}$ ) and reproduced ( $D_{e\_all}$ ) signals of the regarded task it can now be seen that signals of all three muscles get a very high reproduction quality. The signals of the delta muscle and the biceps fit almost one to one, and the reproduced signal of the triceps lateralis (blue stars, right) clearly shows the characteristics of the measured signals, and the deviation to the original signal (green squares) is below the deviations in between repetitions of this task.



**Figure 45:** The reconstruction of the measured EMG signals of the same reaching task and involved muscles, now using ten muscle synergies.

Up to this point, all measured tasks with all repetitions are used to extract the investigated muscle synergies (matrix  $M_{e\_all}$ ). Due to that, it can be argued that the extracted muscle synergies are some kind of data fitting, and only suitable to reproduce measured EMG signals of the scenario that was measured and used to extract the synergies. One major advantage of the optimal control method used in this thesis is, that this approach allows a quite generic description of the tasks to be fulfilled (e.g. reach a point). No further input data for the generated motions (like e.g. motion capture data) is needed. This property should desirably be preserved when using muscle synergies as controls. The generality of the synergies to produce a variety of different motions (output space) is investigated in chapter 4.4.

In a first step, additionally the generality of the extracted synergies on the input space side is evaluated. Therefore, only the EMG signals of a subset of the measured tasks are included in the extraction matrix  $M_e$ , and the extracted synergies are used to reproduce measured EMG signals of tasks, that are not included in the matrix  $M_e$ . The EMG signals of the not included tasks are arranged in the validation matrix  $M_v$ . Then, it is checked if the extracted muscle synergies ( $W$ ) are capable of reproducing the validation matrix  $M_v$ . For this purpose, a customized software written in Matlab is used, which similar as the NMF algorithm (1) minimizes the root-mean-squared residuals between  $M_v$  and  $C \cdot W$ , now with  $M_v$  and  $W$  given (least-square fit algorithm with non-negative values).

In the first case, only EMG signals of reaching motion to target points on the horizontal and vertical line ( $P1, P3, P13, P05, P07, P09, P11, P13, P15, P17$ , see Figure 30) are used as inputs for the NMF algorithm (arranged in the extraction matrix  $M_{e\_hv}$ ). The resulting synergies for  $n_w = 10$  are plotted in Figure 46. As one can see, the characteristic of the resulting synergies remains similar compared with those extracted using matrix  $M_{e\_hv}$  (note that individual synergies may swap their positions). This can be seen as an indication that the extracted muscle synergies reflect and underlying control concept of the CNS and the measured EMG signals are composed by them. In any case, this consistency is a requirement if the synergies should be used as controls with a certain generality.

Then, these synergies ( $W_{hv}$ ) are used, to reconstruct EMG signals of motions, that were not included in the NMF algorithm ( $M_{e\_hv}$ ). Therefore, the EMG signals of reaching motions lying on the bisectrix of the horizontal and the vertical lines ( $P2, P4, P6, P8, P10, P13, P14, P16$ ) are arranged in the validation matrix  $M_{v\_bi}$  that is then reconstructed using the synergy matrix  $W_{hv}$  as described above.

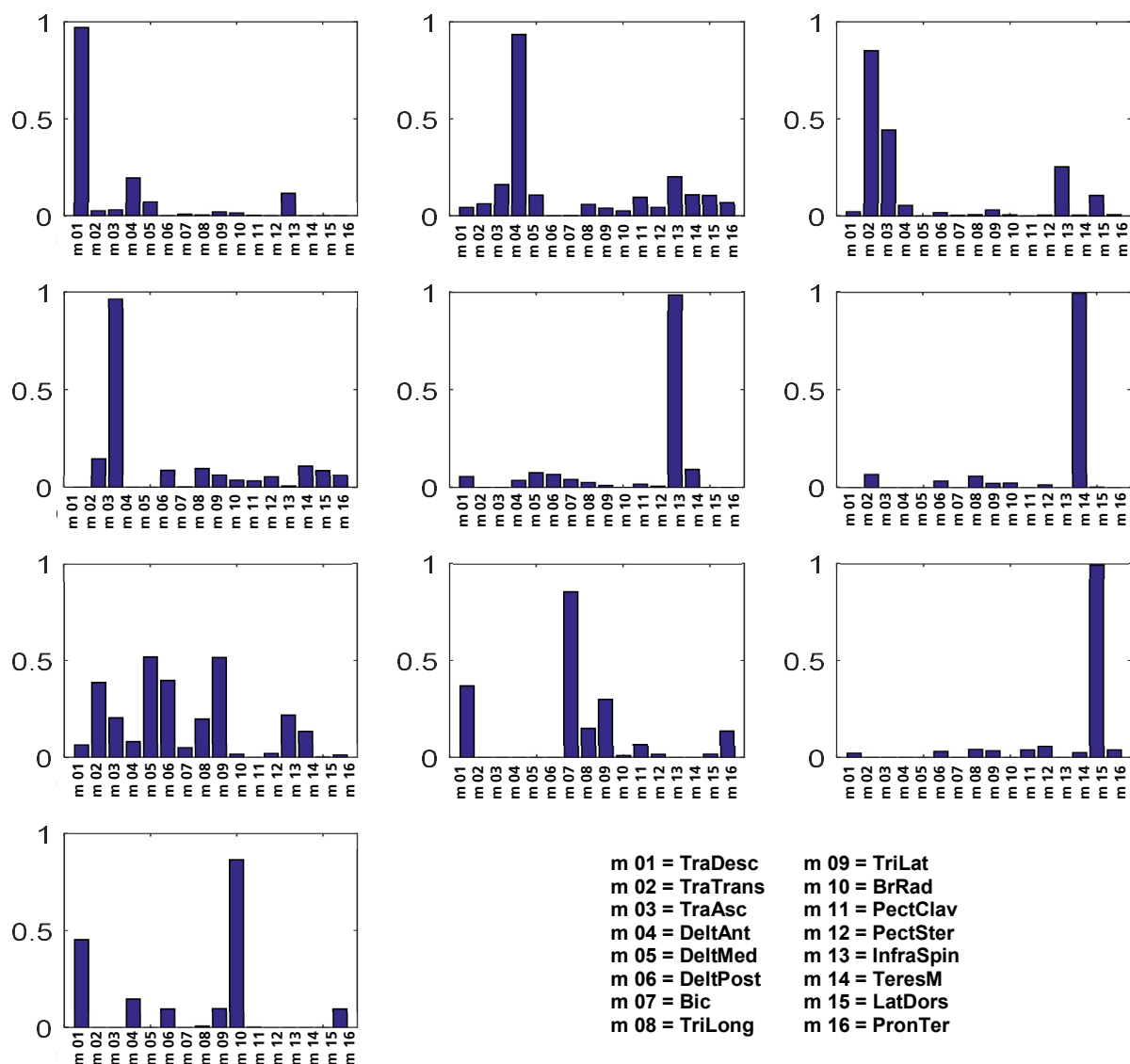


**Figure 46:** Extracted muscle synergies for  $n_w = 10$  remain constant when using only a subset of the measured tasks ( $M_{e_{hv}}$ ) as input for the NMF algorithm.

From these reconstructed EMG signals ( $M_{v_{bi}}$ ) those for the reaching motions to target point P2 are plotted exemplarily in Figure 47. Again the first repetition of the original signal is plotted with green squares and repetitions 2-5 are plotted as colored lines. The reconstruction of the first signal by using the ten muscle synergies extracted from a subset of the measured tasks where P2 is not included ( $M_{e_{hv}}$ ) are plotted as blue stars. As one can see, the measured signal can be very well reproduced by these synergies, which indicates the synergies a certain generality.

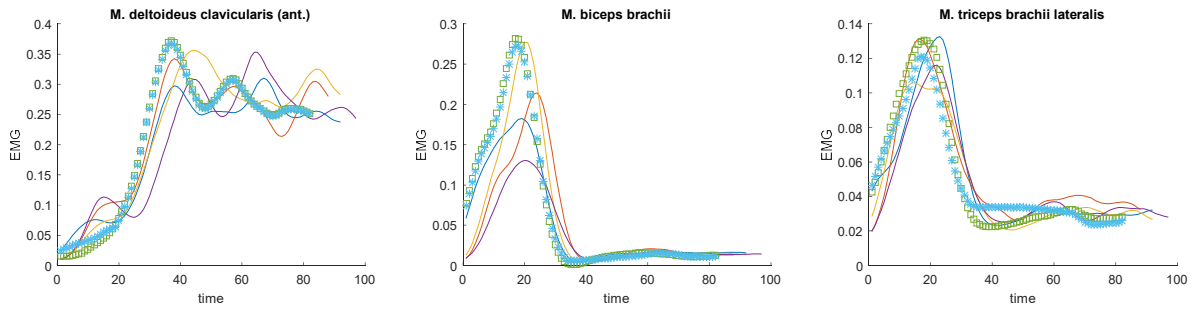


Figure 47: The reconstruction of measured EMG signals of a reaching task using ten muscle synergies – the reconstructed EMG signals were not included in the input Matrix of the NMF algorithm used to extract the synergies.

In a next validation case, only EMG signals of reaching motion that were performed without weight cuff attached to the test person’s wrist (*TS1-TS9*, see Table 2) are used as input for the NMF algorithm ( $M_{e\_nw}$ ). The resulting synergies ( $W_{nw}$ ) are depicted in Figure 48. Again the characteristic of the synergies is preserved (compare with Figure 44 and Figure 46).

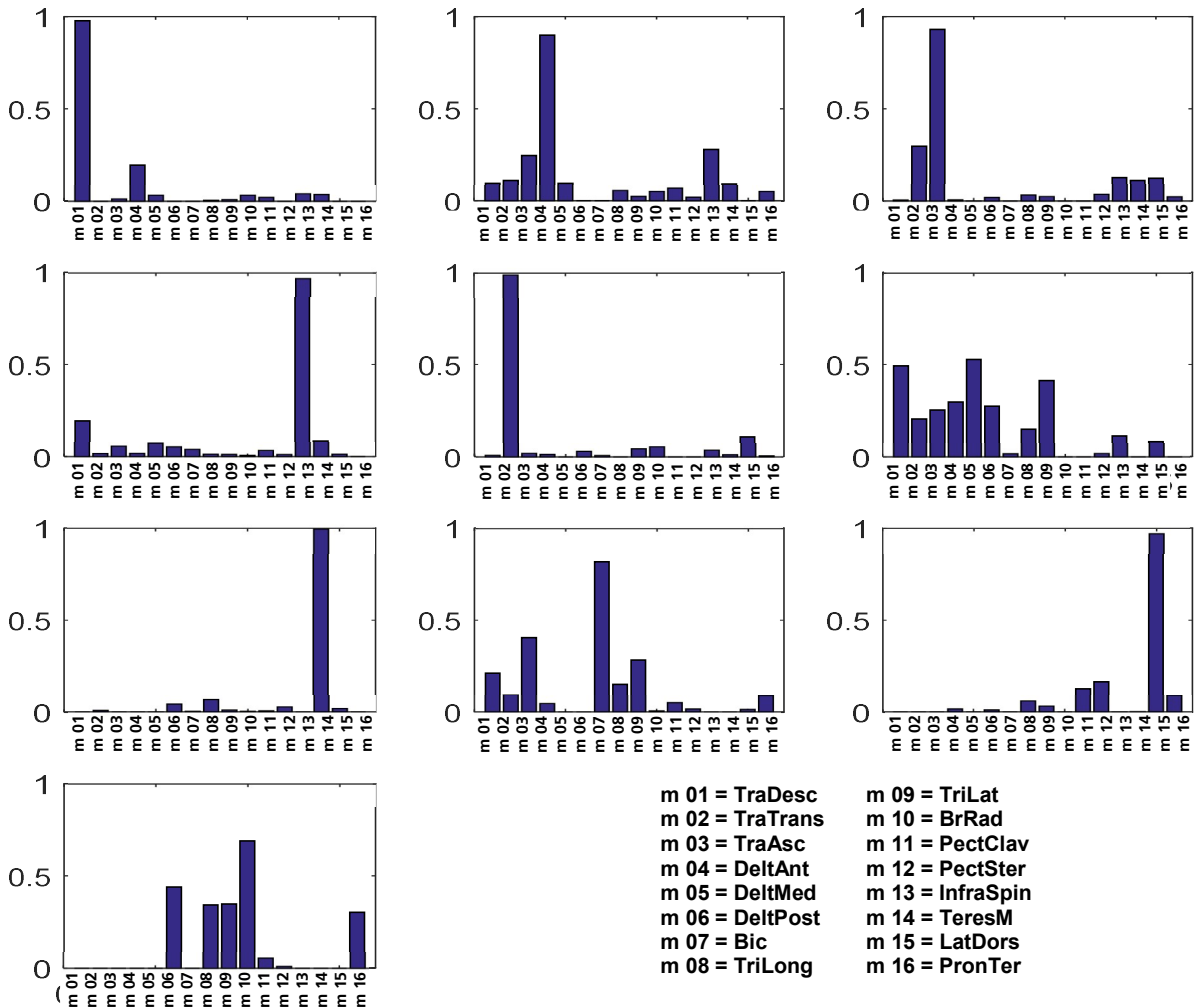
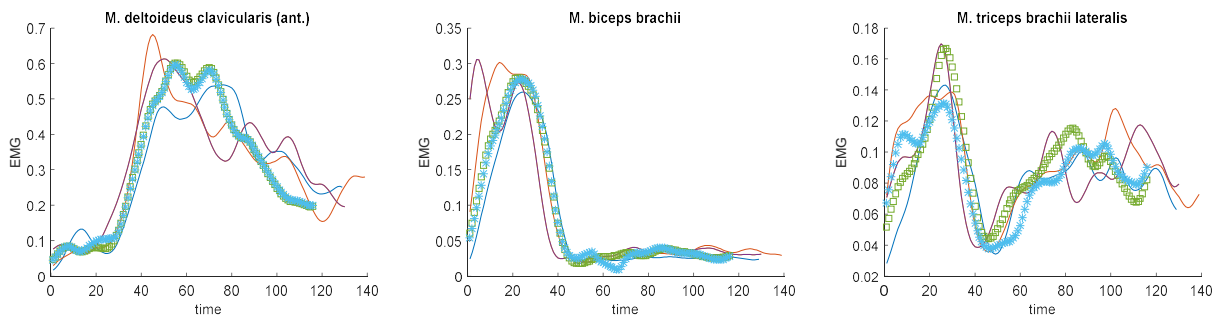


Figure 48: Extracted muscle synergies for  $n_w = 10$  remain constant when using only a subset of the measured tasks ( $M_{e\_nw}$ ) as input for the NMF algorithm.

In Figure 49, the measured EMG signals of a reaching tasks of TS 10 are plotted, where the test person is wearing a weight cuff (1kg) attached to the wrist. The EMG signals of the first repetition (green squares) are reconstructed (blue stars) by the above plotted muscle synergies, that were extracted by using only EMG signals of non-weighted motions as input for the NMF algorithm ( $M_{e\_nw}$ ). Again, measured signals can be very well reproduced.



*Figure 49: The reconstruction of measured EMG signals of a reaching task using ten muscle synergies – the reconstructed EMG signals were not included in the input Matrix to extract the used synergies.*

## 4.4 Simulated test

### 4.4.1 Simulation model and test setup

For simulation, the human arm model introduced in chapter 3.5 is used. As the focus is on reaching in this test, and as test persons are told to keep their shoulder in position and to keep the wrist and hand stiff during the motion, a 5 DOF human arm model is used with three rotational DOF in the shoulder joint and two DOF in the elbow joint, which is adapted to the anthropometry of the test persons.

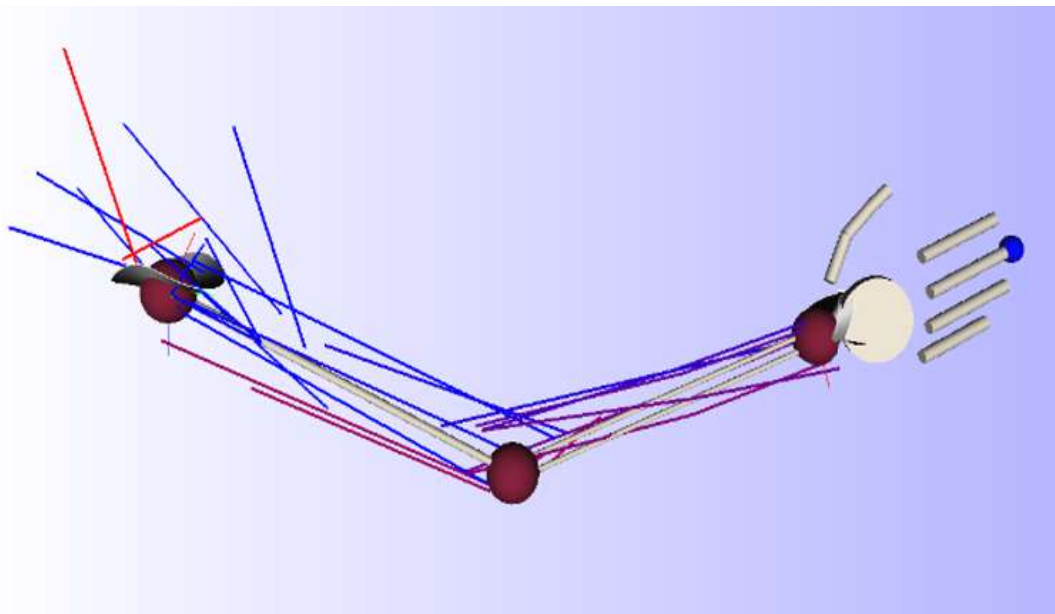


*Figure 50: Human arm model: upper arm, forearm and hand modeled as rigid bodies (grey) connected via joints (5 DOF, red balls with grey ellipsoids delimiting the range of motion) and actuated by Hill-type muscle models (blue and red lines, 29 muscles).*

For a direct muscle actuation (AM-M) and a muscle synergy actuation (AM-S), the model is actuated by the 29 Hill type muscles. For motion evaluation, a virtual marker is introduced in the model, placed at the position of marker HL3R (see Figure 31). For all simulations, the start posture of the model is defined. As goal, the coordinates of the virtual target points have to be reached with the tip of the middle finger (see Figure 50 - blue ball at tip of the middle finger). As test persons in the motion lab are told to move as fast as possible, *minimal time* is used as cost function for all simulations.

#### 4.4.2 Simulated Trajectories

In a first step, the results derived above concerning the quality of the reproduced EMG signals depending on the number of the extracted synergies  $n_w$  is now investigated on the output space side (resulting motions). Therefore, simulations are performed and results compared for different numbers of muscle synergies ( $n_w$ ) as control parameters. Although this is not a direct validation, as the OC controller can freely use the synergies and mix them by calculating corresponding weights (which probably differ to those calculated by the NMF algorithm), it can give an impression of the quality of the resulting motion depending on the number of muscle synergies. To really assess the deviations on the output space side between original signal (measured EMG values e.g.  $M_{e\_all}$ ) and approximated signal reproduced by muscle synergies (e.g.  $D_{e\_all} = C_{all} \cdot W_{all}$ ), the simulation model had to be actuated in a feed forward manner directly by the corresponding signals ( $M_{e\_all}$  respectively  $D_{e\_all}$ ), and resulting motions compared. But also when following this practice, the actuation signals would have to be fed to the same system they were captured from to get meaningful results (which lacks simply by the fact that the underlying EMG signals are captured from living humans).

A multitude of simulations is performed with a number of muscle synergies  $n_w$  between five and ten. In all cases, the goal (reaching for a certain point) can be fulfilled. Overall, the above described observations (input space side) can be confirmed when evaluating the resulting motions. When using just five muscle synergies, the motions look choppy and "robot" like. This effect is reduced when raising the numbers of underlying synergies. When using 10 synergies, the resulting motion become very smooth and human like. In Figure 51, the different trajectories resulting from different numbers of underlying muscle synergies for the same task are plotted. In red, the resulting trajectory when using five muscle synergies is shown ( $n_w = 5$ ), in green for seven muscle synergies ( $n_w = 7$ ) and in yellow for ten muscle synergies ( $n_w = 10$ ).

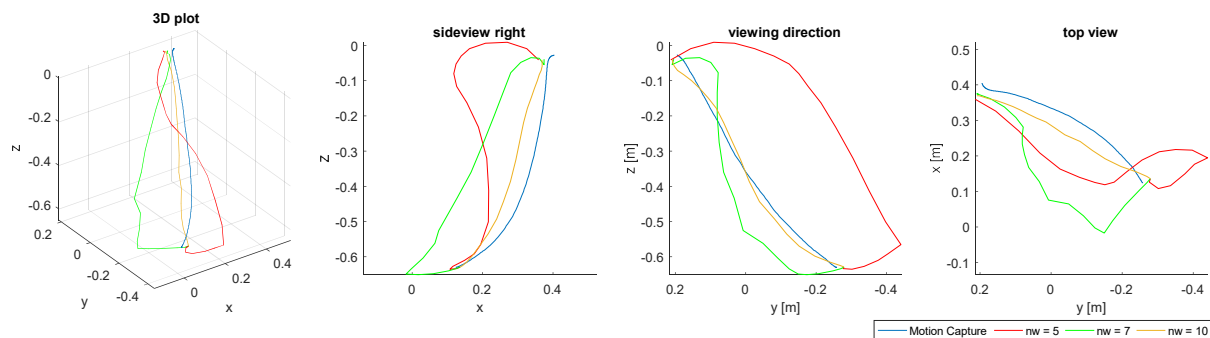


**Figure 51:** Different hand trajectories for the same tasks resulting from a muscle synergy actuation with different numbers of muscle synergies (red  $n_w = 5$ , green  $n_w = 7$  and yellow  $n_w = 10$ ) – in blue the measured trajectory (motion capture) from this task is plotted for validation.



In blue, the in the motion lab measured trajectory for this tasks is plotted as comparison. In the first column the 3D plot is shown, in the second the sideview (right), in the third the viewing direction and in the fourth column the top view. Trajectories resulting from AM-S with five synergies (red) deviate to the one measured in the motion lab (blue). Using seven synergies (green) gets closer to the measured solution, but motions still appear choppy. When raising the number of synergies used as control parameters to ten, the simulation results fit the measured trajectory very well (yellow) and motions appear quite smooth.

In a next step, the influence of the distinct Actuation Modes (joint torque actuation AM-T, direct muscle actuation AM-M and muscle synergy actuation AM-S) is investigated. For all following simulations performed in AM-S, ten muscle synergies are used.

In Figure 52, trajectories of the simulated motions to several target points from distance  $d_1$  using all three Actuation Modes, are compared to the measured trajectories (motion capture). Each row shows different views of the trajectories to one TP (1<sup>st</sup> row TP01, 2<sup>nd</sup> row TP03, 3<sup>rd</sup> row TP05, 4<sup>th</sup> row TP07 and 5<sup>th</sup> row TP17). In the first column the 3D plots are depicted, in the second column the sideview (right), in the third column the test persons viewing direction and in the fourth column the top view. Trajectories measured in the motion lab are colored in blue, trajectories resulting from AM-T in red, from AM-M in green and from AM-S in orange. Note that the origin of each coordinate system (Motion capture and simulation model) is located in the rotation center of the shoulder joint. Due to slightly different start positions of the test persons hand between each repetition of the measured reaching motions, the start positions of simulations and motion capture trajectories can differ to some extent.

For all Actuation Modes and each target point the OC framework converges to a feasible solution. Although trajectories resulting from AM-T differ from those that were measured in the motion lab, the simulated paths at least appears human like and feasible from a subjective point of view when investigating the video data of simulated motions.

Including muscles in the model directly leads to trajectories that are very similar to those that are measured in the lab (note that no other model parameters or constraints are changed or adapted). The observed characteristics of the measured motions (see Chapter 3.2) can be clearly seen in the simulation results as well. In some cases the s- and bow-shape appearance is somewhat exaggerated, but the characteristics are preserved. The use of muscle synergies (AM-S) partly helps to reduce this exaggeration and appears as a "smoothed" version of the motions resulting from AM-M when comparing the resulting motions by investigating the corresponding video data.

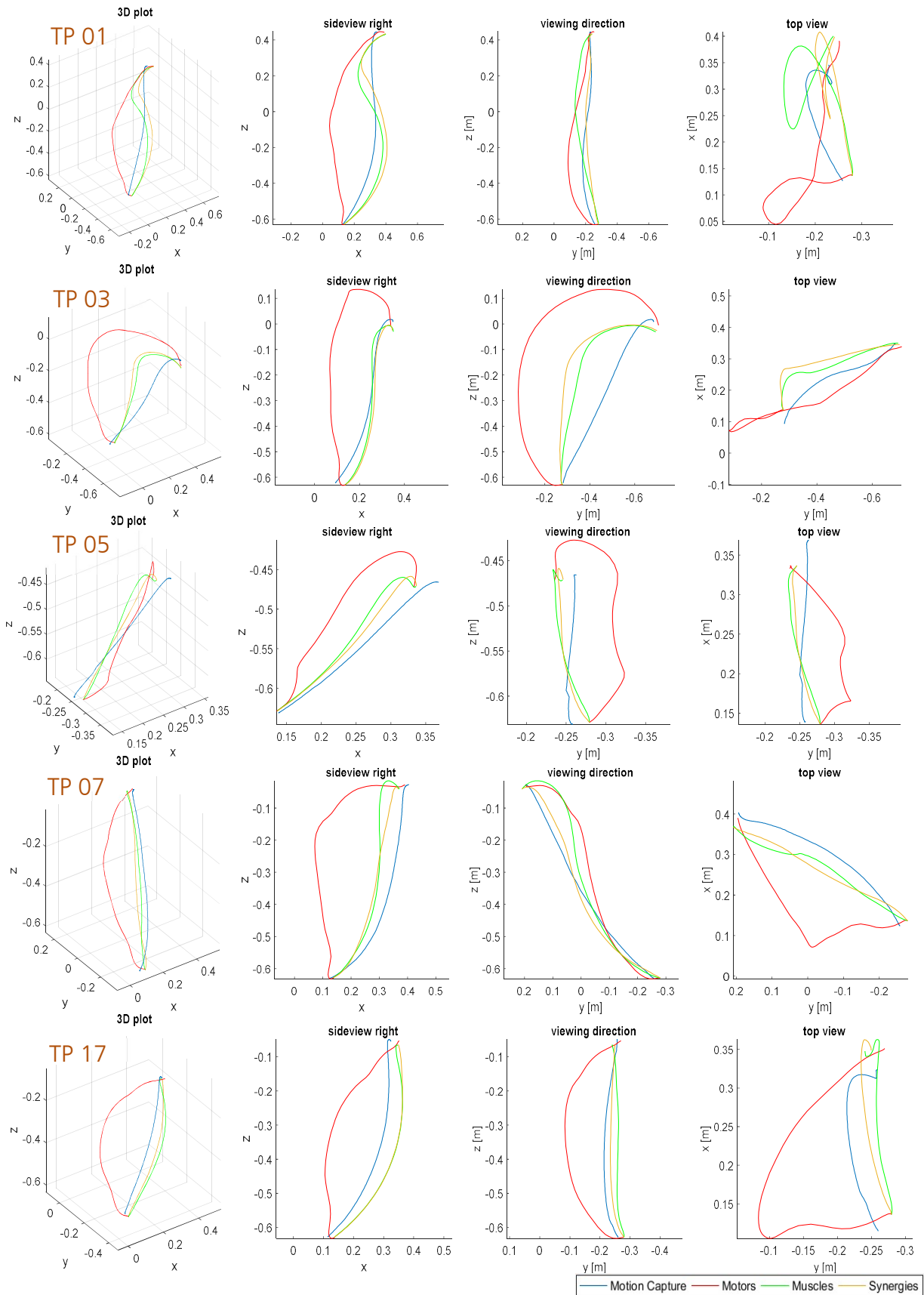


**Figure 52: Comparison of measured (blue lines) and simulated trajectories to different target points (rows) and with different Actuation Modes. Joint torque actuation (AM-T – red) direct muscle actuation (AM-M – green) and muscle synergy actuation (AM-S – yellow).**

### 4.4.3 Simulated velocity profiles

In Figure 53, the velocity profiles (absolute velocities) of reaching motions to several TP's from distance  $d_1$  are plotted for all three Actuation Modes (AM-T, AM-M and AM-S, from left to right).

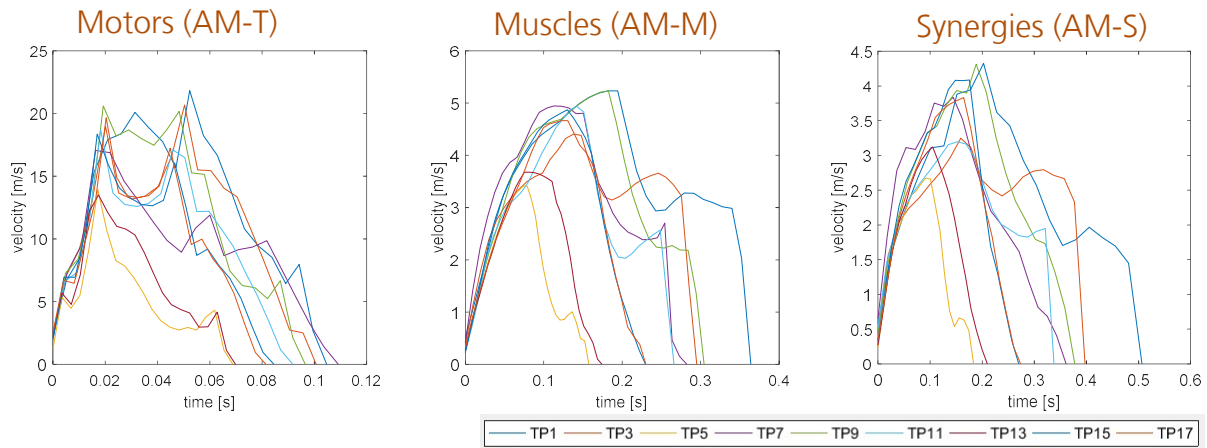


**Figure 53:** Velocity profiles of reaching motions to TP 1-17 (odd numbers only) from Distance  $d_1$  with a neutral final hand orientation: (left) Motors as actuators, (middle) muscles as actuators (right) muscle synergies as control parameters.

When using motors as actuators, the maximum velocity ( $\sim 22\text{m/s}$ ) is about seven times higher compared to the maximum measured values ( $\sim 3\text{m/s}$ ). This leads to motion durations between 0.07s (TP5) and 0.11s (TP1) which are about 10 times faster than the measured values (0.8s and 1.1s, see Chapter 3.2.3). Using muscles as actuators in the model reduces the maximum simulated velocities by factor four. In AM-M, the maximum velocity is about 5.2 m/s which leads to a duration of 0.38s (TP1). In AM-S the maximum velocity is about 4.3 m/s which leads to a motion duration of 0.5s (TP1), which is about twice as fast as the measured value for this point.

It is significant that velocities produced at AM-T are much higher than the measured values (and do not seem to be feasible for a human from a subjective point of view neither). One explanation for this could be that motors in our model have a constant maximum torque, which does not depend on the state of the MBS (joint angles and joint velocities) as it is the case in the human body. Using muscles as actuators (AM-M and AM-S) reduces the produced velocities, which could result from the force-length and force-velocity dependency of the Hill type muscle models which is inspired by nature. Additionally, the velocity profiles produced in AM-M and AM-S have a smoother appearance than those resulting from AM-T. Nevertheless it is conspicuous, that the velocities drop rapidly at the end of the reaching motions (AM-M & AM-S), especially at motions with longer duration and higher velocities. However, that the reaching motions measured in the motion lab involve some precision and visual feedback, as the test persons have to reach a given point and stop exactly in front of the target plane. This could result in a prolonged deceleration phase. Additionally, the test persons were not trained to move as fast as they possibly could (from a physiological point of view).

#### 4.4.4 Simulated EMG values

In Figure 54, the underlying muscle actuation signals for a simulated reaching task are plotted (*TS1-N-TP01*). Shown are all via muscle synergies actuated muscles, each in a distinct subplot. For each muscle, the results from a direct muscle actuation (AM-M, blue lines) and a muscle synergy actuation (AM-S, orange lines) are plotted.

Using a direct muscle actuation, all muscles show a “bang bang” actuation profile. From an optimization point of view this is obvious when aiming on moving the multi body system as fast as possible (*minimal time* used as cost function). When comparing the results with measured EMG values, it is conspicuous that a full actuation ( $a=1$  corresponds to 100%MVC) is higher than the measured values (compare with Figure 38).

is described in the next chapter.

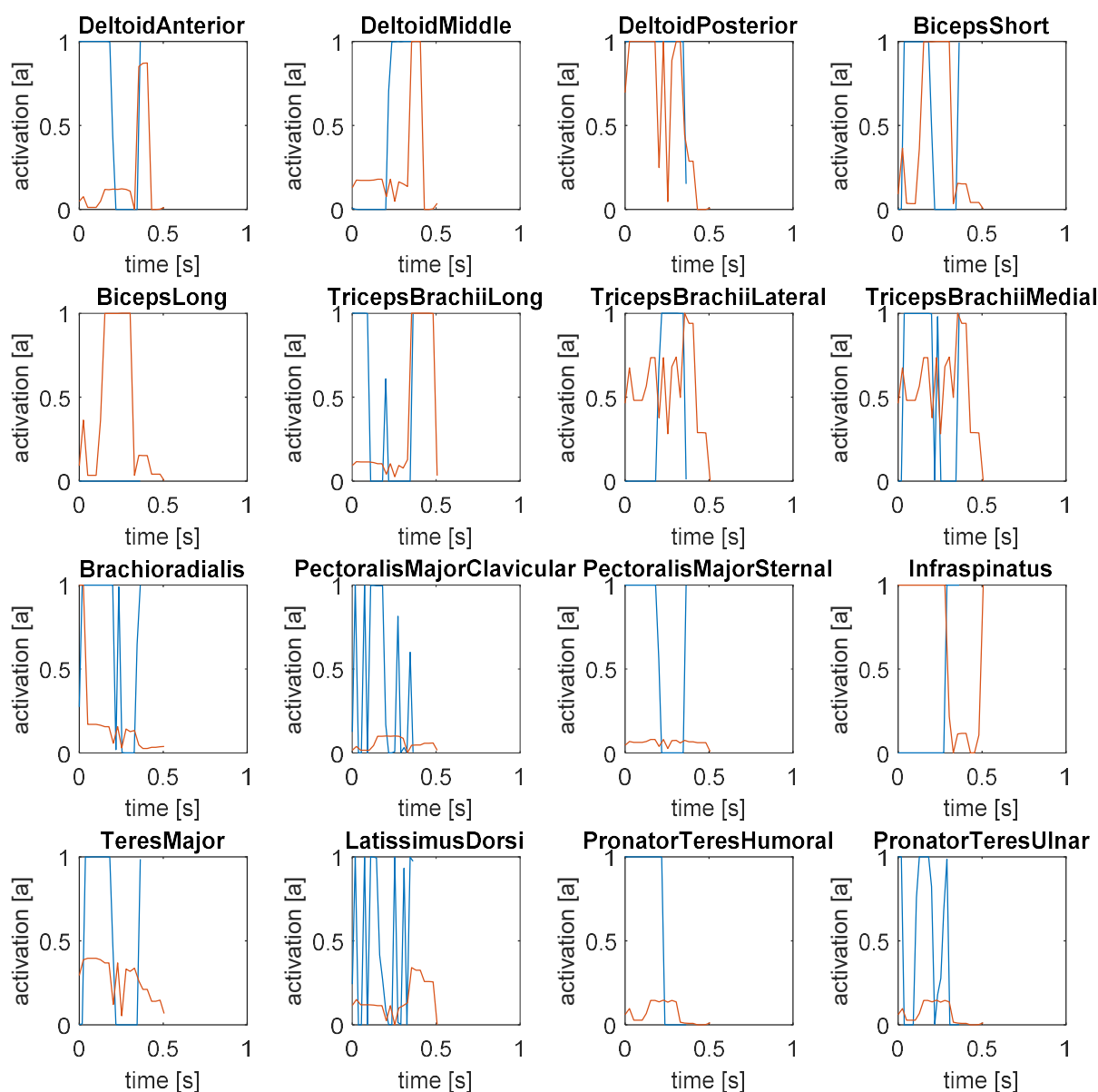


Figure 54: Simulated muscle actuation signals of reaching task *TS1-N-TP01*. Muscle actuation (blue) and muscle synergy actuation (yellow).

---

Using a muscle synergy actuation, this effect is reduced due to the constrained grouping of the muscles by the definition of the synergies as control parameters. Still, those muscle that dominate a synergy are fully actuated ( $a=1$ ).

This characteristic is observed at all simulated tasks when using *minimal time* as cost function, also the resulting trajectories appear very human like and similar to those measured. One option to reduce the effect of the "bang bang" actuation while keeping the realistic behavior concerning the chosen trajectories, could be to mix the used OC cost function (*minimal time*) with other cost function, like e.g. *minimal kinetic energy*, *minimal actuation* or *minimal actuation change*. To investigate the characteristic of each distinct cost function, and how a mixed OC cost function can help to predict human like motions or muscle actuations, the weight lift test is set up, which

## 5 Weight lift test

The *weight lift test* is designed to investigate the characteristics of measured muscle actuations (EMG) of arm muscles and further on allow a comparison with simulated muscle actuation signals. The test persons in the motion lab perform a *flexion* of the elbow joint (“biceps curls”) with different loads, shoulder angles and forearm orientations, which are not changed while motion execution. Beside investigating the influence of a muscle synergy actuation (AM-S) with a direct muscle actuation (AM-M), in this test there is also a special focus on the influence of the minimized OC cost function. The reduced set of kinematical DOF’s leads to a “restriction” of the possible trajectories, and thereby allows to focus on the anatomical redundancy.

### 5.1 Motion Lab measurements

In the following, the experimental setup in the motion lab, restrictions for test execution and measured data are described.

#### 5.1.1 Test setup

At the *weight lift test*, test persons perform a *flexion* of the elbow joint at three different shoulder angles  $\Omega$  (Test Scenario 1–3, angle  $\Omega$  between upper arm and frontal plane) as depicted in Figure 55. In each Test Scenario distinct restricted forearm orientations (neutral and supinated) are measured, each with five different weights (see Table 4). Each particular task (shoulder angle with a certain forearm orientation and a certain weight) is repeated three times. The weights are released in between repetitions, and between tasks performed with high loads (W2-W4) the test subject takes longer time to rest to avoid fatigue. At the start position, the arm is stretched and muscles are relaxed. The test subjects are advised not to change forearm orientation (*supination / pronation*) and to keep shoulder and elbow joint in position while test execution. Motions should be done in a “controlled” manner, with no further specification for motion speed given.

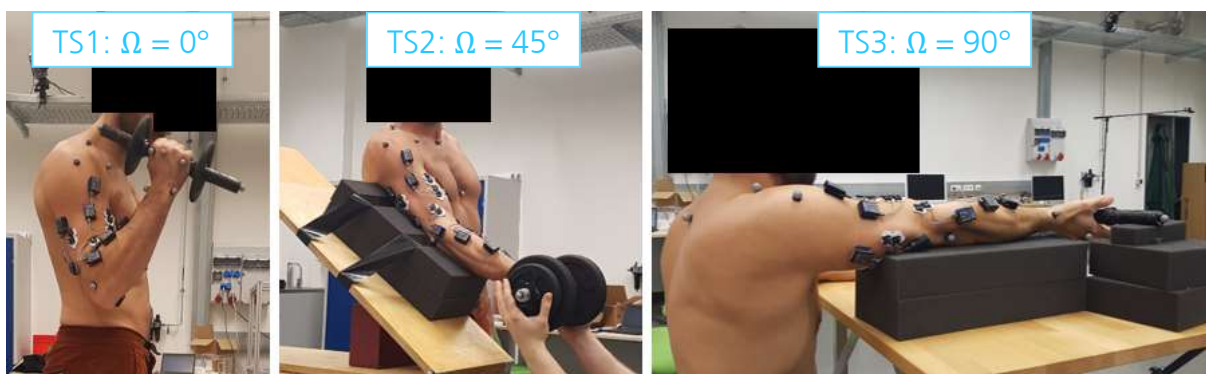


**Figure 55:** The three different Test Scenarios TS1-3 of the weight lift test: Shoulder angle  $\Omega$   $0^\circ$  (left),  $45^\circ$  (middle) and  $90^\circ$  (right). All performed with five weights (W0-W4) and different forearm orientations.

In TS1, the test person is standing in an upright position, with the arm hanging relaxed in natural posture at motion start. The dumbbell is positioned on a table laterally with the height adapted to the position of the hand, so that grasping and releasing can be performed without changing shoulder or body orientation. In this scenario, one additional measurement is performed, where the forearm orientation is not restricted while motion

execution (*free -f*). For *free (-f)* and *neutral (-n)* forearm orientations, the dumbbell is positioned parallel to the sagittal plane on the table at motion start, for supinated (*-s*) forearm orientations it is rotated through  $90^\circ$  (parallel to the frontal plane). All forearm orientations are measured with the five loads cases (*W0-W4*), each task is repeated three times. Weights are released in-between each repetition. In TS-1, a shoulder *flexion* is involved while motion execution, that starts when *flexion* in the elbow joint exceeded  $90^\circ$  (see shoulder orientation in Figure 55 *left*). In TS1-*f*, a continuous *supination* of the forearm is observed while motion execution (from a neutral forearm orientation at start to a supinated at the final position).

**Table 4: Dumbbells weights and weights for test execution**

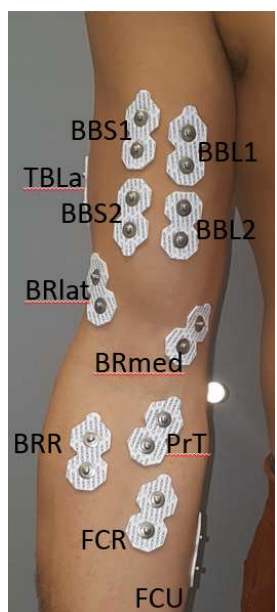
	Handle	Collars (2x)	1 kg plates	2 kg plates
	1750 g	390g	1040g	2050g
W0	0 kg			
W1	1,75kg ( <i>handle only</i> )			
W2	4kg ( <i>handle + collars + 2x 1kg plates</i> )			
W3	10kg ( <i>handle + collars + 4x 2kg plates</i> )			
W4	14kg ( <i>handle + collars + 4x 2kg plates + 4x 1kg plates</i> )			

In TS-2, the test person is standing in an upright position with a shoulder angle  $\Omega=45^\circ$  between upper arm and frontal plane. The upper arm is supported by a foam block, which helps to keep shoulder and upper arm in position while performing the motion (see Figure 55 *middle*). At motion start, the arm is relaxed and extended (elbow joint  $180^\circ$ ) and the dumbbell is positioned by an auxiliary person, which allows grasping and releasing it in between repetitions. Two different forearm orientations are measured (neutral and supinated), that are not changed while performing the motion, again with the weights *W0-W4*.

In TS-3, the shoulder angle between upper arm and frontal plane is  $\Omega=90^\circ$  while performing the motion. The test person is kneeling in front of a table with a foam block supporting the upper arm (Figure 55 *right*). At motion start and before each repetition the arm is relaxed and extended (elbow joint  $180^\circ$ ). The dumbbell is released to a support apparatus for tasks with supinated forearm orientation, and positioned by an auxiliary person for tasks with a neutral forearm orientation. Again, both forearm orientations are measured (neutral and supinated) with the weights *W0-W4*. At high weights (*W3 & W4*), a shoulder *flexion* was observed at motion start (caving in of elbow into foam block and slightly lifting of upper body), which seemed to be necessary to perform the lifting especially in the beginning phase with a stretched arm. Overall, 35 different tasks are measured at the *weigh lift test*, each with three repetitions. Motion capture data of the right shoulder, upper arm, forearm and hand and the thorax as well as EMG data of arm muscles are acquired while test execution. Motions are tracked with an optical system (see Chapter 3.3, 10x Qualisys Opus 7+, 2x Qualisys Opus 5+) and a sample frequency of 300 Hz. The optical markers on the test persons are placed according to the recommendations of the international society of Biomechanics (ISB) as described in [Wu 05]. Additional markers are placed on the hand, to get a higher resolution of hand motions. Palpation of anatomical landmarks is accomplished manually, following the

guidelines of [Van Sint Jan 07]. EMG data was acquired with a Noraxon EMG system at 1500Hz with 12 Channels (NORAXON myoMuscle Desktop DTS).

EMG sensors are placed as depicted in Figure 56, with a special focus on the dominant elbow flexors (Biceps, Brachialis, Brachioradialis), where sensors are positioned according to [Staudemann 14]. One field of attention here is the correlation of biceps short head and long head. To what extent the CNS can actuate different muscle heads individually is an important question when it comes to biomechanical modelling (and control) (see Chapter 2.1.3). Before applying the sensors, the skin is shaved, cleaned with alcohol and rubbed with abrasive gel as recommended in [Freriks 99]. Data recording (motion data as well as EMG signals) for each task started with a signal about one second before the first motion and was recorded continuously during all three repetitions.



Nr.	Short name	Muscle
01	BBS1	M. biceps brachii (short head)
02	BBS2	M. biceps brachii (short head)
03	BBL1	M. biceps brachii (long head)
04	BBL2	M. biceps brachii (long head)
05	BRlat	M. brachialis lateral
06	BRmed	M. brachialis medial
07	BRR	M. brachioradialis
08	PrT	M. pronator teres
09	FCR	M. flexor carpi radialis
10	FCU	M. flexor carpi <i>Ulnar</i> is
11	TBLo	M. triceps brachii long (not depicted)
12	TBLa	M. triceps brachii lateral

**Figure 56: EMG Sensor Placement at the weight lift test. Sensors placed according to [Staudemann 14, Remaley 15 and SENIAM].**

### 5.1.2 Measured Trajectories

In TS-1 a shoulder *flexion* (as well as a slight *adduction* and rotation) is involved while motion execution, and additionally one measurement is performed where the forearm orientation is not restricted and can be changed while motion execution (*TS1-f*). As described above, one objective of the *weight lift test* is to compare measured with simulated muscle actuations. The Test Scenarios TS2 & TS3 are chosen in a way that the kinematical redundancy is limited to a pure elbow *flexion* (at different forearm configurations), which allows to focus on the anatomical redundancy problem. TS1 is set up to overcome the problem of identifying (mixed) OC-cost functions that solve the anatomical redundancy problem in a “human like” manner in kinematical restricted scenarios that would produce nonsensical motions when the number of kinematical DOFs is raised again. So, in this Test Scenario the measured and simulated trajectories are also of interest and are investigated in more detail (compared to *TS2* and *TS3*).



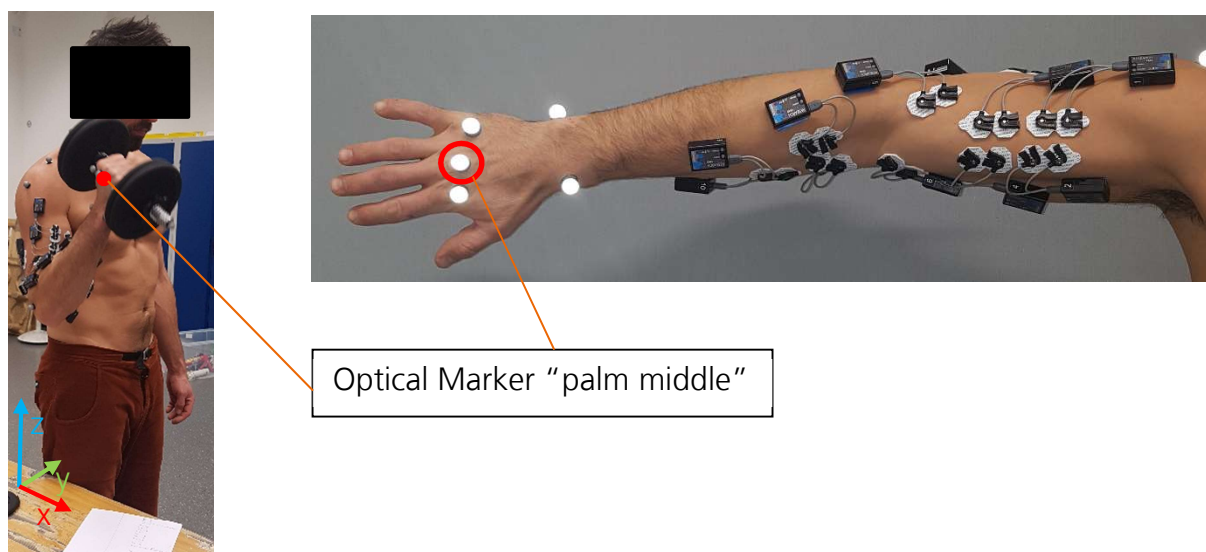


**Figure 57:** Placement of the optical marker plotted for trajectory assessment and orientation of the coordinate system used in the plots.

In the following, the trajectories of the optical marker “palm middle” which is placed analog to the marker “HL3R” at the *basic reaching test* (compare Figure 57 and Figure 31 left) are plotted. The z-direction of the coordinate system for the plots points upwards, x-direction points into the viewing direction of the test person, and y-directions points to its left (see Figure 57 left). In Figure 58, the trajectories for *TS1-f-W0* (line one), *TS1-f-W2* (line two) and *TS1-f-W4* (line three) are depicted. The first column shows the 3D-plots, second column the side view from the right, third column the viewing direction and fourth column the top view. In each plot, all three repetitions of the task are depicted (blue, red and yellow lines).

The trajectories of x-z-plane plots (side view from right side) show a smooth bow shape like characteristic. Due to the involved shoulder *flexion* the appearance is more elliptical compared to a pure 1 DOF elbow *flexion* that should lead to a circular arc like appearance (due to the fact the rotation axis of the elbow joint is not fix and changes while motion execution, also in a restricted 1 DOF case the resulting trajectory is not expected to equal an arc). With higher loads, bending at motion end increases (see Figure 58 line two and three or Appendix A.3 for all measured trajectories). This reflects the observation that shoulder *flexion* is not involved continuously and instead starts at about 90 degree elbow *flexion* and is significantly more distinct at higher loads. This also explains the rougher change of direction at higher loads in column four (top view). In the plots of the y-z-plane (column three – viewing direction) it can be seen that the motion is not performed ideally in parallel to the sagittal plane. Instead, the hand is moved inwards while motion execution, which is mainly caused by a shoulder internal rotation.

The observed characteristic of trajectories remain similar in the Test Scenarios *TS1-n* (forearm orientation restricted to a neutral position at motion start and while motion execution) and *TS1-s* (supinated forearm orientation). For an overview of all measured trajectories of the *weight lift test* see Appendix A.1.

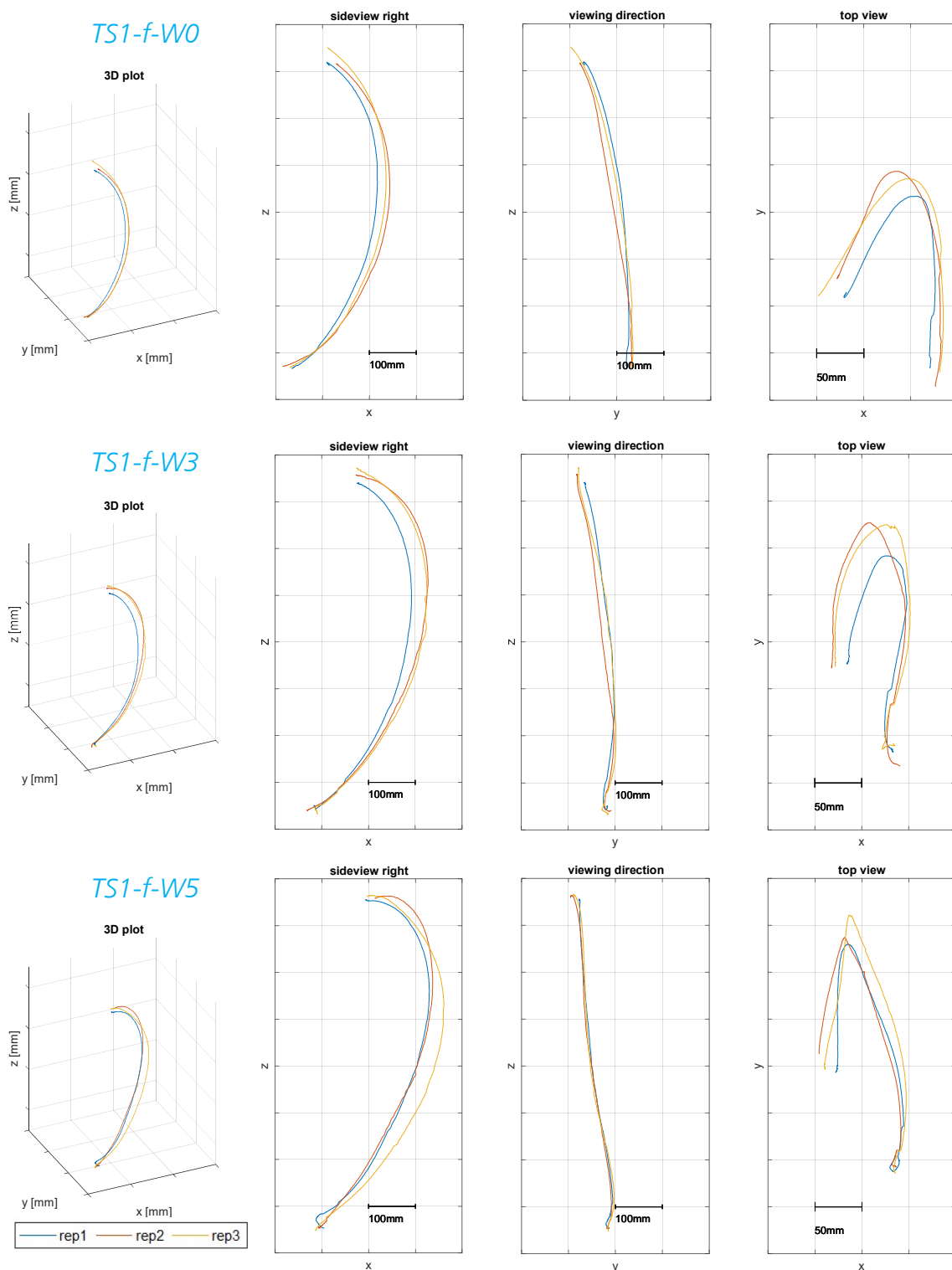


**Figure 58: Measured Trajectories of TS1-f for three different load cases (1<sup>st</sup> row W0, 2<sup>nd</sup> row W2 and 3<sup>rd</sup> row W5).**

In Figure 59, four measured trajectories of TS2 are depicted (TS2-n with weights W0 and W3 and TS2-s with weights W0 and W3). As expected, the side view (x-z plane) shows a circular arc like appearance in this Test Scenario. Also here it can be observed that bending at motion end increases at higher loads. This can be explained by the elasticity of the

supporting foam block (and also the human tissue) which is more compressed at higher loads, especially at motion end, when the forearm is orientated vertically and forces act downwards. In the y-z plane of the unloaded tasks it is noticeable that rotation axis of supinated and neutral forearm orientation differ (*TS2-n-W0* and *TS2-s-W0*, line one and two). In cases with higher loads (like e.g. *TS2-n-W3* *TS2-s-W2*, line two and three) this effect is reduced and trajectories form a more or less straight line, and deviations to the side (y-direction) are reduced (compared to TS1).

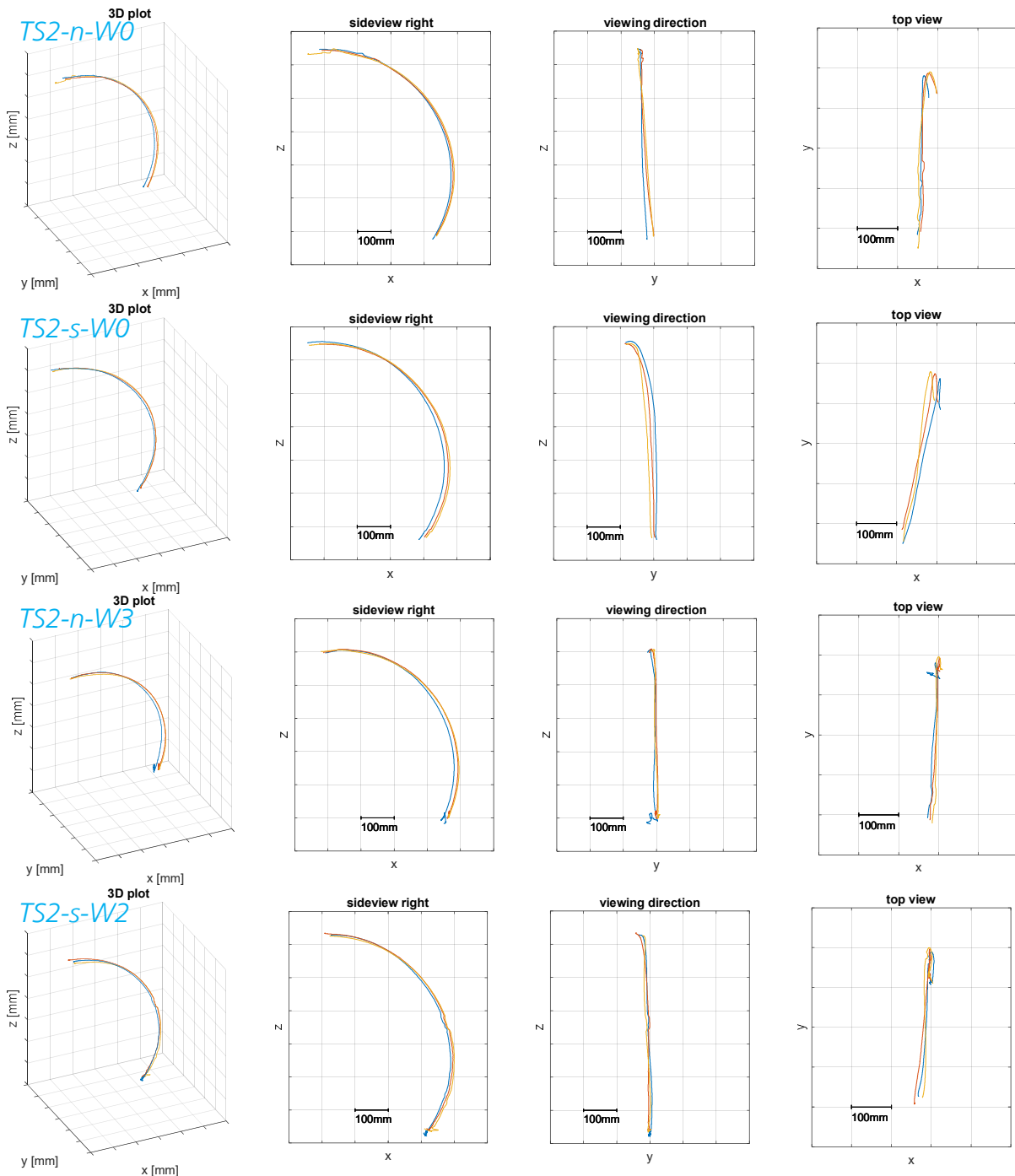
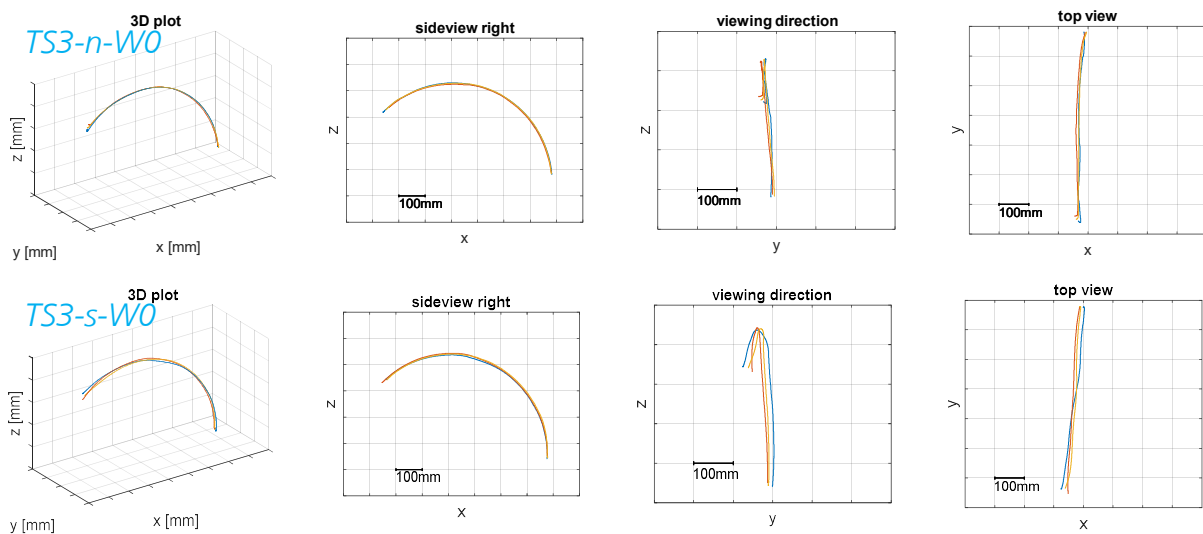


Figure 59: Measured trajectories of Test Scenario TS2-n with weights W0 (1<sup>st</sup> line) and W3 (3<sup>rd</sup> line) and TS2-s with weights W0 (2<sup>nd</sup> line) and W2 (4<sup>th</sup> line).

One explanation for that could be that a completely supinated forearm feels less comfortable with an increasing *flexion* of the elbow joint, which can be avoided by moving the forearm inwards (shoulder internal rotation). Within higher loads, the by that formed lever arm produces a torque in the shoulder, that might make it preferable to choose a non-comfortable joint angle/posture in order to avoid this torque.

This characteristic of the measured trajectories can also be observed in Test Scenario three as shown in Figure 60. Here as well, the effect is reduced with higher loads (see plots in Appendix).



**Figure 60:** Measured trajectories of Test Scenario *TS3-n* (1<sup>st</sup> line) and *TS3-s* (2<sup>nd</sup> line) with weights *W0*.

By visually inspecting video data and the trajectories of *TS2* and *TS3* it can be summed up that the goal to reduce the human motion to one DOF (without a special restriction apparatus) is fulfilled sufficiently.

### 5.1.3 Measured velocity profiles

In Figure 61, the measured velocity profiles of all tasks at the *weight lift test* are depicted. In all Test Scenarios, the highest values are reached at the non-weighted tasks (*W0*, first column) and decrease continuously with higher weights (see lines from left to right). All velocity profiles show a bell shape like characteristics (note that deviations in plots of higher weights – column 3 to column 5 – occur due to tracking problems caused by occlusions of the added weight plates). The highest absolute values are reached in Test Scenario one (*TS1*), where non weighted motions (*W0*) are performed with peak values of about 1,3 m/s and decrease to about 0,7 m/s with the highest weight (*W4*). In Test Scenario two (*TS2*) absolute values are lower with 1 m/s (*W0*) and 0,6 m/s (*W4*) and at Test Scenario three (*TS3*) decrease to 0,8 m/s (*W0*) and about 0,4 m/s (*W4*).

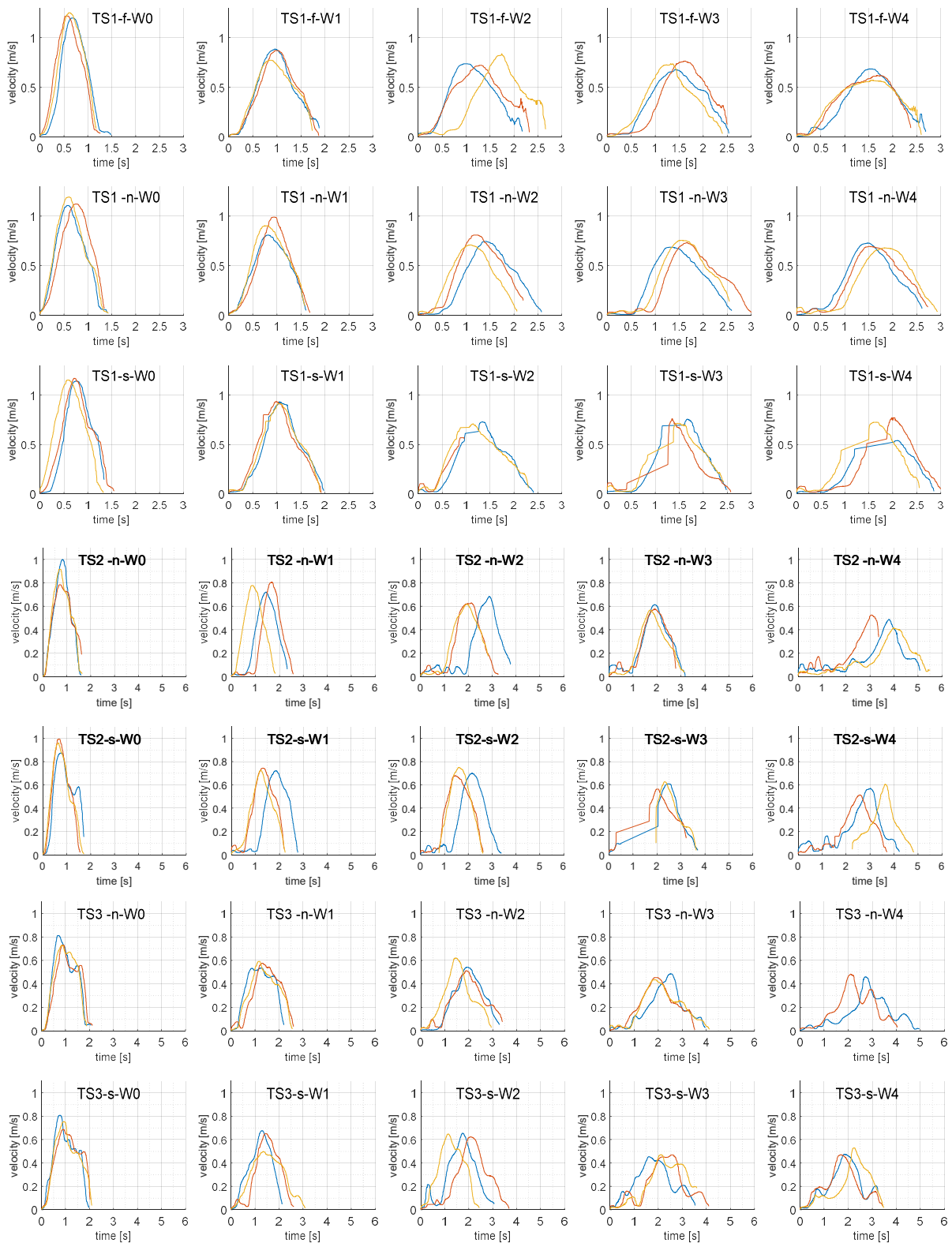
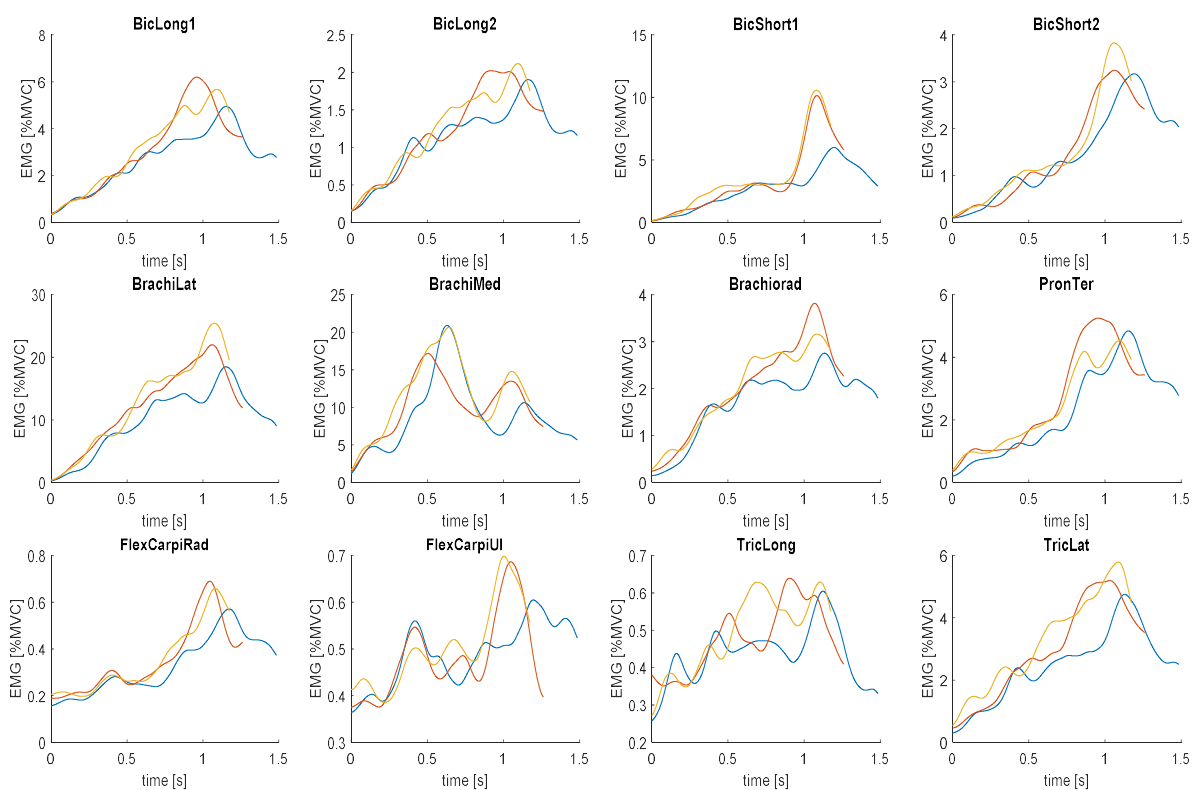


Figure 61: Measure velocity profiles of all Test Scenarios (rows) with all weights (columns) executed at the weight lift test.

### 5.1.4 Measured EMG values

As described above, activity of involved arm muscles is measured with 12 EMG electrodes during task execution, where a special focus is on the dominant elbow flexors Biceps,

Brachialis and Brachioradialis. Each head of the Biceps is measured with two electrodes. This is done to investigate, how much electrode placement influences measuring results during dynamic tasks, as the biceps muscle moves under the electrode during contraction, which might have high influence on the measured signal. For the brachialis muscle there exist no recommendations of electrode placements, and it is discussed controversial if its activity can be measured via surface EMG methods due to the spatial proximity to the biceps muscle [Staudemann 14]. By having two electrodes for each head of the biceps muscle, measured signals can also be compared to the measured signals of the brachialis muscle, to visually determine signal rate of measured crosstalk signals of the biceps muscle. In Figure 62, the measured and filtered EMG signals for all three repetitions for each measured muscle of Test Scenario *TS1-f-W0* are plotted.



**Figure 62: Measured and filtered EMG values of all measured muscles of *TS1-f-W0* (all three repetitions- red, yellow and blue lines).**

Start frames are identified visually by the first visible hand motion, which means that EMG signals of the grasping phase and EMD are included in the plots (as done for all EMG plots of this test). All three repetitions show a similar characteristic and level of activation, which remains valid for all evaluated EMG data in this test (see plots Appendix). In Figure 63, the measured EMG signals of the four biceps electrodes (columns) are plotted for all weights (lines) of Test Scenario *TS1-f*. At lighter weights (line one – *W0* and line two - *W1*), measured values of the Biceps long head (BBL1 & BBL2, column one and two) are about two to three times higher than measured values of the Biceps short head (BBS1 & BBS2, column three and four). Measured values of the two electrodes of one and the same head (BBL2 vs. BBL1 respectively BBS2 vs. BBS1) are about factor two higher at *W0*, at *W1* this is only the case at the long head and short head values become similar (note that Y-axis values differ at lighter weights, line one - line three).

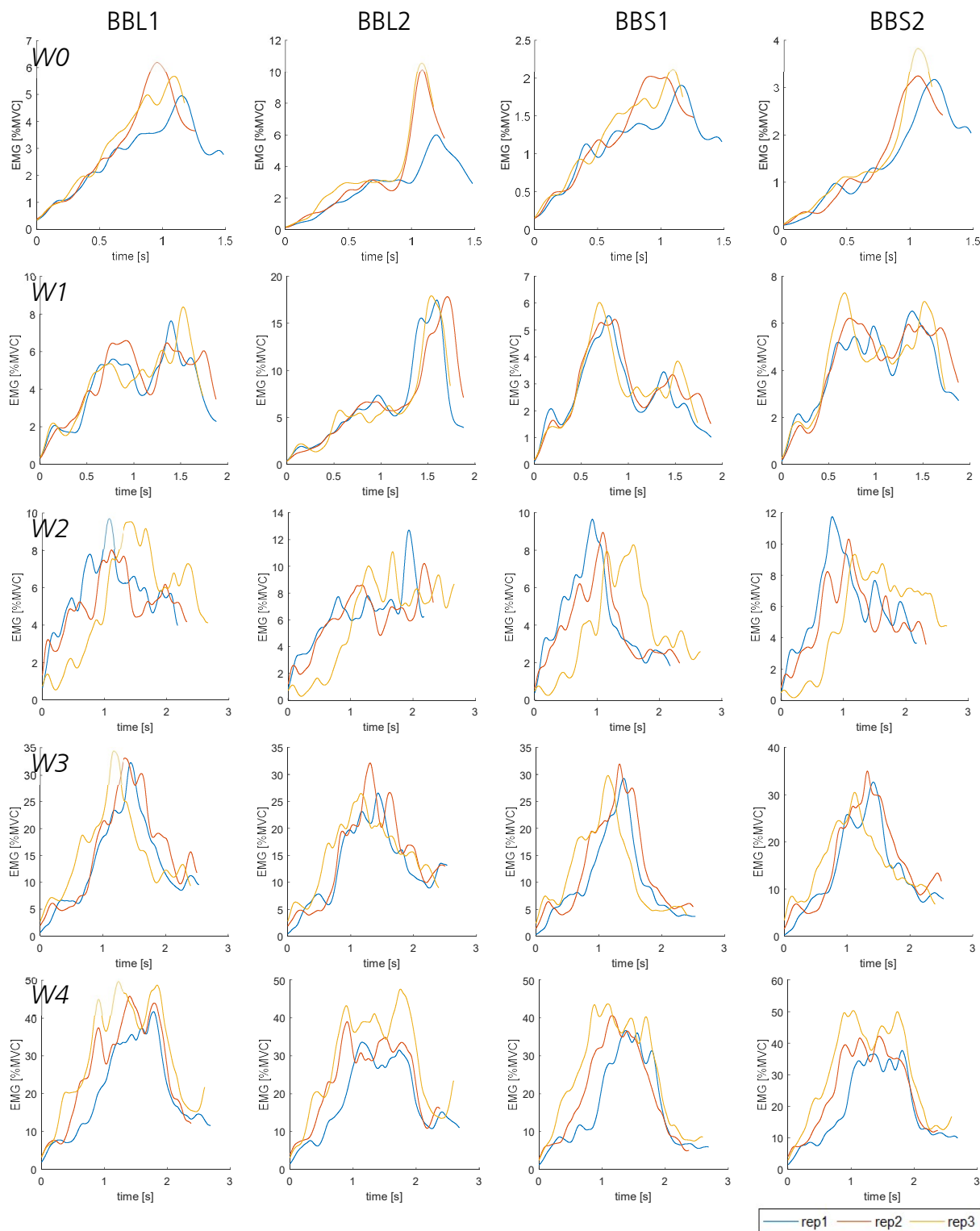


**Figure 63: Measured EMG signals of all four Biceps electrodes (columns) for all weights (rows) of TS1-f.**

Within higher weights, this effects is reduced, so that the measured values for all four electrodes show similar results. In all measurements, the brachialis muscle consistently shows the highest measured values (normalized to MVC – see Appendix), which corresponds with the fact that it is the dominant elbow flexor. The measured values of

the triceps muscle grow by factor three from  $W0$  to  $W4$ , which indicates its contribution (for joint stabilization) also in pure *flexion* tasks. The observed characteristics remain similar in  $TS1-n$  and  $TS1-s$ .

In Test Scenario  $TS2$ , observed characteristics remain similar for lighter weights. At higher loads ( $W3$  and  $W4$ ), the orientation of the forearm has an influence to the magnitude of the measured signal of Biceps, Brachialis and Brachioradialis muscle. A supinated forearm orientation produces EMG signals with peaks at about 100% MVC for all the dominant forearm flexors, whereas values for a pronated forearm orientation are at about 80% MVC. In Test Scenario  $TS3$ , this influence is not measurable, here at the highest weight ( $W4$ ) a supinated as well as a neutral forearm orientation produces peak values of about 80% MVC with the exception of the medial part of the Brachialis, which in both forearm orientations has peak values of 100% MVC.

## 5.2 Simulated test – Test Scenario 1

In  $TS1$ , measurements in the motion lab are performed in an upright standing position. The motions measured in this scenario include beside the elbow *flexion* a shoulder abduction and in  $TS1-f$  additionally a continuous *supination* of the forearm while motion execution. Test persons are advised to keep shoulder center in position while motion execution. As described above, the idea of the *weight lift test* is to reduce the number of DOFs of the performed motion, in order to focus on the anatomical redundancy problem and investigate the influence of the OC cost functions and the Actuation Mode (AM-S vs. AM-T) to the resulting muscle actuations. To avoid the problem of identifying simulation parameters that produce good results (muscle actuations) in one DOF cases, which solve the kinematical redundancy problem in a nonsensical way (compared to human motions) when the number of DOFs is raised, in measurements (and simulations) in  $TS1$  there is also a focus on how the kinematical redundancy is solved.

### 5.2.1 Simulation model and test setup

To keep the simulated motion data comparable with results from the *basic reaching test*, the same simulation model is used to simulate  $TS1$  (5 DOF, 29 muscles - see Figure 64). This also means that no adaptations concerning muscle parameters like maximum muscle forces are done. As shown in chapter 5.1.4, measured EMG values reach 80%-100% MVC at higher weights ( $W3$  &  $W4$ ). As the test subject performing the weight lifting is a much trained person (and stated that lifting tasks with the highest weights are at the limit), this might lead to the problem that motions cannot be performed with the "default" muscle force parameter with the simulation model.

Given is the start configuration (joint angles), and as goal it is defined to lift the center of the wrist over a certain height. No further specifications for the final hand orientation or position are defined. In  $TS1-N$  and  $TS1-S$ , the orientation of the forearm is defined as "constraint" during motion execution and not by restricting the corresponding DOF in the model.

This means that the model has to "hold" the orientation by choosing a convenient muscle actuation. In contrast, if a certain DOF is restricted in the model, the joint can absorb forces in the direction of this DOF, which means that e.g. no muscle forces would be needed to prevent a *supination / pronation* when the forearm should be kept stable in a neutral position. As two dominant forearm flexors (Brachioradialis and Biceps) also induce



a *supination* of the forearm, the way of modelling most probably influences the resulting muscle actuation, also the kinematical motions might be the same or look similar.

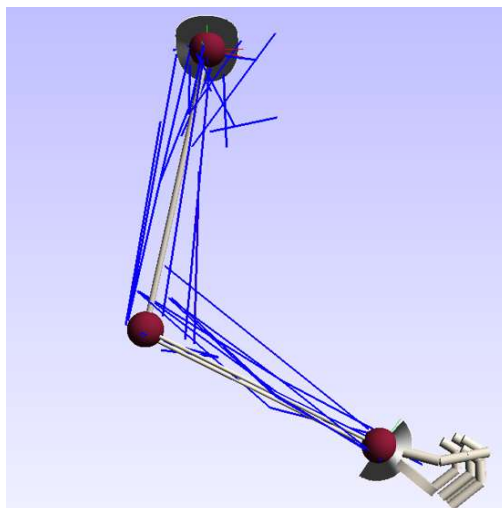


**Figure 64:** simulation model of the weight lift test (rigid bodies representing the human bones visualized in “thin” mode to make muscles visible).

As the fingers in the simulation model are only actuated by joint torque, they are not considered in the simulation, which means that grasping forces are not simulated. So, for simplification, the dumbbell and dumbbell grasping is not simulated. Instead, the weight of the palm in the simulation model is raised according to the weight of the simulated Test Scenario (*W1-W4*).

The muscle synergies used for simulations in Actuation Mode AM-S are those identified and used at the basic reaching test as well. This is also done to keep simulation data comparable, and also to check if muscle synergies are applicable in simulation scenarios which are different to those they were extracted from.

### 5.2.2 Simulated Trajectories – minimal time

In Figure 65, the simulated motion sequences of *TS1-f-W0* for minimal time as cost function are plotted. In the first row motions resulting from a joint torque actuation (AM-T) are shown, in the second row results from a direct muscle actuation (AM-M) and in the third row resulting motions from a muscle synergy actuation (AM-S). As first picture in each row, the start position is depicted and in the following pictures (columns 2-5) each fifth frame of the simulated motion is shown. At the motion resulting from a joint torque actuation (AM-T, 1<sup>st</sup> row), the hand is moved inwards quite far to perform the lifting task. This trajectory does not look unnatural, but differs to the observed motion in the motion lab. Further on, the hand is “oscillating” (*pronation – supination*) while motion execution, which was already observe at the *basic reaching test* when optimizing on minimal time and which appears conspicuously non-natural. Still, the final hand orientation is chosen in a posture that matches the observed final posture in the motion lab quite well.

At a single muscle actuation (AM-M, 2<sup>nd</sup> row) the hand itself is kept in parallel to the sagittal plane while motion execution (as observed in the motion lab). In contrast to the captured motion in the lab, a shoulder *extension* is involved at motion begin and the elbow is turned outwards a bit more pronounced. But overall, the resulting motion looks

very natural and similar to what has been measured. At a muscle synergy actuation (AM-S, 3<sup>rd</sup> row) the shoulder *extension* is reduced and the elbow is also kept in the same plane (parallel to the sagittal plane) as the hand while motion execution. Further on, the final posture matches the one observed in the motion lab very well (forearm steep, almost parallel to frontal plane).

Overall it can be stated that the characteristics observed at the basic reaching test concerning the different Actuation Modes are affirmed by these simulation results. Actuation mode AM-T delivers motions which are – beside an oscillation of the forearm - looking natural but differ to the motions measured at the motion lab. By using muscles as actuators, a single muscle actuation is leading to good and realistic trajectories which are similar to those measured in the motion lab, with some minor deviations on a detail level. The muscle synergies as control parameters for the muscles can reduce these deviations and create an overall more smooth looking version of the motion produced at AM-M.

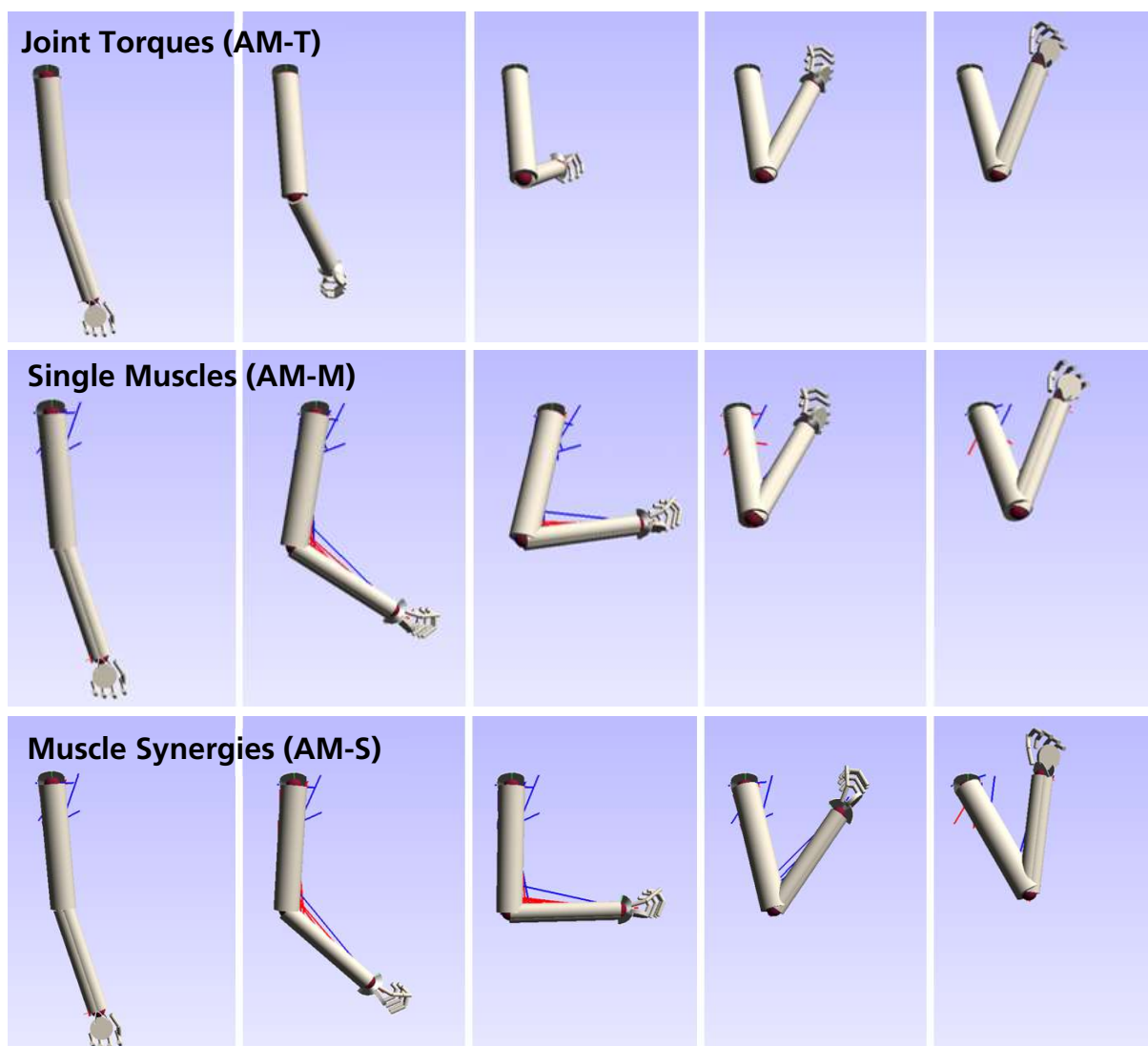
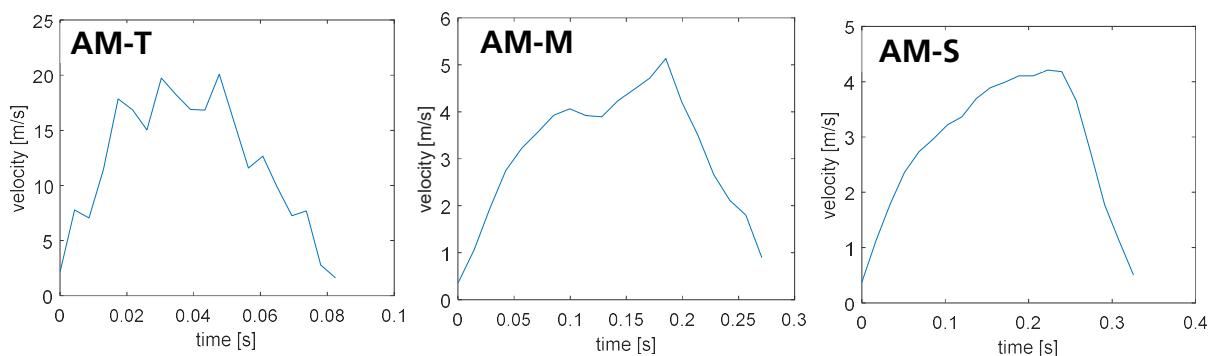


Figure 65: Simulated motions of TS1-f-W0 with minimal time as cost function for the three different Actuation Modes joint torque actuation (AM-T - first row), single muscle actuation (AM-M - second row) and muscle synergy actuation (AM-S - third row).

### 5.2.3 Simulated velocity profiles – minimal time

In Figure 66, the corresponding velocity profiles to the above shown trajectories are plotted (*TS1-f-W0 – min time as cost function*). At the profile resulting from a joint torque actuation (AM-T, *left*) the zigzagging of the plot is salient and caused by the described oscillating of the forearm. The overall appearance has a bell shape like characteristics (when visualizing a line of best fit) similar as the measured velocity profiles (compare with Figure 61), but maximum velocity is with 20m/s about factor 15 higher than the measured peak (1,3 m/s) which leads to a total motion duration of 0,08s (in contrast to 1,2 s measured). Even though the objective for the test persons in the motion lab was to perform the motions “controlled” (and not as fast as possible which would be according to the solved cost function *minimal time*), the simulated velocities are most probably much faster than a human could perform them.



**Figure 66: Velocity profiles of simulation of Test Scenario TS1-f-W0 with minimal time as cost function and the three different Actuation Modes AM-T (left), AM-M (middle) and AM-S (right).**

A direct muscle actuation (AM-M, *middle*) delivers a much more realistic velocity profile. Still the peak velocity is with 5m/s about factor 4 higher than what has been measured in the motion lab, but it is in a level that could probably be reached when the objective is to move *as fast as possible*. Conspicuous is the hard edge representing the peak, which appears to be unnatural and has not been observed at measured velocity profiles.

The muscle synergy actuation (AM-S, *right*) does not show such sudden changes in direction, and the overall shape of the velocity curve reflects the above described observation of the motion as a “smoothed” version of the motion resulting from a direct muscle actuation and matches the measured velocity profiles very well. Also the peak velocity of 4 m/s seems very realistic (compare e.g. with max velocities of 3 m/s at the basic reaching test, Figure 37, where test persons were advised to move fast, but the test setup still involved some precision, which reduces motion speed).

### 5.2.4 Simulated muscle actuations – different cost functions

The above described trajectories and velocity profiles resulting from the three different Actuation Modes AM-T, AM-M and AM-S and the minimized cost function *minimal time* confirmed observations of *the basic reaching test*. Especially a single muscle and a muscle synergy actuation can simulate human trajectories in a predictive manner very well (note that at the simulated *weight lift test* even the muscle synergies were identified in another test, so motion lab measurements are exclusively done and used for validation – no measured parameters are used to adapt the simulation model before simulation).

In a next step, the focus is on the underlying Hill muscle activations used to create these motions in AM-M and AM-S (as in AM-T the model is actuated via joint torques, here obviously no Hill muscle signals can be investigated and compared).

The Hill muscles in the simulation model can be activated between zero and one ( $a \in [0, 1]$ ) – see chapter 3.5.3), so that “1” corresponds to 100% MVC when comparing the simulated activations with measured EMG values (normalized to MVC).

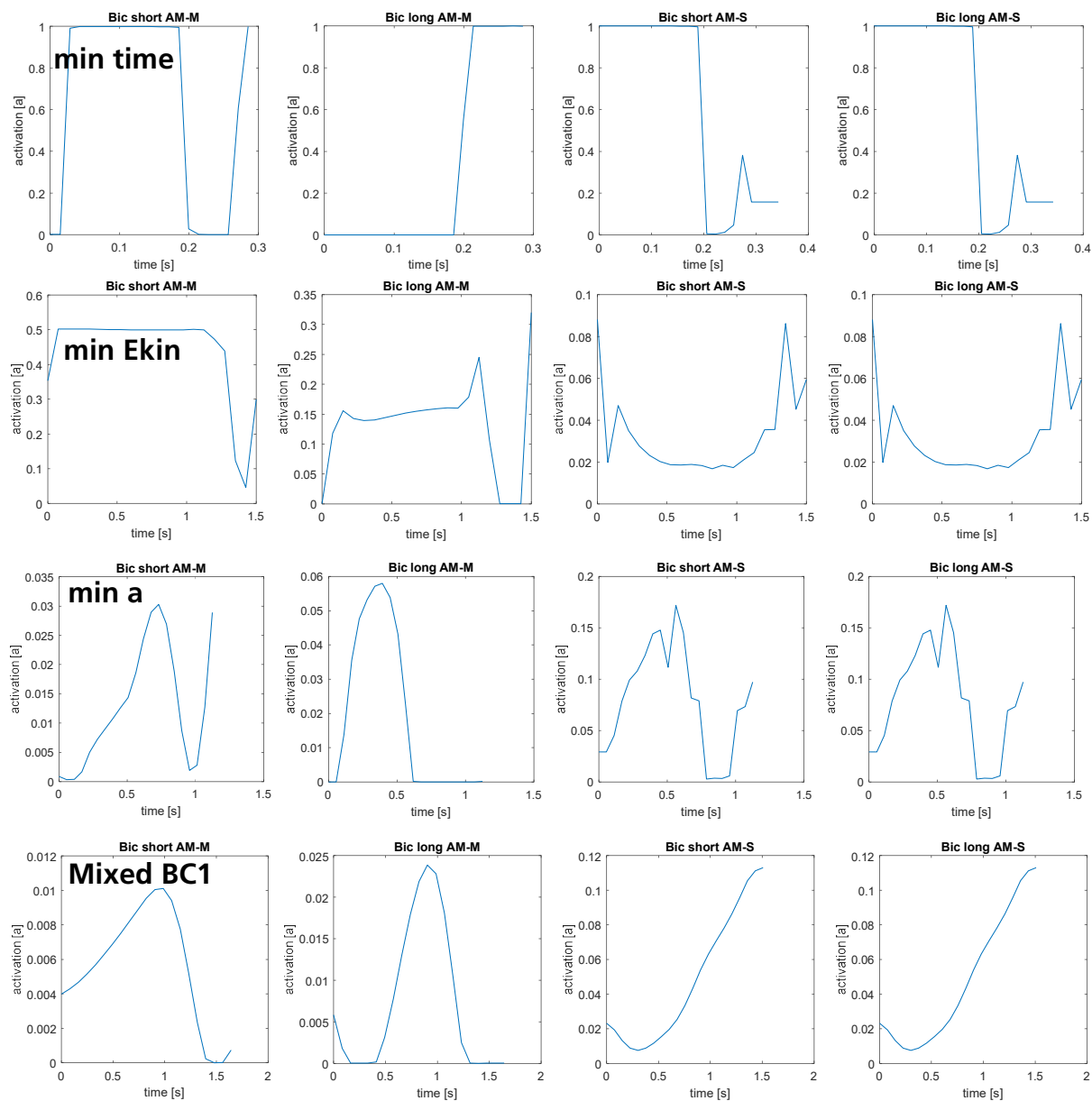


**Figure 67:** Activation level  $a$  ( $a \in [0, 1]$ ) of the Hill type muscles of the biceps long -and short head for a direct muscle actuation (AM-M, column 1&2) and muscle synergy actuation (column 3&4) for simulation of TS1-f-W0. Different OC cost functions (rows).

In Figure 67, the simulated muscle activations for TS1-f-W0 and different OC cost functions (rows, see chapter 3.6) are depicted. Plotted are the signals of the Biceps short head (*Bic short*) and Biceps long head (*Bic long*), each for a single muscle actuation AM-M (column 1 and 2) and for a muscle synergy actuation AM-S (column 3 and 4). Note that at the used muscle synergies the underlying control parameters for *Bic short* and *Bic long*

have a one-to-one correlation (see Chapter 4.3), which leads to the identical activations in AM-S for both heads (column 3 and 4). In all cases, the resulting trajectories appear human like and similar to those shown above whereas velocity profiles differ. When time is minimized (line one), the optimization makes use of the maximum muscle forces, which leads to a “bang-bang” actuation in a single muscle actuation (AM-M). When using a muscle synergy actuation (AM-S), this effect is moderated, but still the actuation level reaches  $a = 1$ , which corresponds to 100% MVC (in contrast, maximum measured values reach about 12% MVC – see Figure 63 BBS2). When minimizing kinetic energy (second row) activation levels vary less with a maximum activation of 50% ( $a = 0,5$ ) using a single muscle actuation (AM-M). With a muscle synergy actuation, the maximum activation level is about 9% ( $a = 0,9$ ), which is very close to the measured values (12%MVC). As described in chapter 3.6, start- and end time ( $t_0$  and  $t_F$ ) are set as free parameters and result from the simulation, whereas they are constrained to a limit set by the user. When minimizing kinetic energy, the optimization exploits the given time limit for the simulation, so that the maximum duration time is reached. The limit in this simulation is set to 1,5s, corresponding to the measured time in the motion lab.

Minimizing the activation  $a$  itself (third row) shows smooth curves in AM-M with a good match of maximum values for the long head of the biceps (Bic long AM-M  $a = 0,05$  vs. 5%MVC BBL Fig.3), but short head values are factor four lower ( $a = 0,03$ . vs. 12% MVC measured). The maximum activations resulting from a muscle synergy actuation (AM-S) are less influenced and remain almost constant (14% min Ekin vs. 16% min  $a$ ). The last row shows the resulting muscle activations when minimizing the mixed OC cost function BC1 (Biomechanical cost function 1). This was derived by investigating the characteristics and properties of each single cost function to the resulting trajectories, velocity profiles and underlying muscle activations. The single cost functions were then used as “controllers” to reduce or reinforce certain properties until the resulting motion matched the measured motion quite well concerning trajectories and velocities (evaluated by comparing simulation results with video data). Activation Levels from BC1 in AM-M are smooth but with  $a = 0,01$  (BIC-short) and  $a = 0,02$  (BIC-long) very low, whereas maximum activation levels in AM-S 11% ( $a = 0,11$ ) as well as the characteristics of the activation curve resemble measured values very well. The predicted duration of the motion is in AM-S (1,4s) as well as in AM-M (1,6s) very close to the measured motion duration (1,2s-1,5s).

Overall it can be stated that a muscle synergy actuation (AM-S) appears to be more robust concerning the maximum values of the produced muscle activation signals compared to a direct muscle actuation (AM-M) in *TS1-f-W0*. Whereas at AM-S the maximum values of the activation  $a$  range between 9% and 16%, at a direct muscle actuation (AM-M) values range between 2% and 50% (excepted when optimizing on time where in both Actuation Modes a full actuation ( $a = 1$ ) is reached. This is particularly noticeable when considering that in both cases the resulting velocity profiles and “global” trajectories are, beside the above described deviations, very similar to one another. In a next step, *TS1-f* is simulated for the weights *W1-W4*, each scenario again with the four different cost functions *minimal time*, *minimal activation (a)*, *minimal kinetic energy* and the derived mixed cost function *BC1* and the two Actuation Modes *AM-M* and *AM-S*. The resulting trajectories remained very similar and natural for the weights *W0-W2*, and the corresponding velocity profiles showed reduced peak velocities and an increased overall duration with higher weights as observed in the motion lab. At high weights (*W3 & W4*), the resulting motion

in a direct muscle actuation (AM-M) changed totally for all cost functions. The hand started to move inwards quite far (internal rotation compared with a horizontal *adduction*) to perform the lifting. The trajectory did not seem undoable for a human, but it appeared unnatural and deviated from what has been observed in the motion lab. From a subjective point of view, it does also not seem a plausible solution for heavy weight lifting, but this has not been proven or tested anyhow. Using a muscle synergy actuation, the optimizer could not find a solution to perform the weight lifting for the weights  $W3$  &  $W4$  in all cases (cost functions).

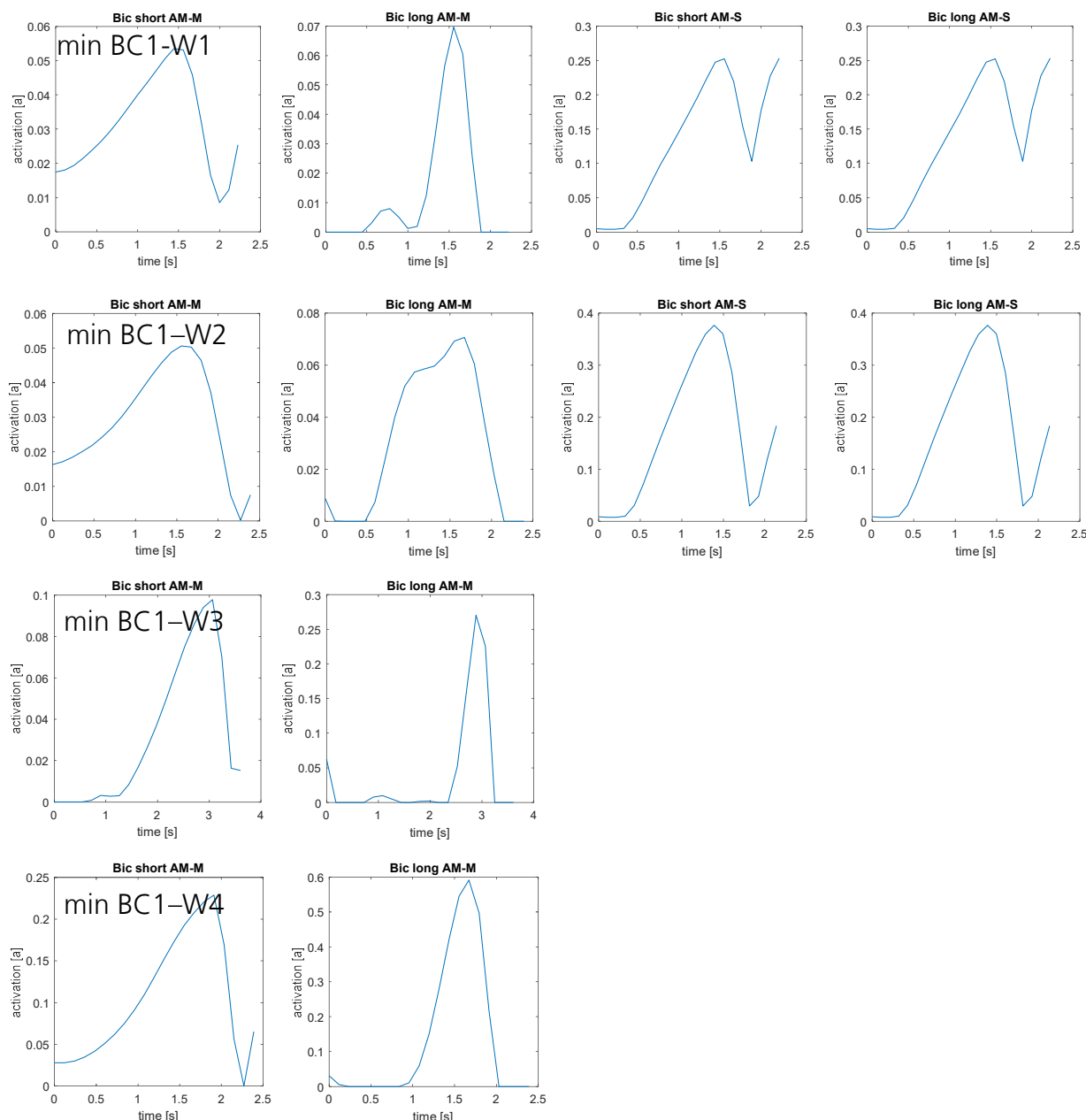


**Figure 68:** Activation level  $a$  ( $a \in [0, 1]$ ) of the Hill type muscles of the biceps long -and short head for a direct muscle actuation (AM-M, column 1&2) and muscle synergy actuation (column 3&4) when simulating TS1-f and solving BC1 as cost function. In each row, a different weight is simulated ( $W1$ - $W4$ ). At a muscle synergy actuation (AM-S), the OC solver could not find a solution for the weights  $W3$  and  $W4$ .

The observed characteristics of the underlying muscle actuation signals remained similar for higher weights ( $W1$ - $W4$ ) when minimizing time. The optimizer made use of a “bang-bang” actuation as observed for  $W0$  in both Actuation Modes. When minimizing kinetic energy, in AM-S the peaks reached full actuation already for  $W1$  &  $W2$ . In AM-M, the peaks remained constant for  $W0$ - $W3$  and reached 100% for  $W4$  &  $W5$ , which is not really comparable as the resulting motions totally deviated from measurements. For comparison, measured peak MVC values of the Biceps muscle are 20%  $W1$ , 14%  $W2$ , 40%  $W3$  and 50%  $W4$ . When minimizing the actuation itself (min a), in AM-S the peak values grew steady (20%  $W1$ , 60%  $W2$ ). In AM-M peak values were lower (10%  $W1$ , 20%  $W2$ , 30%  $W3$  and 70%  $W4$ ). Also here, values for  $W3$  and  $W4$  are not really comparable, as trajectories were different. In Figure 68, the resulting muscle actuations (a) for the mixed cost function BC1 are plotted, which produced natural looking motions and a good match of muscle actuations in AM-S in  $TS1$ - $f$ - $W0$ . For weights  $W1$  &  $W2$ , the peak values reached 25% and 40% in AM-S, which appears plausible (constantly growing with higher weights), but exceeds measured values. In AM-M, simulated peak values remain constant and very low for  $W1$  &  $W2$  (7%), and for the highest weights ( $W3$  &  $W4$ ), as for the other cost functions, data is not comparable due to deviations of the motions.

For higher weights ( $W1$ & $W2$ ), the peaks of the underlying muscle activations in AM-S deviate more in between results of different OC cost functions than it has been observed in  $TS1$ - $f$ - $W0$ . The resulting motions of the derived cost function BC1 appear natural for these weights as well, and the underlying control signals here seem plausible and grow steady with higher weights with similar control curves. The highest weights ( $W3$  &  $W4$ ) cannot be lifted in AM-S and in AM-M the resulting trajectories appeared very unnatural. Here it has to be considered that no model parameters were adapted, and that a one arm biceps curl with 14kg ( $W4$ ), which has been performed by a well-trained person in this test, might not be doable for an averagely trained person as well. From that point of view, the resulting solutions from AM-S can be realistic as weights might simply be too heavy using the “default” model parameters. Overall, simulated (predicted) trajectories of a muscle synergy actuation (AM-S) combined with the derived OC cost function BC-1 delivers very natural looking trajectories in all cases a solution is found, underlying muscle actuations for the biceps seem plausible but higher than those measured. This might be caused due to model parameters which are too low in that case (maximum muscle forces), which would also explain that no solution is found for the highest weights ( $W3$  &  $W4$ ). This can also be seen as “robustness”, as it might be preferable not to find any solution instead of a unnatural one in those cases when working with a DHM. As described above, Test Scenario  $TS1$  was also set up to have a focus on the simulated trajectories, to not identify parameters (cost functions / Actuation Modes) that deliver good results (muscle actuations) in one DOF cases, which would deliver unnatural trajectories when the number of kinematical DOFs is raised again. Here, the derived biomechanical cost function BC1 in combination with a muscle synergy actuation (AM-S) delivered best results and will be further investigated in the Test scenarios  $TS2$  and  $TS3$ , where kinematical DOFs are reduced to one.

### 5.3 Simulated test – Test Scenario 2

As described above, in Test Scenario  $TS2$ , the upper arm of the test person in the motion lab is supported by a foam block so that the angle between upper arm and body (*Humerus*

and sagittal plane) remains at 45 degree while test execution. Further on, the foam block absorbs forces in direction of gravity, so that the positions of the upper arm does not need to be stabilized by a torque produced in the shoulder joint. In the simulation model, this is reproduced idealized by modelling the shoulder joint as “rigid” (meaning that the upper arm is fixed in the root coordinate system). All other model parameters remain similar to those used in the above described model (TS1).

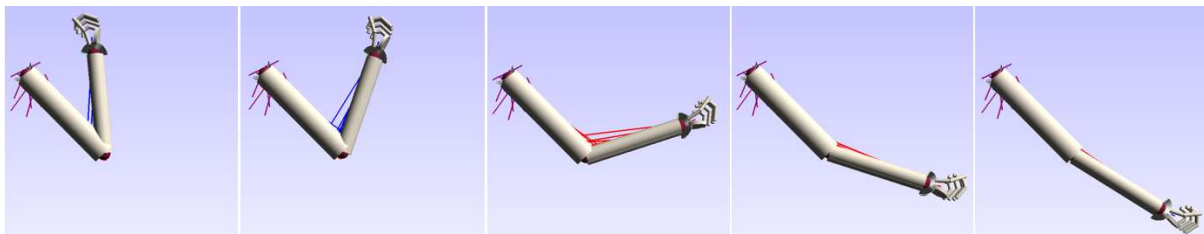


**Figure 69: Simulation of TS2-s – plotted is every 5<sup>th</sup> frame of the resulting motion.**

For simulation, the start- and the end- configuration of the elbow joint is defined, as shown in Figure 69 *right* and *left*. A forearm rotation (*supination / pronation*) is restricted by constraints (with plus minus five degree deviation allowed), and not by “locking” this DOF in the joint, so that the position has to be stabilized by muscle actuations while motion execution.

In Figure 70, the simulated velocity profiles of the resulting motions for a direct muscle actuation AM-M (first row) and a muscle synergy actuation AM-S (second row) when simulating TS2-S and solving BC1 as cost function are depicted. Each column shows the results for a different weight (W0-W4), whereas for W4 no solutions are found (the closest results are plotted). Both simulation modes show very similar velocity profiles, which also match those observed in the motions lab (concerning total duration, shape and peak values) very well (compare with Figure 61 5<sup>th</sup> row – note that in measured velocity profiles grasping phases are included).

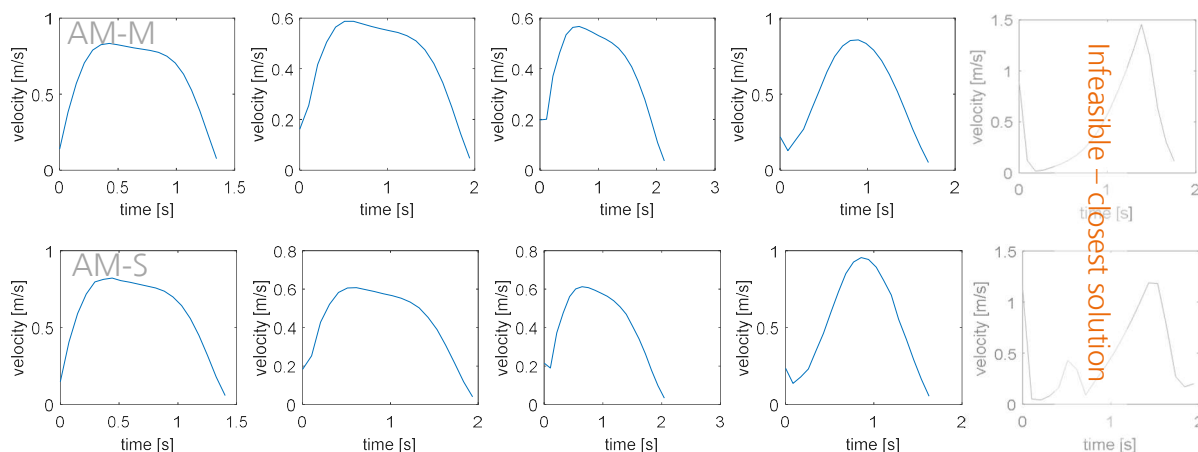


**Figure 70: Simulated velocity profiles for weights W0-W4 (columns) of Test Scenario TS2 when solving BC1 as cost function – a direct muscle actuation (first row) compared with a muscle synergy actuation (second row). Highest weight (W4 – last column) is infeasible, the closest solution is plotted.**

In Figure 71, the simulated muscle actuations of TS2-S for the Biceps short and long head of a direct muscle actuation (Column 1 & 2) and a muscle synergy actuation (Column 3 & 4) when solving the cost function BC1 are compared. In each row, the results



for the different weights (W0 in line one – W4 in line 5) are depicted. As described, when simulation the weight lifting with the highest weight (W4) both Actuation Modes (AM-M and AM-S) failed to find a possible solution.

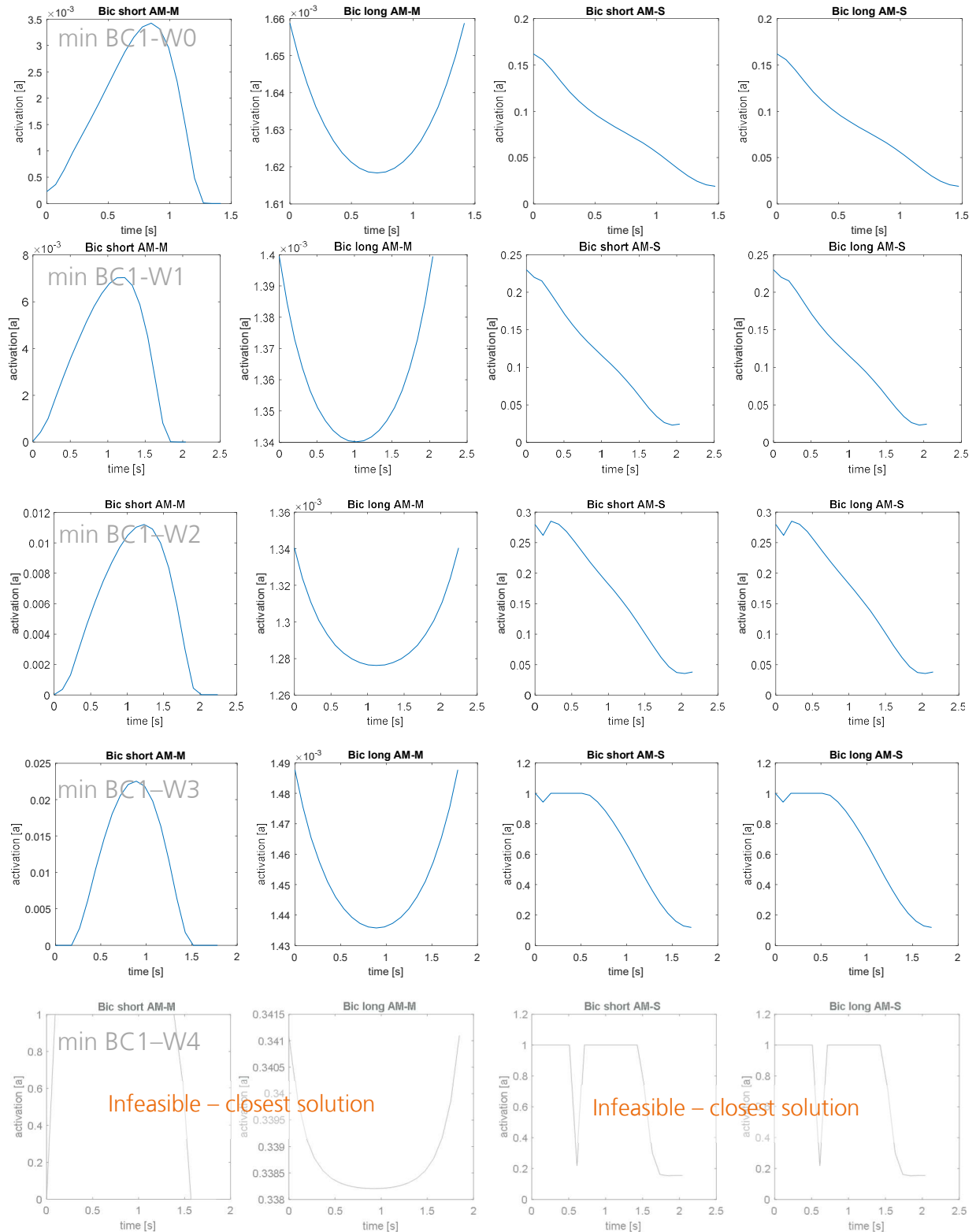


Figure 71: Simulated muscle actuation for Test Scenario TS2-S for all weights (rows) and the cost function BC1. Highest weight (W4 – last row) is infeasible, the closest solution is plotted.

Here again it seems that the weights are simply too high to be lifted with the default muscle parameters. In contrast to TS1, both Actuation Modes fail to find a possible solution in this case. One explanation for this might be that, in contrast to TS1, the solver cannot find a solution in AM-M by choosing a deviating (unnatural) trajectory to solve the problem. This would underline the results of a muscle synergy actuation in TS1 as robust, as in the restricted cases both Actuation Modes converge to similar solutions (although the solver in AM-M can exploit single muscles (muscle heads) independently, it cannot find a solution if the measured (human like) trajectory has to be adhered to).

The peaks of the simulated muscle actuations in AM-S seem very plausible and grow steady from 16% ( $\cong a=0,16$ ) at W0 over 23%(W1), 30%(W2) to 100% (W3). As comparison, measured muscle peaks of the biceps muscle are 5%MVC (W0), 10%MVC (W1), 20%MVC (W2), 60%MVC (W3) and 100%MVC (W4) – see Appendix.

Simulated muscle actuation in AM-M in contrast are very low and never exceed 2,5% activation, which is far below the measured values.

#### 5.4 Simulated test – Test Scenario 3

Test scenario TS3, is set up as one DOF problem similar as Test scenario TS2, but now with an angle between upper arm and body (*Humerus* and sagittal plane) of 90° while test execution. Again, the upper arm in the motion lab is supported by a foam block to keep the angle constant while test execution and to avoid high torques in the shoulder joint. For simulation, the same model and idealization is used as in TS2 (upper arm is fixed in the root coordinate system), with the shoulder angle adapted accordingly to 90°.

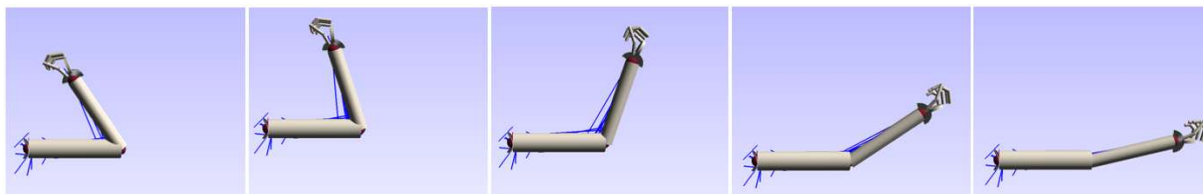


**Figure 72: Simulated motion of TS3 -. BC1 as cost function solved.**

Simulation boundary conditions and constraints are chosen similar as in TS2, the start- and the end- configuration of the elbow joint is defined, as shown in Figure 72 *right* and *left*. A forearm rotation (*supination / pronation*) is restricted by constraints (with plus minus five degree deviation allowed), and not by “locking” this DOF in the joint, so that the position has to be stabilized by muscle actuations while motion execution.

In Figure 73, the simulated velocity profiles of the resulting motions for a direct muscle actuation AM-M (first row) and a muscle synergy actuation AM-S (second row) when simulating TS3-S are depicted. Each column shows the results for a different weight (W0-W4). In this Test Scenario, the OC solver could not find a solution for the weights W3 and W4 (the closest results are plotted). Both simulation modes show very similar velocity profiles, which also match those observed in the motions lab (concerning total duration, shape and peak values) very well (compare with Figure 61 7<sup>th</sup> row – note that in measured velocity profiles grasping phases are included).

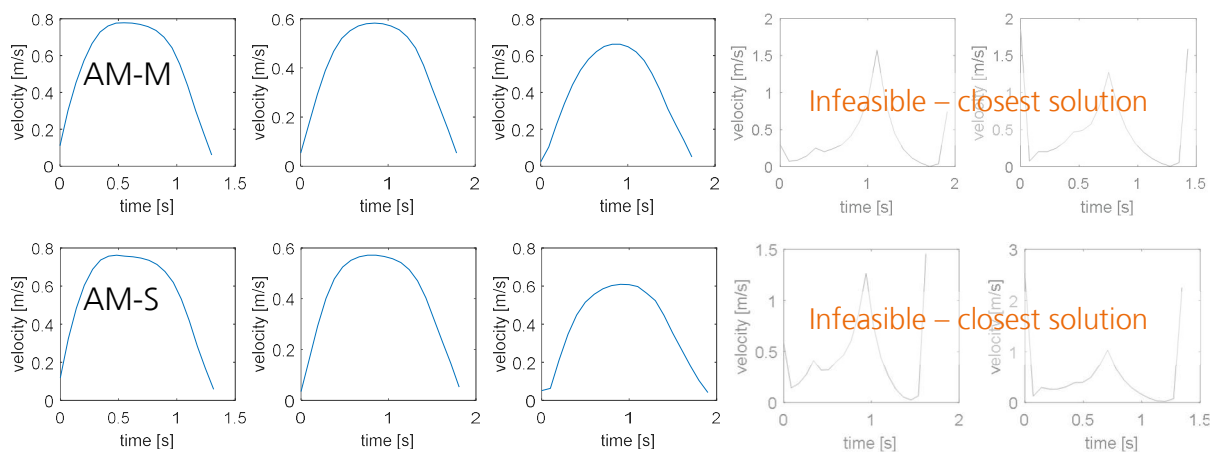


**Figure 73: Simulated velocity profiles for weights  $W_0$ - $W_4$  (columns) of Test Scenario TS3 when solving BC1 as cost function – a direct muscle actuation (first row) compared with a muscle synergy actuation (second row). The weights  $W_3$  and  $W_4$  (3<sup>rd</sup> and 4<sup>th</sup> column) are infeasible, the closest solution is plotted.**

In Figure 74, the simulated muscle actuations of TS3-S for the Biceps short and long head of a direct muscle actuation (Column 1 & 2) and a muscle synergy actuation (Column 3 & 4) when solving the cost function BC1 are compared. In each row, the results for the different weights ( $W_0$  in line one –  $W_4$  in line 5) are depicted. In Test scenario TS3, the OC solver did not find a solution to perform the weight lifting for the weights  $W_3$  and  $W_4$  for both Actuation Modes (AM-M and AM-S). Here again the closest solutions that were found are plotted.

At a muscle synergy actuation (AM-S, column 3 & 4), the simulated Hill-muscle actuation peaks are almost constant for  $W_0$  and  $W_1$ , whereas the activation curves (and the resulting velocity profiles) differ. For the weight  $W_2$ , the peak value of the activation level increases to about 35% with a similar activation curve as for  $W_1$  (and also similar resulting velocity profile). As comparison, measured MVC values are 4%MVC at ( $W_0$ ), 8%MVC ( $W_1$ ), 20%MVC ( $W_2$ ), 50%MVC ( $W_3$ ) and 80%MVC ( $W_4$ ) – see Appendix. For the weights  $W_3$  and  $W_4$  the lifting task cannot be performed. As described above, also in the motion lab the test persons are not able to perform the lifting in this cases in a “clean” way (shoulder flexion involved to achieve an elbow flexion for motion start). Interpreting the plots of the closest solutions (Figure 74, line 4 and 5 - column 3 & 4), it seems that also in the simulation most forces are needed in the start phase (activation level  $a=1$ ) and are simply not high enough (and due to the idealization and constraints in the simulation model, the solver cannot make use of a shoulder flexion / caving in of the elbow joint).

Although the resulting velocity profiles of a muscle synergy actuation (AM-S) and a direct muscle actuation (AM-M) are very similar, the underlying muscle activation levels of the biceps muscle strongly differ. In AM-M, the activation curves of biceps short head (column 1) and biceps long head (column 2) are almost inversely proportional. Also measured values of biceps short- and long head do differ in measurements especially with low weights, this is mainly about the activation level and activation curves are mostly very similar. As already observed in TS-2, the activation levels of the biceps muscle resulting from a direct muscle actuation are far below the values measured in the motion lab. Same as in AM-S, the weights  $W_3$  and  $W_4$  cannot be lifted in AM-M.

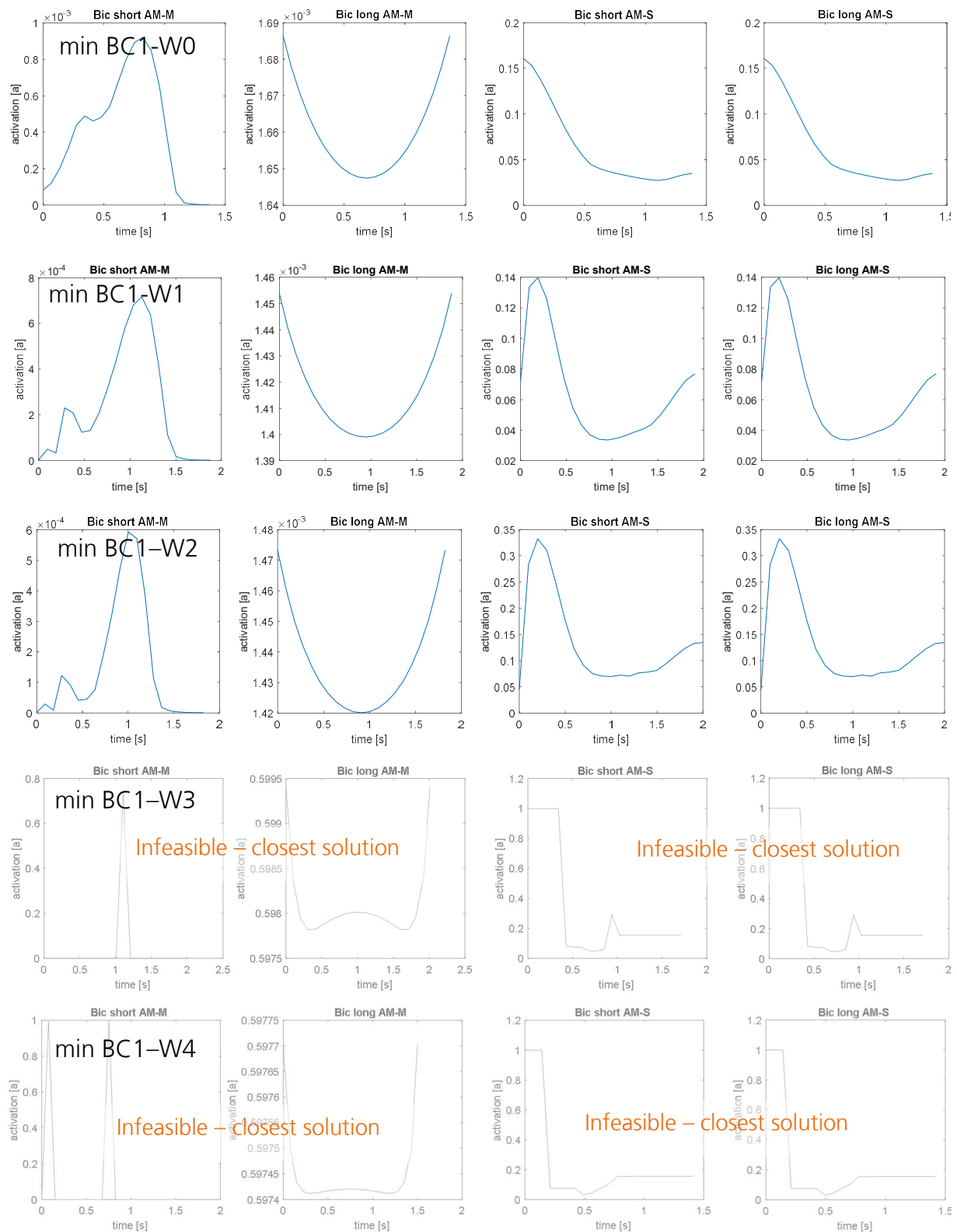


Figure 74: Activation level  $a$  ( $a \in [0, 1]$ ) of the Hill type muscles of the biceps long - and short head for a direct muscle actuation (AM-M, column 1&2) and muscle synergy actuation (column 3&4) when simulating TS3-s and solving BC1 as cost function. In each row, a different weight is simulated (W1-W4). The OC solver could not find a solution for the weights W3 and W4 (4<sup>th</sup> and 5<sup>th</sup> row), the closest solution is plotted.

## 6 Industry use case – box lifting

In this chapter, first investigations are done with a full body digital human model simulating a relevant use case from industry, to determine if the derived simulation approach can be applied in realistic and relevant and also more complex scenarios.

### 6.1 Motivation from industry

Lifting objects like boxes and cartons, as shown in Figure 75, is a common work task in many industry branches as e.g. logistics, often performed highly repetitive per shift. To reduce the risk of injury and work related musculo-skeletal disorders, workers are e.g. instructed on proper lifting techniques, cycle times are reduced and loads exceeding a certain weight are restricted. Still, overload or fatigue leading to adverse postures and motions cause injuries, health and safety issues.



*Figure 75: Cardboard box lifting task in industrial application. From [iStock.com/KatarzynaBialasiewicz].*

To better understand the effects of object lifting on the human body, an ergonomic study was commissioned by a big logistic company, where a multitude of lifting scenarios in the motion lab were performed. In these studies, motion capture data as well as EMG data of the involved muscles were acquired, to identify cases and motions leading to high muscle actuations and by that may cause fatigue in repetitive tasks. The derived ergonomic findings of these studies allow to optimize the existing processes like cycle times, limits for maximum weights or lifting techniques. Still, when e.g. planning new work stations of a logistic center, a simulation tool to predict those results would be very helpful, as in this state no existing processes to assess are given. Further on, motion lab experiments are very time consuming and expensive and in principle only valid for the measured use case and test person. To investigate how far the in this work derived approach and identified control parameter are suitable to simulate more complex use cases, one lifting tasks of the above described measurements is simulated with a full human body model, and simulation results are compared with the acquired data of the motion lab experiments.

## 6.2 Motion Lab test description

As a validation case, the in Figure 76 depicted *box lifting test* is chosen. In this Test Scenario, test persons grab a box from a table placed in front of them, and lift the box to about shoulder height where it should be hold static for one second. The test is performed with different weights and also with different boxes.

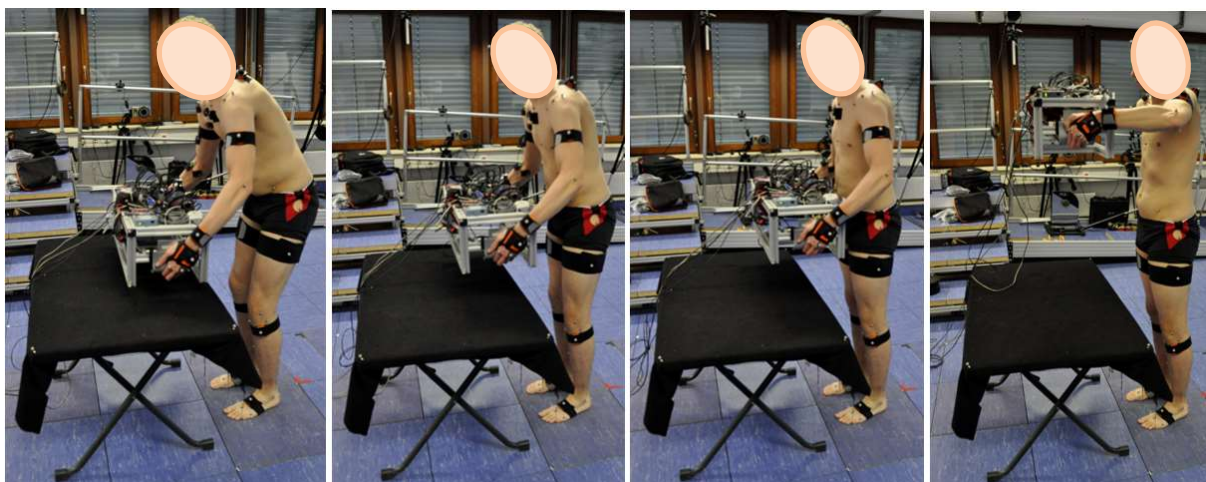


**Figure 76:** Motion Lab measurements of the “Box Lift test” with a force measurement box.

Beside the depicted force measurement box, where pressure sensors are placed at a defined grip and effects and behavior at heavier weights are investigated, tests are also performed with simple cartons, where no grips are available and the test persons have to grab the box with the flat hand and freely choose the grasp position on the side (lateral surface) of the carton, similar as in Figure 75. In these cases, also a pressing force between both hands has to be applied to create the needed friction force to be able to lift the carton. This case is chosen for simulation, as the free grip position and the needed pressing forces add some complexity to the task to be solved.

Resulting from the EMG measurements, especially in cases with lower weights, no dominant muscle was identified for fulfilling the task. Instead, all muscles of the upper extremity like shoulder girdle, shoulder, elbow and radioulnar joint as well as of wrist and hand are involved. In cases with higher loads, some muscles (e.g. Trapezius, Teres Major and Delta) showed higher contribution in single phases, but still the interaction of all muscles was most dominant with increasing activations of all muscles.

## 6.3 Simulated Test

For simulating the “box lifting test”, a full body human model is used as depicted in Figure 77. The legs, torso and head are modelled simplified as rigid bodies connected via joints (red balls) and actuated by joint torques. Attached to the torso is the already introduced arm model with 29 Hill muscles (now for left and right arm and 7 DOF) with a modified hand. To simulate the friction contact gripping, the hand is modelled flat and rectangular for simplification. The wrist is modelled as two revolute joints and controlled completely by the Hill muscles (*Ulnar / radial deviation* as well as *flexion* and *extension*). The carton is modelled as rigid body with a certain weight.

As start condition, the orientation of the human model is given as shown in Figure 77 left, with the box placed in front of the manikin on a table. The table, the box and the manikin itself are considered as collision geometries in the simulation.

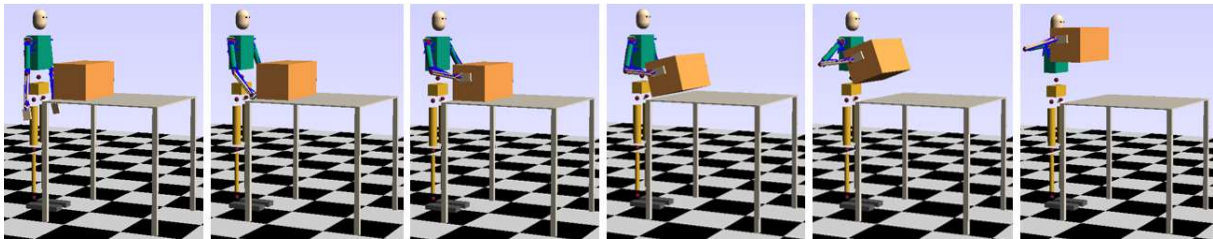


**Figure 77:** Simulated test results of the “box lifting” with arbitrary grip position on the side of the carton. Both arms with 7 DOF each fully actuated by 29 Hill muscles, creating normal forces for frictional contact as well as lifting forces.

As goal it is defined to lift the center of the box to a certain height (about shoulder height, no further orientation defined), whereas the lateral surfaces of the box are given as possible grip areas. The exact position for grasping is a free parameter of the optimization problem, as well as the applied pressing force to produce a proper normal force for friction contact (Coulomb friction, coefficient of static friction  $\mu_s = 1$ ). The test is simulated with the in Chapter 5 derived biomechanical cost function BC1 as optimization criteria and a direct muscle actuation (AM-M) as well as a muscle synergy actuation (AM-S). In both cases the “global” strategy is very similar. The simulation model chooses the grip points in the vertical symmetry axis of the carton and slightly above the center of mass (horizontal symmetry axis). After lifting the carton from the table it is moved to the body and then lifted close to the upper body.

As observed before, the motions resulting from a muscle synergy actuation are slightly slower and appear a bit smoother compared to a direct muscle actuation, but not as significant as observed at other Test Scenarios. The underlying muscle actuations also differ for the different Actuation Modes (see Appendix). In both cases all muscles are involved with different magnitudes in a lower activation range. At a direct muscle actuation the *extensor carpi radialis longus* and *teres minor* are with 40% activation ( $\alpha = 0,4$ ) slightly more dominant than the other involved muscles. At a muscle synergy actuation the *Teres Major* muscle is with 60% activation ( $\alpha = 0,6$ ) significant higher than the other involved muscles.

## 6.4 Results and Discussion

First simulation results of the *box lift test* indicate, that the derived approach and the OC control framework are also suitable to simulate realistic use cases and can by that deliver important information concerning human motions, underlying muscle activations and resulting forces, which can support design engineers to achieve a human centered and ergonomic workplace layout without the need of physical prototypes.

At the *box lift test*, the free parameter of choosing a grip point, the frictional contact, the weight of the box, the resulting kinematical closed loop when grabbing the box with both arms and the 14 kinematical DOFs of the arms controlled by 58 Hill muscles (plus the other DOFs of the simplified human body model) bring a high complexity in the system. Still, the solver converges to a very realistic and human like solution just by defining a very

generic goal. This shows that the used optimal control framework can be a convenient control strategy to predict motions of a digital human model. The use of Hill muscles as actuators resulted in human like trajectories at the *basic reaching test*. At the *box lift test* it is now shown that this actuation principle is not only suitable in simplified examples. The solver converges and the simulated trajectories are human like, also the complexity is much higher. The use of Hill muscles transfers the underlying actuation properties of the dynamic system from humans to the DHM (as e.g. force-length and force velocity dependency of muscles), which might be the reason why the optimizer converges to similar trajectories as humans choose to fulfill a task. This would be a big achievement, as it would allow to predict human behavior and motions for completely new scenarios, including the optimization on not only postures, but also velocities, accelerations, external forces and dynamic quantities like inertia effects.

Muscle synergies as control principle showed smoother velocity profiles at *the basic reaching test* and *the weight lift test*, which were closer to those measured in the motion lab. Further on, the investigated muscle actuation signals appeared to be more realistic (human like). *The box lift test* shows now, that the actuation principle can be applied to more complex used cases, and also here the resulting motions appeared as a smoothed version of those resulting from a direct muscle actuation. As already discussed above, this could be the reason due to the fact that the synergies have been extracted from measurements at humans, so they might capture some human like activation characteristics. The synergies used in all three tests are extracted at *the basic reaching test*, which attributes them a certain generality. Muscle synergies might capture activation characteristics of the CNS resulting from e.g. the need for a joint stabilization by muscles in humans, which is not the case in the used DHM approach (and by that not predicted by the optimizer).

Overall, from evaluating simulation results from *the box lift test*, the used control framework appears to be quite promising concerning the central issue of predicting human like motions in unknown scenarios for ergonomic assessment. The detailed human arm model with 29 Hill muscles showed, that a human like control and actuation principle can lead to human like motions in a predictive manner. Muscle synergies are transferred as control parameters to the DHM and have shown their applicability also in this use case with raised complexity. The in this thesis simulated use cases are all limited to the range of motion of the simplified shoulder model. To simulate the whole range of motion of the human shoulder joint, it would be necessary to develop a more detailed model of the shoulder including all four sub joints (see chapter 2) including the relevant muscles for actuation. This refinement can be performed with the used OC MBS framework. Concerning the rest of the human body, the use of a joint torque actuation might be sufficient in a first step, as many cases concerning ergonomics mainly effect the upper extremities. Further on, many muscles of the trunk are activated isometrically for stabilization of the body, so that they do not change their length a lot and properties of muscles force generation do not have such a big effect here. Due to that, to predict muscle forces of these muscles (e.g. for ergonomic assessment), a “workaround” by the use of muscle synergies similar as in [Razavian 18] could e.g. be used, where calculated forced of the controller are “mapped” to a set of muscle actuations by the use of muscle synergies.



## 7 Conclusion and Outlook

In the work presented in this thesis, the author developed a control and validation approach for a biomechanical digital human model, with the overall goal to simulate human like motions in a predictive manner for the use in ergonomic assessment. For motion generation, a pre-existing optimal control framework is used, which allows to build up human models or to model parts of the human body by the use of a multibody system code. Bones are modeled as rigid bodies connected via joints, which can be limited to the human range of motion. The model can be actuated via joint torques or by simplified Hill muscle models. The OC code then calculates the actuation signals in a way, that a certain goal is fulfilled, while minimizing some cost function and considering the side constraints that the equations of motion of the MBS are fulfilled. In contrast to most other control strategies, the goal can be described in a quite generic manner and no further control signals have to be defined. It was assumed, that human like control and activation principles, especially the use of Hill muscles as actuators and *time invariant muscle synergies* as control policy can lead to human like motions (trajectories, velocity profiles) and muscle actuations. Muscle synergies result from the field of neuroscience, and are one hypothesis how the human central nervous system could simplify control. Several studies on animals and humans, which are reviewed in the first part of the thesis, give evidence for the existence of muscle synergies in vertebrates. Instead of activating each muscle in particular, muscles are grouped into building blocks (or synergies), where each muscle is present in each synergy with a fixed amplitude that does not change over time. Muscle activations can now be generated by activating those building blocks and sum up the output for each muscle from each block. By that, the number of control parameters is reduced as the number of synergies (building blocks) is smaller than the number of muscles. To transfer muscle synergies into a control policy for a digital human model, develop a concept for motion validation (in order to assess how „human like“ a solution is) and investigate the characteristics of the different Actuation Modes (joint torques, muscles and muscle synergies), several sub steps have been performed in this thesis.

First, the basics of human motion generation are treated. The anatomical background is summarized, with a special focus on bones and joints of the human arm, as the main experiments performed later in this thesis work focus on human arm motions. The principles of human force generation by muscles are treated, including activation properties of moto neurons and the electrical excitability of muscle tissue. Muscles are attached to the bones via tendons, and by contraction they create pulling forces which lead to motions. Due to the nature of the underlying principle of force generation by the filament proteins, muscles have a force-length and a force-velocity dependency. When a limb is moved, the muscle insertion point is moving, which means that e.g. the angle between the muscle tendon and bone are changing, which leads to a different lever arm and by that influences the resulting joint torque. These are important properties of the human locomotor system, which are transferred to the digital human model by simplified Hill muscles. In later on performed and validated simulations it is shown that this actuation principle applied to a digital human model already leads to trajectories very close to those a human chooses (in contrast to trajectories resulting from a joint torque actuation).

Afterwards, the approach for control and validation developed in this thesis is treated and the relevant details of each sub step are explained. From experiments in the motion lab

trajectories are captured, and muscle activation signals are recorded by the use of electromyography measurements. Muscles are excited electrically by the central nervous system and EMG measurements allow to measure the summed up signals of all active muscle fibers at the surface of the muscle (skin). So, the height of the measured signal correlates to the number of active muscle fibers and by that to the produced force. To normalize the measured signals, the *maximum voluntary contraction* is estimated for each muscle, the highest EMG value that is measured when as much force as (voluntary) possible is produced. From EMG values, muscle synergies can be extracted (see below), which can then be used as control policy in the optimal control framework. The experimental setup is then simulated in the OC framework under similar conditions as done in the motion lab, whereas the influence of different Actuation Modes (joint torques, muscles, muscle synergies) and OC cost functions can be investigated. By comparison with measured values, it can be assessed how "human like" a solution is.

The derived approach was applied to three specific test setups, each with a special focus. At the *basic reaching test*, test persons performed a multitude of different reaching motions to target points on a plane, from different distances and orientations towards the plane. Additionally, at some tests, a weight cuff was attached to the test person's wrist. From these tests, trajectories were measured by the use of an optical tracking system, and muscle activities of 16 arm and shoulder muscles were measured via EMG measurements. The measured EMG signals were then arranged in a matrix and muscle synergies were extracted, using a *non-negative matrix factorization* algorithm. The NMF algorithm searches for a subset of *basis vectors*, which allow to reproduce the matrix of measured signals with minimum error. These basis vectors are interpreted as the *time invariant muscle synergies*, whereas the number of synergies is a free parameter of the algorithm and has to be defined by the user. The quality of the extracted synergies was assessed for different numbers of synergies by calculating the *Variance Account For*, visual inspections of original and reproduced signal, and by further crosschecks (testing how good measured EMG signals can be reproduced with synergies where these reproduced EMG signals were not used as input for the NMF algorithm). Due to the nature of the NMF algorithm (*least square fit*), EMG signals with smaller amplitudes have a smaller influence on the error between measured and reproduced signal (compared to EMG signals with higher amplitudes). VAF values reached the common threshold of 90% already with five synergies. Visual inspections showed that in this case errors of EMG signals with smaller amplitudes were neglected, although these signals appeared consistently at repetitions of the same task. In this thesis it was argued that these EMG signals, as they are constantly reproduced by the CNS, must be important for human motor control as well. By continuously raising the number of the muscle synergies and visually comparing original and versus muscle synergies reproduced signal, the number of synergies regarded as sufficient was raised to ten.

In a next step the measured reaching tasks were set up in the OC simulation framework. In these simulations, a five DOF human arm model was used, actuated by joint torques or 29 implemented Hill muscles and adapted to the test person's anthropometries. The extracted muscle synergies were transferred as control parameters in the OC framework. Similar as in the motion lab, start and final configuration of the arm were defined, and *minimal time* was solves as *cost function*, as test persons were advised to move as fast as possible. Motions resulting from a joint torque actuation looked realistic on a first glance (assessing slow-motion video data), but the chosen trajectories were different to those

---

measured in the motion lab and velocities were much too high. A direct muscle actuation delivered trajectories very similar to those measured in the motion lab and maximum velocities became close to those measured. A muscle synergy actuation with ten synergies delivered similar trajectories, whereas maximum velocity and especially velocity profiles became much closer to those observed in the lab (bell shaped characteristic). Control simulation with a reduced set of synergies confirmed the approach of visual inspections of EMG signals and did not deliver good results. *Minimal time* as cost function resulted in a *bang bang* actuation, which was moderated by a muscle synergy actuation, but still muscle activities were much higher than those measured in the lab.

To further investigate underlying muscle activities, the *weight lift test* was set up. Test persons in the motion lab performed elbow flexions (*biceps curls*) with five different weights and at different upper arm and forearm orientations. At all tests, beside the Test Scenario 1 (upright standing), the motions were reduced to one kinematical DOF to focus on the anatomical redundancy. Test scenario 1 was in a first step simulated with *minimal time* as cost function and confirmed results of the *basic reaching test*. Hill muscles as actuators delivered very similar trajectories to those measured in the motion lab, whereas muscle synergies as control parameters showed smoother velocity profiles. Then, the influence of different OC *cost functions*, (*time, kinetic energy, control, control change*) to the resulting motions and muscle actuations, was investigated. From these investigations, a mixed OC cost function was derived (*biomechanical cost function BC1*), which delivered very realistic motions and muscle activations in non-weighted cases for the biceps muscle. This cost function was then used to simulate the other Test Scenarios with raising weights. A direct muscle actuation thereby showed very low values for the simulated biceps activations and additionally high variations of the values of the different muscle heads (biceps short and long head). A muscle synergy actuation in contrast appeared to be very robust concerning the variations of the underlying muscle actuations. Although simulated absolute activations values were higher in the simulation than those measured, the simulated biceps values grew constantly with higher weights in the simulation (as it was the case in the measurements). One simple reason for the difference of absolute values could be that the parameter for the maximum muscle force of the simulation model did not match the maximum muscle force of the test person (in contrast to the anthropometry values, the parameters for maximum muscle forces were not adapted to the test persons as there is no simple in-vivo procedure existing to estimate those parameters).

The last simulated test was the *box lift test*, where a cartoon box was lifted from a table with both arms to about shoulder height. This test was performed to check, if the derived control approach is also applicable in a more complex and realistic scenario. In the simulation, the box could be grabbed on a free position on the sides, lifted by creating a normal force (frictional contact), and each arm of the full body model had seven kinematical DOFs and was fully controlled by 29 Hill muscles. Also this brought a high complexity into the system, the OC solver converged to a very human like solution just by defining the very generic goal of grabbing and lifting the box to a desired height. Here again, the motions resulting from a muscle synergy actuation appeared as "smoothed version" of those resulting from a direct muscle actuation.

Overall the developed control and validation approach showed promising results. The developed validation concept allowed for an assessment of how "human like" a simulation result is, comprising the chosen trajectories, velocity profiles as well as muscle

activations. Of course, muscle activation signals are the most challenging aspect here and still inherit uncertainties, which holds true for the measured EMG signals as well as the simulated actuation signals. But here one has to be aware of that even a rough prediction of the (peak) values of physiological muscle strains resulting from a work task would be of high use for ergonomic workplace layout. Using (simplified) muscles as actuators raises complexity of the model, especially due to the redundant nature of human muscle actuation principles (more muscles than kinematical DOFs). The comparison of measured motions (motion lab) with simulated motions showed that the used and investigated OC control framework cannot only handle this complexity but that the use of this actuation principle in a simulation model leads to human like trajectories and velocities. Although the resulting trajectories were very realistic, the underlying muscle activations differed from those that were measured. This was improved when muscle synergies were used as control parameters. Further on, the resulting motions appeared as “smoothed” version of those resulting from a direct muscle actuation with velocity profiles being very similar to those measured in the motion lab.

**In future work**, the developed control and validation approach should be applied to further use cases, to see if the results of this work can be confirmed also in other scenarios. As in this thesis work only the human arms were actuated by muscles (with the shown advantages), the developed approach should be extended to the whole human body. The most challenging part remains the prediction of EMG data. To achieve reliable data for muscle activities, simulated and measured muscle actuation signals need to be investigated in more detail. This comprises the analyses of muscle data of all involved muscle of use cases measured and simulated in this work, but also setting up further tests designed with a specific focus on this topic. This could e.g. be done by focusing on further joints or other motions of the investigated elbow joint (e.g. weighted extension). Muscle synergies seem to be a promising approach to transfer human muscle activation characteristics to a DHM, especially in cases where these activations result from properties that are not present in the simplified model (e.g. the need for joint stabilization by muscle co-activation). One limit here is that the used method of surface EMG does not allow to measure deep layer muscles. Here, future algorithms for separation of surface and deep layer muscle signals of surface EMG could be expedient, as first results are shown in [Koshio 2012]. Alternatively fine wire EMG could be used, which is an invasive procedure allowing only for isometric motions, which complicates experimental design and execution. Another challenging issue are muscle parameters, which are highly relevant when it comes to validity of simulation results (e.g. assessing if a worker will be able to lift a part independently or if a support tool or second person is needed). As maximum muscle forces cannot be measured directly, a special procedure e.g. by the use of laboratory measurements in combination with some kind of optimization methods needs to be developed. This might allow to estimate worker specific data, which would enable personalized workplace layout, or with sufficient data, to generate averaged parameter sets (e.g. for the population of a plant). The derived approach showed promising results and a further development could be a big improvement for state of the art digital human models used for ergonomic workplace layout.

# A Experimental and Simulation results

## A.1 Weight lift test data

In the following, all measured data of the weight lift test (see chapter 5) is plotted. In A1.1 the measured trajectories for all Test Scenarios (TS1-TS3) are shown, in A.1.2 the velocity profiles, in A.1.3 the measured EMG data and in A.1.4 simulation results.

### A.1.1 Weight lift test - Measured Trajectories

In this subsection, the measured trajectories for all Test Scenarios are plotted. For each task, all three repetitions are overlaid in one plot (blue, red and yellow lines).

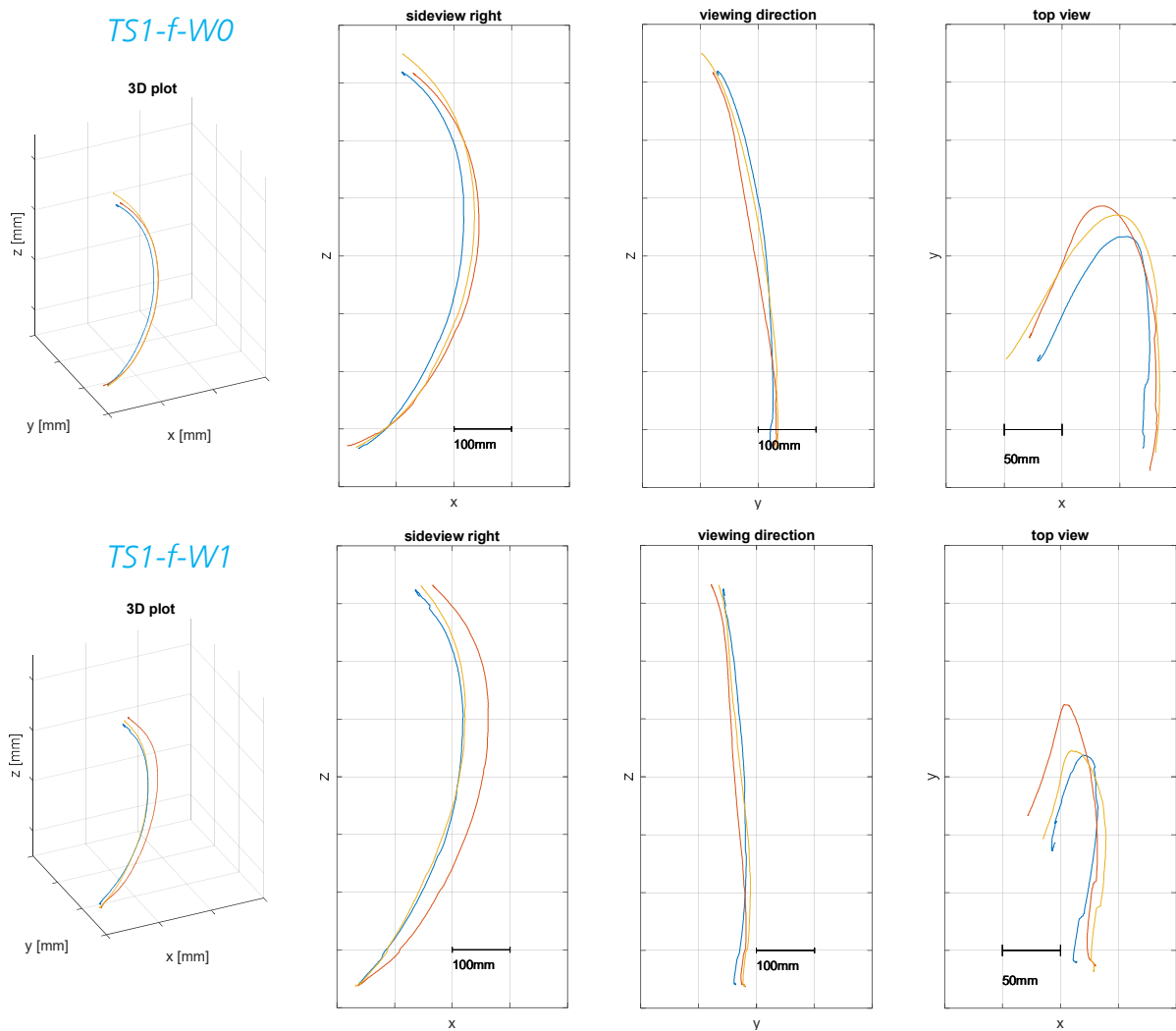


Figure 78: Weight lift test - Measured Trajectories

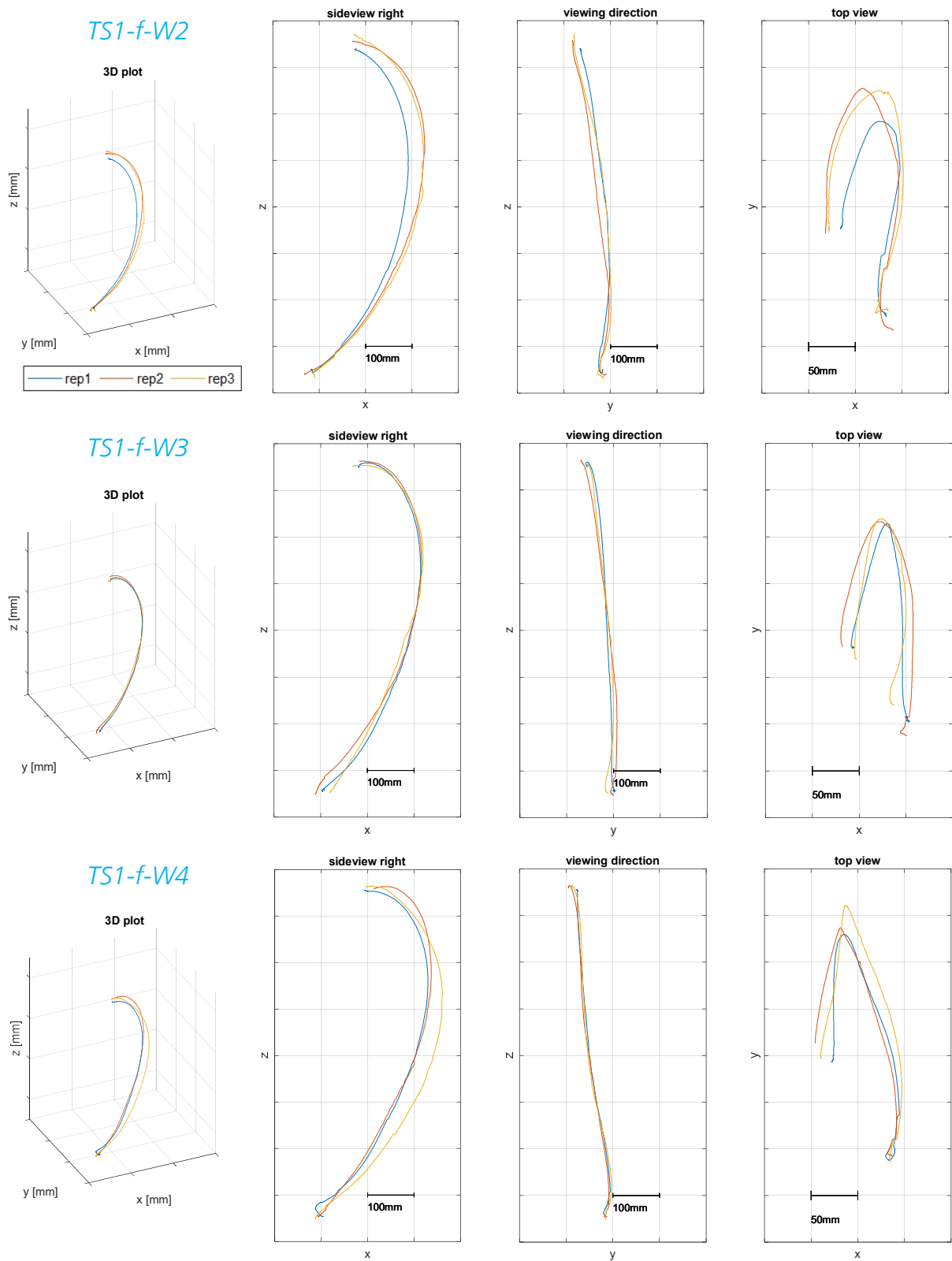


Figure 79: Weight lift test - Measured Trajectories

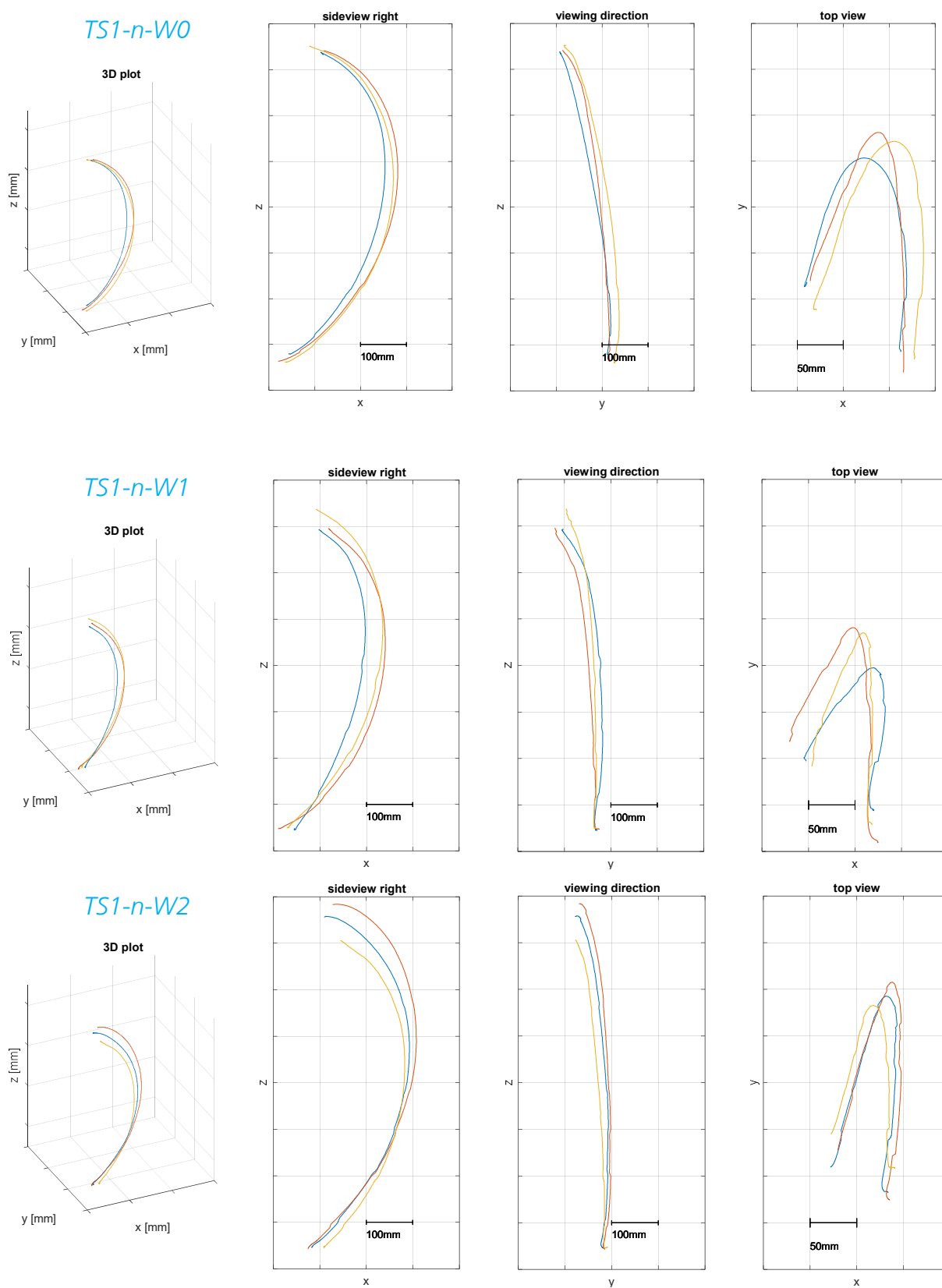


Figure 80: Weight lift test - Measured Trajectories

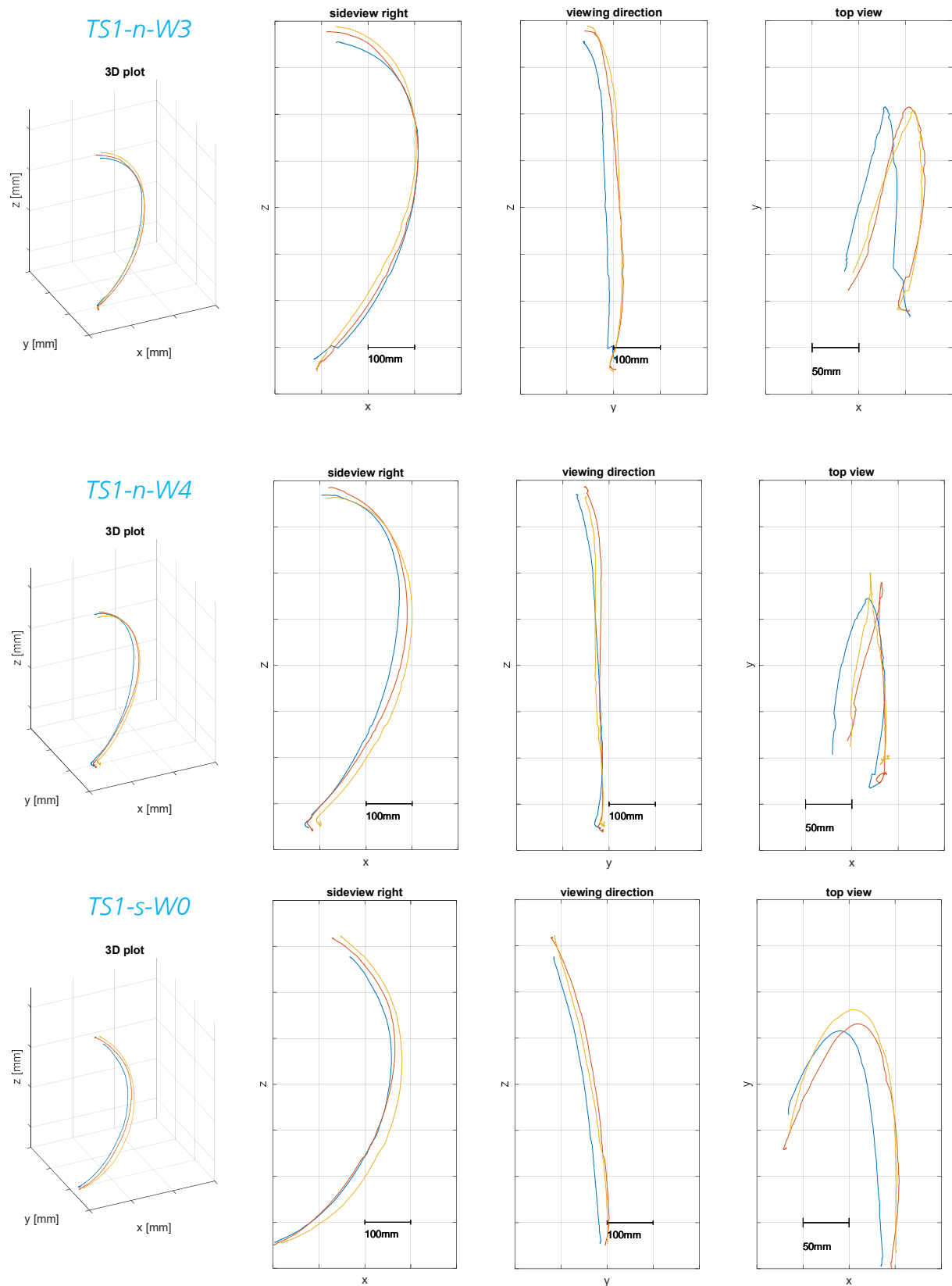


Figure 81: Weight lift test - Measured Trajectories



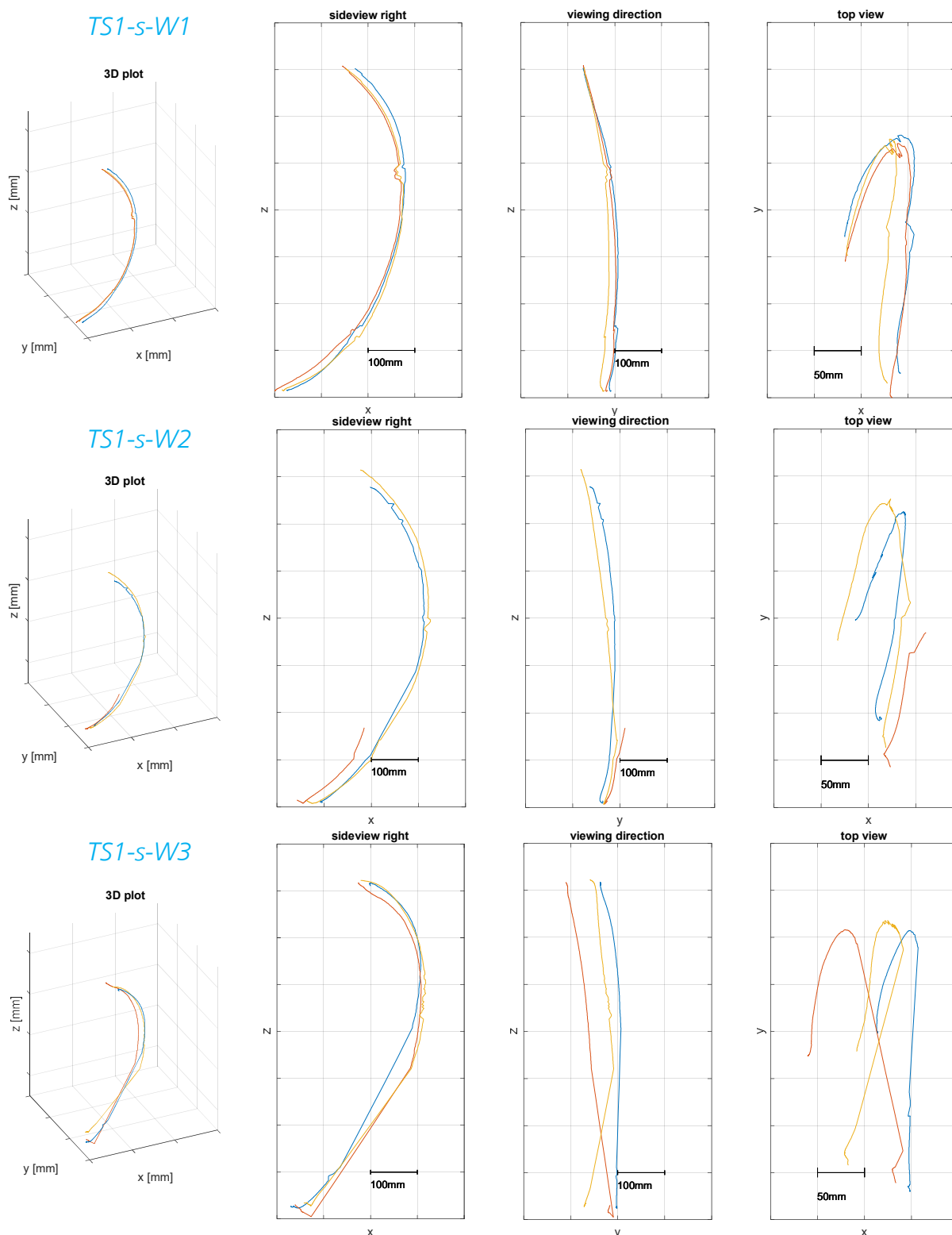


Figure 82: Weight lift test - Measured Trajectories

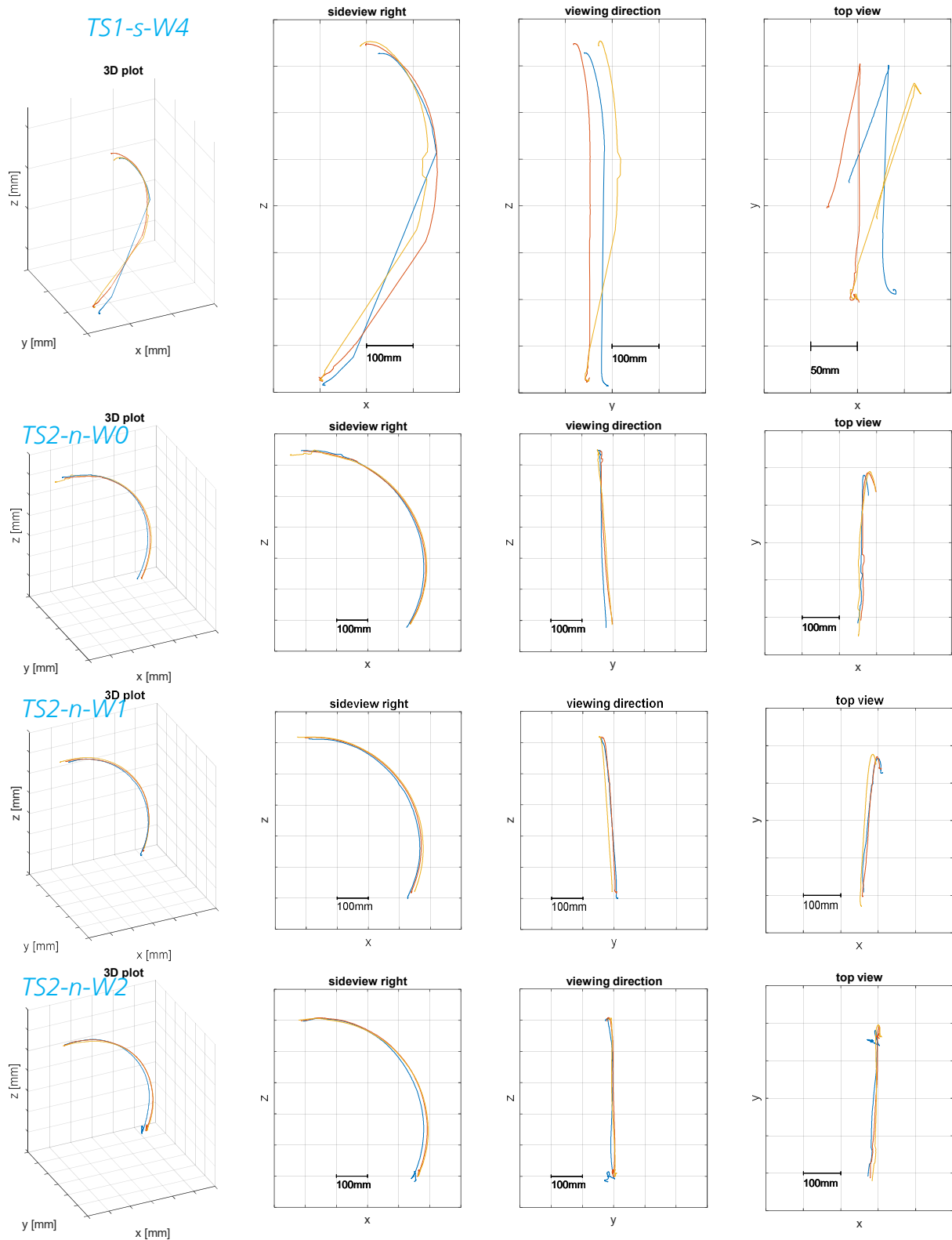


Figure 83: Weight lift test - Measured Trajectories

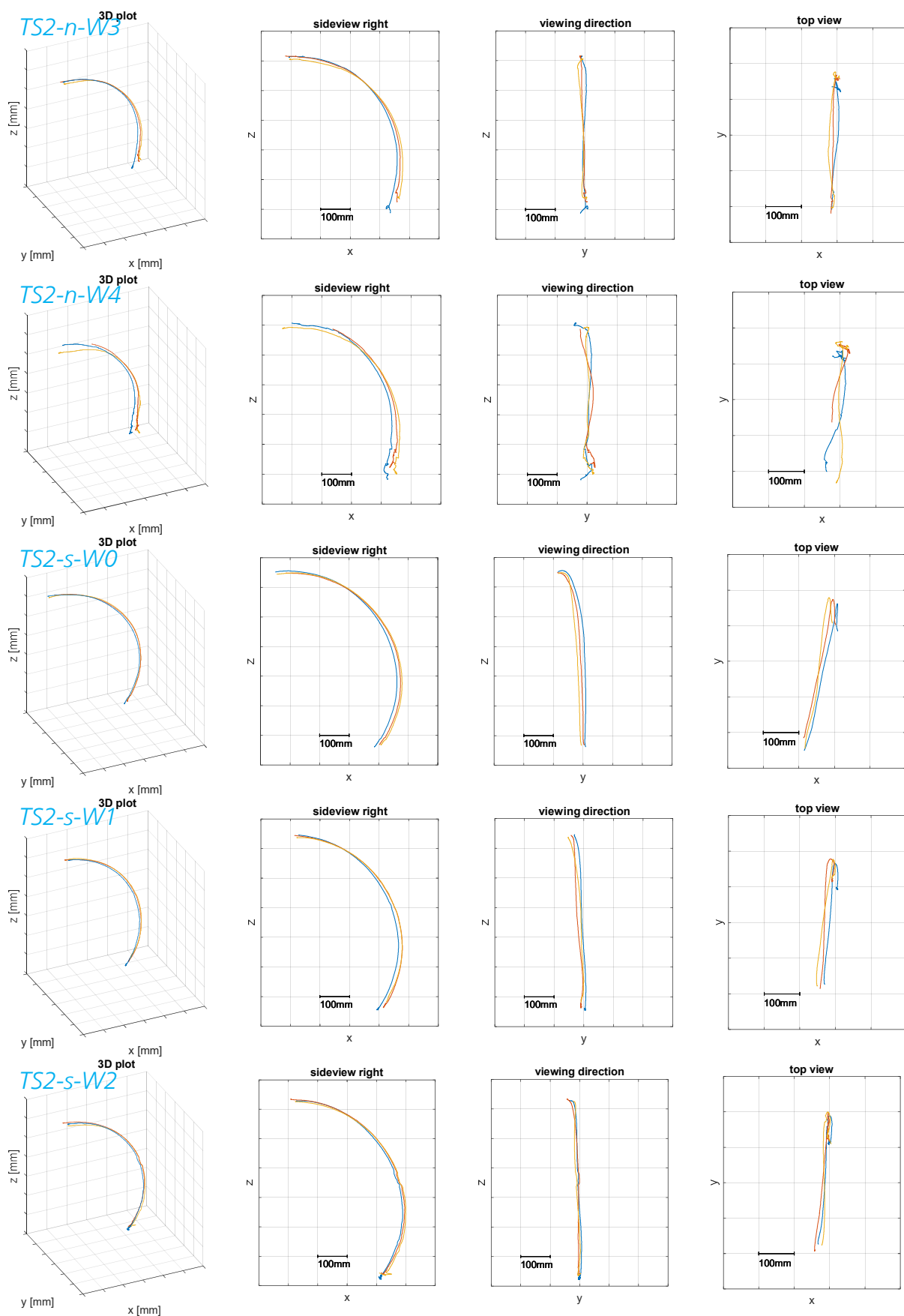


Figure 84: Weight lift test - Measured Trajectories

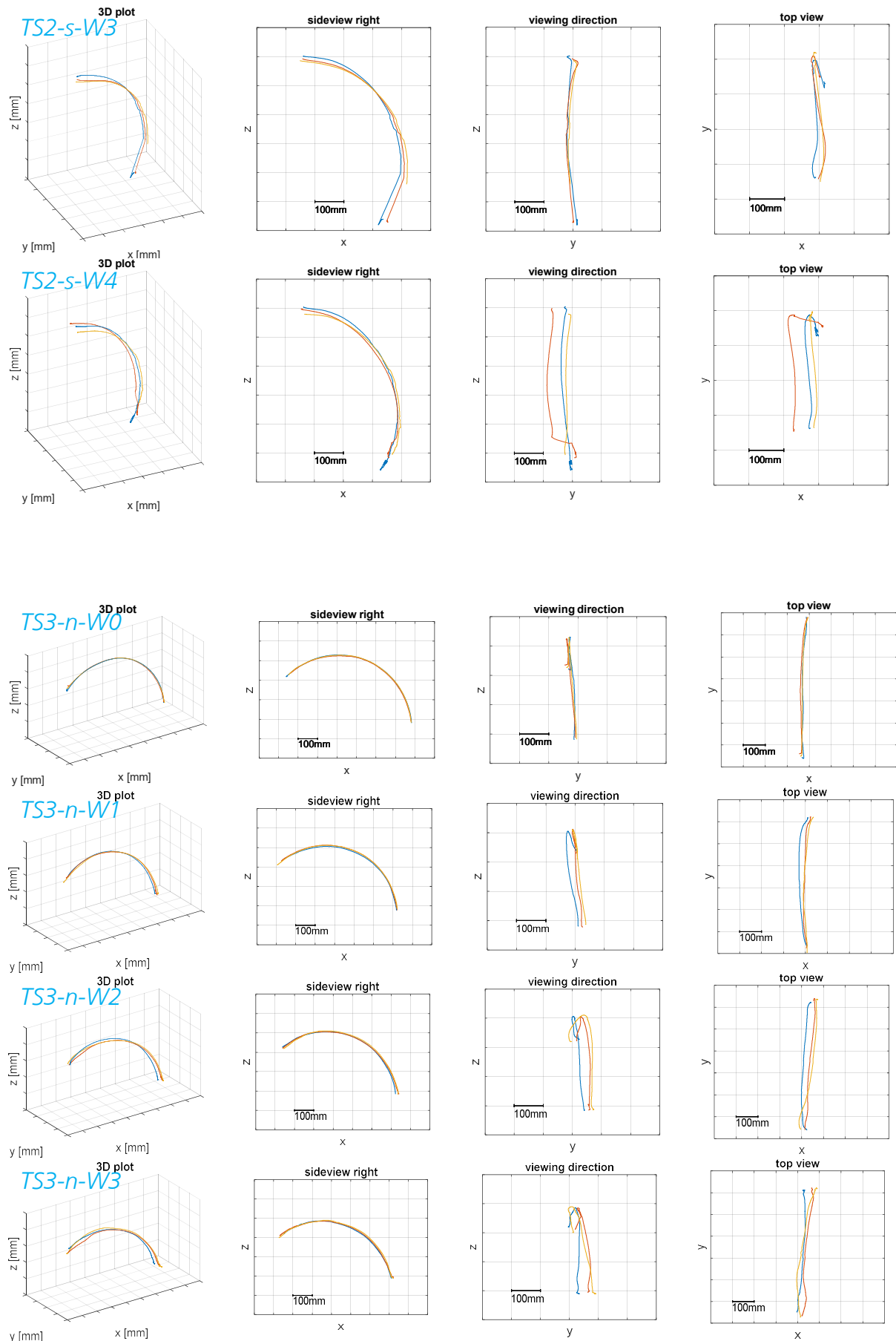


Figure 85: Weight lift test - Measured Trajectories

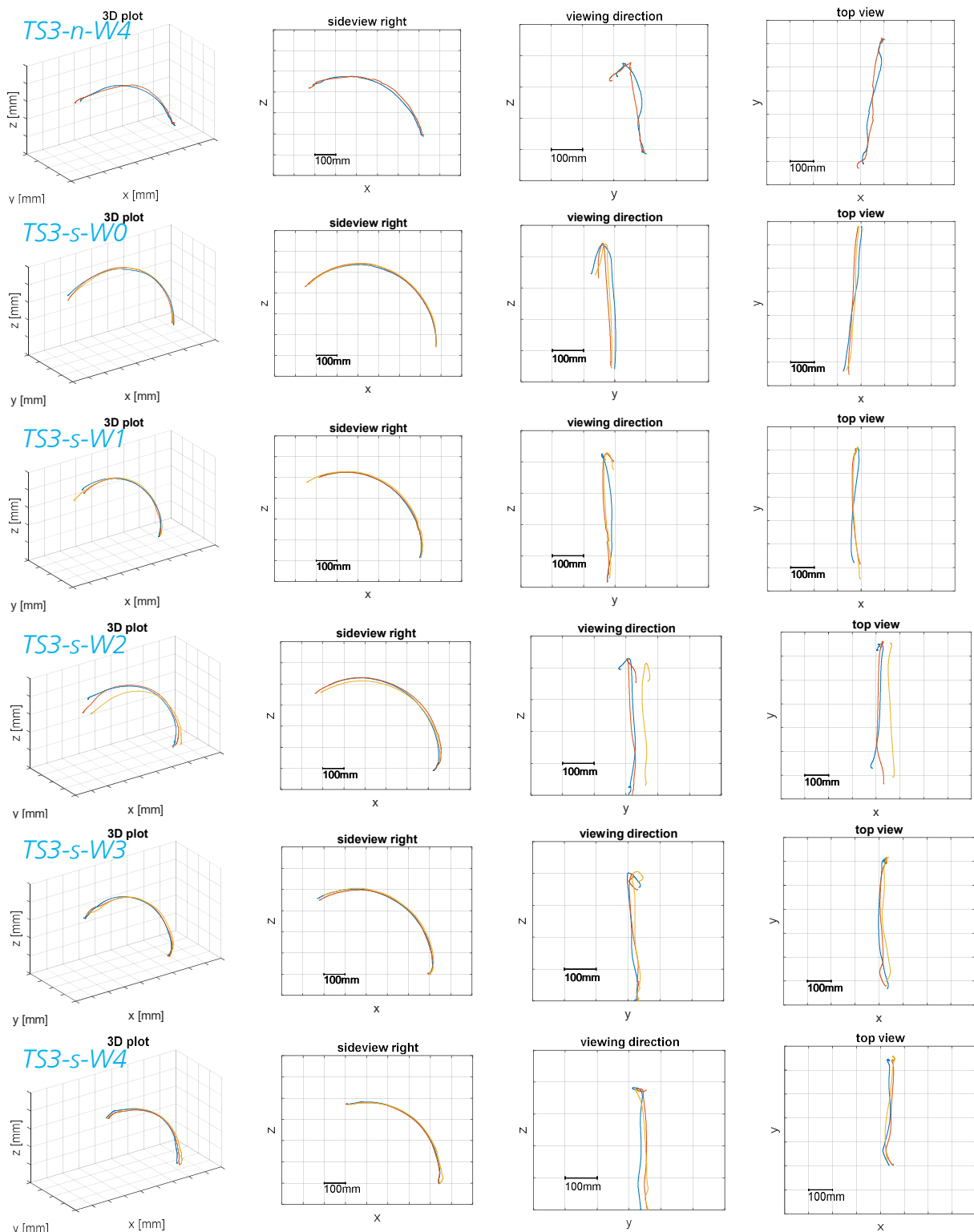


Figure 86: Weight lift test - Measured Trajectories

### A.1.2 Weight lift test - Measured Velocity profiles

In this subsection, the measured velocity profiles for all Test Scenarios are plotted. For each task, all three repetitions are overlaid in one plot (blue, red and yellow lines).

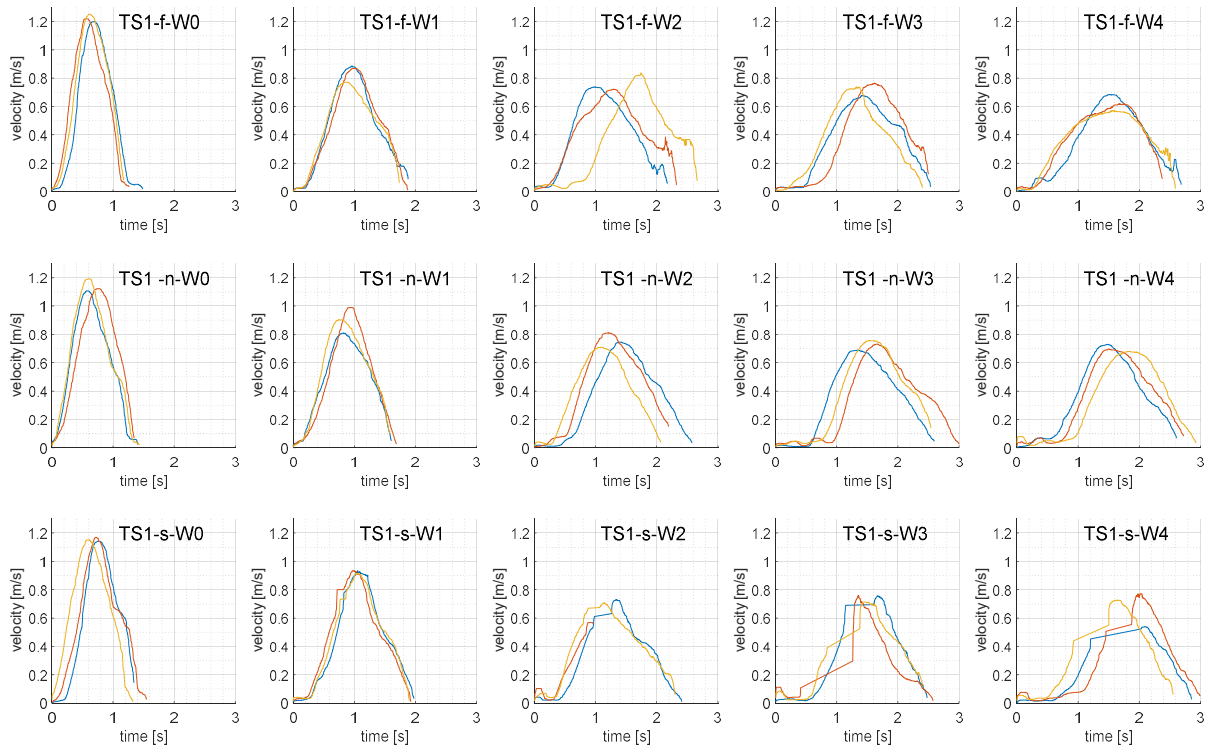


Figure 87: Measured velocity profiles of TS1 (shoulder angle  $\Omega = 0^\circ$ ), filtered with median filter

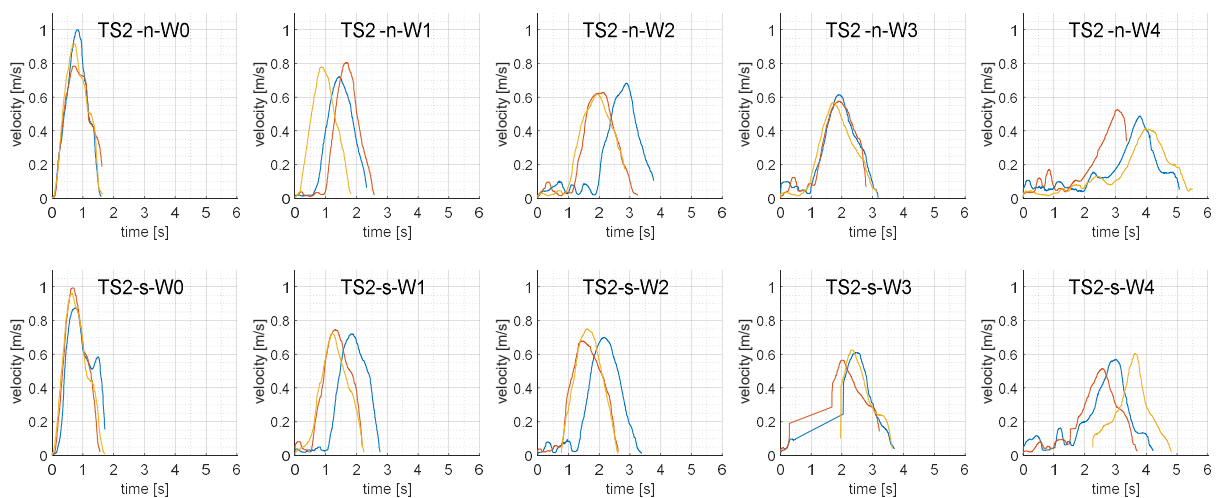


Figure 88: Measured velocity profiles of TS2 (shoulder angle  $\Omega = 45^\circ$ )

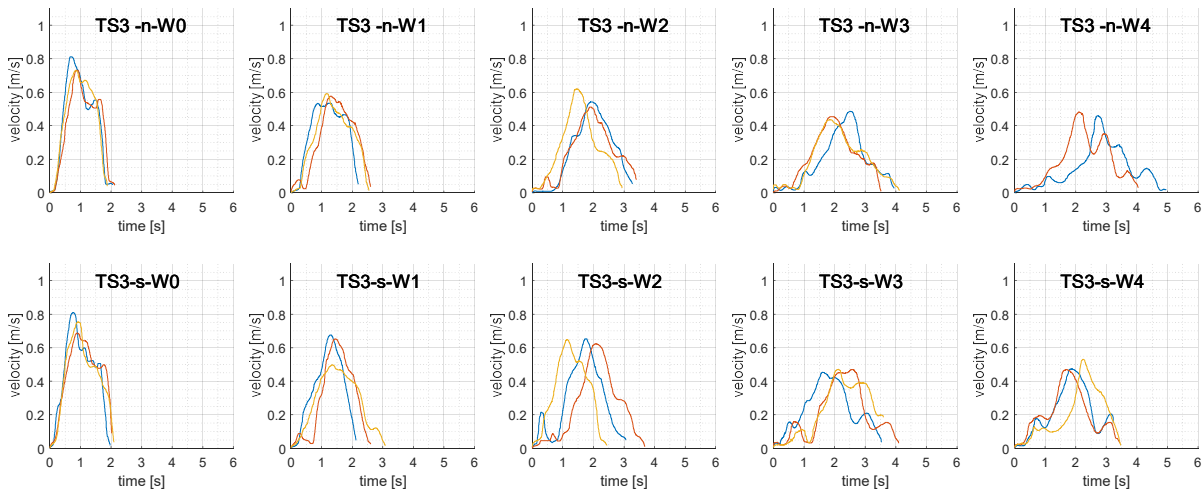


Figure 89: Measured velocity profiles of TS3 (shoulder angle  $\Omega = 90^\circ$ )

### A.1.3 Weight lift test - Measured EMG data

In the following, the measured and filtered EMG values of all 12 electrodes are plotted for all measured tasks. For each task, all three repetitions are overlaid in one plot (blue, red and yellow lines).

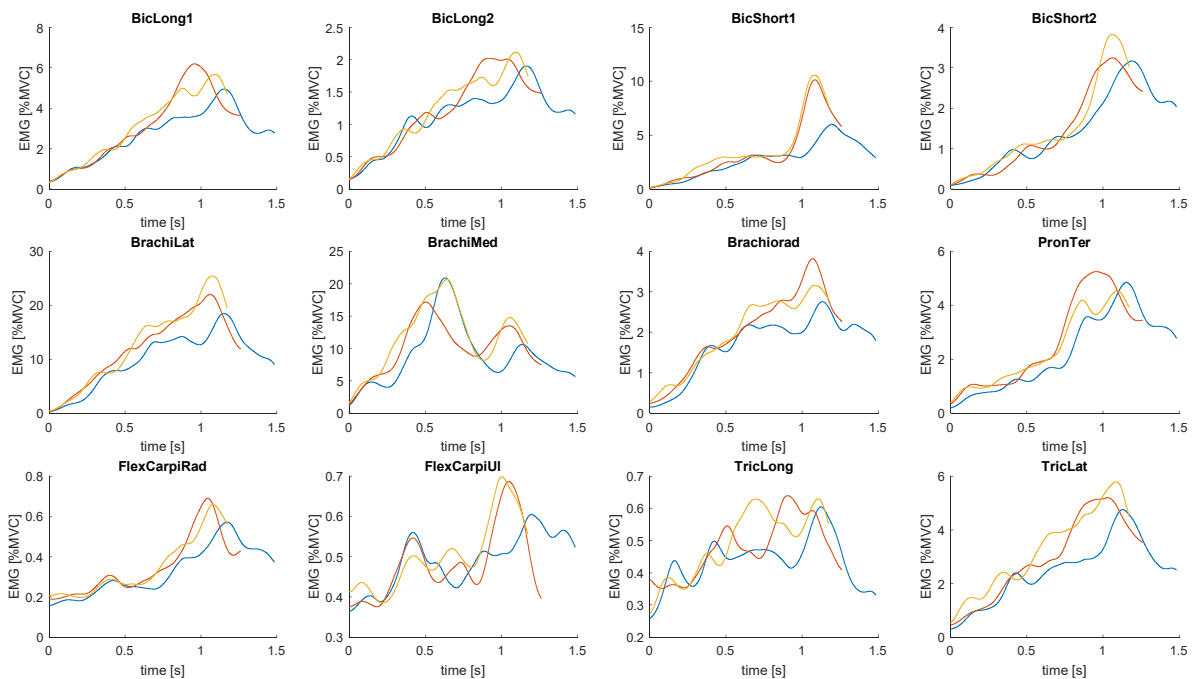


Figure 90: Weight lift test - Measured EMG data of TS1-f-W0

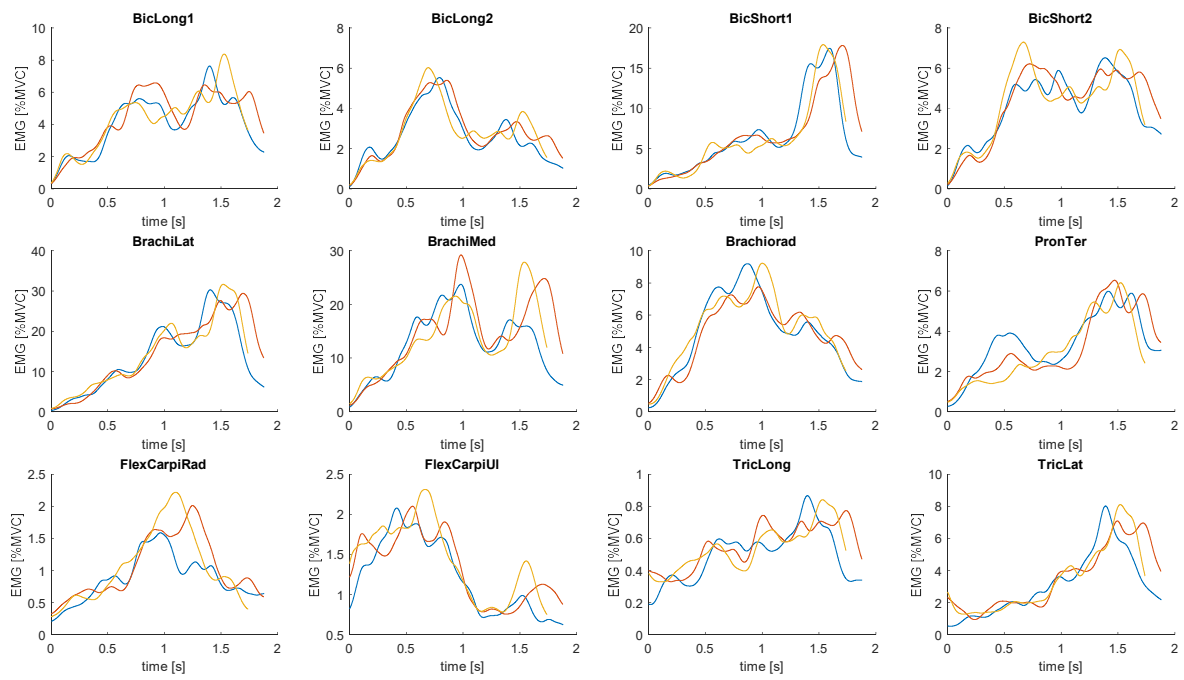


Figure 91: Weight lift test - Measured EMG data of TS1-f-W1

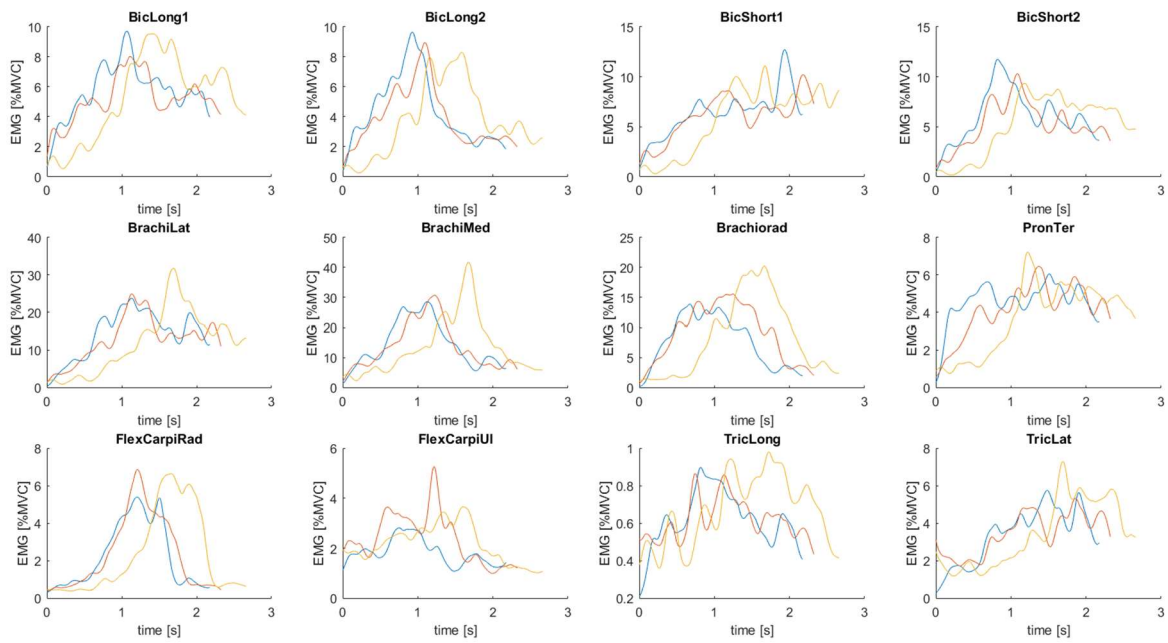


Figure 92: Weight lift test - Measured EMG data of TS1-f-W2



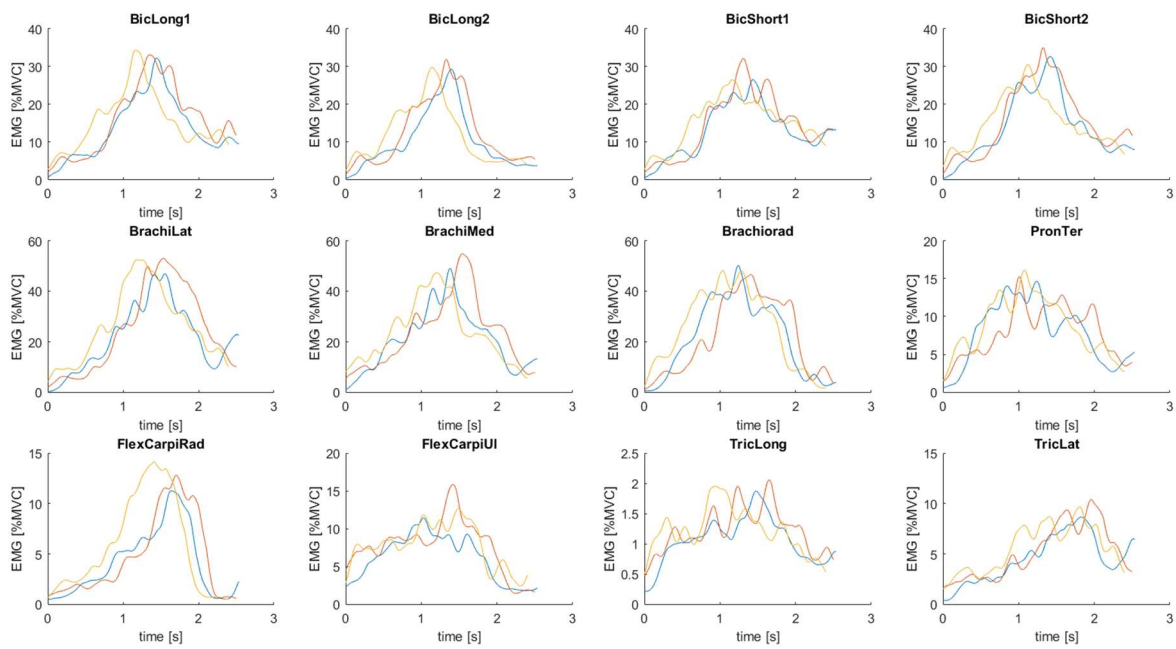


Figure 93: Weight lift test - Measured EMG data of TS1-f-W3

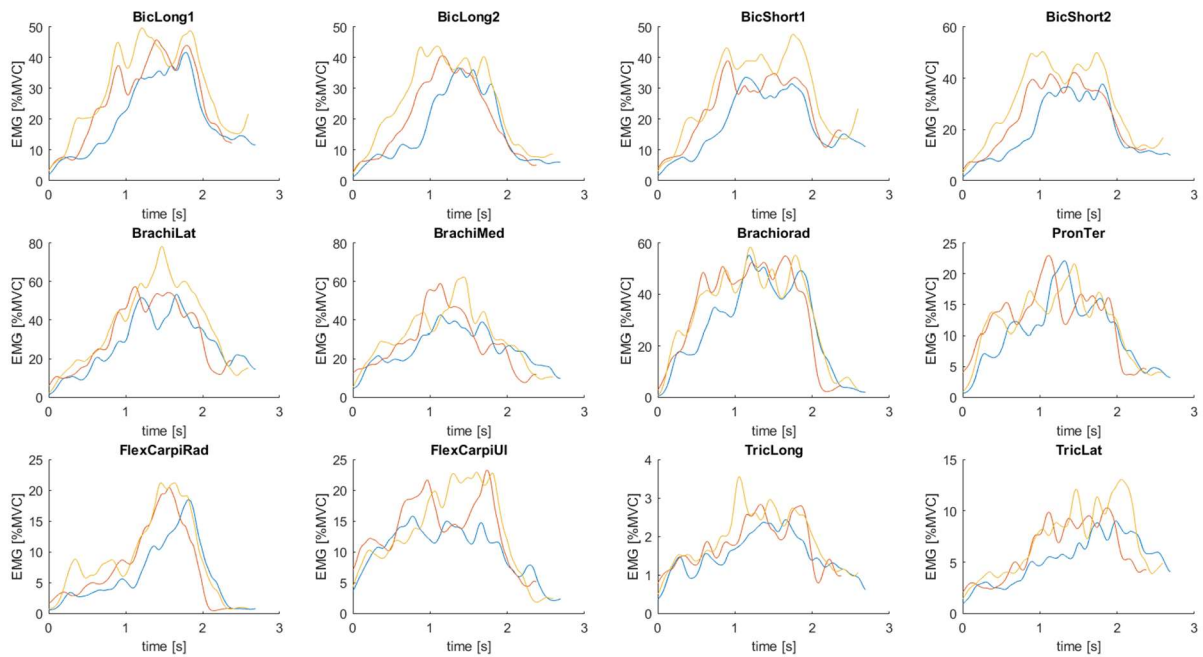


Figure 94: Weight lift test - Measured EMG data of TS1-f-W4

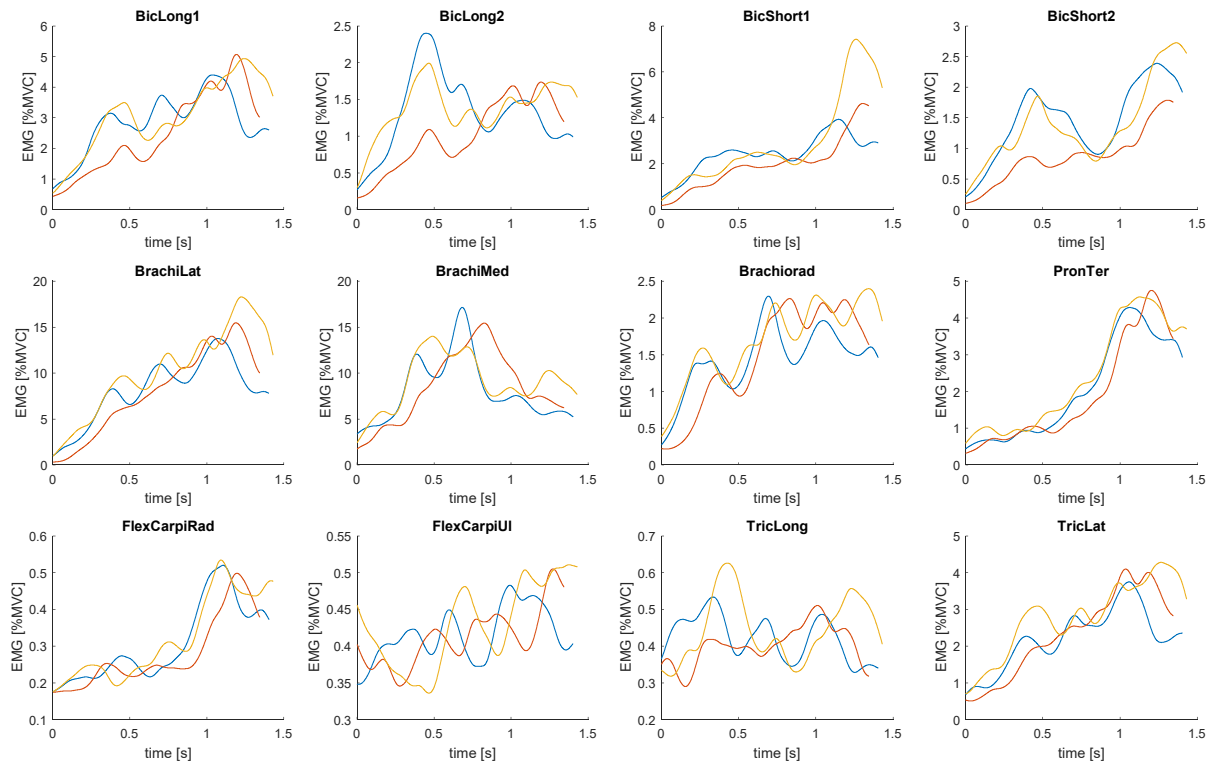


Figure 95: Weight lift test - Measured EMG data of TS1-n-W0

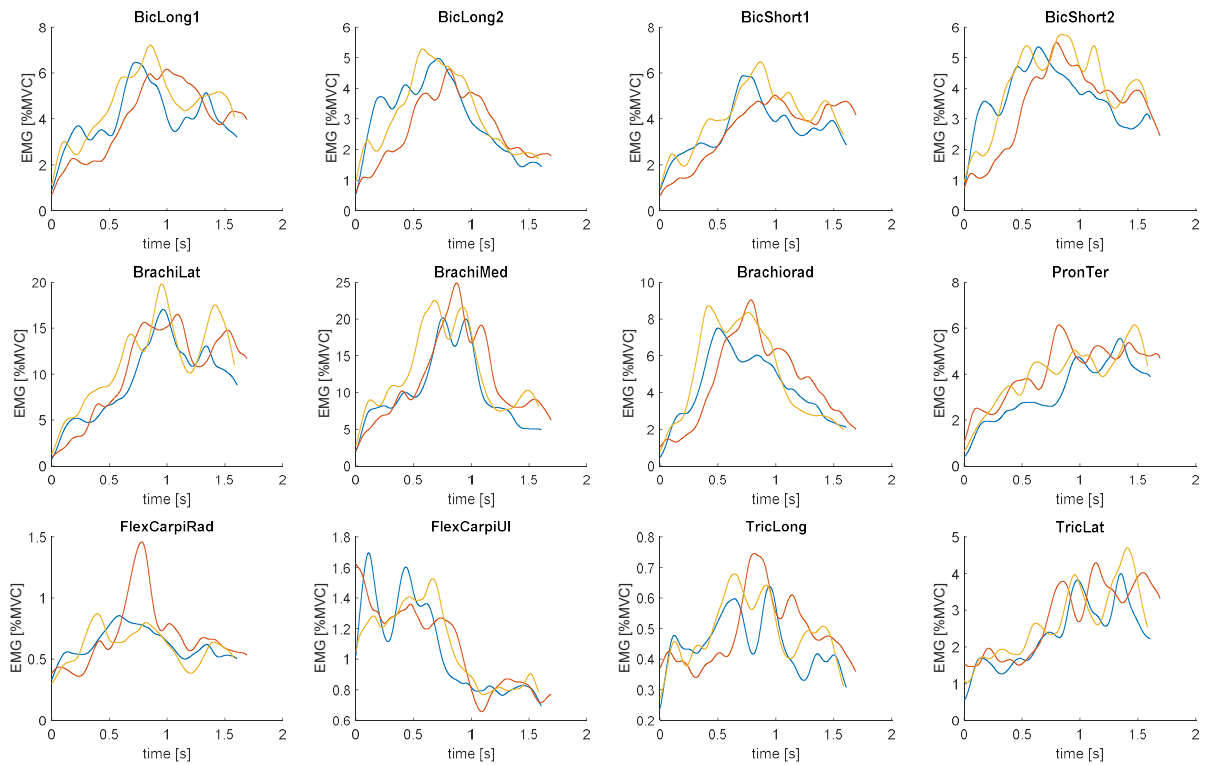


Figure 96: Weight lift test - Measured EMG data of TS1-n-W1

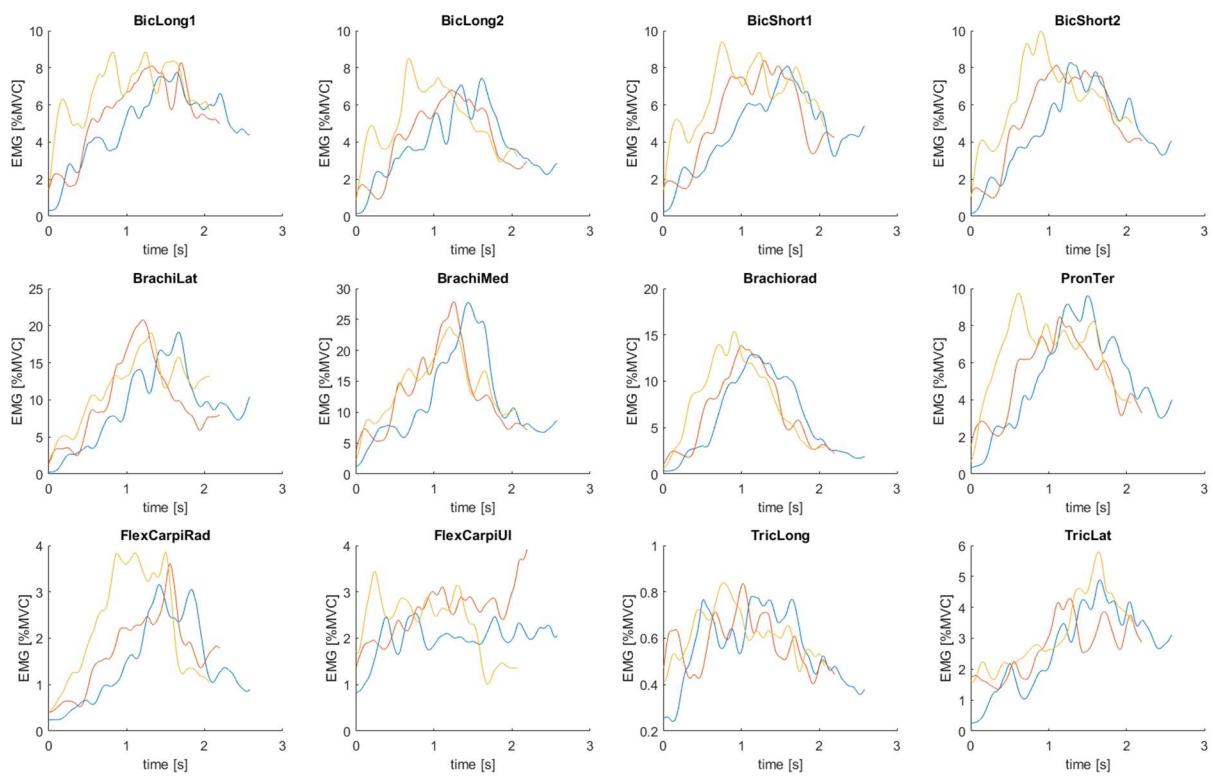


Figure 97: Weight lift test - Measured EMG data of TS1-n-W2

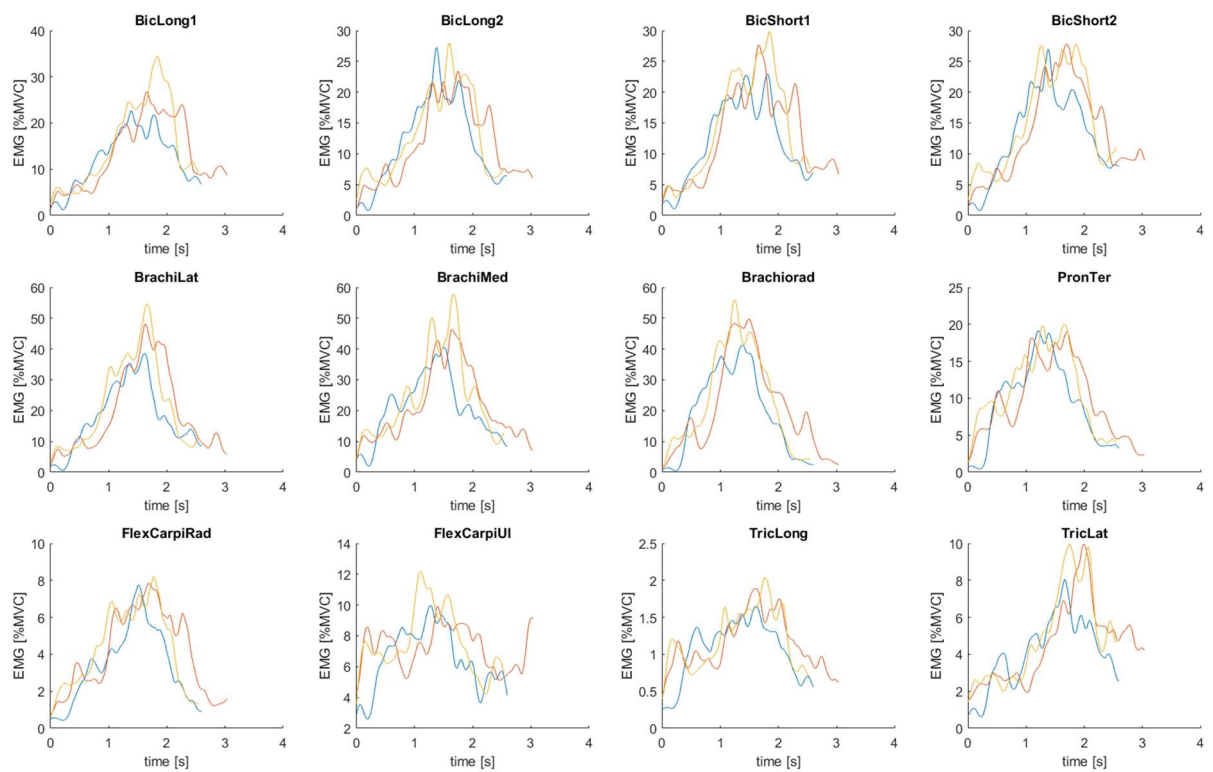


Figure 98: Weight lift test - Measured EMG data of TS1-n-W3

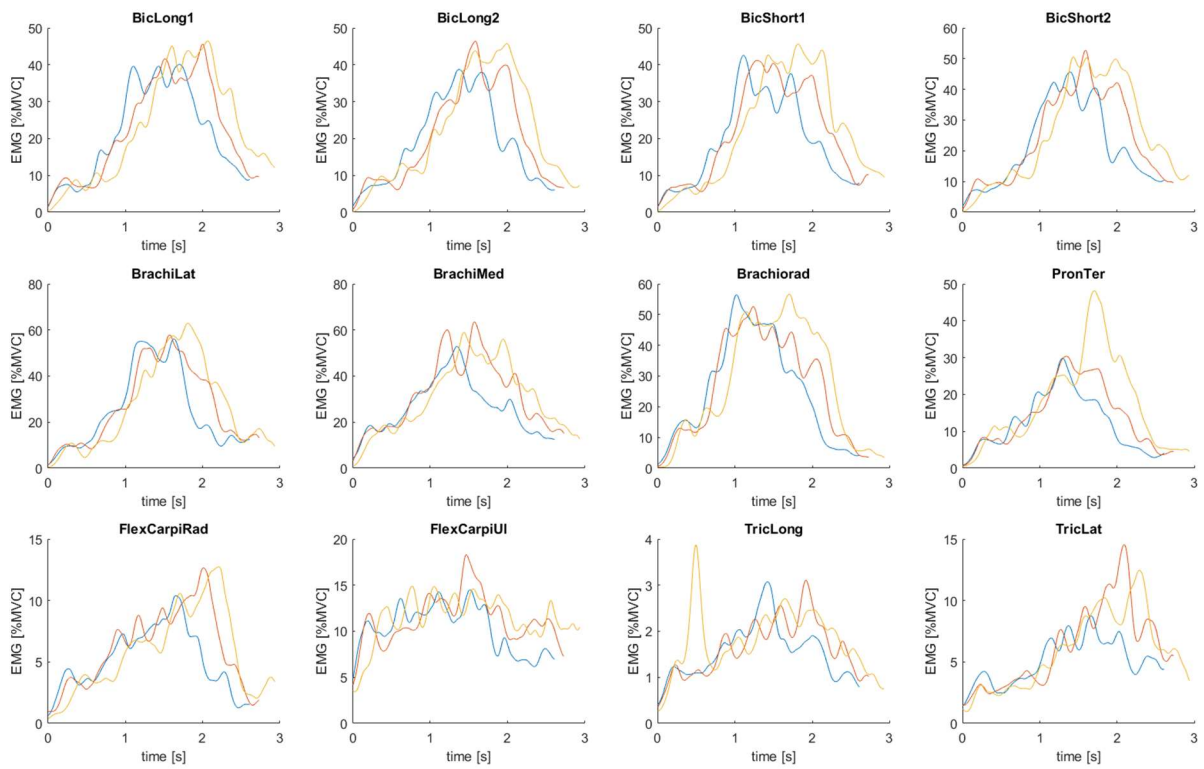


Figure 99: Weight lift test - Measured EMG data of TS1-n-W4

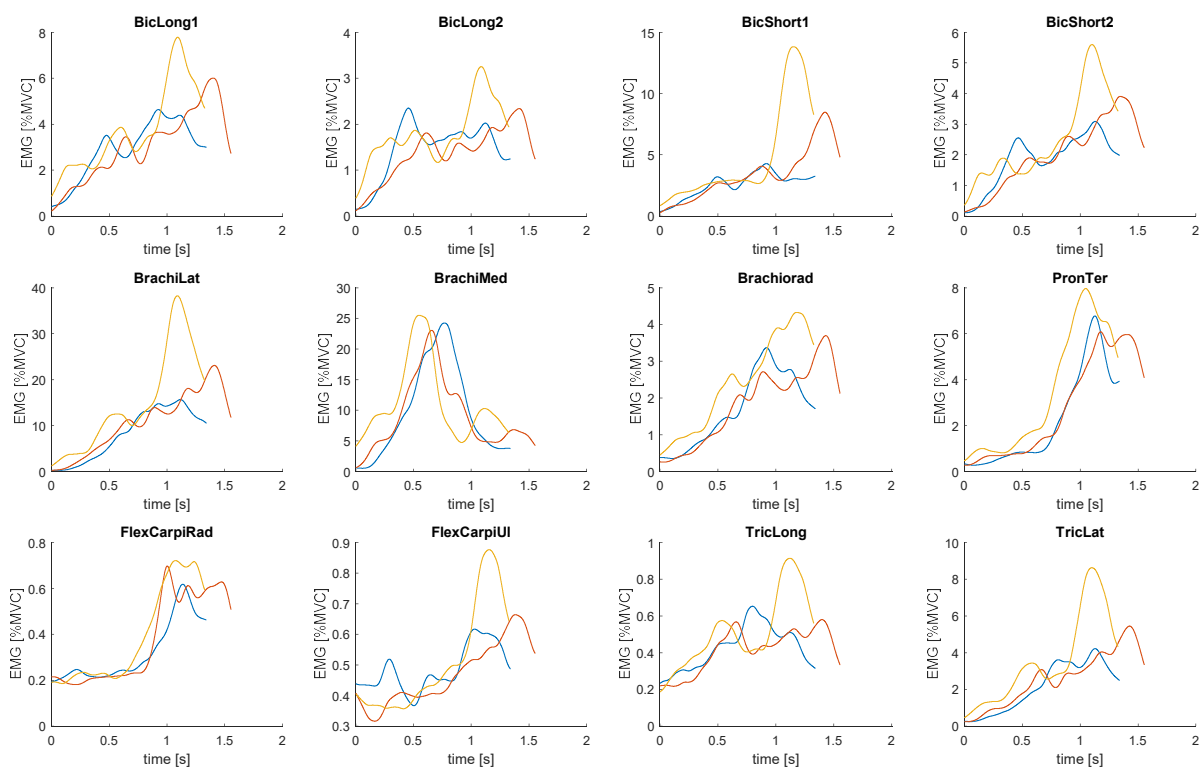


Figure 100: Weight lift test - Measured EMG data of TS1-s-W0

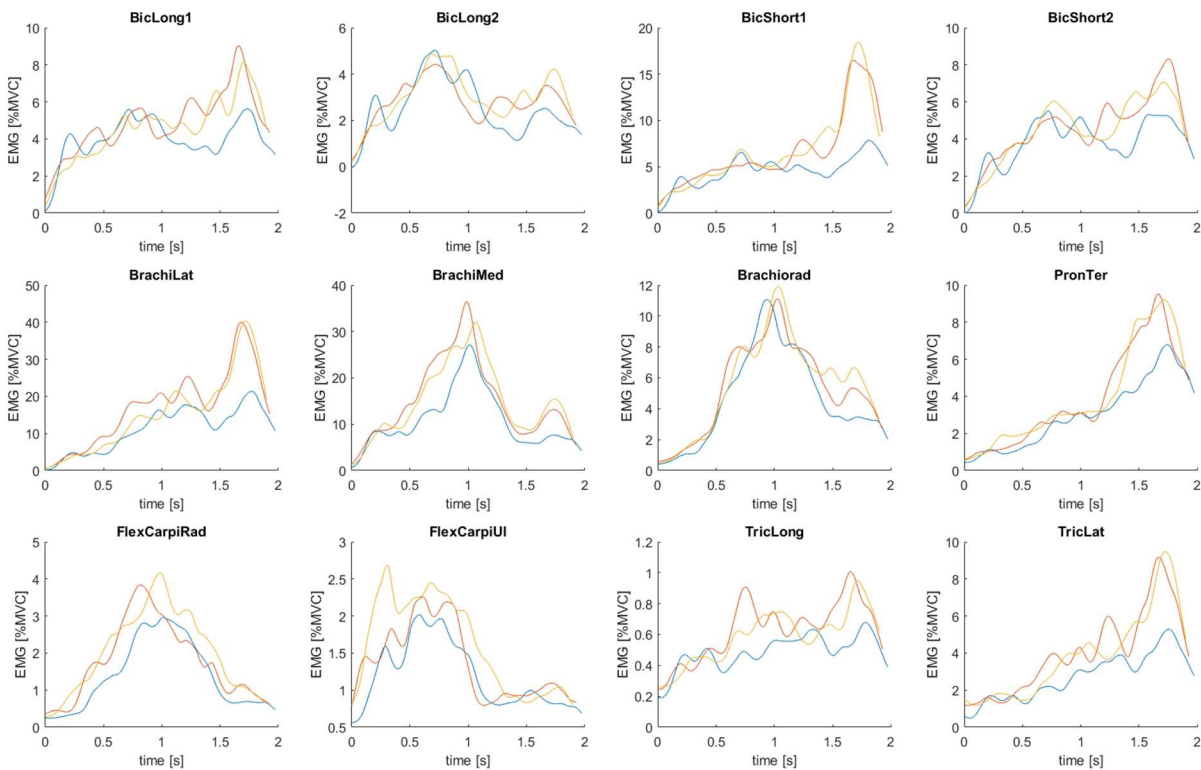


Figure 101: Weight lift test - Measured EMG data of TS1-s-W1

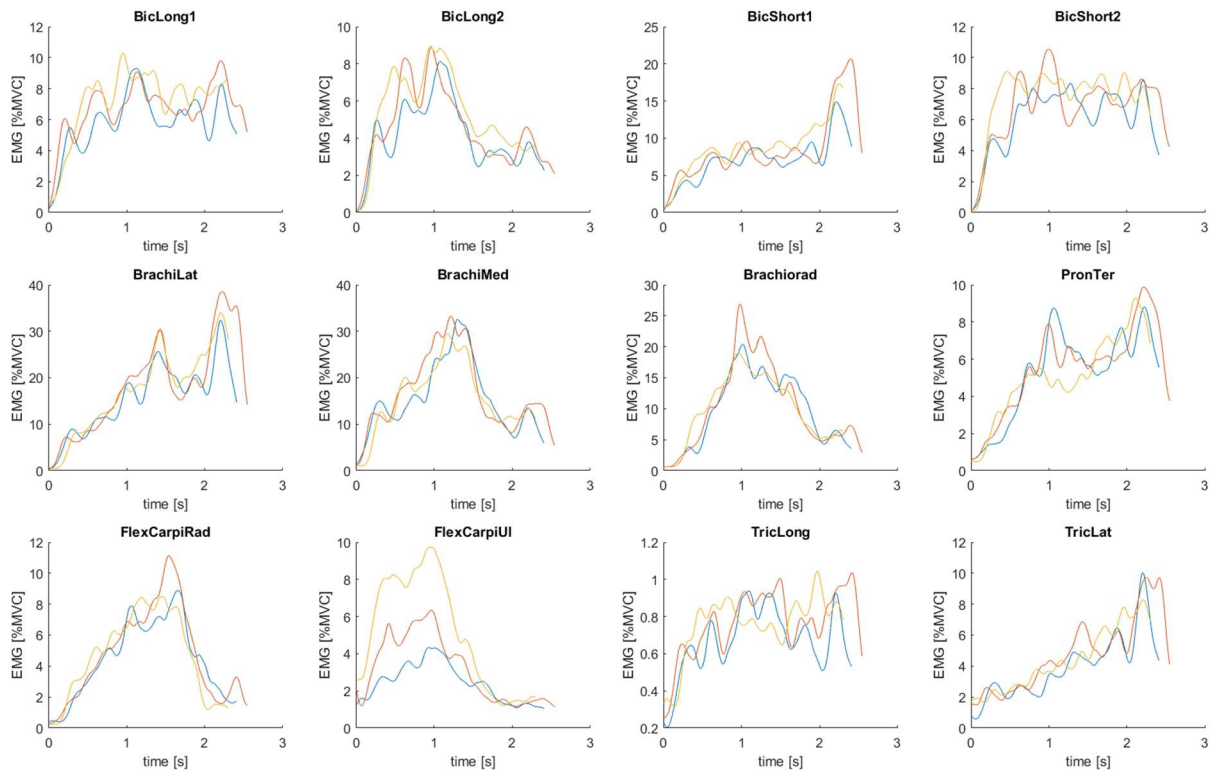


Figure 102: Weight lift test - Measured EMG data of TS1-s-W2

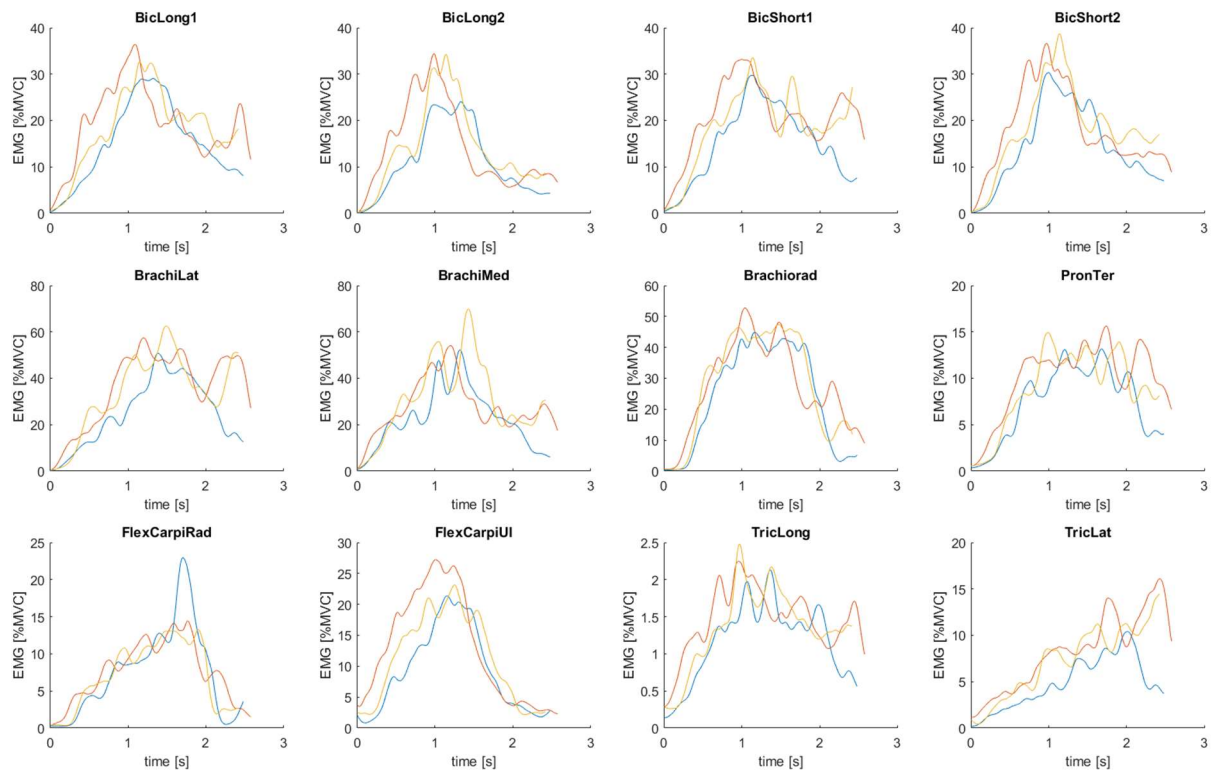


Figure 103: Weight lift test - Measured EMG data of TS1-s-W3

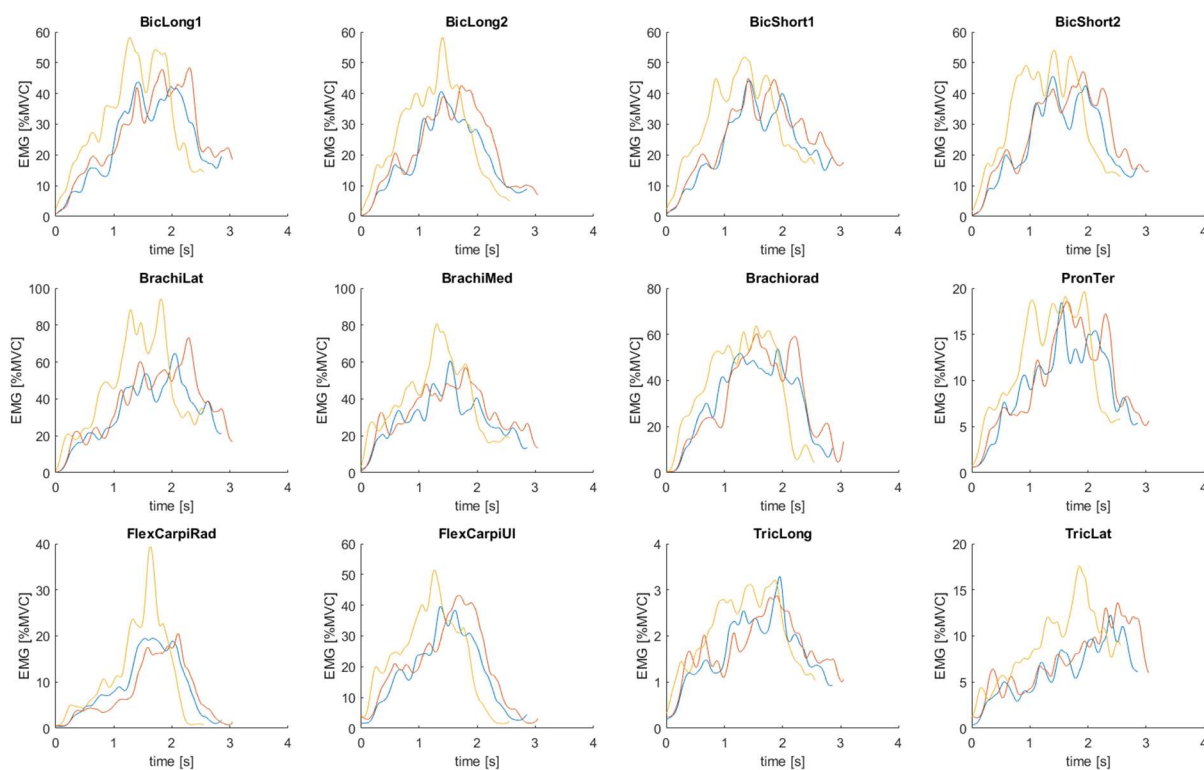


Figure 104: Weight lift test - Measured EMG data of TS1-s-W4

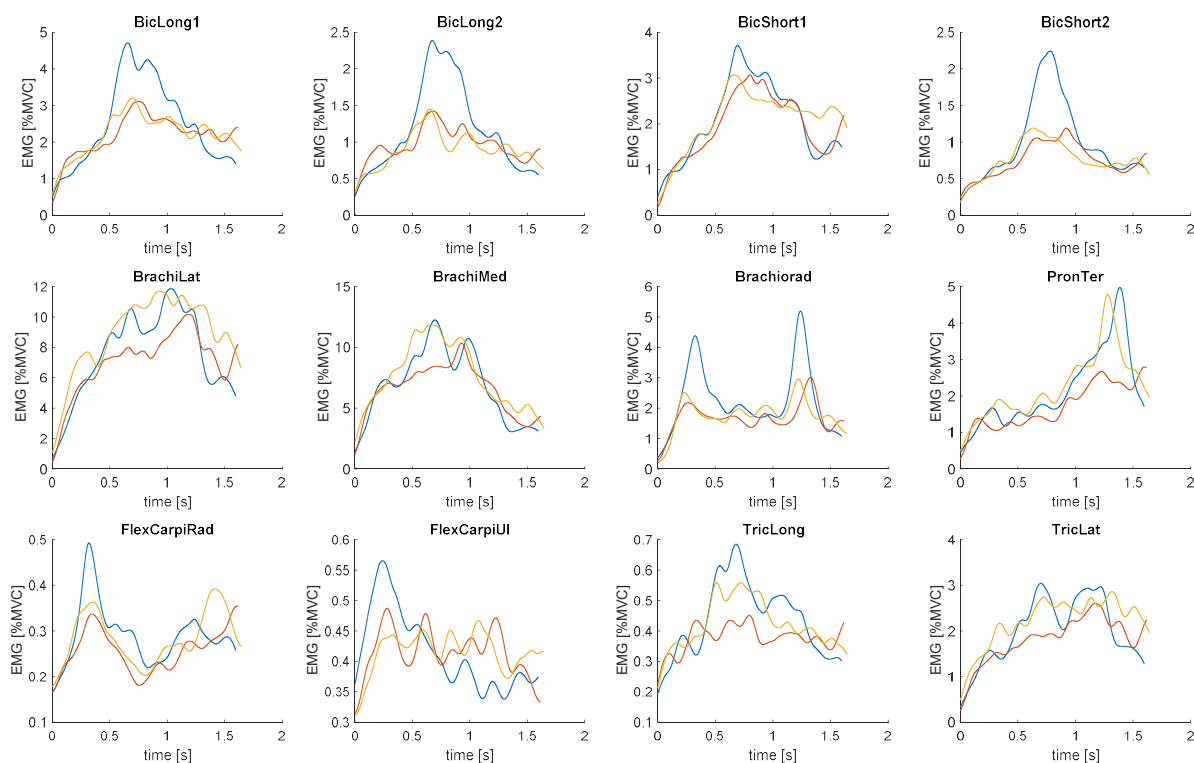


Figure 105: Weight lift test - Measured EMG data of TS2-n-W0

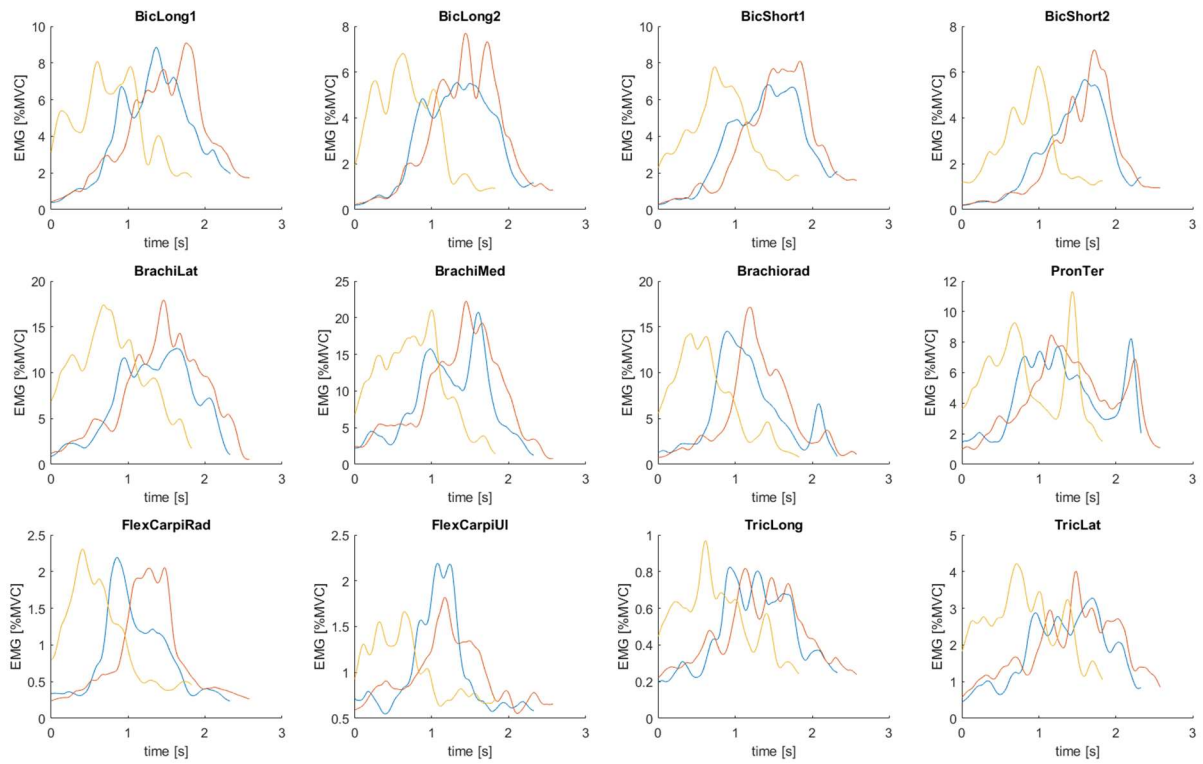


Figure 106: Weight lift test - Measured EMG data of TS2-n-W1

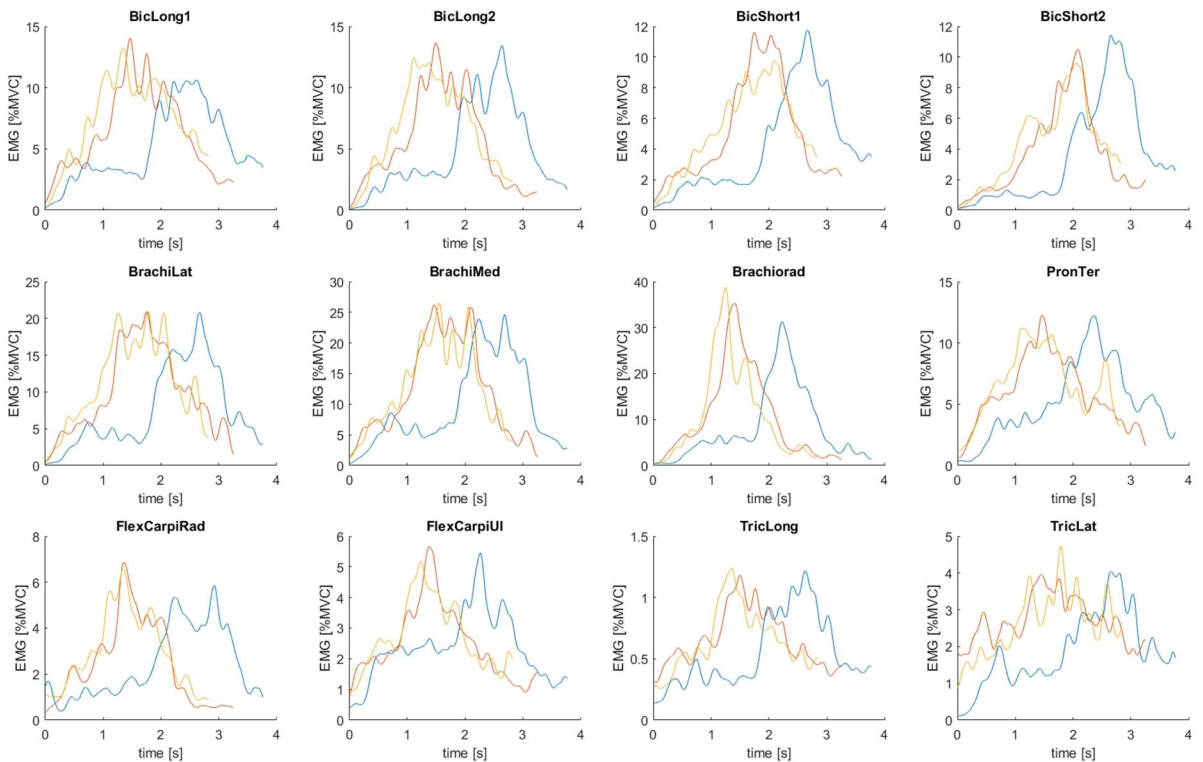


Figure 107: Weight lift test - Measured EMG data of TS2-n-W2



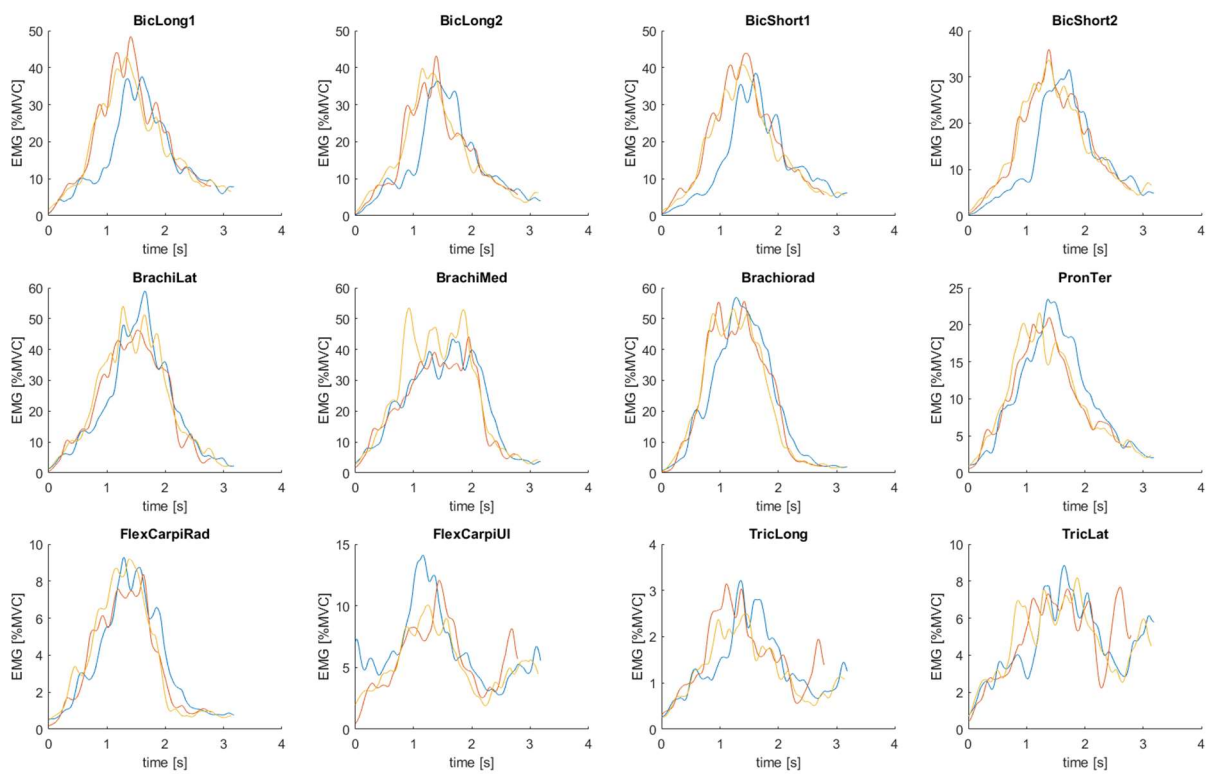


Figure 108: Weight lift test - Measured EMG data of TS2-nW3

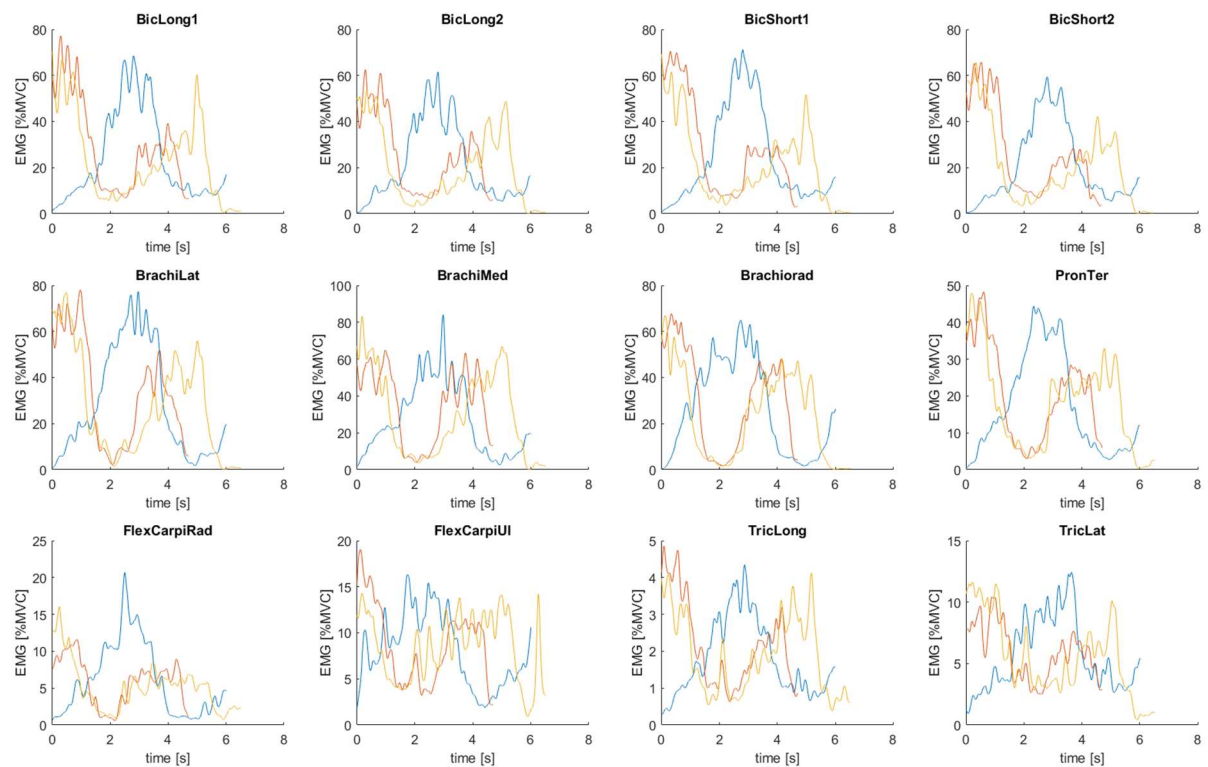


Figure 109: Weight lift test - Measured EMG data of TS2-nW4

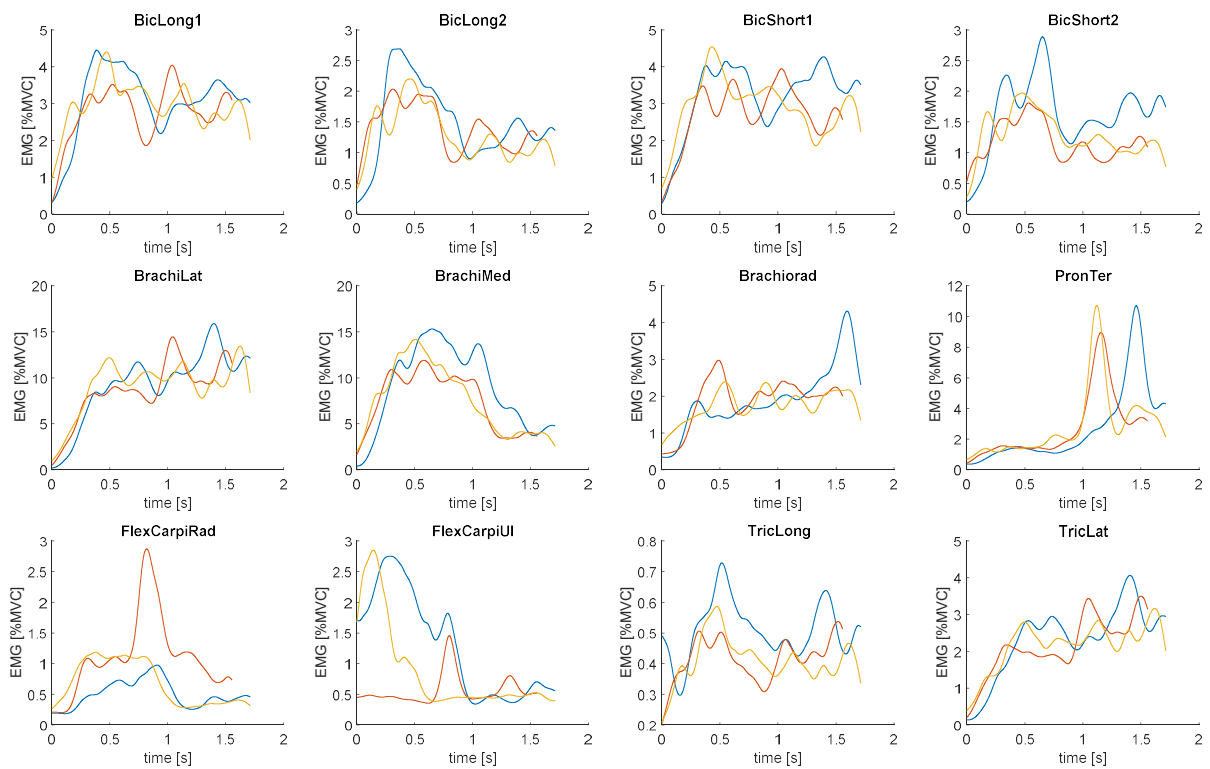


Figure 110: Weight lift test - Measured EMG data of TS2-s-W0

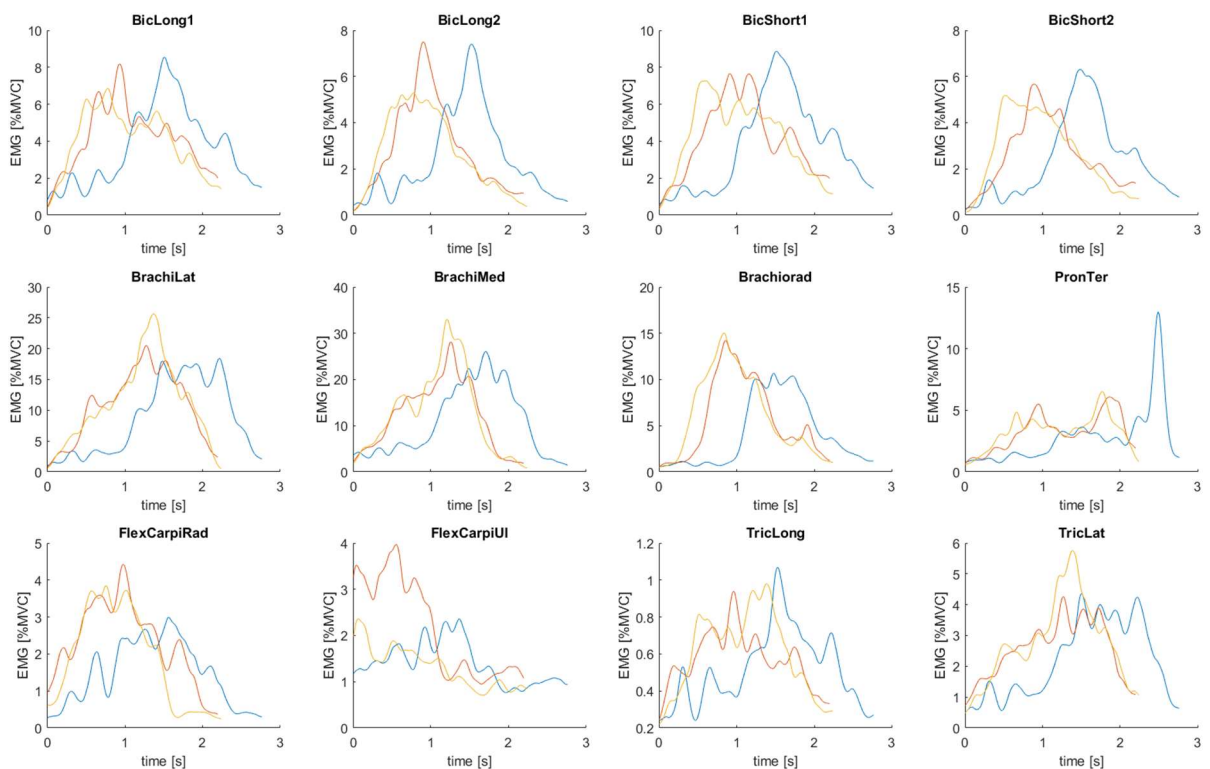


Figure 111: Weight lift test - Measured EMG data of TS2-s-W1

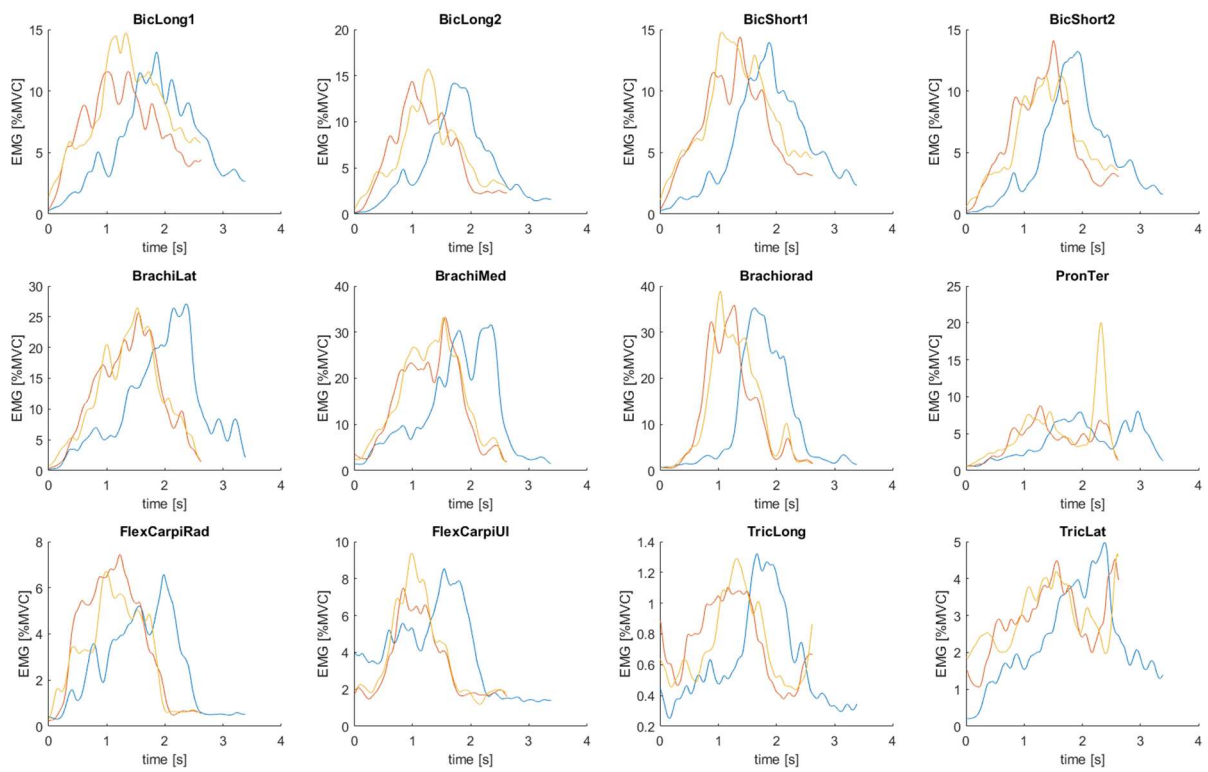


Figure 112: Weight lift test - Measured EMG data of TS2-s-W2

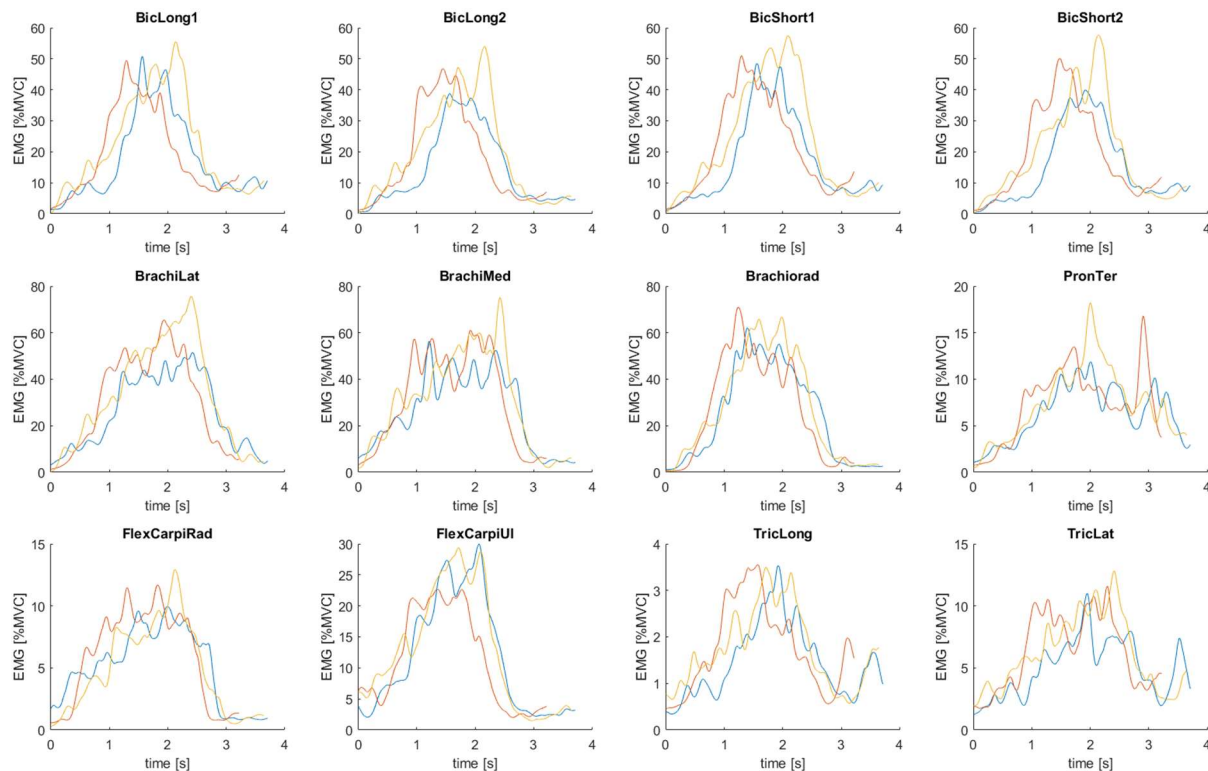


Figure 113: Weight lift test - Measured EMG data of TS2-s-W3

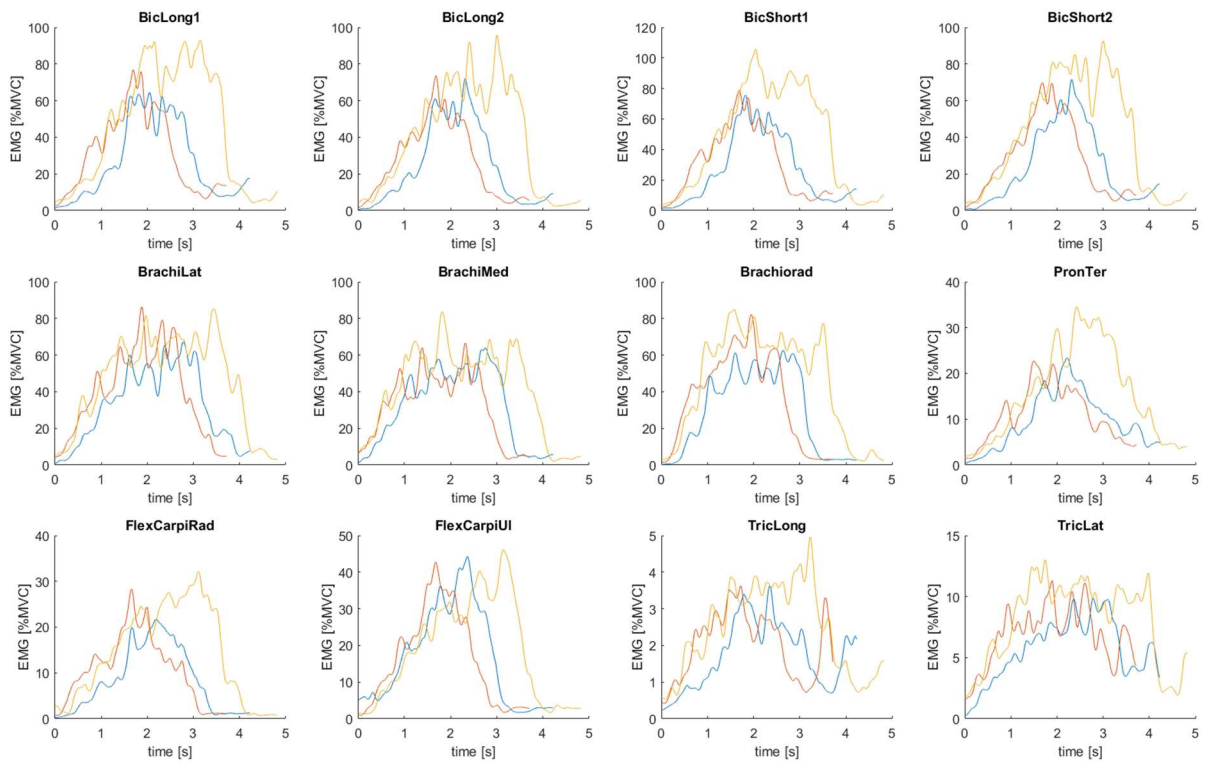


Figure 114: Weight lift test - Measured EMG data of TS2-s-W4

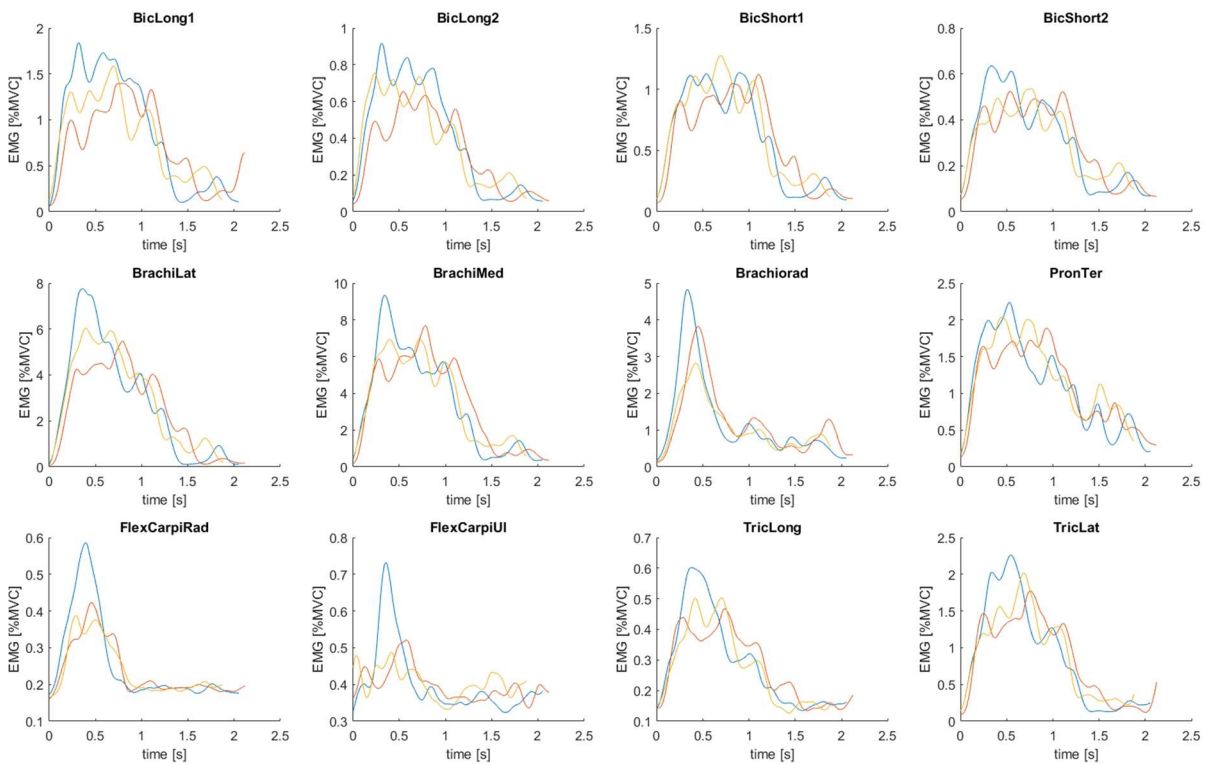


Figure 115: Weight lift test - Measured EMG data of TS3-n-W0

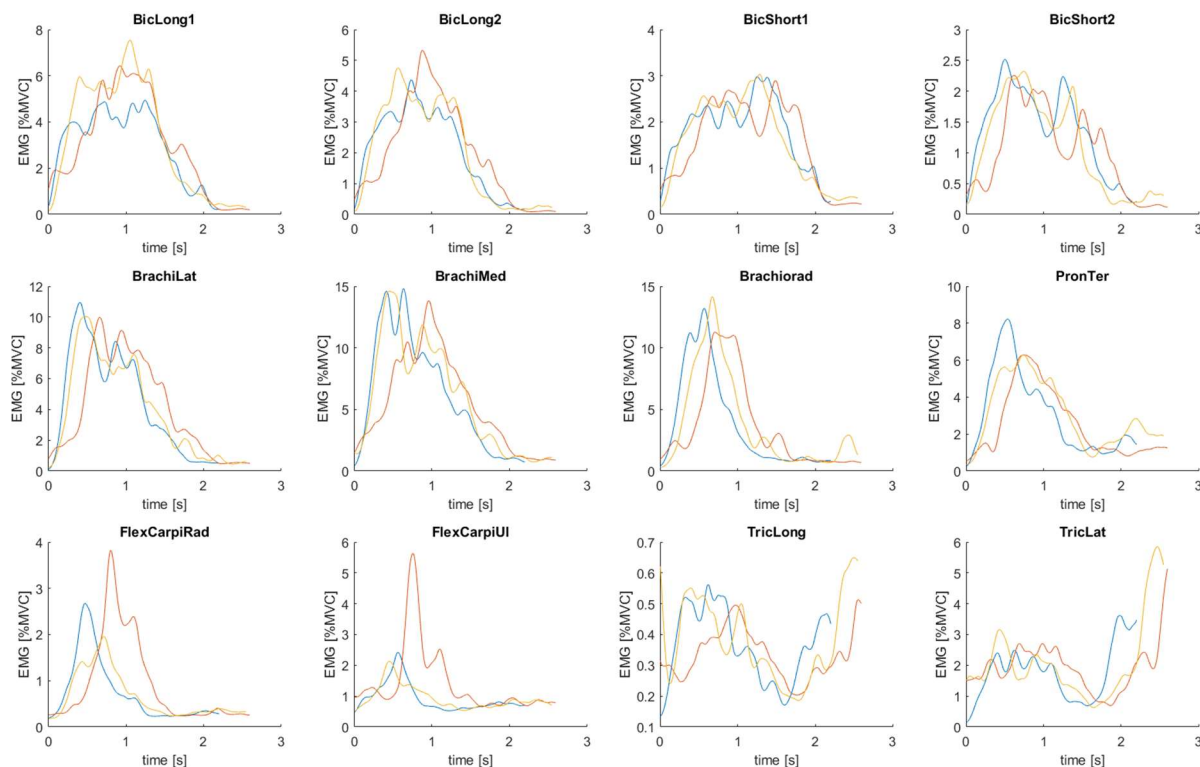


Figure 116: Weight lift test - Measured EMG data of TS3-n-W1

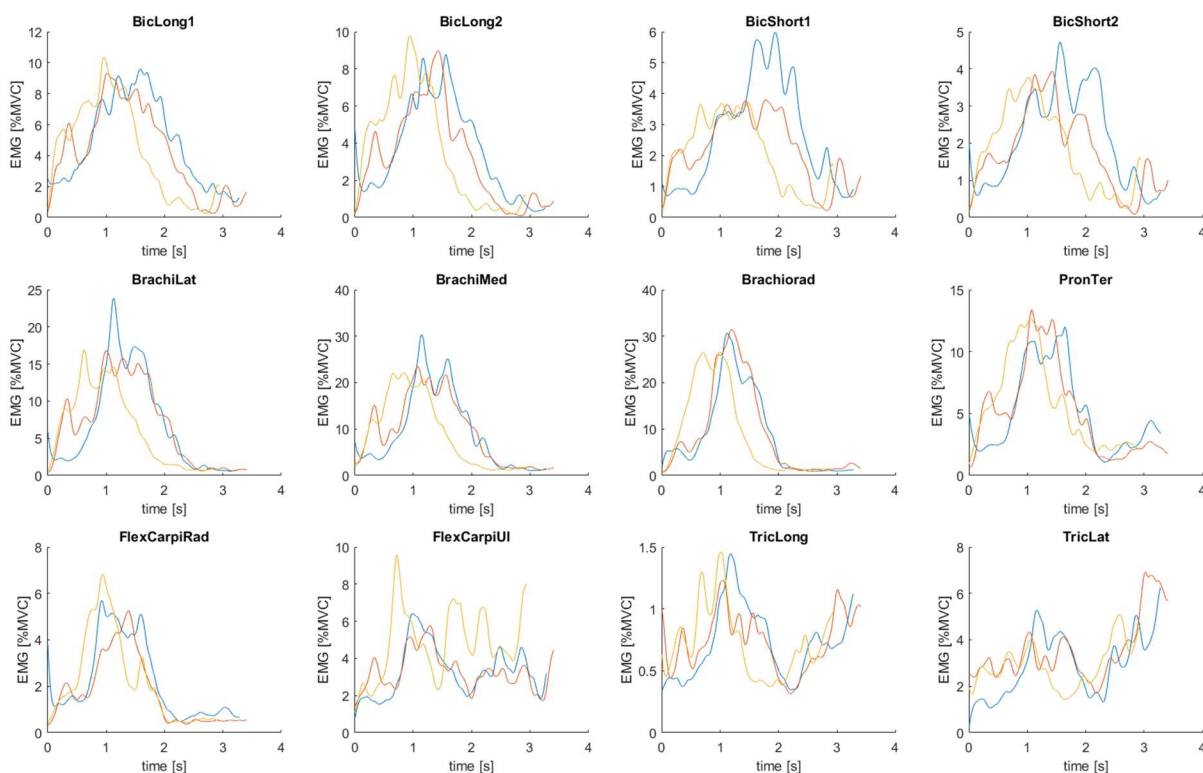


Figure 117: Weight lift test - Measured EMG data of TS3-n-W2

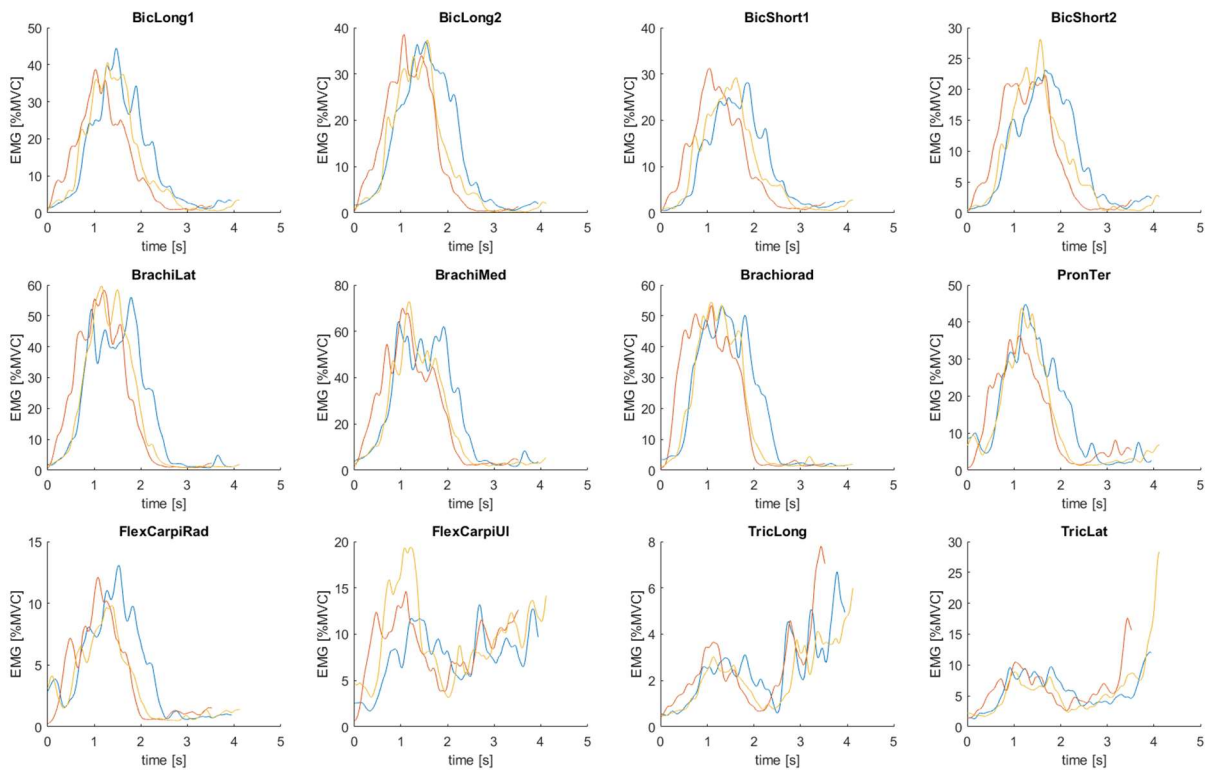


Figure 118: Weight lift test - Measured EMG data of TS3-n-W3

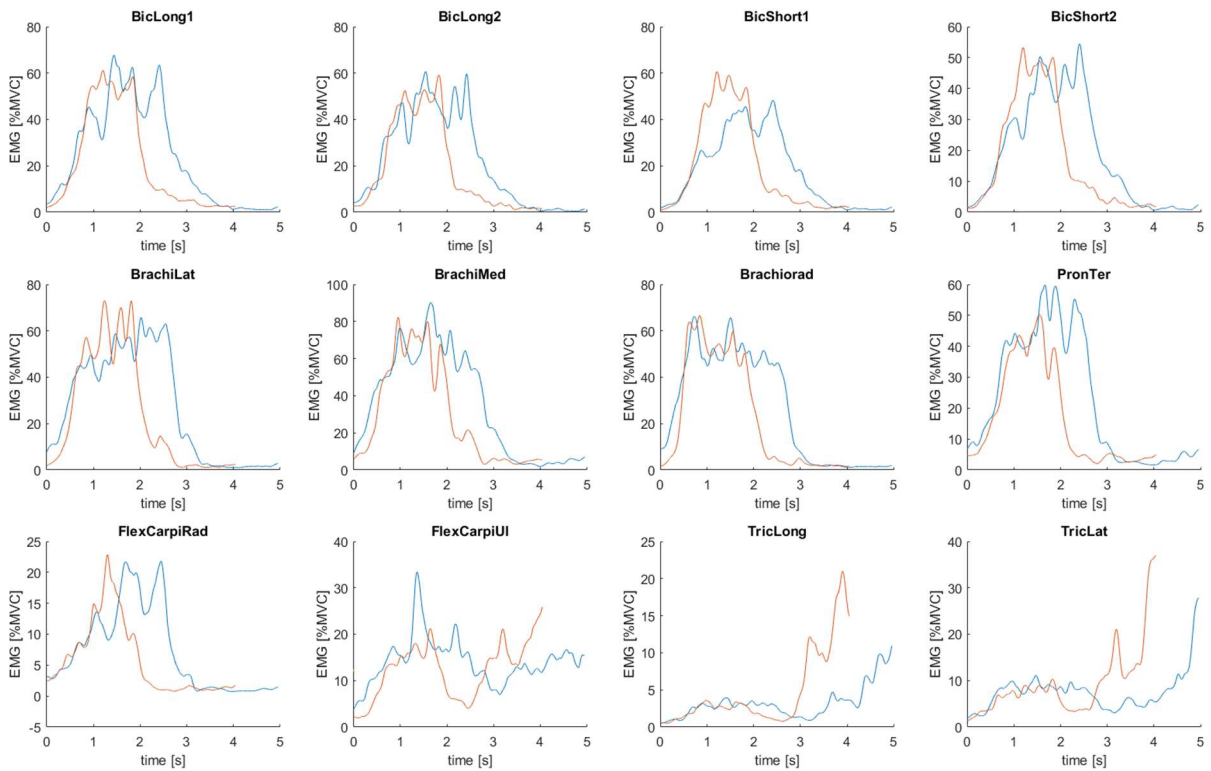


Figure 119: Weight lift test - Measured EMG data of TS-n-W4

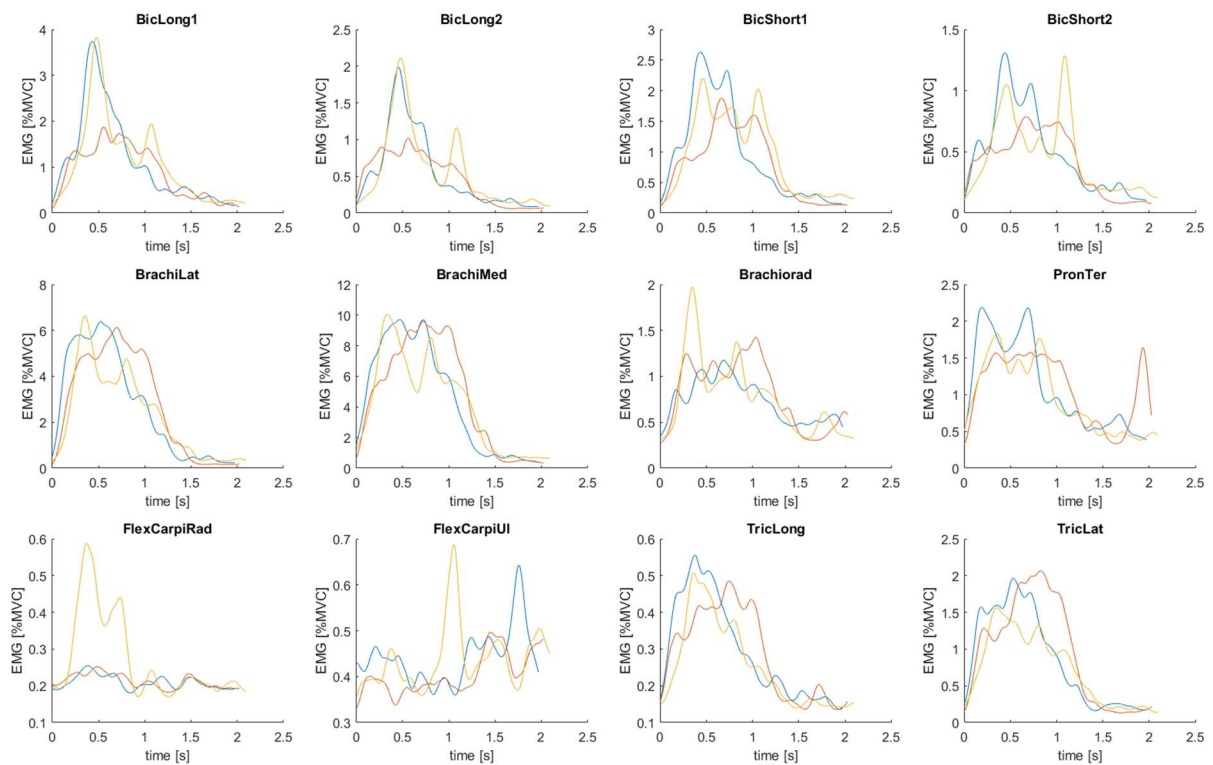


Figure 120: Weight lift test - Measured EMG data of TS3-s-W0

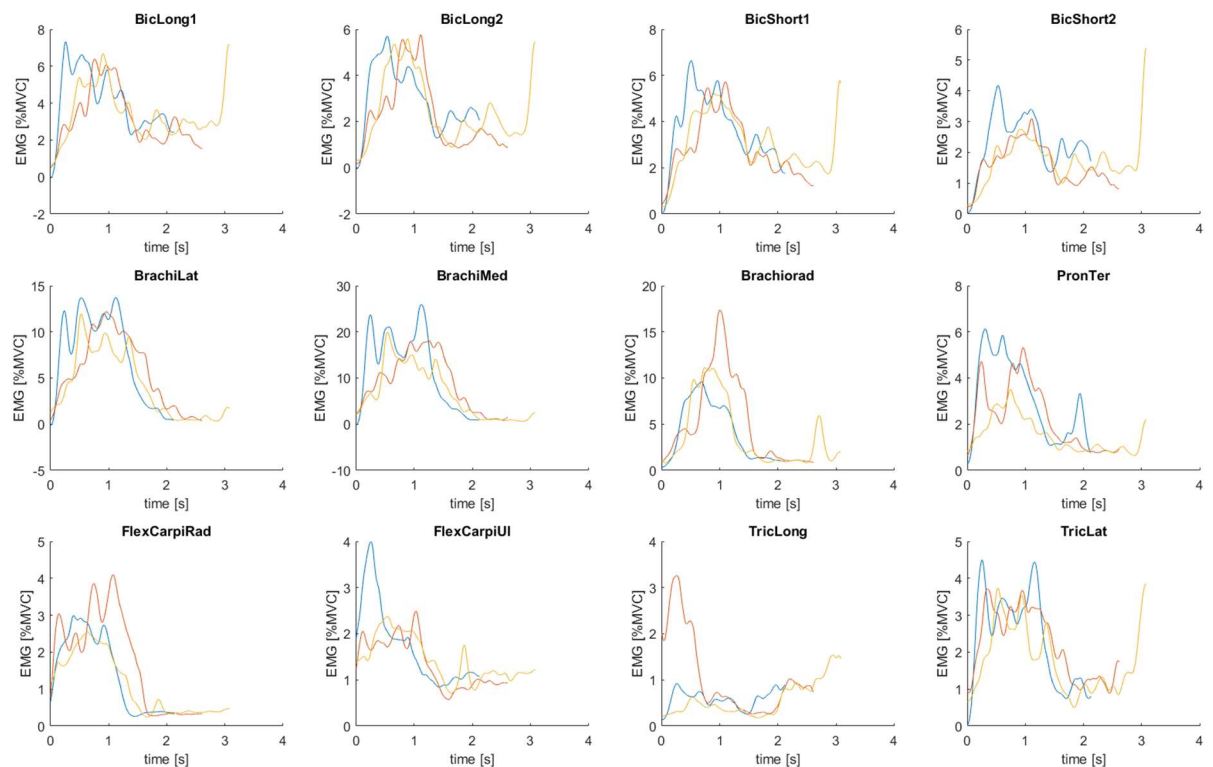


Figure 121: Weight lift test - Measured EMG data of TS3-s-W1

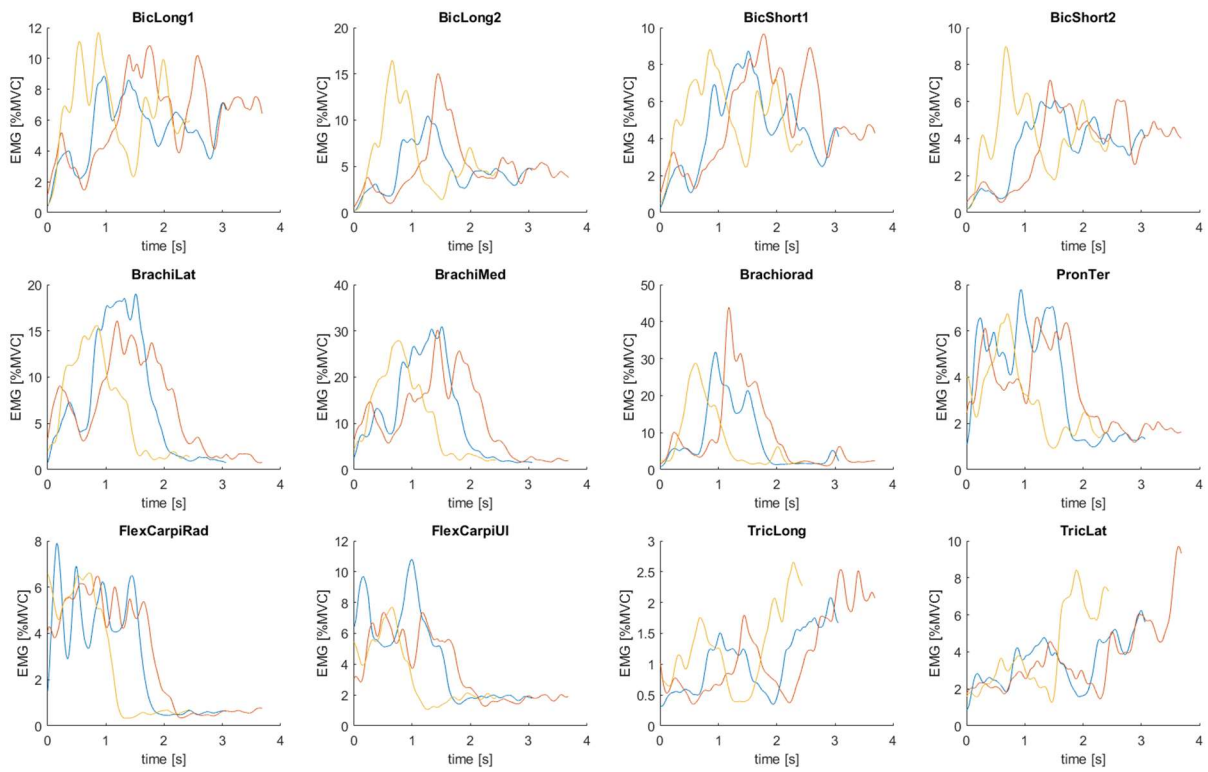


Figure 122: Weight lift test - Measured EMG data of TS3-s-W2

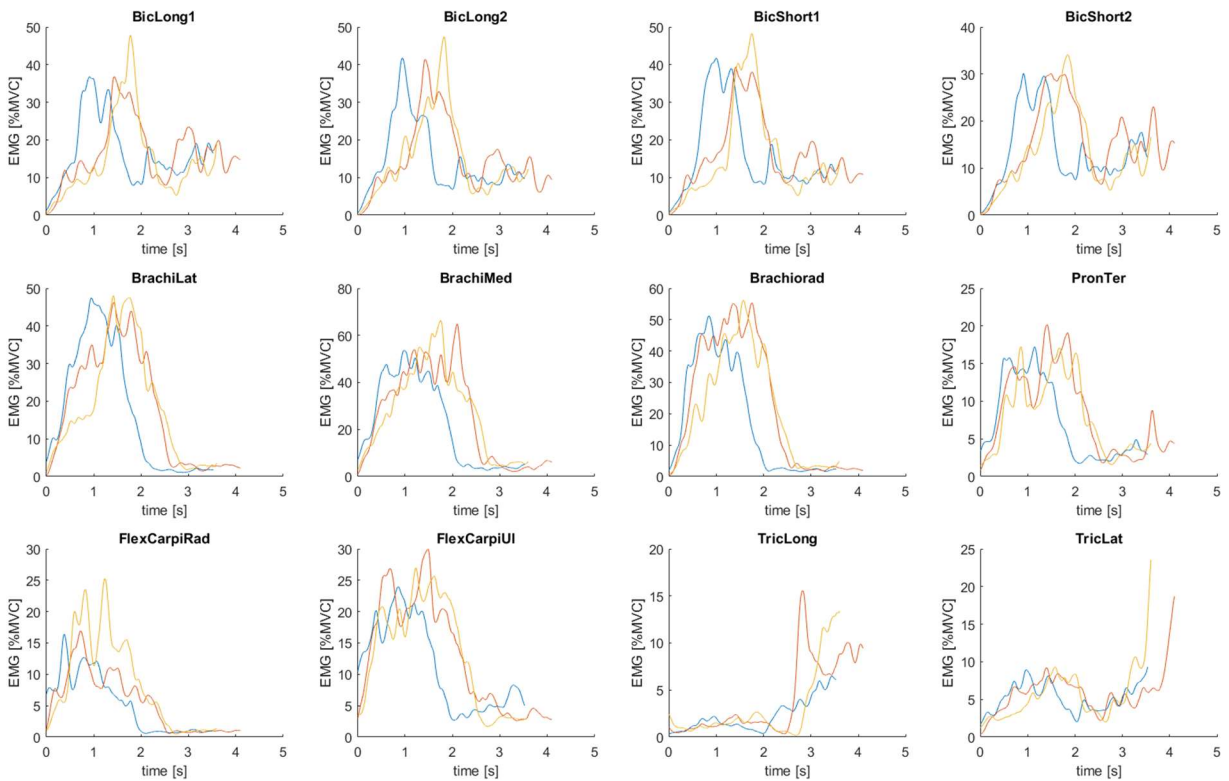


Figure 123: Weight lift test - Measured EMG data of TS3-s-W3



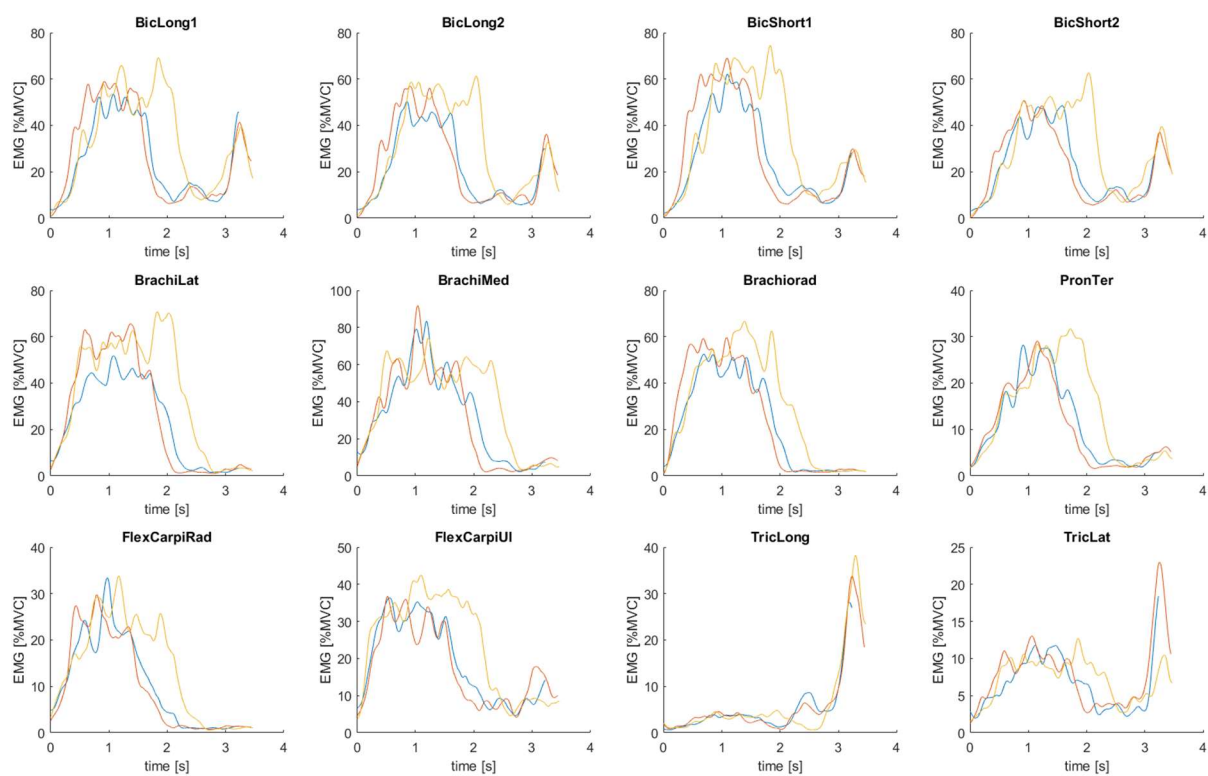


Figure 124: Weight lift test - Measured EMG data of TS3-s-W4

### A.1.4 Simulated muscle actuations TS1-f

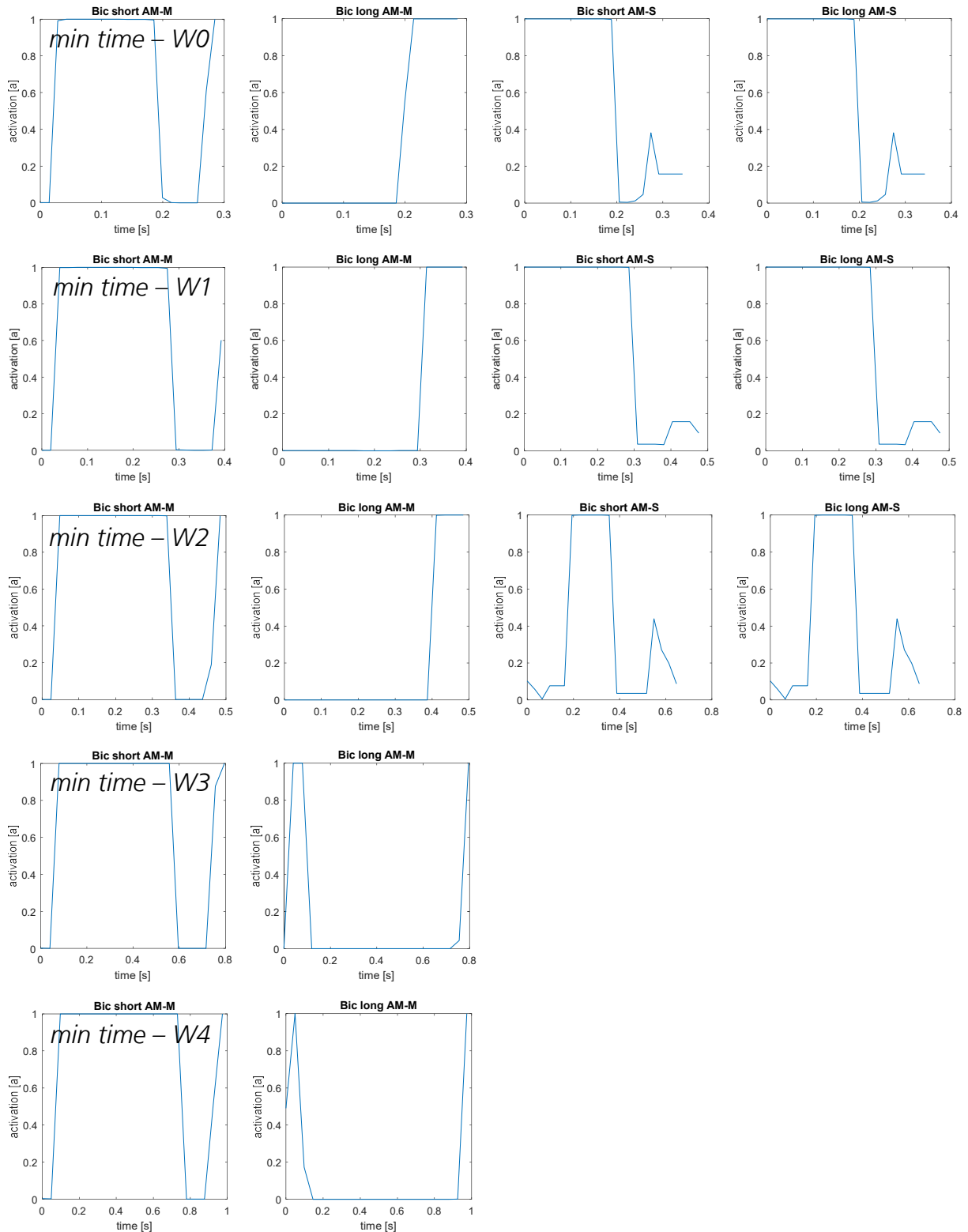


Figure 125: Simulated muscle actuations of Biceps short and long head for a AM-M (column 1&2) and AM-S (column 3&4) for Test Scenario TS-1-f for weights  $W_0$ - $W_4$  – minimal time as cost function

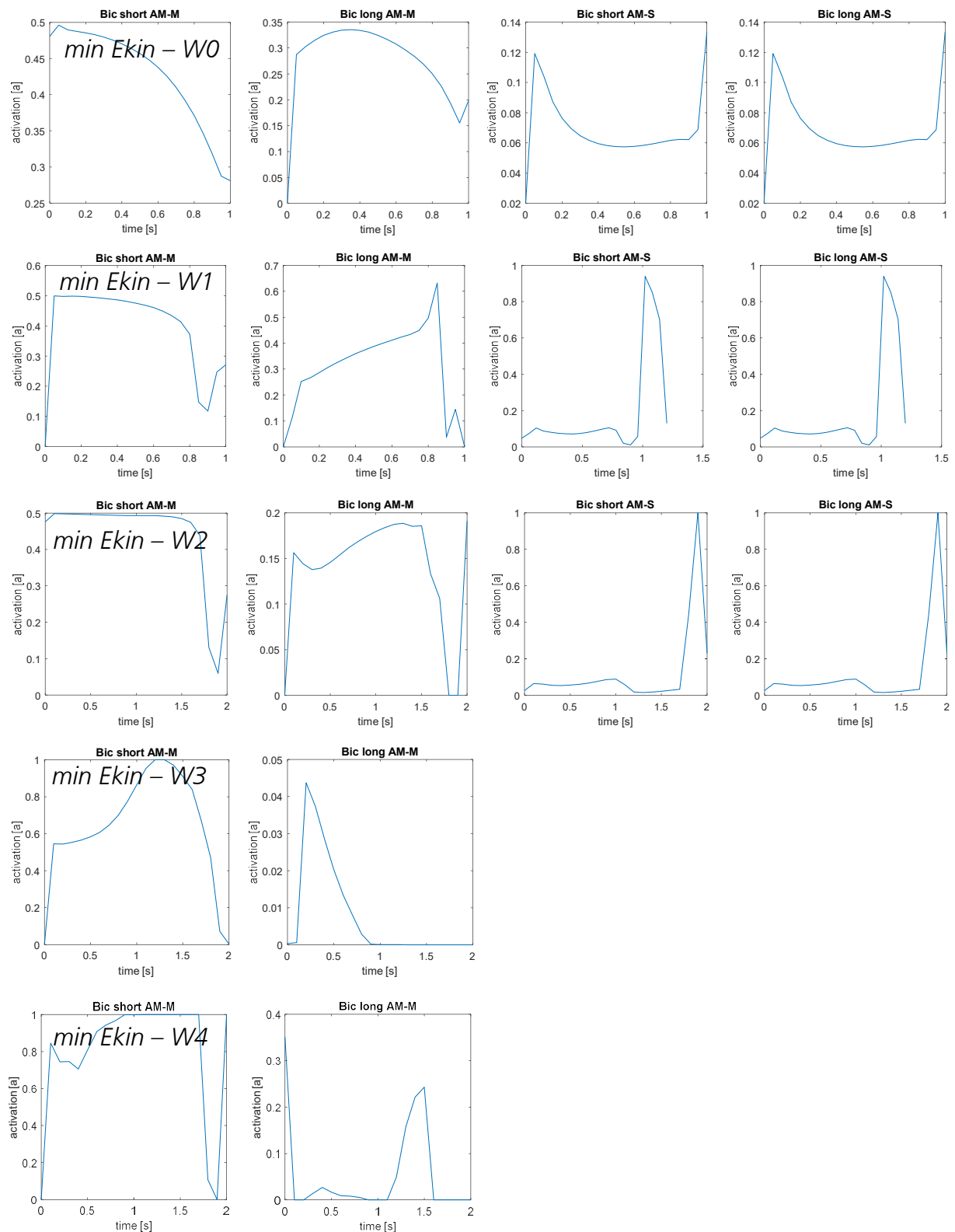


Figure 126: Simulated muscle actuations of Biceps short and long head for a AM-M (column 1&2) and AM-S (column 3&4) for Test Scenario TS-1-f for weights W0-W4 – minimal kinetic Energy as cost function

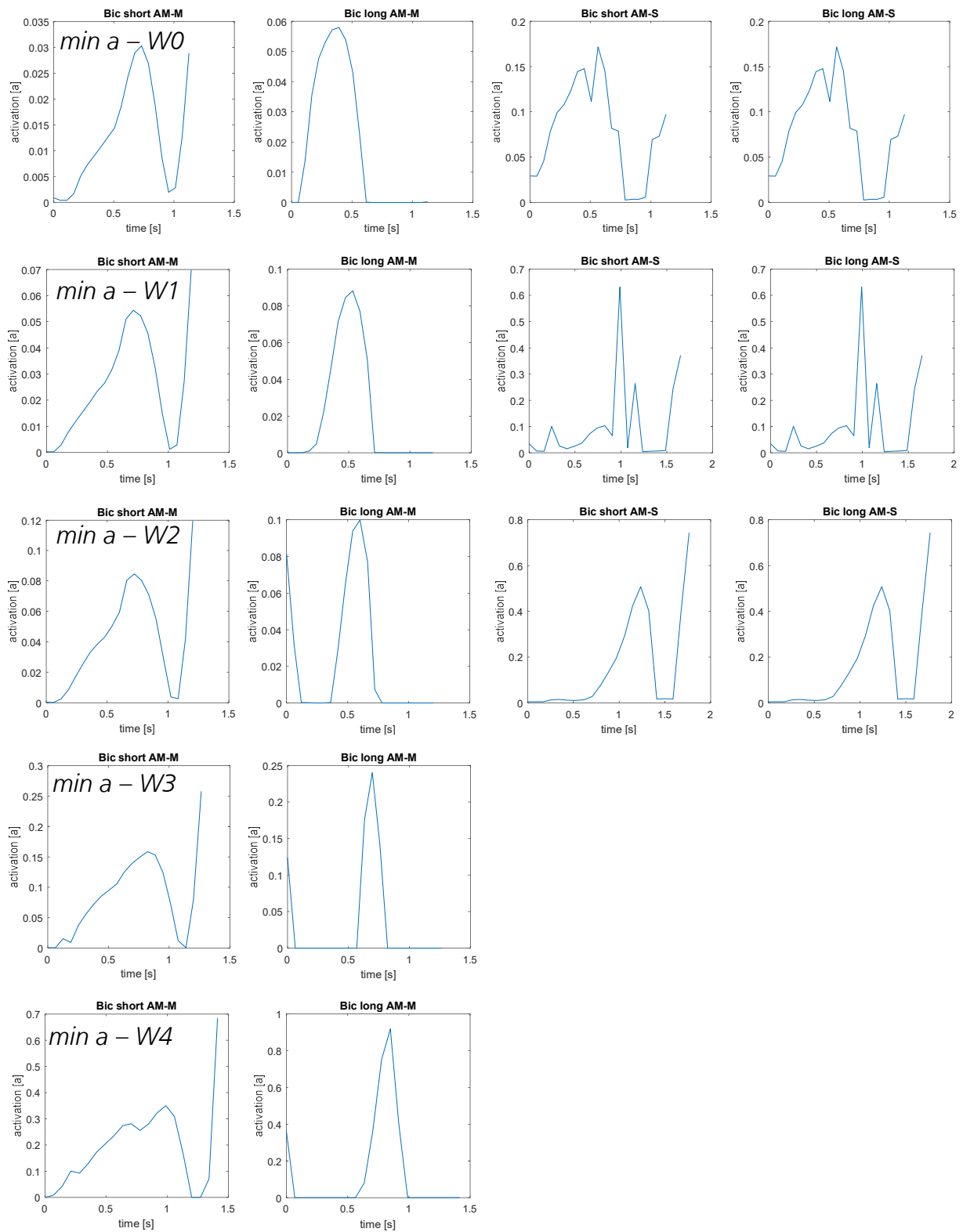


Figure 127: Simulated muscle actuations of Biceps short and long head for a AM-M (column 1&2) and AM-S (column 3&4) for Test Scenario TS-1-f for weights W0-W4 – minimal control (a) as cost function

## A.2 Box lift – simulated muscle actuations

### A.2.1 Direct muscle actuation

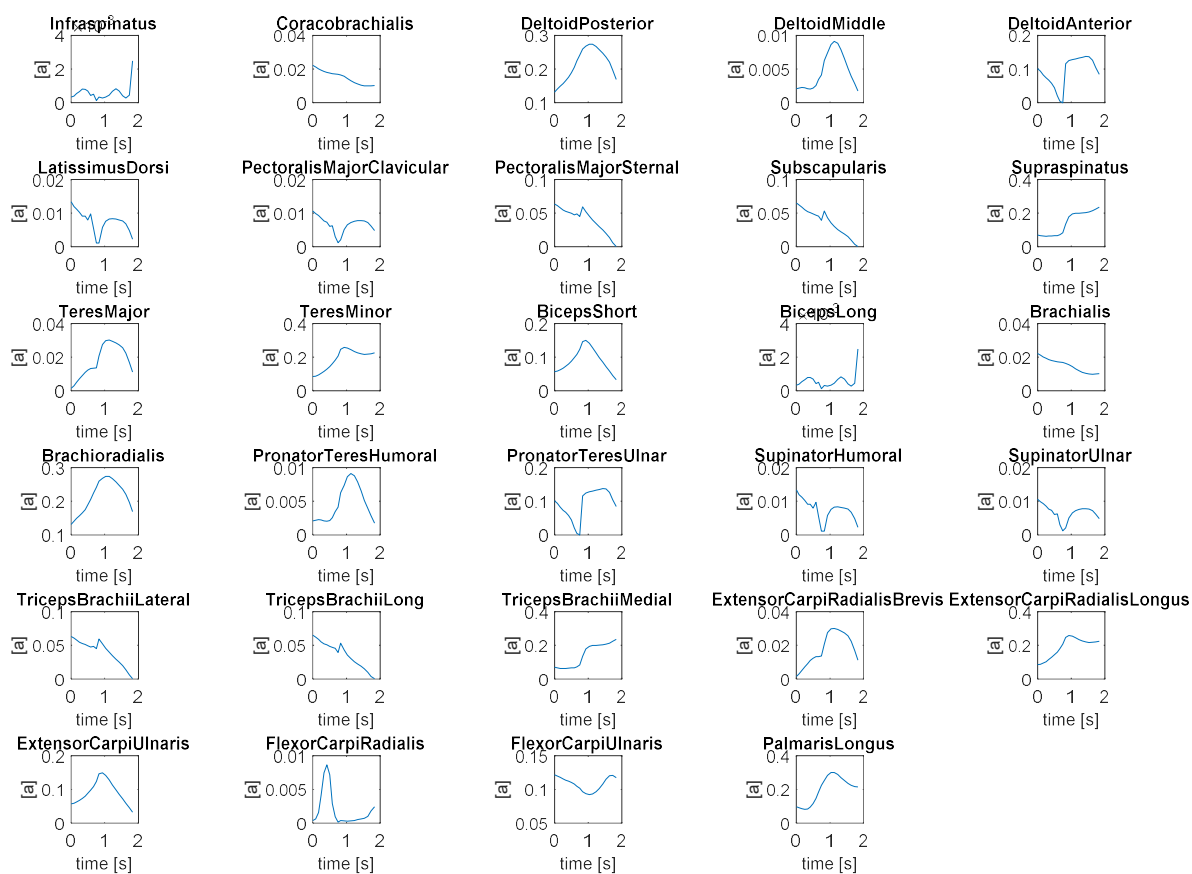


Figure 128: Box lift test – simulated muscle actuation – all muscles – BC1 as cost function – direct muscle actuation (AM-M)

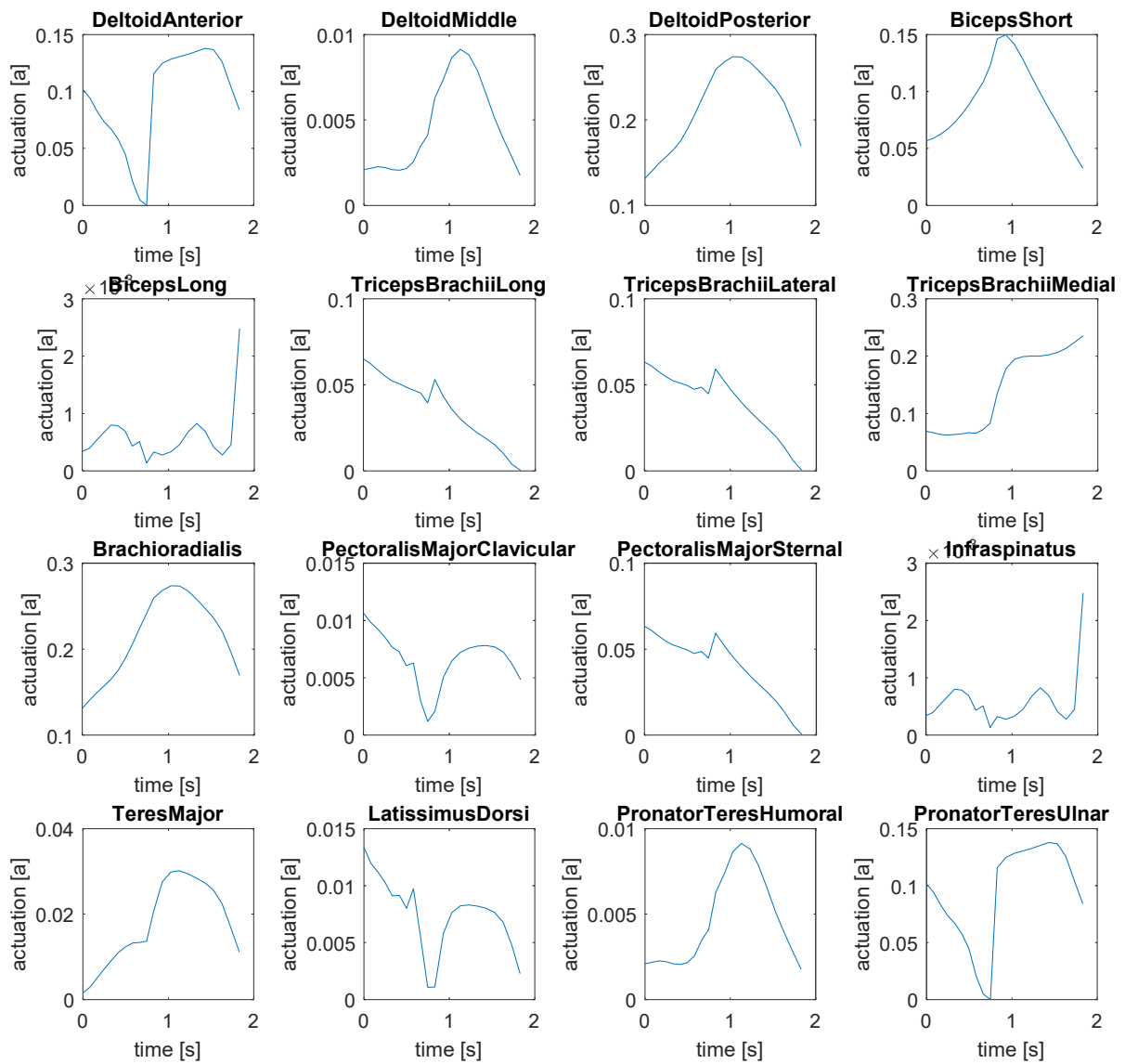


Figure 129: Box lift test – simulated muscle actuation – only muscles which are included in synergies (for comparison) – BC1 as cost function – direct muscle actuation (AM-M)

### A.2.2 Synergetic muscle actuation

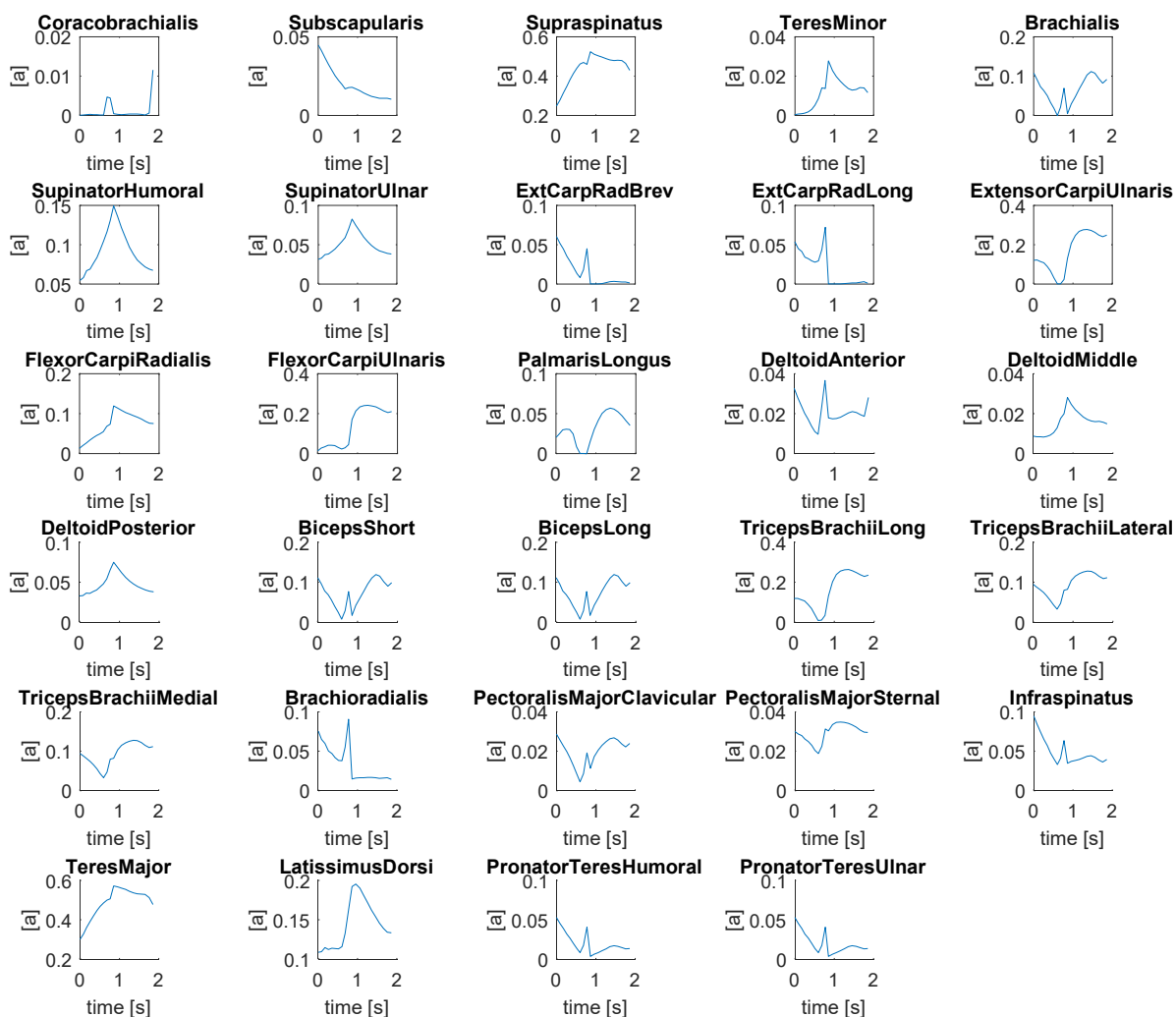
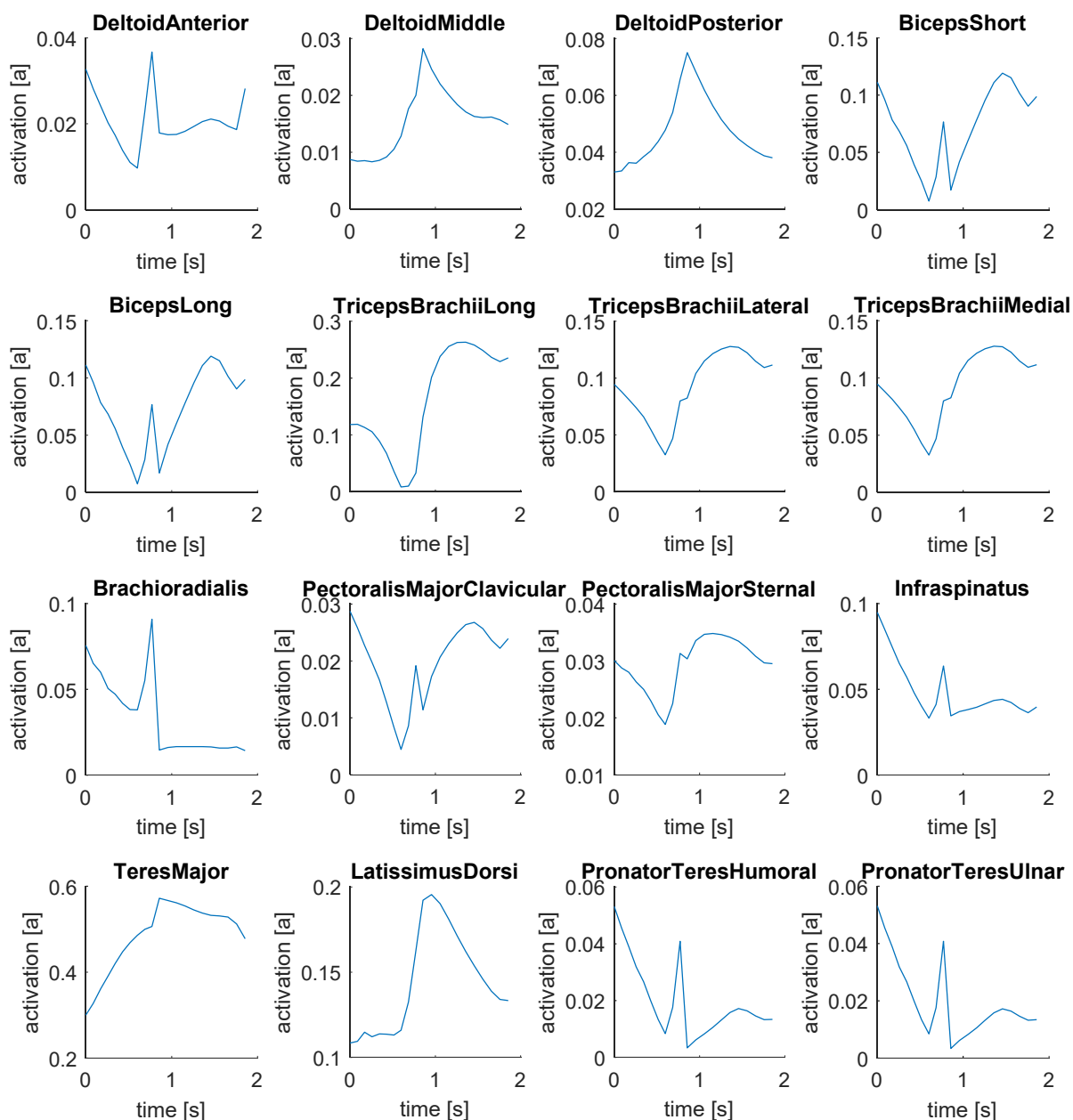


Figure 130: Box lift test – simulated muscle actuation – all muscles – BC1 as cost function – synergetic muscle actuation (AM-S)



*Figure 131: Box lift test – simulated muscle actuation – only muscles which are included in synergies (for comparison) – BC1 as cost function – synergetic muscle actuation (AM-S)*



## Bibliography

- [Abdel-Malek 07] Abdel-Malek, K., Yang, J., Kim, J., Marler, T., Beck, S., Swan, C., Frey-Law, L., Mathai, A., Murphy, C., Rahmatallah, S., and Arora, J. (2007). Development of the virtual-human santos. In *Digital Human Modeling*, V. D. (Ed.), Springer-Verlag Berlin Heidelberg, pp. 490–499.
- [Afzal 17] Afzal, T., Iqbal, K., White G., Wright, A., B.(2017). A method for locomotion mode identification using muscle synergies. *IEEE Transactions on Neural Systems and Rehabilitation Engineering*. 2017;25(6):608–617. doi: 10.1109/tnsre.2016.2585962.
- [Alessandro 13] Alessandro, C., Delis, I., Nori, F., Panzeri, S., & Berret, B. (2013). Muscle synergies in neuroscience and robotics: from input-space to task-space perspectives. *Frontiers in computational neuroscience*, 7, 43. doi:10.3389/fncom.2013.00043
- [Allen 12] Allen, J. L., & Neptune, R. R. (2012). Three-dimensional modular control of human walking. *Journal of biomechanics*, 45(12), 2157–2163. doi:10.1016/j.jbiomech.2012.05.037
- [Anderson 17] Anderson, P., Fels, S., Harandi, N., et al (2017). FRANK A Hybrid 3D Biomechanical Model of the Head and Neck. *Biomechanics of Living Organs*. 10.1016/b978-0-12-804009-6.00020-1
- [Andrews 87] Andrews, JG. (1987). The functional roles of the hamstrings and quadriceps during cycling: Lombard's Paradox revisited. *Journal of Biomechanics* 20 (6): 565–75. doi:10.1016/0021-9290(87)90278-8. PMID 3611133.
- [Badler 97] Badler, N. I.(1997). Virtual humans for animation, ergonomics, and simulation. In: *Proceedings of the IEEE workshop on non-rigid and articulated motion*. pp. 28–36.
- [Berniker 09] Berniker, M., Jarc, A., Bizzi, E., Tresch, MC.(2009).Simplified and effective motor control based on muscle synergies to exploit musculoskeletal dynamics. *Proceedings of the National Academy of Sciences of the USA* 2009;106:7601–7606.
- [Bernstein 67] Bernstein, N. (1967). *The Coordination and Regulation of Movements*. Oxford: Pergamon Press
- [Bio 14] Image source: internet <https://biomechanicsforeverybody.wordpress.com/2013/02/04/as-simple-as-possible/>. Accessed on 26.09.2019
- [Bizzi 08] Bizzi, E., Cheung, V. C., d'Avella, A., Saltiel, P., & Tresch, M. (2008). Combining modules for movement. *Brain research reviews*, 57(1), 125–133. doi:10.1016/j.brainresrev.2007.08.004

- [Bizzi 91] Bizzi, E., Mussa-Ivaldi, F.A., Giszter, S.F.(1991). *Computations underlying the execution of movement: a biological perspective. Science. 1991; 253:287–291. [PubMed: 1857964]*
- [Björkenstam 16] Björkenstam, S., Delfs, N., Carlson, J.S., Bohlin, R., Lennartson, B.(2016). Enhancing digital human motion planning of assembly tasks through dynamics and optimal control. *Procedia CIRP*, 44, 20-25.
- [Björkenstam 18] Björkenstam, S., Leyendecker, S., Linn, L., Carlson, J.S., Lennartson, B.(2018). Inverse Dynamics for Discrete Geometric Mechanics of Multibody Systems With Application to Direct Optimal Control. *ASME. Journal The Journal of Computational and Nonlinear Dynamics*. 13(10):101001-101001-15.
- [Blanchonette 09] Blanchonette P.(2009). Jack human modelling tool: A review. *Technical report - Air Operations Division Defence Science and Technology Organisation. Australia.*
- [Brown 07] Brown, J.M., Wickham, J.B., McAndrew, D.J., Huang, X.F. (2007). Muscles within muscles: Coordination of 19 muscle segments within three shoulder muscles during isometric motor tasks. *Journal of Electromyography and Kinesiology*. 17(1):57-73. PMID 16458022 doi:10.1016/j.jelekin.2005.10.007
- [Cardoso 98] Cardoso, J.-F.(1998) Blind signal separation: statistical principles. *Proceedings of the IEEE*, vol. 86, no. 10, pp. 2009-2025, Oct. 1998
- [Cheung 05] Cheung, V. C.-K. K.(2005). Central and Sensory Contributions to the Activation and Organization of Muscle Synergies during Natural Motor Behaviors. *Journal of Neuroscience* 25 (27) (2005) 6419–6434. doi:10.1523/JNEUROSCI.4904-04.2005.
- [Chiovetto 13] Chiovetto, E., Berret, B., Delis, I., Panzeri, S., Pozzo, T. (2013). Investigating reduction of dimensionality during single-joint elbow movements: a case study on muscle synergies. *Frontiers in computational neuroscience*, 7, 11. doi:10.3389/fncom.2013.00011
- [Cholewicki 95] Cholewicki, J., McGill, S.M., Norman, R.W. (1995). Comparison of muscle forces and joint load from an optimization and EMG assisted lumbar spine model: Towards development of a hybrid approach. *Journal of Biomechanics*, Volume 28, Issue 3, 1995, Pages 321-331, ISSN 0021-9290,
- [Cimolato 16] Cimolato, A., Piovanelli, E., Bortoletto, R., Menegatti, E., Pagello, E. (2016). Muscle synergies for reliable NAO arm motion control: An online simulation with real-time constraints. *IEEE International Conference on Simulation, Modeling, and Programming for Autonomous Robots (SIMPAR)*, San Francisco, CA, 2016, pp. 191-196.

- [d'Avella 14] d'Avella, A. (2014). Muscle synergies and neuromotor recovery. *Presentation on COST Winter School on Computational Methods for Neurorehabilitation*. Hotel Schütz, Obertauern, Austria January 29th, 2014.
- [Damsgaard 06] Damsgaard, M. Rasmussen, J. Christensen, S.T., Mark de Zee, E.S. (2006). Analysis of musculoskeletal system in the AnyBody modeling system. *Simulation Modeling practice and theory*, 14:1100-1111.
- [d'Avella 06] d'Avella, A., Portone, A., Fernandez, L., & Lacquaniti, F. (2006). Control of fast-reaching movements by muscle synergy combinations. *The Journal of neuroscience: the official journal of the Society for Neuroscience*, 26(30), 7791–7810. doi:10.1523/JNEUROSCI.0830-06.2006
- [De Magistris 13] De Magistris, G., Micaelli, A., Evrard, P., Andriot, C. Savin, J., Gaudez, C., Marsot J. (2013). Dynamic control of DHM for ergonomic assessments, *International Journal of Industrial Ergonomics*, Volume 43, Issue 2, 2013, Pages 170-180, ISSN 0169-8141.
- [de Rugy 13] de Rugy, A., Loeb, G. E., Carroll, T. J. (2013). Are muscle synergies useful for neural control? *Frontiers in Computational Neuroscience*, 7(March):1{13.
- [Dhillon 05] Dhillon, I.S., Sra, S. (2005). Generalized nonnegative matrix approximations with Bregman divergences. In *Proceedings of the 18th International Conference on Neural Information Processing Systems (NIPS'05)*, Y. Weiss, B. Schölkopf, and J. C. Platt (Eds.). MIT Press, Cambridge, MA, USA, 283-290.
- [Drillis 64] Drillis, R., Contini, R., Bluestein, M. (1964). Body segment parameters; a survey of measurement techniques. *Artif. Limbs* 1964, 8, 44–66.
- [Eames 07] Eames, M.H.A., Bain, G.I., Fogg, Q.A., van Riet, R.P. (2007). Distal Biceps Tendon Anatomy: A Cadaveric Study. *The Journal of Bone & Joint Surgery*. 89(5):1044–1049, MAY 2007:DOI: 10.2106/JBJS.D.02992.PMID: 17473142
- [Ebied 18] Ebied, A. Kinney-Lang, E., Spyrou, L., Escudero, J. (2018). Evaluation of matrix factorisation approaches for muscle synergy extraction. *Medical Engineering & Physics*, Volume 57, 2018, Pages 51-60, ISSN 1350-4533.
- [Enoka 89] Enoka, R.M. (1989). A review of: Neuromechanical basis of kinesiology. Human Kinetic Books, Champaign, ISBN 0-87322-179-6, *Ergonomics*, 32:10, 1252, DOI: 10.1080/00140138908966896
- [Featherstone 14] Featherstone, R. (2014). Rigid body dynamics algorithm. *Springer*
- [Ferré 95] Ferré, L. (1995). Selection of components in principal component analysis: a comparison of methods. *Computational Statistics and Data Analyses* 19, 669–682.

- [Freriks 99] B. Freriks, H.J. Hermens. European Recommendations for Surface ElectroMyoGraphy, results of the SENIAM project, ISBN: 90-75452-14-4, 1999.
- [Gerdts 11] Gerdts, M. (2011). *Optimal Control of ODEs and DAEs*. Berlin, Boston: De Gruyter.
- [Giszter 93] Giszter, S.F., Mussa-Ivaldi, F.A., Bizzi, E. (1993). Convergent force fields organized in the frog's spinal cord. *Journal of Neuroscience*, 13 (2) 467-491; DOI: 10.1523/JNEUROSCI.13-02-00467.
- [Haiss 05] Haiss, F., Schwarz, C. (2005). Spatial segregation of different modes of movement control in the whisker representation of rat primary motor cortex. *The Journal of neuroscience : the official journal of the Society for Neuroscience* 25 (6) (2005) 1579–87. doi:10.1523/JNEUROSCI.3760-04.2005.
- [Hamill 14] Hamill, J., Knutzen, K., Derrick, T. (2014). Biomechanical Basis of Human Movement. *LIPPINCOTT RAVEN*. ISBN-13: 978-1451177305
- [Hanson 19] Hanson, L., Högberg, D. Carlson, J.S. Industrial path solutions - intelligently moving manikins. *DHM and Posturography* (115-124). London: Academic Press, 2019.
- [Heald 18] Heald, J. B., Franklin, D. W., & Wolpert, D. M. (2018). Increasing muscle co-contraction speeds up internal model acquisition during dynamic motor learning. *Scientific reports*, 8(1), 16355. doi:10.1038/s41598-018-34737-5
- [Heidlauf 14] Heidlauf, T., Röhrle, O. (2014). A multiscale chemo-electro-mechanical skeletal muscle model to analyze muscle contraction and force generation for different muscle fiber arrangements." *Frontiers in physiology* vol. 5 498. 23 Dec. 2014, doi:10.3389/fphys.2014.00498
- [Herman 16] Herman, I.P. (2016). Physics of the Human Body. *Springer International Publishing* ISBN 978-3-319-23932-3
- [Herrmann 19] Herrmann, S., Kebbach, M., Grawe, R., Kelsey, K., Ingr, K., Bader, R., Woernle, C. (2019). A Detailed Kinematic Multibody Model of the Shoulder Complex After Total Shoulder Replacement. *Proceedings of the 9<sup>th</sup> ECCOMAS Thematic Conference on Multibody Dynamics*. Duisburg.
- [Hill 38] Hill, A. (1938). The heat of shortening and the dynamic constants of muscle. *Proceedings of the Royal Society of London. Series B, Biological Sciences*, vol. 126, no. 843, pp. 136–195, 1938.
- [Högberg 16] Högberg D., Hanson L., Bohlin R. (2016). Creating and shaping the DHM tool IMMA for ergonomic product and production design. *International Journal of the Digital Human*, 2016, 1(2), 132-152.

- [Horita 87] Horita, T., Ishiko, T. (1987). Relationships between Muscle Lactate Accumulation and Surface EMG Activities During Isokinetic Contractions in Man. *European Physical Journal Applied Physics* 56,18-23.
- [imk 19] Image Source: <https://www.imk-automotive.de/newsleser/neue-ema-version-1610-verfuegbar.html> - 30.09.2019
- [Israely 18] Israely, S., Leisman, G., Machluf, C. C., & Carmeli, E. (2018). Muscle Synergies Control during Hand-Reaching Tasks in Multiple Directions Post-stroke. *Frontiers in computational neuroscience*, 12, 10. doi:10.3389/fncom.2018.00010
- [Jöllenbeck 99] Jöllenbeck, T., Wank, V. (1999). Electromechanical Delay of the Knee Extensor Muscles and Relation to the Initial Muscle Length. In: SANDERS R.H./GIBSON, B.J. (eds.): ISBS '99 – XVI International Symposium of Biomechanics in Sports. Perth: Scientific Proceedings. pp. 125-128
- [Kapandji 16] Kapandji, I.A., Rehart, S. (2016) Funktionelle Anatomie der Gelenke. Thieme, Stuttgart 6. Auflage 2016 ISBN: 9783131422163
- [Konrad 11] Konrad, P. (2011). EMG-FIBEL: Eine praxisorientierte Einführung in die kinesiologische Elektromyographie. Noraxon INC. USA
- [Koshio 2012] Koshio, T., Sakurazawa, S., Toda, M., Akita, J., Kondo K., Nakamura, Y. (2012). Identification of surface and deep layer muscles activity by surface EMG. *Proceedings of SICE Annual Conference (SICE)*, Akita, 2012, pp. 1816-1821.
- [Krouchev 06] Krouchev, N., Kalaska, J.F., Drew, T. (2006). Sequential activation of muscle synergies during locomotion in the intact cat as revealed by cluster analysis and direct decomposition. *Journal of Neurophysiology*. 96(4):1991–2010.
- [Le 17] Le, P., Best, T.M., Khan, S.N., Mendel, E., Marras, W.S. (2017). A review of methods to assess coactivation in the spine. *Journal of Electromyography and Kinesiology*. 32: 51–60. doi:10.1016/j.jelekin.2016.12.004. PMID 28039769.
- [Leidholdt 16] Leidholdt, W., Fritzsche, L., Bauer, S. (2016). Editor menschlicher Arbeit (ema). 10.1007/978-3-662-50459-8\_20. Chapter from book *Homo Sapiens Digitalis - Virtuelle Ergonomie und digitale Menschmodelle* (pp.355-362)
- [Lemay 01] Lemay, M.A., Galagan, J.E., Hogan, N., Bizzi, E. (2001). Modulation and Vectorial Summation of the Spinalized Frog's Hindlimb End-Point Force Produced by Intraspinally Electrical Stimulation of the Cord. *IEEE Transactions of Neural Systems and Rehabilitation Engineering*. 2001; 9(1)
- [Lemay 04] Lemay, M.A., Grill, W. M. (2004). Modularity of motor output evoked by intraspinal microstimulation in cats. *Journal of neurophysiology* 91 (1) (2004) 502–14. doi:10.1152/jn.00235.2003.

- [Leyendecker 10] Leyendecker, S., Ober-Blöbaum, S., Marsden, J., Ortiz M. (2010). Discrete mechanics and optimal control for constrained systems. *Optimal control applications & methods*, 31(6), 505–528, 2010.
- [Lombard 07] Lombard, W.P., Abbott, F.M. (1907). The mechanical effects produced by the contraction of individual muscles of the thigh of the frog. *American Journal of Physiology*, 20, 1-60.
- [Lundy-Ekman 13] Lundy-Ekman, L. (2013). *Neuroscience - E-Book: Fundamentals for Rehabilitation (4th ed.)*. Elsevier Health Sciences. pp. 190–220. ISBN 9780323266482.
- [Maas 14] Maas, R. (2014). Biomechanics and optimal control simulations of the human upper extremity. *Doctoral thesis*, Friedrich-Alexander-University Erlangen-Nürnberg (FAU).
- [Maas 13] Maas, R., Leyendecker, S. (2013). Biomechanical optimal control of human arm motion. *Journal of Multi-Body Dynamics* 227(4) 375-389.
- [Marshall 10] Marshall Cavendish Corporation. (2010). *Mammal Anatomy: An Illustrated Guide*. Cavendish Square Publishing. New York. ISBN 9780761478829
- [McKay 08] McKay, J. L., Ting, L. H. (2008). Functional muscle synergies constrain force production during postural tasks. *Journal of biomechanics*, 41(2), 299–306. doi:10.1016/j.jbiomech.2007.09.012
- [Mörle 12] Mörl, F., Siebert, T., Schmitt, S., Blickhan, R., Günther, M. (2012). Electro-Mechanical Delay in Hill-Type Muscle Models. *Journal of Mechanics in Medicine and Biology*, 12(05):1250085, 2012. doi: 10.1142/S0219519412500856.
- [Mostafa 10] Mostafa, S. N., Mostafa, G., Masoud, M. (2010). Optimal trajectory planning of a mobile robot with spatial manipulator for obstacle avoidance, *ICCAS 2010*, Gyeonggi-do, 2010, pp. 314-318. doi: 10.1109/ICCAS.2010.5670217
- [Mühlstedt 12] Mühlstedt J. (2012). Entwicklung eines Modells dynamisch-muskulärer Arbeitsbeanspruchungen auf Basis digitaler Menschmodelle. *Doctoral thesis*, Chemnitz, Technical University. *Universitätsverlag Chemnitz*.
- [Mussa-Ivaldi 92] Mussa-Ivaldi, F., Giszter, S. (1992). Vector field approximation: a computational paradigm for motor control and learning. *Biological Cybernetics*. 1992; 67:491–500.
- [Mussa-Ivaldi 94] Mussa-Ivaldi, F.A., Giszter, S.F., Bizzi, E. (1994) Motor learning through the combination of primitives. *Proceedings of the National Academy of Sciences of the USA*. 91:7534–7538. [PubMed: 8052615]
- [Mussa-Ivaldi 97] Mussa-Ivaldi, FA. (1997). Nonlinear force fields: a distributed system of control primitives for representing and learning movements. *Proceedings of the*

- 1997 *IEEE International Symposium on Computation Intelligence in Robotics and Automation*. Los Alamitos, CA: IEEE Computer Society Press; 1997.; p. 84-90.
- [Neptune 09] Neptune, R. R., Clark, D. J., Kautz, S. A. (2009). Modular control of human walking: a simulation study. *Journal of biomechanics*, 42(9), 1282–1287. doi:10.1016/j.jbiomech.2009.03.009
- [Obentheuer 17] Obentheuer, M., Roller, M., Björkenstam, S., Berns, K., Linn, J. (2017). Human like Motion Generation for Ergonomic Assessment - a Muscle Driven Digital Human Model Using Muscle Synergies. *Proceedings of the 8<sup>th</sup> ECCOMAS Thematic Conference on Multibody Dynamics*, pp. 847-856, June 19-22, Prague, Czech Republic.
- [Obentheuer 18] Obentheuer, M., Roller, M., Björkenstam, S., Berns, K., Linn, J. (2018). Comparison of different Actuation Modes of a biomechanical human arm model in an optimal control framework. *Proceedings of the 5<sup>th</sup> IMSD Joint International Conference on Multibody System Dynamics*, Lisbon.
- [Obentheuer 19] Obentheuer, M., Roller, M., Björkenstam, S., Berns, K., Linn, J. (2019). Comparison of Measured EMG Data with Simulated Muscle Actuations of a Biomechanical Human Arm Model in an Optimal Control Framework – Direct Vs. Muscle Synergy Actuation. *Proceedings of the 9<sup>th</sup> ECCOMAS Thematic Conference on Multibody Dynamics*, pp. 26-33, July 15-18, Duisburg.
- [Ott 13] Ott, C., Henze, B., Lee, D. (2013). Kinesthetic teaching of humanoid motion based on whole-body compliance control with interaction-aware balancing. *IEEE/RSJ International Conference on Intelligent Robots and Systems*, Tokyo, 2013, pp. 4615-4621. doi: 10.1109/IROS.2013.6697020
- [Overduin 08] Overduin, S.A., D’Avella, A., Roh, J., Bizzi, E. (2008). Modulation of Muscle Synergy Recruitment in Primate Grasping. *Journal of Neuroscience* 28 (4) (2008) 880–892. doi:10.1523/JNEUROSCI.2869-07.2008
- [Overduin 14] Overduin, S. A., D’Avella, A., Carmena, J. M., Bizzi, E. (2014). Muscle synergies evoked by microstimulation are preferentially encoded during behavior. *Frontiers in computational neuroscience* 8 (March) (2014) 20. doi:10.3389/fncom.2014.00020.
- [Pérot 96] Pérot, C., André, L., Dupont, L., Vanhoutte, C. (1996). Relative contributions of the long and short heads of the biceps brachii during single or dual isometric tasks. *Journal of Electromyography and Kinesiology*. Volume 6, Issue 1, 1996, ISSN 1050-6411.
- [Peters 18] Peters, M., Quadrat, E., Nolte, A., et.al (2018. )Biomechanical Digital Human Models: Chances and Challenges to Expand Ergonomic Evaluation. *Proceedings of the 1st International Conference on Human Systems Engineering and Design (IHSED2018): Future Trends and Applications*. October 25-27, 2018, CHU-Université de Reims Champagne-Ardenne, France"

- [Platzer 14] Platzer, W. (2014) Color Atlas of Human Anatomy: Vol 1. Locomotor System. *Thieme*; 7th edition. ISBN-13: 978-3135333076
- [Pollard 02] Pollard, N.S., Hodgins, J.K., Riley, M., Atkeson, C.G. (2002). Adapting human motion for the control of a humanoid robot. *Proceedings 2002 IEEE International Conference on Robotics and Automation (Cat. No.02CH37292)*, 2, 1390-1397 vol.2.
- [Porter 90] Porter, J.M., Freer, M., Bonney, M.C. (1990). Computer aided ergonomics and workspace design., in *Evaluation of Human Work: A Practical Ergonomics Methodology*. J.R. Wilson and E.N. Corlett, Editors. 1990, *Taylor and Francis*. p. 575.
- [Rasool 16] Rasool, G., Iqbal, K., Bouaynaya, N., White, G. (2016). Real-Time Task Discrimination for Myoelectric Control Employing Task-Specific Muscle Synergies. *IEEE Transactions on Neural Systems and Rehabilitation Engineering*, vol. 24, no. 1, pp. 98-108.doi: 10.1109/TNSRE.2015.2410176
- [Razavian 15] Razavian, R.S. Ghannadi, B., McPhee, J. (2015). Control of a musculoskeletal arm model using muscle synergy. *International Society of Biomechanics*. Glasgow, UK
- [Razavian 16] Razavian, R.S., McPhee, J. (2016). A motor control framework for the fast control of a 3D musculoskeletal arm motion using muscle synergy. Conference Proceedings. *International Multibody Systems Dynamics*. Montreal, Canada
- [Razavian 18] Razavian, R.S. Ghannadi, B., McPhee, J. (2018). A synergy-based motor control framework for the fast feedback control of musculoskeletal systems. *Journal of Biomechanical Engineering*. 141. 10.1115/1.4042185.
- [Remaley 15] Remaley, D. T., Fincham, B., McCullough, B., Davis, K., Nofsinger, C., Armstrong, C., & Stausmire, J. M. (2015). Surface Electromyography of the Forearm Musculature During the Windmill Softball Pitch. *Orthopaedic journal of sports medicine*, 3(1), 2325967114566796. doi:10.1177/2325967114566796
- [Riemann 02] Riemann, B.L., Lephart, S.M. (2002). The Sensorimotor System, Part II: The Role of Proprioception in Motor Control and Functional Joint Stability. *Journal of Athletic Training*. 37 (1): 80–84. ISSN 1062-6050. PMC 164312. PMID 16558671.
- [Röhrle 16] Röhrle, O., Sprenger, M., Schmitt, S. (2016). A two-muscle, continuum-mechanical forward simulation of the upper limb. *Biomechanics and modeling in mechanobiology*. 16. 10.1007/s10237-016-0850-x.
- [Roller 17] Roller, M., Björkenstam, S., Linn, J. Leyendecker, S. (2017) Optimal control of a biomechanical multibody model for the dynamic simulation of working tasks.



- ECCOMAS Thematic Conference on Multibody Dynamics* June 19-22, 2017, Prague, Czech Republic
- [Sartori 13] Sartori, M., Gizzi, L., Lloyd, D. G., Farina, D. (2013). A musculoskeletal model of human locomotion driven by a low dimensional set of impulsive excitation primitives. *Frontiers in computational neuroscience*, 7(June):79.
- [Schünke 18] Schünke, M., Schulte, E., Schumacher, U. (2018) PROMETHEUS Allgemeine Anatomie und Bewegungssysteme - LernAtlas der Anatomie. *Lehrbuch / Bildatlas*. 5. überarbeitete Auflage 2018. ISBN 978-3-13-242083-0
- [Seekircher 17] Seekircher, A., Visser, U. (2017) A Closed-Loop Gait for Humanoid Robots Combining LIPM with Parameter Optimization. In: Behnke S., Sheh R., Sarel S., Lee D. (eds) RoboCup 2016: Robot World Cup XX. RoboCup 2016. *Lecture Notes in Computer Science*, vol 9776. Springer, Cham
- [SENIAM] The European Recommendations for Surface Electromyography (SENIAM) Web Link: <http://www.seniam.org/> - 30.09.2019
- [Singh 18] Singh, R.E., Iqbal, K., White, G., Hutchinson, T.E. (2018). A Systematic Review on Muscle Synergies: From Building Blocks of Motor Behavior to a Neurorehabilitation Tool. *Applied Bionics and Biomechanics*. 2018;2018:3615368. Published 2018 Apr 22. doi:10.1155/2018/3615368
- [Staudemann 14] Staudemann, D., Taube, W. (2014). Brachialis muscle activity can be assessed with surface electromyography. *Journal of Electromyography and Kinesiology*, Volume 25, Issue 2,2015,Pages 199-204,ISSN 1050-6411,
- [Steele 13] Steele, K. M., Tresch, M. C., Perreault, E. J. (2013). The number and choice of muscles impact the results of muscle synergy analyses. *Frontiers in computational neuroscience*, 7(August):105.
- [Stepniewska 05] I. Stepniewska, P.-C., Fang, J. H. (2005). Microstimulation reveals specialized subregions for different complex movements in posterior parietal cortex of prosimian galagos. *Proceedings of the National Academy of Sciences of the United States of America* 102 (13) (2005) 4878–83. doi:10.1073/pnas.0501048102.
- [Taborri 18] Taborri, J., Agostini, V., Artemiadis, P. K., Ghislieri, M., Jacobs, D. A., Roh, J., Rossi, S. (2018). Feasibility of Muscle Synergy Outcomes in Clinics, Robotics, and Sports: A Systematic Review. *Applied bionics and biomechanics*, 2018, 3934698. doi:10.1155/2018/3934698
- [Tillmann 05] Tillmann, B.N. (2005). Atlas der Anatomie des Menschen. Berlin, Heidelberg, New York. *Springer-Verlag*
- [Ting 05] Ting, L.H., Macpherson, J.M. (2005). A Limited Set of Muscle Synergies for Force Control During a Postural Task. *Journal of Neurophysiology*,2005; 93:609–613.

- [Ting 08] Ting, L. H., McKay, J. L. (2007). Neuromechanics of muscle synergies for posture and movement. *Current opinion in neurobiology*, 17(6), 622–628. doi:10.1016/j.conb.2008.01.002
- [Todorov 04] Todorov, E. (2004). Optimality principles in sensorimotor control. *Nature neuroscience*, 7(9), 907–915. doi:10.1038/nn1309
- [Torres-Oviedo 06] Torres-Oviedo, G., Macpherson, J.M., Ting, L.H.. Muscle synergy organization is robust across a variety of postural perturbations. *Journal of neurophysiology* 96 (3) (2006) 1530–1546. doi:10.1152/jn.00810.2005.
- [Tresch 09] Tresch, M. C., Jarc, A. (2009). The case for and against muscle synergies. *Current opinion in neurobiology*, 19(6), 601–607. doi:10.1016/j.conb.2009.09.002
- [Tresch 99] Tresch, M.C., Bizzi, E. (1999) Responses to spinal microstimulation in the chronically spinalized rat and their relationship to spinal systems activated by low threshold cutaneous stimulation. *Experimental Brain Research*. 1999; 129:401–416. [PubMed: 10591912]
- [Tresch 06] Tresch, M.C., Cheung, V.C., d'Avella, A. (2006) Matrix factorization algorithms for the identification of muscle synergies: evaluation on simulated and experimental data sets. *Journal of Neurophysiology* 2006 Apr;95(4):2199-212. Epub 2006 Jan 4.
- [Trinler 19] Trinler, U., Schwameder, T., Baker, R., Alexander, N. (2019). Muscle force estimation in clinical gait analysis using AnyBody and OpenSim. *Journal of Biomechanics*, Volume 86,2019, Pages 55-63,ISSN 0021-9290.
- [Tsai 13] Tsai, M. J., Lee, H. W., Kumar, V. Schmiedeler, J., Sreenivasan, S. V., Su, H.J. (2013). Automatic Full Body Inverse Dynamic Analysis Based on Personalized Body Model and MoCap Data" in *Advances in Mechanisms, Robotics and Design Education and Research*. 2013 Springer International Publishing, Heidelberg, pages 305—322 isbn978-3-319-00398-6
- [Van der Meulen 07] Van der Meulen, P., Seidl, A. (2007). Ramsis – the leading cad tool for ergonomic analysis of vehicles. In *Digital Human Modeling*, V. D. (Ed.), ed., Springer-Verlag Berlin Heidelberg, pp. 1008–1017.
- [Van Sint Jan 07] Van Sint Jan, S., Allard, P., Wu Ge. (2007) Color Atlas of Skeletal Landmark Definitions: Guidelines for Reproducible Manual and Virtual Palpations. *Churchill Livingstone*; Auflage: 1 (13. April 2007)
- [Vaupel 15] Vaupel, P., Mutschler, E., Schaible, H.G. (2015) Anatomie, Physiologie, Pathophysiologie des Menschen. *Wissenschaftliche Verlagsgesellschaft*; Auflage: 7 ISBN-10: 9783804729797

- [Wächter 06] Wächter, A., Biegler, L.T. (2006). On the Implementation of a Primal-Dual Interior Point Filter Line Search Algorithm for Large-Scale Nonlinear Programming. *Mathematical Programming* 106(1), pp. 25-57, 2006.
- [Weiss 04] Weiss, E. J., Flanders, M. (2004) Muscular and postural synergies of the human hand. *Journal of neurophysiology* 92 (1) (2004) 523–35. doi:10.1152/jn.01265.2003.
- [Westover 16] Westover, L. M., Sinaei, N., Küpper, J. C., Ronsky, J. L. (2016). Quantifying *in vivo* laxity in the anterior cruciate ligament and individual knee joint structures. *Computer Methods in Biomechanics and Biomedical Engineering*. 19:14, 1567-1577, DOI: 10.1080/10255842.2016.1170122
- [Wibawa 13] Wibawa, A. D. (2013). A validation study on muscle activity prediction of a lower limb musculoskeletal model using EMG during normal walking. *3rd International Conference on Instrumentation, Communications, Information Technology and Biomedical Engineering (ICICI-BME)*, Bandung, 2013, pp. 260-264. doi: 10.1109/ICICI-BME.2013.6698504
- [Winter 09] Winter, D.A. (2009). *Biomechanics and Motor Control of Human Movement*, Fourth Edition. John Wiley & Sons, Inc. ISBN: 978-0-470-39818-0
- [Willert 01] Willert et al (2001). *Taber's cyclopedic medical dictionary* (Ed. 19, illustrated in full color ed.). Philadelphia: F.A.Davis Co. ISBN 0-8036-0655-9.
- [Wu 05] Wu, G., van der Helm, F.C.T., Veeger, H.E.J, Makhsous, M., van Roy, P., Anglin, C. et al. (2005) recommendation on definitions of joint coordinate systems of various joints for the reporting of human joint motion—Part II: shoulder, elbow, wrist and hand. *Journal of Biomechanics* 38 (5), S. 981–992. DOI: 10.1016/j.jbiomech.2004.05.042, 2005
- [Zhang 19] Zhang, X., Chaffin, D. (2019). Digital human modeling for computer-aided ergonomics.

## Academic CV – Marius Obentheuer

Since 2019	Employee at Fraunhofer ITWM Department Mathematics for the Digital Factory
2015 - 2020	PhD Research Robotics Research Lab Department of Computer Science TU Kaiserslautern Research Focus: Digital Human Modelling
2002 – 2014	Diploma Mechanical Engineering Combined with Applied Informatics Majoring in Construction and CAD TU Kaiserslautern